The quality of GRACE monthly solutions and potential improvements by the use of the Global Tide and Surge Model

Marenka Brussee

TU Delft

The quality of GRACE monthly solutions and potential improvements by the use of the Global Tide and Surge Model

by

Marenka Brussee

to obtain the degree of Master of Science
at the Delft University of Technology,
to be defended publicly on Tuesday August 27, 2019 at 9:30 AM.

Student number:	4186249	
Faculty:	Civil Engineering and Geosciences	
Master track:	Geoscience and Remote Sensing	
Thesis committee:	Dr. P. G. Ditmar,	TU Delft
	Dr. ir. D. C. Slobbe,	TU Delft
	Prof. dr. ir. M. Verlaan,	TU Delft, Deltares

TU Delft

Abstract

Climate change causes alterations in large scale mass transport patterns in the ocean, cryosphere and hydrology. The Gravity Recovery and Climate Experiment (GRACE) satellite mission which has been operational in the years 2002-2017 has already improved our understanding of large scale mass transport on Earth, but improvement of data quality is still needed. This will increase the quality of our current estimates of the effects of climate change on one hand and help in the validation and initiation of climate models on the other, which improves the accuracy of future predictions.

Noise in GRACE Level-2 data (monthly gravity field solutions) is caused by various reasons. The measurements themselves are already executed and their quality is fixed but better data processing algorithms and background models can reduce the current noise level. This is also relevant for the GRACE Follow On mission which might have a higher measurement precision. Over the ocean, these GRACE monthly solutions ideally only show mass exchange between continents and ocean and effects of self-attraction and loading. Therefore, the signal over the ocean is expected to consist predominantly of a linear trend and a seasonal variability. For certain oceanic regions this is not the case. In these areas still a signal variance representing interannual differences in the mass-derivative and large residuals with respect to a low-pass filtered signal are observed. This low-pass filtered signal contains only signals of a frequency lower than the semiannual cycle. These signal variance and residuals are unexpected and can be caused by inaccuracies in the currently applied oceanic background models in GRACE data processing.

For various Release 5 and Release 6 monthly solutions the noise variance, signal variance and residuals as aforementioned are estimated. The noise and signal variance are estimated by Variance Component Estimation (VCE). Additionally, numerical experiments are performed to analyze different regularization functionals and set-ups in the VCE. The oceanic regions where the largest signal variance and residuals are observed correlate. These areas are for GRACE Release 5 data the Baltic Sea, Black Sea, Arafura Sea, East Siberian Arctic Shelf, Argentine Basin and Hudson Bay. For GRACE Release 6 data a significant drop of this signal variance and residuals can be observed for the Hudson Bay and East Siberian Arctic Shelf.

Consequently, the oceanic background models for these releases are compared against each other and against the Global Tide and Surge Model (GTSM) which is a 2D hydrological model based on the Delft3D Flexible Mesh software developed by Deltares. For the whole ocean both 3/6-hourly time-series and monthly time-series are analyzed. For the shallow regions up to 200 m, the Black Sea and the Red Sea, GTSM shows significant differences with respect to the current applied oceanic background models. When comparing the oceanic background models of different releases it can be observed that the regions where the signal variance and residuals decreased for GRACE Release 6 with respect to Release 5 correlate to regions where the differences between these models is significant. This indicates that oceanic background models do significantly influence the quality of GRACE monthly solutions over the ocean.

Furthermore, it is investigated whether it can be expected that GTSM will improve the GRACE monthly solutions. For this, monthly time-series of the current applied oceanic background models are added back to the GRACE monthly solutions; consequently, by GTSM computed monthly time-series are removed. Compared to GRACE Release 5 monthly solutions, GTSM shows a reduction in the signal variance and residuals for the Hudson Bay, East Siberian Arctic Shelf, Black Sea, Baltic Sea, North Sea, Arafura Sea and certain parts of the Arctic and Southern ocean. Compared to GRACE Release 6, a reduction in the signal variance and residuals is observed for the East Siberian Arctic Shelf, Black Sea, Baltic Sea, North Sea and Arafura Sea. For these regions it is most expected that GTSM can improve GRACE monthly solutions. Since the quality of monthly solutions over the oceans is clearly influenced by the oceanic background models significant alterations in GRACE monthly solutions are expected for the shallow regions up to 200 m, Black Sea and Red Sea when applying GTSM in the GRACE data processing. Whether these will be improvements or not should be analyzed by implementing GTSM-based 3-hourly time-series in the GRACE data processing to create a new GRACE Level-2 data product.

Preface

While finalizing this master thesis also my study trip through the TU Delft will end. It has been no direct route with a first-year degree in Architecture, a bachelor in Chemical Engineering, a minor in Applied Mathematics and finally the master Geoscience and Remote Sensing as specialization track of Applied Earth Sciences. I am very happy to have experienced these different study areas because I have been able to learn different aspects from each area and I have met many different people with a variety of knowledge and opinions. By doing this master research project I developed a lot of practical skills which I think are useful in future. Before this research, I never wrote in Python or LaTeX, worked in a Linux environment or understood a bit of Fortran. To work and do computations with terabytes of data was new for me and I am happy that my codes worked in the end to handle this size of data. One thing I like very much about the master Geoscience and Remote Sensing is the interdisciplinary character and the applicability in our current world of climate change. In future, I hope I can work in an interdisciplinary environment and contribute in some way to our challenge to handle properly with climate change.

I would like to thank several institutes and people. First of all I am very thankful that the TU Delft allows students to schedule their studies flexibly which made it for me possible to follow this master beside a full-time study in classical music performance at the University for the Arts in Rotterdam. This made it possible to broaden my horizon by developing myself in two different directions of engineering on one side and musicianship on the other side. I would like to thank Deltares for their perfect work environment (also digitally) and pleasant atmosphere. I would like to thank my three supervisors a lot for their help and knowledge. Pavel, thank you especially for all your detailed comments, your fast and strict responding and your interest in results which seemed for me (in first instance) not so useful. Cornelis, thank you especially for your very practical attitude. During meetings you helped a lot by suggesting practical solutions and new steps in my research and by being clear about the quality (or not) of results. Martin, thank you especially for your restful attitude which made me dare to speak my thoughts during meetings and for your help to start-up at Deltares. Also I am thankful for your good advice in time of a concussion. Besides this, I would like to thank my family, boyfriend, friends and fellow students for speaking about my research from a broader perspective and for your support and friendship in general.

Marenka Brussee
Delft, August 2019

Contents

Abstract iii

Preface v

1 Introduction 1
- 1.1 Context . . . 1
- 1.2 Gravity Recovery and Climate Experiment . . . 2
- 1.3 Problem statement . . . 4
- 1.4 Research question, sub-questions and outline report . . . 5

2 Estimation of signal and noise in mass-anomaly time-series 9
- 2.1 Theory . . . 10
  - 2.1.1 Combination of mass-anomaly time-series and regularization . . . 10
  - 2.1.2 Description of the linear functional models . . . 11
  - 2.1.3 Finding the noise variances and the regularized solution . . . 12
- 2.2 Numerical study . . . 13
  - 2.2.1 Generating noisy time-series . . . 14
  - 2.2.2 Determination of noise variance and bias in combined and/or regularized mass-anomaly time-series . . . 17
- 2.3 Case study for the Baltic Sea . . . 17
  - 2.3.1 Comparison of a GRACE based time-series to a tide-gauge based time-series . . . 18
  - 2.3.2 Comparison of several combined GRACE-based time-series to a tide-gauge based time-series . . . 19
- 2.4 Results and discussion . . . 21
  - 2.4.1 Numerical study . . . 21
  - 2.4.2 Case study for the Baltic Sea . . . 33
- 2.5 Summary and remarks . . . 35

3 Quality of GRACE Release 5 and 6 monthly solutions 37
- 3.1 Theory . . . 37
  - 3.1.1 Earth's gravitational potential . . . 37
  - 3.1.2 Coordinate systems . . . 39
  - 3.1.3 Conversion of Stokes coefficients to mass anomalies at the Earth's surface . . . 40
  - 3.1.4 GRACE Release 5 and 6 Level-2 data . . . 42
  - 3.1.5 Degree-1 and C20 coefficients . . . 43
- 3.2 Method . . . 44
  - 3.2.1 Computation of mass-anomaly time-series from different GRACE Level-2 data . . . 44
  - 3.2.2 Chosen set-up in the VCE and computation of regional estimates . . . 45
  - 3.2.3 Definition of oceanic and continental regions . . . 47
  - 3.2.4 Estimation of non-seasonal and high-frequency residuals in ITSG monthly solutions . . . 48
- 3.3 Results and discussion . . . 49
- 3.4 Summary and remarks . . . 68

4 Comparison of GTSM to oceanic background models currently used in GRACE data processing 71
- 4.1 Theory . . . 71
  - 4.1.1 Ocean variability . . . 71
  - 4.1.2 Global Tide and Surge Model . . . 72
  - 4.1.3 Atmosphere and Ocean non-tidal De-aliasing product . . . 74

4.2 Method . . . 77
4.2.1 Computation of mass-anomaly time-series from ocean tide and AOD1B products . 78
4.2.2 Configurations in GTSM . . . 78
4.2.3 Creation of GTSM products comparable to the AOD1B products . . . 78
4.2.4 Conversion of mass-anomaly time-series at a structured grid to Stokes coefficients . . . 80
4.2.5 3/6-hourly time-series comparison between GTSM and AOD1B products . . . 81
4.2.6 Monthly time-series comparison between GTSM and AOD1B products . . . 83
4.3 Results and discussion . . . 83
4.3.1 3/6-hourly time-series comparison . . . 83
4.3.2 Fourier analysis of basin average 3/6-hourly time-series . . . 91
4.3.3 Monthly time-series comparison . . . 94
4.4 Summary and remarks . . . 99

5 Potential improvements to GRACE monthly solutions by the use of GTSM 101
5.1 Method . . . 101
5.2 Results and discussion . . . 102
5.3 Summary and remarks . . . 117

6 Conclusions and recommendations 119
6.1 Conclusions regarding the sub-questions . . . 119
6.2 Main conclusions . . . 121
6.3 Recommendations . . . 122

A Standard deviations of reported results in section 2.4 125

B Complete set of figures of estimated signal and noise in chapter 3 135

C Supplementing set of figures for section 4.3 143

D Strange features in GTSM when run with only tidal forcing 149

Bibliography 155

1 Introduction

In this chapter the context and some theoretical background for the research will be given. The problem will be described in a separate section which leads to the goal of this research. Thereafter, the main question of this research and the sub-questions follow together with an outline for this report.

1.1. Context

Impacts of climate change are among others visible in large-scale mass transport. Melting of land ice, increasing and intensifying drought periods at certain land areas and sea level rise [12] [39] are examples of large-scale mass transport. In the context of climate change, accurate measurements of large-scale mass transport are useful for at least two reasons. Firstly, to have good estimates of the current effects of climate change and secondly to validate and initiate climate models which can provide future predictions.

An example of the need to have accurate measurements of mass transport is in the scope of sea level rise. It has to be known when the sea level with respect to land will increase by what amount. Countries as for example The Netherlands should make their protection mechanisms on time (for example figure 1.1) and eventually evacuate (parts of) their country on time. The range in predicted sea level rise is large. According to IPCC [40] global mean sea level has risen at an average rate of 1.7 (1.5-1.9) mm/y between 1900 and 2010 and at an average rate of 3.2 (2.8-3.6) mm/y between 1993 to 2010. For the Dutch coast, current projections in sea level rise for 2100 with respect to 1995 are 0.3 m (lower bound) to 2.0 m (upper bound) if the global temperature rise is 2°C by 2100. If the global temperature rise is 4°C by 2100 the upper bound is 3.0 m. [34] The range between upper and lower bound is among others large due to the unknown level of increased ice melt at Antarctica. [34] Accurate measurements of each contributing process to sea level rise are needed to improve the predictions.

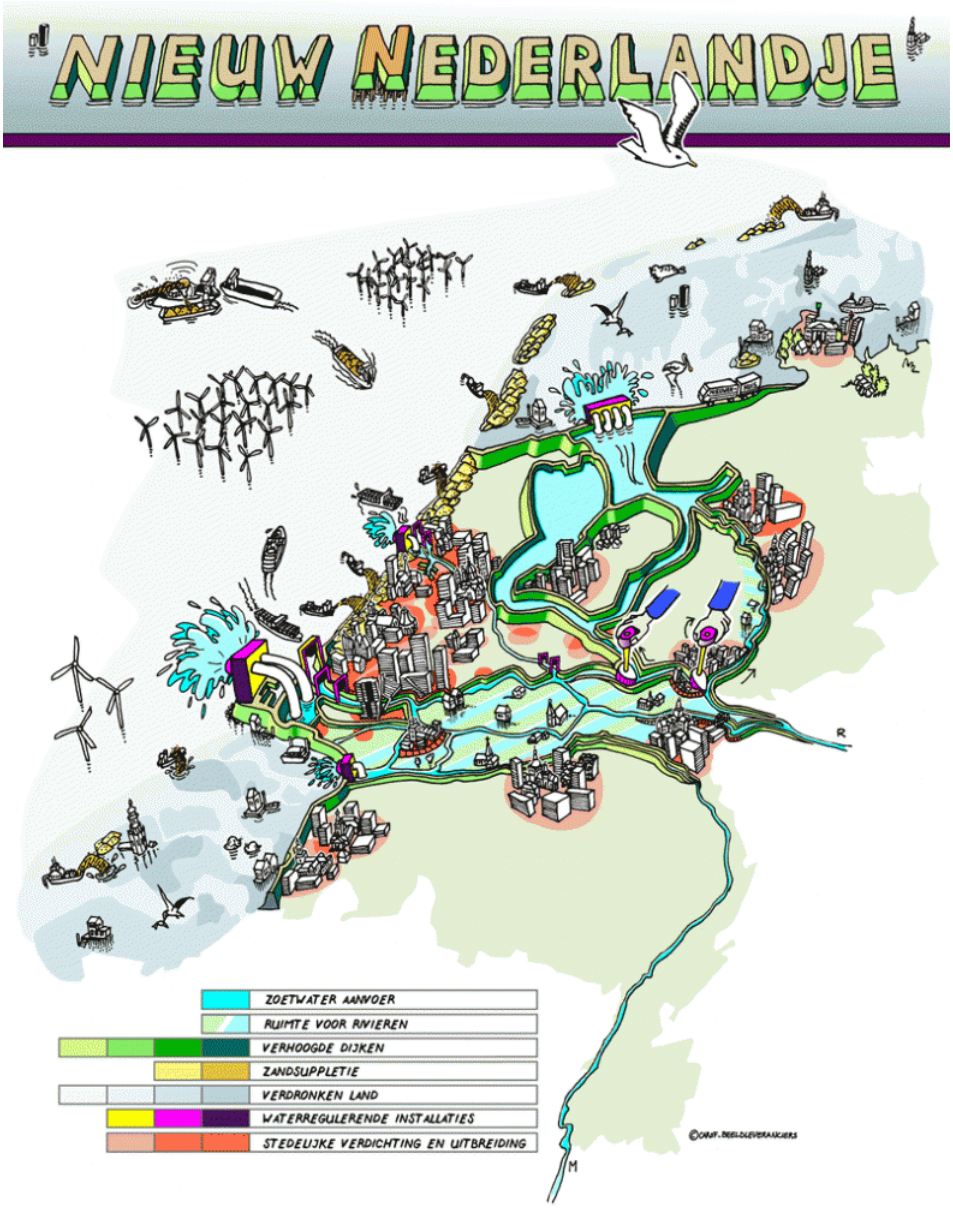

Figure 1.1: Possible consequences for the Netherlands at the time of sea level rise of several meters: an impression by Carof Beeldleveranciers [72].

For the period 2002-2017 measurements of large scale mass transport were made by the Gravity Recovery and Climate Experiment (GRACE) [32]. This experiment gives estimates of large scale mass transport in the Earth's system at the monthly and longer time-scales. Since the launch of GRACE in 2002, satellite gravimetry has been widely used for this type of observations [4] and it is one of the most important ways to study large-scale mass transport in the Earth's system [24]. GRACE gives insight in to what extent the melt of glaciers and ice sheets, and changes in hydrology are contributing to sea level rise. [48] GRACE distinguishes these from changes caused by thermal expansion of the water. Measurements by GRACE can thus contribute to the determination and prediction of the effects of climate change in especially the ocean and cryosphere.

1.2. Gravity Recovery and Climate Experiment

The GRACE mission is a satellite mission which has been operational in the period March 2002 to October 2017. The principal objective of the GRACE mission is to obtain accurate estimates of the mean and time-variable gravity field of the Earth. [10] It has as setup two twin satellites orbiting one

behind the other with a distance of about $220\ km$ in between [32]. This can be seen in the artist's impression in Figure 1.2. The twin spacecraft co-orbit in a near circular, near polar orbit (orbit inclination = 89°, eccentricity = 0.001) and started at an initial altitude of $500\ km$. [23]

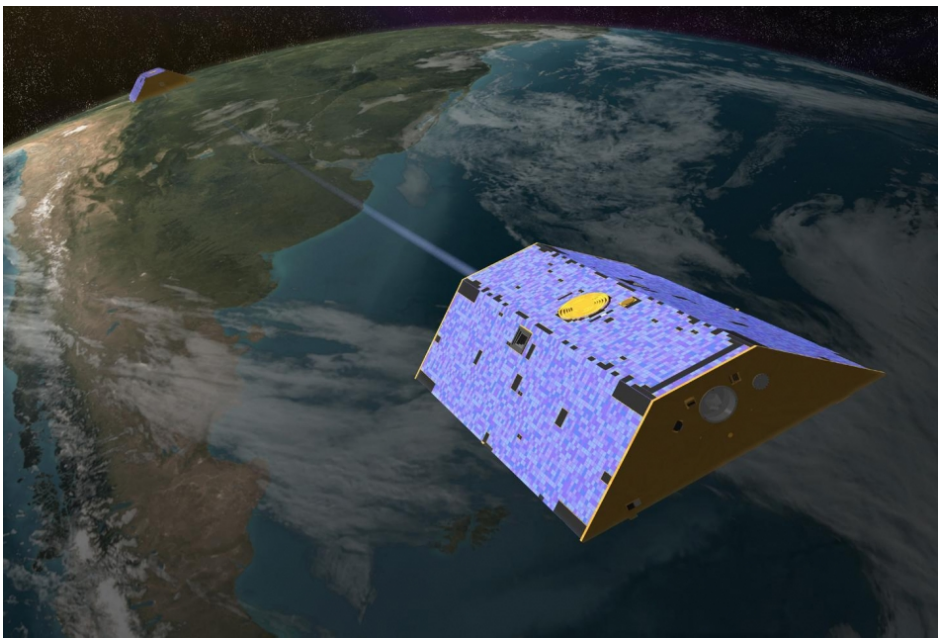

Figure 1.2: GRACE satellites: an artist's impression [33].

The distance between the two satellites changed by small accelerations and decelerations of the satellites due to varying mass below these spacecrafts [32] since a local increase in mass leads to an increase of the gravitational attraction on a satellite [3]. The gravitational field of the Earth is determined by how Earth's material is distributed throughout the Earth's system. Mass is not equally distributed due to a varying material density distribution which also varies over time [3].

The changes in distance between the two satellites can be in the order of kilometers and are measured by a microwave ranging system (a K-band ranging system) with a micrometer precision [10] [37] [23]. The range change data are processed to produce monthly mean solutions of the Earth's exterior gravitational potential [10] which are provided as Level-2 data product. For this ancillary data are needed. These are measurements of non-gravitational forces such as atmospheric drag and solar radiation pressure by an accelerometer [32] [10], measurements of the satellite orientation and position which are determined by two star cameras and a GPS receiver [10], and data from background models.

The changes in Earth's gravitational potential give an estimate of the mass movement (changes in the distribution of mass) taking place in the Earth's system. [35] The by GRACE provided Level-2 data product consists of monthly mean gravity field solutions and thus gives an indication of mass transport at the monthly and longer time-scales. Furthermore, the spatial resolution of GRACE based estimates of mass transport is $300 - 400\ km$ [23]. Estimates of mass transport retrieved from this Level-2 data product are thus averaged over an area of the size of two times the Netherlands and a month of time [32].

GRACE has improved our understanding of changes in underground water, melting ice sheets, sea level rise and solid earth changes [32]. A few discoveries by GRACE in its active period are [32]:

- A third of the largest groundwater basins is rapidly depleted.
- Greenland looses about 280 gigatons of ice per year.
- Antarctica looses about 120 gigatons per year.
- Both Greenland and Antarctica show increasing melt rates.
- The sea level drop and change in precipitation pattern caused by the 2011 La Niña event.
- The movement of viscous mantle material under the Earth's crust due to water mass changes near the surface like ice sheet loss and groundwater depletion and thereby caused changes in Earth's rotation.

Importantly the GRACE mission covers the whole Earth's surface and it observes mass re-distribution directly without needing additional information [23]. The GRACE mission gives insight in changes of mass of water and solid Earth at locations where humans cannot go. [32]

After the success of the GRACE mission, GRACE Follow-On (GRACE-FO) was launched in May 2018 to continue the data record of GRACE. The GRACE-FO is equipped with an additional ranging instrument beside the K-band ranging system, a laser ranging interferometer, which is expected to produce more accurate measurements. [32] The measurement precision of the distance between the two satellites influences the accuracy of the derived gravity field solutions and thus using a laser ranging instrument might lead to a better spatial resolution and accuracy of the gravity field solutions. [28] The GRACE-FO furthermore uses three star camera's instead of two for the attitude control and this makes the attitude determination more robust. [28] The accelerometer and GPS receiver are also evolved versions of the ones used for GRACE. [28]

1.3. Problem statement

GRACE solutions are used in the interpretation of various geophysical processes in the Earth's system and calibration of geophysical models. [79] Therefore, improvements in the quality of these solutions is desirable. Some points of improvement are related to the mission itself and can only be improved in a future mission and thus for a different time span. Other points of improvement are related to the data processing. Reduction of error sources in the data processing can improve GRACE solutions also for the period 2002-2017. This research focuses on an error source in the data processing.

This error source in currently available GRACE solutions is related to the problem of temporal aliasing. [80] Temporal aliasing is caused by high frequency mass variations which are present in hydrology, atmosphere and ocean. [80] [35] [79] These high frequency geophysical phenomena induce short-term variations in the external gravitational potential which can even be in the order of a few hours. These can not be captured by the GRACE satellites because their repeat period is much larger and can consequently alias in the GRACE solutions when not appropriately removed from the measurements. Various geophysical background models are considered to estimate and remove the high-frequency geophysical phenomena to overcome the problem of temporal aliasing. [29] Unfortunately, the models are not perfect and their errors can alias in the final GRACE solutions.

Over the ocean, the most dominant contributors to the temporal aliasing are the oceanic tides of the daily and sub-daily period and non-tidal variations in both atmosphere and ocean at the scale of a few hours. [53] Short-term oceanic water redistribution can induce deviations of the sea surface heights from their mean values by several meters. [15] Over the oceans, all signals not related to mass exchange between land and ocean and effects due to self-attraction and loading should be removed from GRACE measurements. This would results in a signal of predominantly a linear trend and seasonal variability. Regions where this is not the case are expected to suffer from aliasing errors due to inaccurate background models.

Temporal aliasing, due to inaccuracies in the ocean tide model and the non-tidal ocean and atmosphere models [28] [80] [23] [79], is one of the dominant contributors to the error in GRACE monthly solutions beside inaccuracies in the inter-satellite distance measurements [80] and accelerometer error [28] [23]. In the context of the GFO, which might show intersatellite ranging measurements of higher accuracy, the dominant barriers to further improve the gravity field solutions are the temporal aliasing errors and accelerometer noise. [80] [53] [79] [28] All these error sources contribute to the total noise in GRACE monthly solutions.

Ditmar et al. [25] introduced a method to estimate and reduce the level of the random noise in GRACE monthly solutions. This method is based on Variance Component Estimation (VCE) with inclusion of a regularization functional. In a similar way to them, the noise in GRACE monthly solutions will be estimated in chapter 3. The regularization in their proposed method is in the time domain and based on the minimization of Month-to-month Year-to-year Double Differences (MYDD). This regularization functional will be discussed in further detail in section 2.1. By considering this regularization functional in the VCE, signal variance can be estimated which represents interannual differences in the mass-derivative. This signal variance is expected to be zero over the oceans when all tidal and non-tidal variability are properly modeled and removed. In chapter 3 it can be observed that this is not the case. GRACE monthly solutions are thus in need for improvement over the ocean, and especially in regions of high signal standard deviation.

This research focuses on the part of the temporal aliasing caused by inaccuracies in tidal and non-tidal oceanic background models. At the moment, separate models are used for the tidal part (for example EOT11a and FES2014b) and the non-tidal part which is provided as a so-called Atmosphere and Ocean De-aliasing product (AOD1B). In this research it is investigated whether the Global Tide and Surge Model (GTSM) has the potential to improve GRACE monthly solutions. This model is recently developed by Deltares and is a global ocean model that includes both tidal and meteorological forcing. When this model is more accurate than the currently used oceanic background models, it might be able to decrease the aliasing errors in GRACE monthly solutions

One improvement of GTSM with respect to the currently used oceanic background models might be that the non-linear interaction between tidal and meteorological forced dynamics is included in GTSM. Another advantage of GTSM is that is has a unstructured computational grid. This grid has smaller grid cells ($\sim$5 km) in shallow coastal areas and larger grid cells ($\sim$ 50 km) in deep ocean parts [51]. Also, in areas with high bathymetry gradients like at ocean ridges and trenches there is a grid densification. [41] This can reduce the problem of inadequate (too rough) discretization in the horizontal direction. Some other differences with respect to the currently used oceanic background models is that GTSM is a 2D horizontal (2DH) model instead of a 3D model and that the internal time-step of the model is maximal 2.5 minutes instead of 20-90 minutes in the currently applied oceanic background models. GTSM will be discussed in detail in section 4.1.2. It will be investigated how GTSM performs in comparison to the oceanic background models currently used in GRACE data processing and if it might be advisable to use GTSM in future to create better GRACE monthly solutions.

1.4. Research question, sub-questions and outline report

This research is about the quality of GRACE Level-2 data and about the performance of GTSM compared to the oceanic background models currently used in the generation of GRACE Level-2 data product.

The main question for this research is:

(i) What is the global distribution of the quality of GRACE Release 5 and 6 monthly solutions and (ii) is it expected that these solutions will be improved by the use of the Global Tide and Surge Model as oceanic background model?

The quality of GRACE Level-2 data is assessed in different ways. Firstly, noise variance in the GRACE Level-2 data is estimated for the whole world. Secondly, a signal variance is estimated. This signal variance quantifies interannual differences in the mass-derivative which should be close to zero over the ocean. Thirdly, residuals with respect to a low-pass filtered signal or analytical function are estimated for certain GRACE Level-2 data. The low-pass filtered signal contains only frequencies smaller than the semi-annual cycle. The analytical function contains only a linear trend and seasonal variability. Over the ocean, these residuals should also be close to zero. For a certain region the quality of GRACE monthly solutions is regarded higher when the estimated noise variance is smaller than the global average. For a certain oceanic region the quality of GRACE monthly solutions is regarded higher when the signal variance and residuals are estimated smaller than the oceanic average. After an analysis of the differences between the GTSM and the currently used oceanic background models, it is investigated if the signal variance and residuals reduce by the use of monthly time-series generated by GTSM. This gives an indication if it is expected that GTSM can improve GRACE Level-2 data.

The main question gives rise to four sub-questions which are addressed in the corresponding chapters as explained below. Most of these chapters contain a theoretical and methodological part after which a part with results and discussion follows. The four sub-questions and the outline of these four chapters are:

- Which regularization functional should be used in Variance Component Estimation to identify the noise variance and signal in time-series which consist predominantly of a seasonal variability and linear trend?

  In this chapter the method to estimate noise variance and recover the signal in mass-anomaly time-series by Variance Component Estimation (VCE) is described. Numerical experiments are performed to evaluate different set-ups in the VCE among which the use of a different regularization functional. The amount of time-series which are processed together in the VCE is varied

which is similar to processing multiple time-series derived from GRACE Level-2 data of different research centers. The influence of the use of multiple time-series, different signals and different noise levels, as well as the impact of cross-correlation in noise realizations are investigated. Conclusions are made about the influence of these differences in simulated time-series and processing strategy to the accuracy of the estimated noise variance and recovered signal. When the regularization functional is used which is based on MYDD minimization, a signal variance is estimated which represents interannual differences in the mass derivative. Estimates of this signal variance for different signals are also reported. With this analysis the estimates of signal and noise variance in future chapters can be better interpreted.

Besides the numerical experiments, VCE is applied to GRACE-based mass-anomaly time-series. The effect of a different regularization functional or no regularization functional at all in the VCE set-up is analyzed for the Baltic Sea. For this, the GRACE-based time-series are compared against a tide-gauge based time-series for this area. The GRACE-based mass-anomaly time-series are derived from monthly GRACE Release 5 solutions. Basin average time-series are compared. For this comparison, ocean variability predicted by the oceanic background models is added to the combined solution retrieved by VCE. Also signal leakage is taken into account by using scaling factors and output of a hydrological model.

- What are the global distributions of signal and noise variance in GRACE Release 5 and 6 monthly solutions?

  In this chapter the quality of the currently available GRACE monthly solutions is addressed. Solutions of different research centers and of different releases are considered. First theoretical differences between these solutions in their applied geophysical background models are described before estimating the noise variance and signal variance for the different GRACE monthly solutions by VCE. When MYDD-minimization is the considered regularization functional in the VCE, this signal variance represents interannual differences in the mass-derivative. Three Release 5 GRACE monthly solutions (CSR Release 5, GFZ Release 5 and ITSG 2016) and three Release 6 GRACE monthly solutions (CSR Release 6, ITSG 2018 and JPL Release 6) will be considered. Beside the estimation of noise and signal variance, residuals with respect to a low-pass filtered signal and an analytical function are estimated for the ITSG monthly solutions. The low-pass filtered signal contains only frequencies small than the half-year periodicity. The analytical function is estimated by least-squares and is a combination of a linear trend, annual and semiannual periodicity. Areas where the noise variance is large w.r.t. the global mean and signal variance or residuals are large w.r.t. the oceanic mean are identified.

- Which regions show significant differences between 3-hourly, 6-hourly and monthly mass-anomaly time-series generated by GTSM and those generated by the oceanic background models currently used in GRACE data processing?

  In this chapter GTSM is described and differences in modeling strategy between GTSM and the currently used oceanic background models are listed. Then the method to convert GTSM output to make it comparable to the currently used background models is described. This means that the inverted barometer effect, the presence of a static residual atmospheric pressure field and the subtraction of a long-term mean have to be taken into account in a similar way when considering time-series by GTSM. For the monthly time-series comparison GTSM output is compared to both the non-tidal product only and the combination of non-tidal and tidal products provided by GRACE data processing centers. For this, GTSM is run with only meteorological forcing and both tidal and meteorological forcing. For the 3-hourly and 6-hourly time-series comparison GTSM is only compared to only the non-tidal product. Also a frequency analysis is performed for these 3-hourly and 6-hourly time-series comparison to observe in which frequency range the differences are larger.

- For which regions does the quality of GRACE monthly solutions increase by the use of monthly mass-anomaly time-series generated by GTSM?

  In this chapter the method of addition and subtraction (MAS) to the GRACE Level-2 data is explained. By adding monthly mass-anomaly time-series generated by the currently used oceanic

background models and consequently removing monthly mass-anomaly time-series generated by GTSM from the Level-2 data it is investigated if GTSM has a potential to improve the latter. This is done for the combination of tidal and non-tidal products as well as for the non-tidal product only. It is investigated if the signal variance and residuals (as described for the second sub-question) decrease for certain areas. Also the bathymetry is considered in this comparison by showing the changes versus bathymetry. Time-series of monthly time-series before and after the MAS are shown to observe the effect in the time domain.

After these four chapters, a chapter with conclusions and recommendations follows.

2

Estimation of signal and noise in mass-anomaly time-series

This chapter is about the first sub-question:

- Which regularization functional should be used in Variance Component Estimation to identify the noise variance and signal in time-series which consist predominantly of a seasonal variability and linear trend?

This question is assessed to find a good VCE set-up for the analysis of GRACE-based monthly solutions in the chapter 3. Furthermore, results shown in this chapter lead to a better interpretation of the results shown in chapters 3 and 5. First, the method to estimate signal and noise in mass-anomaly time-series by using Variance Component Estimation (VCE) will be described. This description is adapted from Koch and Kusche [45] and Ditmar et al. [25]. In this chapter two types of mass-anomaly time-series are considered. The first type are synthetic data. These mass-anomaly time-series are a combination of a self-defined signal and white noise. The second type are GRACE-based mass-anomaly time-series. By applying VCE different mass-anomaly time-series can be combined to compose a new mass-anomaly time-series by assigning appropriate weights to the original ones. The VCE allows also a regularization functional to be incorporated. One of the regularization functionals which will be investigated is the one that minimizes the year-to-year difference of the time-derivative of mass-anomalies. This regularization functional is proposed and analyzed by Ditmar et al. [25].

True mass-anomaly time-series derived from GRACE monthly solutions consist over the ocean predominantly of a seasonal variability and linear trend. The GRACE-based mass-anomaly time-series also contain a certain amount of noise which can be cross-correlated. Numerical experiments with the synthetic data are performed to investigate by which VCE set-up noise and signal are estimated best for time-series which resemble GRACE-based mass-anomaly time-series over the ocean. The self-constructed signal in the mass-anomaly time-series are varied in the size of amplitude of the annual variability since the size of seasonal variations is different for different regions. Also two types of short-term signals are considered in the construction of mass-anomaly time-series to investigate how well these signals can be estimated by VCE. These short-term signals can be true signals in GRACE-based mass-anomaly time-series or an indication of an error in these time-series. Since the size of the noise in GRACE monthly solutions is regionally different, time-series are constructed with different noise levels. Because a part of the noise in GRACE monthly solutions can be cross-correlated, also time-series are constructed with cross-correlated noise. The numerical experiments will thus be performed to analyze the effect of:

- processing a different number of mass-anomaly time-series together
- using different regularization functionals or no regularization at all
- processing mass-anomaly time-series with different noise levels
- processing mass-anomaly time-series with or without cross-correlated noise
- processing mass-anomaly time-series with an annual variability of different amplitude

- processing mass-anomaly time-series which show short-term variations like an instantaneous increase in mass in a certain year or an increased amplitude of annual variations within a half-year interval

To investigate the effect of the use of a different regularization functional in the VCE for true GRACE-based mass-anomaly time-series a certain area is selected to compare the combined mass-anomaly time-series against a mass-anomaly time-series measured by a different technique. The chosen area is the Baltic Sea. For the Baltic Sea, the combined (regularized) mass-anomaly time-series retrieved from three input time-series using VCE are compared to a tide-gauge derived mass-anomaly time-series. This area is chosen because for this area a comparison of a GRACE-based time-series against a tide-gauge based time-series is already performed by Virtanen et al. [69]. Therefore, a tide-gauge based time-series, a hydrological leakage time-series and a steric signal for this area are available which makes it possible to do a similar comparison. Furthermore, it can be observed that the basin-average mass-anomaly time-series for this area consists mainly of a linear trend and seasonal variability which is similar to our assumption for the construction of the synthetic data. Furthermore, it is assumed that the basin-average time-series for the Baltic Sea is representative for oceanic signals in general because of the presence of a linear trend and seasonal variability in this time-series. The applied method by Virtanen et al. [69] will be described as well as how the method in this study deviates from their study.

2.1. Theory

In this section the method to combine several mass-anomaly time-series into one and simultaneously estimate the noise variance of these time-series will be described. In this research, these mass-anomaly time-series are derived from GRACE monthly solutions or they are synthesized data resembling GRACE-based mass-anomaly time-series. These mass-anomaly time-series are thus supposed to be available for the same total period. When considering GRACE-based mass-anomaly time-series, different GRACE solutions are provided by several research centers. These GRACE solutions should contain the same signal but are different by containing their own errors due to different data processing strategies of the research centers. In this chapter first synthetic data resembling GRACE-based mass-anomaly time-series are considered. The method which will be used to combine the mass-anomaly time-series into one is based on the VCE technique [45]. By introducing a set of pseudo-observations besides the mass-anomaly time-series, regularization can be incorporated. Different regularization functionals are addressed.

2.1.1. Combination of mass-anomaly time-series and regularization

The combined mass-anomaly time-series $H(t)$ will be found by minimizing the following objective function:

$$\Phi[H] = \sum_{i=1}^{P} \sum_{j \in N_i} \frac{1}{\sigma_{d_i}^2} \left(H(t_j) - H_j^i \right)^2 + \frac{1}{\sigma_0^2} \Omega[H], \tag{2.1}$$

where P is the number of mass-anomaly time-series, N_i is the set of observation moments of the specific dataset i, H_j^i is the mass-anomaly of the specific dataset i at observation moment j, t_j is the time in years corresponding to observation moment j, $H(t)$ is the combined and/or regularized mass-anomaly as a continuous function of time, $\Omega[H]$ is the regularization functional, $\sigma_{d_i}^2$ is the noise variance of data set i and σ_0^2 is the error variance of the pseudo-observations. The pseudo-observation equations are defined in line with the chosen regularization functional. The error variance of the pseudo-observations thus represent how much the regularized signal deviates from a signal which totally meets the requirements of a certain regularization functional. This error variance of the pseudo-observations will also be called signal variance in the following sections and chapters. Equation 2.1 holds when it is assumed that the data noise and the noise in the pseudo-observations is white. When no regularization is included the last term in equation 2.1 is absent.

The regularization functional $\Omega[H]$ represents the regularization used. The regularization functionals that will be addressed in this chapter are the Tikhonov zero-order, first-order and second-order functionals, as well as the regularization functional proposed in [25] which minimizes the year-to-year differences of the time-derivative of mass-anomaly.

The zero-order Tikhonov regularization functional is defined as:

$$\Omega\left[H\right] = \int \left[H\left(t\right)\right]^2 \, dt \tag{2.2}$$

with $H\left(t\right)$ the regularized mass-anomaly time-series. When this functional is used, the mass-anomalies themselves will be minimized. This will favor a solution close to zero.

The first-order Tikhonov regularization is defined as:

$$\Omega\left[H\right] = \int \left[\dot{H}\left(t\right)\right]^2 \, dt, \tag{2.3}$$

where $\dot{H}\left(t\right)$ is the time-derivative of the regularized mass-anomaly time-series. When this functional is used the time derivative of mass-anomaly will be minimized. Since in this chapter the temporal sampling of input data is one month, the month-to-month differences are minimized in practice. In this way solutions that are relatively flat (i.e. constant) will be favored.

The second-order Tikhonov regularization is defined as:

$$\Omega\left[H\right] = \int \left[\ddot{H}\left(t\right)\right]^2 \, dt, \tag{2.4}$$

where $\ddot{H}\left(t\right)$ is the second time-derivative of the regularized mass-anomaly time-series. When this functional is used, month-to-month double differences are minimized in practice. In this way solutions that are smooth (i.e. with a constant slope) will be favored. [7]

The regularization functional proposed in [25] is defined as follows:

$$\Omega\left[H\right] = \sum_{k=1}^{K-1} \int_0^1 \left[\dot{H}\left(k+1+\tau\right) - \dot{H}\left(k+\tau\right)\right]^2 \, d\tau, \tag{2.5}$$

where K is the total number of years considered and τ the time in years ($0 \leq \tau \leq 1$) of a specific year k. By applying this regularization functional, month-to-month year-to-year double differences will be minimized in practice. The regularization functional is based on the expectation that GRACE-based mass-anomaly time-series show predominantly a combination of a seasonal variability and linear trend. So with this choice the bias introduced by regularization will be reduced. [25] When referring to this regularization functional the term MYDD (Month-to-month Year-to-year Double Difference) will be used.

2.1.2. Description of the linear functional models

The input data for the regularization and noise estimation method are mass-anomaly time-series in meters of equivalent water height (EWH). The mass-anomaly time-series can be GRACE-based and available for each grid point in the spatial domain or simulated time-series. The mass-anomaly time-series are considered as data vectors which contain both signal and noise. The data vectors are represented by $\mathbf{d}_i$ for each mass-anomaly time-series i. The data vectors can be related to an unknown vector ($\mathbf{x}$), which is the discrete analogue of $H\left(t\right)$ in equation 2.1. By VCE, this vector $\mathbf{x}$ is estimated as a combined and/or regularized mass-anomaly time-series. The notation for the estimate of this unknown vector is $\hat{\mathbf{x}}$. The following description of the linear functional models is based on Koch and Kusche [45], Ditmar et al. [25] and Aster et al. [7].

The linear functional model which relates the data vectors to the unknown vector $\mathbf{x}$ is:

$$\mathbf{A}_i\mathbf{x} = \mathbf{d}_i \text{ for each } i \tag{2.6}$$

with $\mathbf{A}_i$ the design matrices. This matrix contains only zeros and ones in such a way that there is a one-to-one relation for each epoch between mass-anomalies in the vectors $\mathbf{d}_i$ and $\mathbf{x}$. When $\mathbf{d}_i$ and $\mathbf{x}$ have the same length this would exactly result in an identity matrix. Otherwise, $\mathbf{A}_i$ contains as many ones as the length of $\mathbf{d}_i$ and their location in the matrix $\mathbf{A}_i$ is determined by the epochs of the data vector $\mathbf{d}_i$.

The noise covariance matrices of the data vectors can be represented as:

$$\mathbf{C}_i = \sigma_{d_i}^2 \mathbf{P}_i^{-1} \tag{2.7}$$

with $\mathbf{P}_i$ the known weight matrices of the data vectors $\mathbf{d}_i$ which are in this case defined as identity matrices because it is assumed that the data noise is white. Furthermore, $\sigma_{d_i}^2$ are unknown noise variances to be estimated for each data vector $\mathbf{d}_i$.

An additional set of linear equations is added to the linear functional model 2.6 when regularization is used. This additional set of linear equations is related to the chosen regularization functional and defined as follows:

$$\mathbf{D}\mathbf{x} = \mathbf{0}, \tag{2.8}$$

where $\mathbf{D}$ is the finite-difference analog of the differentiation operator present in the squared brackets in the integrals of equations 2.2, 2.3, 2.4 and 2.5. So $\mathbf{D}$ depends on the chosen regularization functional.

When the zero-order Tikhonov regularization functional is used, matrix $\mathbf{D}$ becomes the identity matrix:

$$\begin{bmatrix} 1 & 0 & 0 & 0 & 0 & \dots & 0 \\ 0 & 1 & 0 & 0 & 0 & \dots & 0 \\ \vdots & \ddots & \ddots & \ddots & \ddots & \ddots & \vdots \\ 0 & \dots & 0 & 0 & 0 & 1 & 0 \\ 0 & \dots & 0 & 0 & 0 & 0 & 1 \end{bmatrix}. \tag{2.9}$$

When the first-order Tikhonov regularization functional is selected, matrix $\mathbf{D}$ becomes:

$$\begin{bmatrix} -1 & 1 & 0 & 0 & 0 & \dots & 0 \\ 0 & -1 & 1 & 0 & 0 & \dots & 0 \\ \vdots & \ddots & \ddots & \ddots & \ddots & \ddots & \vdots \\ 0 & \dots & 0 & 0 & -1 & 1 & 0 \\ 0 & \dots & 0 & 0 & 0 & -1 & 1 \end{bmatrix}. \tag{2.10}$$

When the second-order Tikhonov regularization functional is preferred, matrix $\mathbf{D}$ becomes:

$$\begin{bmatrix} 1 & -2 & 1 & 0 & 0 & \dots & 0 \\ 0 & 1 & -2 & 1 & 0 & \dots & 0 \\ \vdots & \ddots & \ddots & \ddots & \ddots & \ddots & \vdots \\ 0 & \dots & 0 & 1 & -2 & 1 & 0 \\ 0 & \dots & 0 & 0 & 1 & -2 & 1 \end{bmatrix}. \tag{2.11}$$

When the regularization functional proposed by Ditmar et al. [25] is used, matrix $\mathbf{D}$ becomes:

$$\begin{bmatrix} 1 & -1 & 0 & 0 & 0 & 0 & 0 & 0 & 0 & 0 & 0 & 0 & -1 & 1 & 0 & 0 & \dots & 0 \\ 0 & 1 & -1 & 0 & 0 & 0 & 0 & 0 & 0 & 0 & 0 & 0 & 0 & -1 & 1 & 0 & \dots & 0 \\ \vdots & \ddots & \ddots & \ddots & \ddots & \ddots & \ddots & \ddots & \ddots & \ddots & \ddots & \ddots & \ddots & \ddots & \ddots & \ddots & \ddots & \vdots \\ 0 & \dots & 0 & 1 & -1 & 0 & 0 & 0 & 0 & 0 & 0 & 0 & 0 & 0 & 0 & -1 & 1 & 0 \\ 0 & \dots & 0 & 0 & 1 & -1 & 0 & 0 & 0 & 0 & 0 & 0 & 0 & 0 & 0 & 0 & -1 & 1 \end{bmatrix}. \tag{2.12}$$

Furthermore, since it is assumed that the pseudo-observations are contaminated by white noise, their noise covariance matrix becomes:

$$\mathbf{C}_0 = \sigma_0^2 \mathbf{P}_0^{-1}, \tag{2.13}$$

where $\mathbf{P}_0$ is defined as an identity matrix and σ_0^2 is an unknown signal variance to be estimated. Since the pseudo-observations are always zero, the noise variance of the pseudo-observations can be interpreted as signal variance.

2.1.3. Finding the noise variances and the regularized solution

The finite-difference analog of the objective function (equation 2.1) is:

$$\Phi[\mathbf{x}] = \sum_i \frac{1}{\sigma_{d_i}^2} (\mathbf{d}_i - \mathbf{A}_i\mathbf{x})^T \mathbf{P}_i (\mathbf{d}_i - \mathbf{A}_i\mathbf{x}) + \frac{1}{\sigma_0^2} (\mathbf{D}\mathbf{x})^T \mathbf{P}_0 (\mathbf{D}\mathbf{x}), \tag{2.14}$$

where $\mathbf{A}_i$ are identity matrices. When no regularization is applied the term $\frac{1}{\sigma_0^2} (\mathbf{D}\mathbf{x})^T \mathbf{P}_0 (\mathbf{D}\mathbf{x})$ is absent in equation 2.14.

By minimizing function 2.14, the least-squares solution $\hat{\mathbf{x}}$ of the combined system of the linear equations 2.6 and 2.8 can be found. This estimate $\hat{\mathbf{x}}$ of the unknown vector $\mathbf{x}$ which is the combined and/or regularized mass-anomaly time-series can be found by solving the normal equations [45]:

$$\left(\sum_i \frac{1}{\sigma_{d_i}^2}\mathbf{A}_i^T\mathbf{P}_i\mathbf{A}_i + \frac{1}{\sigma_0^2}\mathbf{D}^T\mathbf{P}_0\mathbf{D}\right)\hat{\mathbf{x}} = \sum_i \frac{1}{\sigma_{d_i}^2}\mathbf{A}_i^T\mathbf{P}_i\mathbf{d}_i. \tag{2.15}$$

Accordingly, the expression to estimate vector $\hat{\mathbf{x}}$ becomes:

$$\hat{\mathbf{x}} = \left(\sum_i \frac{1}{\sigma_{d_i}^2}\mathbf{A}_i^T\mathbf{P}_i\mathbf{A}_i + \frac{1}{\sigma_0^2}\mathbf{D}^T\mathbf{P}_0\mathbf{D}\right)^{-1}\sum_i \frac{1}{\sigma_{d_i}^2}\mathbf{A}_i^T\mathbf{P}_i\mathbf{d}_i. \tag{2.16}$$

The noise variances $\sigma_{d_i}^2$ and the signal variance σ_0^2 can be estimated with the VCE method. This method is iterative. First, initial estimates $\hat{\sigma}_{d_i}^2$ and $\hat{\sigma}_0^2$ of respectively $\sigma_{d_i}^2$ and σ_0^2 are defined to be $1\ m^2$ taking into account that the mass-anomaly time-series are given in meters of EWH. From these initial noise variances, an initial estimate $\hat{\mathbf{x}}$ can be computed with equation 2.16. Then the iterative procedure starts. Updated estimates of the noise variances can be computed as follows:

$$\left(\hat{\sigma}_{d_i}^2\right)_{new} = \frac{1}{n_i - \hat{\tau}_{d_i}}\left(\mathbf{d}_i - \mathbf{A}_i\hat{\mathbf{x}}\right)^T\mathbf{P}_i\left(\mathbf{d}_i - \mathbf{A}_i\hat{\mathbf{x}}\right) \text{ for each } i \tag{2.17}$$

with n_i the length of the data vector $\mathbf{d}_i$ and

$$\hat{\tau}_{d_i} = trace\left[\frac{1}{\left(\hat{\sigma}_{d_i}^2\right)_{old}}\mathbf{A}_i^T\mathbf{P}_i\mathbf{A}_i\left(\sum_i \frac{1}{\left(\hat{\sigma}_{d_i}^2\right)_{old}}\mathbf{A}_i^T\mathbf{P}_i\mathbf{A}_i + \frac{1}{\left(\hat{\sigma}_0^2\right)_{old}}\mathbf{D}^T\mathbf{P}_0\mathbf{D}\right)^{-1}\right].$$

And in a similar way:

$$\left(\hat{\sigma}_0^2\right)_{new} = \frac{1}{m - \hat{\tau}_0}\left(\mathbf{D}\hat{\mathbf{x}}\right)^T\mathbf{P}_0\left(\mathbf{D}\hat{\mathbf{x}}\right) \tag{2.18}$$

with m the number of pseudo-observations and

$$\hat{\tau}_0 = trace\left[\frac{1}{\left(\hat{\sigma}_0^2\right)_{old}}\mathbf{D}^T\mathbf{P}_0\mathbf{D}\left(\sum_i \frac{1}{\left(\hat{\sigma}_{d_i}^2\right)_{old}}\mathbf{A}_i^T\mathbf{P}_i\mathbf{A}_i + \frac{1}{\left(\hat{\sigma}_0^2\right)_{old}}\mathbf{D}^T\mathbf{P}_0\mathbf{D}\right)^{-1}\right].$$

The improved estimates of the noise variances $\sigma_{d_i}^2$ and the signal variance σ_0^2 are then used to compute an improved estimate $\hat{\mathbf{x}}$ with equation 2.16, etc. This iterative process by successively using the expressions 2.17, 2.18 and 2.16 can be continued until convergence. Convergence is achieved when:

$$\frac{\left|\left(\hat{\sigma}_{d_i}^2\right)_{new} - \left(\hat{\sigma}_{d_i}^2\right)_{old}\right|}{\left(\hat{\sigma}_{d_i}^2\right)_{new}} \leq \epsilon \text{ for each } i \text{ and } \frac{\left|\left(\hat{\sigma}_0^2\right)_{new} - \left(\hat{\sigma}_0^2\right)_{old}\right|}{\left(\hat{\sigma}_0^2\right)_{new}} \leq \epsilon \tag{2.19}$$

and/or the maximum number of iterations is reached. In this research $\epsilon = 0.001$ is used and the maximum number of iterations is defined to be 100.

2.2. Numerical study

In this section numerical experiments are presented. These numerical experiments are performed to investigate the effect of using a different number of time-series and different regularization functionals or no regularization at all in the VCE technique. The synthetic time-series are constructed as a combination of a signal and a time-series of white noise. The signal always contains a seasonal variability and linear trend. Additionally, signals with a non-seasonal variability are considered. The constructed time-series have different signal-to-noise ratios and contain cross-correlated or uncorrelated noise.

2.2.1. Generating noisy time-series

The noisy time-series are generated by adding white noise to a certain signal. In table 2.1 all combinations of signal and added noise are shown. For each combination 1000 realizations are synthesized to make the obtained statistics sufficiently representative.

Each signal contains a linear trend and seasonal variations. The linear trend is defined to be 2.1 mm/y which is the part (66%) of the global mean sea level rise for the period 1993-2010 which is not due to thermal expansion reported by IPCC [39]. Also Wouters et al. [77] reported that between 2002 and 2012 60-80% of the global mean sea level rise can be explained by mass change (and 20-40% is caused by thermosteric sea level rise). They showed a mass-induced global mean sea level rise of 1.6 mm/y for the period 2003-2013 as measured by GRACE. For the North Pacific they showed a mass-induced sea level rise of 3.2 mm/y for the period 2003-2013 as measured by GRACE. The chosen linear trend of 2.1 mm/y for the numerical experiments is thus also in the reported range by Wouters et al. [77]. The seasonal variability is defined as:

$$H_j^i = -A \sin\left(2\pi t_j\right) \tag{2.20}$$

in which H_j^i is the mass anomaly of time-series i at time t_j. The time is defined in years and the period under consideration is 2003-2013. Since all constructed time-series have mass anomaly values at the same moments in time, j is not dependent on i. Furthermore, A is the amplitude as defined in table 2.1. The considered amplitudes are on the one hand based on observed amplitudes in GRACE based time-series considered in Chapter 3, which show peak-to-peak amplitudes of $3-5$ cm. On the other hand they are selected by taking into account GRACE based seasonal variability reported by Chambers et al. [13]. They reported global ocean mass variations of a 8.4 ± 1.1 mm annual amplitude for the period August 2002 to December 2003. Furthermore, Dobslaw et al. [27] reported that the seasonal variation of globally averaged ocean bottom pressure due to barystatic sea-level variability is about 1 hPa which is equivalent to about 1 cm EWH. Therefore, the chosen peak-to-peak amplitudes for the numerical experiments are 1, 2, 3 and 4 cm.

Table 2.1: Considered combinations of signal and noise

Amplitude of seasonal variability (cm)	Step function in signal	Amplified seasonal variability during a half-year	Standard deviation of white noise (cm)	Cross-correlated noise
0.5	No	No	1.0	No
0.5	No	No	1.5	No
0.5	No	No	2.0	No
0.5	No	No	2.5	No
1.0	No	No	1.0	No
1.0	No	No	1.5	No
1.0	No	No	2.0	No
1.0	No	No	2.5	No
1.5	No	No	1.0	No
1.5	No	No	1.5	No
1.5	No	No	2.0	No
1.5	No	No	2.5	No
1.5	Yes	No	1.0	No
1.5	Yes	No	1.5	No
1.5	Yes	No	2.0	No
1.5	Yes	No	2.5	No
1.5	No	Yes	1.0	No

Table 2.1: Considered combinations of signal and noise

Amplitude of seasonal variability (cm)	Step function in signal	Amplified seasonal variability during a half-year	Standard deviation of white noise (cm)	Cross-correlated noise
1.5	No	Yes	1.5	No
1.5	No	Yes	2.0	No
1.5	No	Yes	2.5	No
1.5	No	No	1.0	Yes
1.5	No	No	1.5	Yes
1.5	No	No	2.0	Yes
1.5	No	No	2.5	Yes
1.5	Yes	No	1.0	Yes
1.5	Yes	No	1.5	Yes
1.5	Yes	No	2.0	Yes
1.5	Yes	No	2.5	Yes
1.5	No	Yes	1.0	Yes
1.5	No	Yes	1.5	Yes
1.5	No	Yes	2.0	Yes
1.5	No	Yes	2.5	Yes
2.0	No	No	1.0	No
2.0	No	No	1.5	No
2.0	No	No	2.0	No
2.0	No	No	2.5	No

Oceans do not only show seasonal variations and a linear trend. This can for example be observed in time-series shown in chapter 3. Non-seasonal variability can be caused by for example an El Niño or La Niña. [77] [13] Not only regionally interannual sea level variations are observed. Even the global mean sea level (GMSL) shows interannual variations [13] and it is more likely that interannual variations in GMSL are due to changes in water cycling between oceans and continents than due to changes in heat storage [77]. Another example of a non-seasonal variability is a sudden big melt of ice sheets of Greenland or Antarctica. To analyze the effect of non-seasonal and non-linear signals in the time-series two types of such signals are included for the time-series with a seasonal variability of $3\ cm$ peak-to-peak amplitude. The considered two types of non-linear and non-seasonal signals are a sudden step-wise increase in mass-anomaly and an amplification of the seasonal variability during a half-year period by a foctor of 2. The sudden increase in mass anomaly is a step of $6\ mm$ of EWH at a random moment in the set of times $2003.5, 2004, 2004.5, ..., 2012, 5\ yr$. The amplification of the seasonal variability during a half-year period happens for a randomly chosen interval from the set $2003.5 - 2004, 2004.5 - 2005, 2005.5 - 2006, ..., 2012.5 - 2013\ yr$. Examples of the constructed signals can be found in figure 2.1.

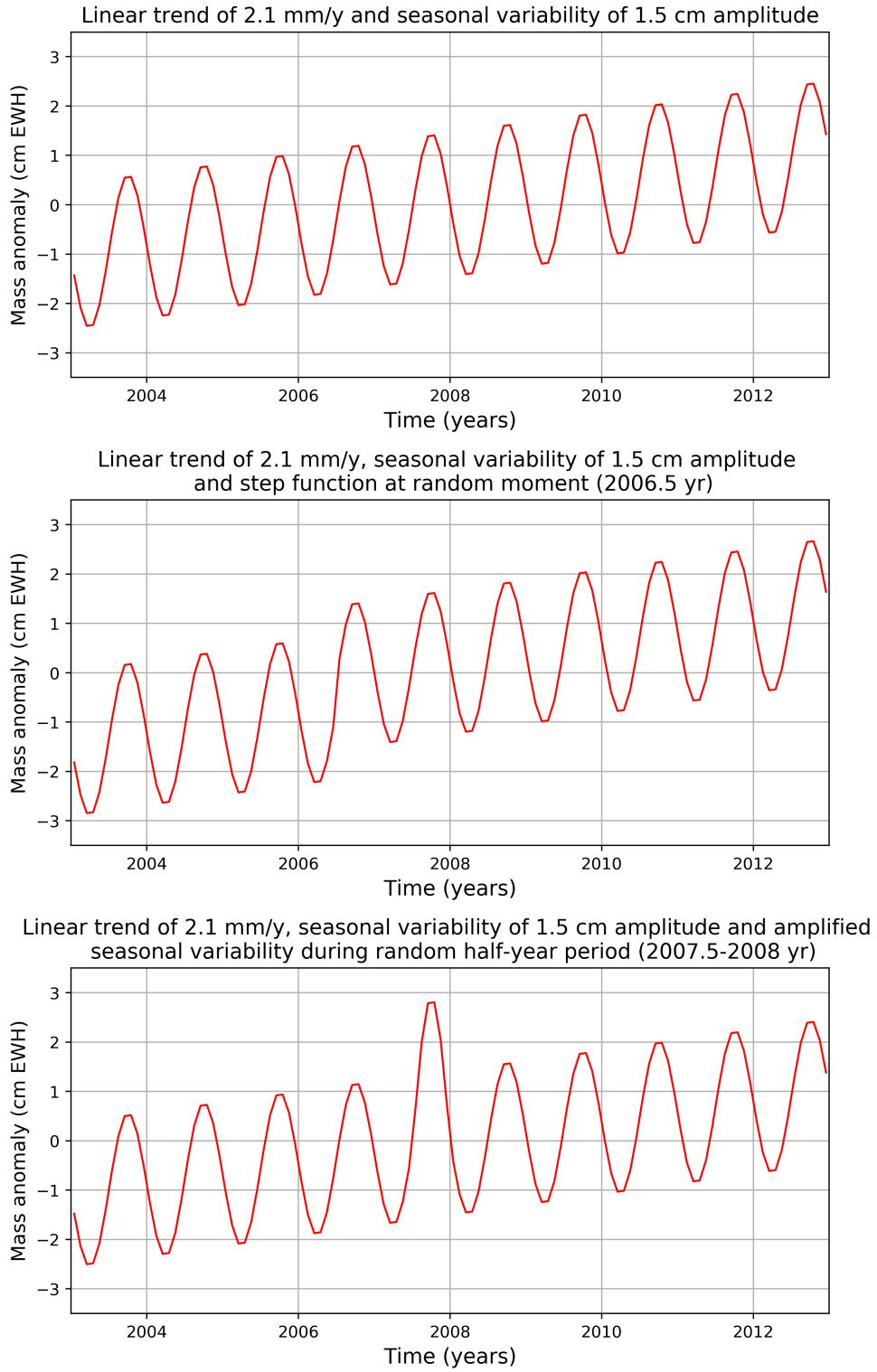

Figure 2.1: Examples of constructed signals for the numerical experiments.

Finally, white noise is added to the constructed signals. The standard deviation of this noise is 1, 1.5 , 2 or 2.5 cm as can be seen in table 2.1. These values are chosen based on estimates of standard deviation of random noise in real data as shown in chapter 3. The global averages of these estimates ranged between 1.3 and 3.4 cm for GRACE Release 5 data and between 1.0 and 1.6 cm for GRACE Release 6 data. For the signals with a seasonal variability of 3 cm amplitude, data-realizations with both cross-correlated and uncorrelated noise are constructed. Data-realizations with cross-correlated

noise are constructed by adding exactly the same time-series of white noise to the signal for a certain realization. Each of the 1000 realizations thus contain a different noise realization but the time-series considered together (2, 3 or 4) in the VCE are exactly similar by containing the same signal and same noise. The long-term mean over the total simulation period is subtracted from the constructed mass anomaly time-series.

2.2.2. Determination of noise variance and bias in combined and/or regularized mass-anomaly time-series

For all created time-series as shown in table 2.1, the effect of various regularization functionals (no regularization, zero-order, first-order, second-order Tikhonov regularization and the MYDD minimization, and various numbers of time-series (1, 2, 3 or 4) are analyzed. Note that when only one time-series is used in the VCE method, regularization is a must. It is investigated how different signal-to-noise ratio's, correlation in noise and interannual variations in the signal influence the quality of the different VCE set-ups. For this, the estimated noise, the noise reductions and introduced biases will be reported.

The standard deviation of random noise is estimated by the VCE method explained in section 2.1.3. These estimates will be reported together with the actual standard deviations of random noise (table 2.1). Since for every signal 1000 data realizations are made the mean and standard deviation (std) of the estimated noise standard deviation will be reported. Consequently, the root mean square error (RMSE) of the combined and/or regularized solutions is computed. The RMSE contains both regularized random noise and the introduced bias to the true signal [25].

To estimate biases noise-free mass-anomaly time-series are combined according to equation 2.16. Noise-free time-series are combined to have no leakage of noise in the bias estimates. The signal and noise variances in this equation are the ones estimated by VCE. For the combined and/or regularized time-series consequently the bias in the amplitude of seasonal variability, the linear trend and eventually step function or the amplification of the seasonal variability are estimated. These parameters are re-estimated by using least-squares. Consequently, the true parameters are subtracted from these re-estimated ones and the difference is regarded as bias. For both the RMSE and the bias the mean and corresponding standard deviation based on the 1000 data realizations are reported.

Finally, when the MYDD minimization is used, also the estimate of the signal standard deviation ($\hat{\sigma}_0$) will be reported. In this way, it is possible to see the influence of the level of simulated random noise, the cross-correlation of noise and the number of simultaneously processed time-series to the estimated signal standard deviation.

The true signal standard deviations are also computed and reported. These are computed in two steps as shown in equation 2.21 and 2.22:

$$\mathbf{s} = \mathbf{D}\mathbf{d}_i, \tag{2.21}$$

where $\mathbf{d}$ is the time-series of noise-free data, $\mathbf{D}$ is the MYDD operator as defined in 2.12, and

$$\sigma_0^{true} = \sqrt{\frac{1}{N-13}\sum_{j=1}^{N-13}\left(s_j\right)^2}, \tag{2.22}$$

where N is the length of the time-series $\mathbf{d}$ and s_j are elements of the vector $\mathbf{s}$. Since 1000 realizations of noise-free data are realized the mean of 1000 σ_0^{true} values will be reported as the true signal standard deviation. Note that in the case of no interannual variability the 1000 realizations of noise-free data are exactly similar and is not necessary to calculate a mean σ_0^{true}.

2.3. Case study for the Baltic Sea

This section is about the comparison of GRACE-based time-series against a tide-gauge based time-series for the Baltic Sea. This comparison is performed to investigate the effect of a different regularization functional in the context of real GRACE data. First an experiment performed by Virtanen et al. [69] is explained. It is described, since the experiment in this research is very similar. Then the exact methodology of the experiment in this research follows and adjustments to their experiment are mentioned. The Baltic Sea is chosen because of the availability of a basin-average tide-gauge time-series, a time-series of leakage due to hydrological phenomena and a time-series of the steric effects for this

area. Also, it can be observed that the GRACE-based unregularized time-series for this area contain a linear trend and seasonal variability besides some noisy higher frequency fluctuations which seem representative for the ocean in general.

2.3.1. Comparison of a GRACE based time-series to a tide-gauge based time-series

This theoretical section is about an experiment performed by Virtanen et al. [69]. The exact period for which all time-series were constructed and reported is April 2003 to December 2006. Virtanen et al. [69] computed GRACE-based mass-anomaly time-series from CSR Release 4 Level-2 data provided which were provided set of Stokes coefficients. The solutions up to degree 60 were used. For this conversion they used the following equation:

$$\Delta H_w(\theta,\lambda) = \sum_{l=0}^{\infty}\sum_{m=-l}^{l} \frac{a\rho_E(2l+1)}{3(1+k_l)\rho_w}\Delta\bar{C}_{l,m}\bar{Y}_{l,m}(\theta,\lambda), \tag{2.23}$$

where $\Delta H_w(\theta,\lambda)$ are mass-anomalies in equivalent water height (EWH), θ is the geocentric co-latitude, λ is the longitude, a is the Earth's mean radius, ρ_E is the Earth's mean density, ρ_w is the water density defined as $\rho_w = 1000\ kg/m^3$, k_l are the load Love numbers [70], $\bar{C}_{l,m}$ are temporal variations of the provided Stokes coefficients and $\bar{Y}_{l,m}(\theta,\lambda)$ are the 4π-normalized surface spherical harmonics. The degree and order of the temporal surface spherical harmonics and Stokes coefficients are represented by l and m respectively. Equation 2.23 resembles 3.18 which is the equation used in this research to convert temporal variations of Stokes coefficients to mass anomalies in EWH. The difference is that Virtanen et al. [69] assume that mass transport takes place at the surface of the sphere with as radius the Earth's mean radius. In this research it is assumed that mass transport takes place at a sphere but it is assumed that this sphere is different for each latitude. The full explanation can be found in section 3.1.3.

To compute basin averages time-series for the Baltic Sea Virtanen et al. [69] adapted a method explained by Swenson and Wahr [64]. In this method basin averages were computed by using an averaging kernel which was defined by the convolution of a Gaussian filter with a function describing the basin (1 inside the basin, 0 outside the basin). The chosen Gaussian filter in this process was a Gaussian filter of 400 km half-width. Before calculating the basin averages, they added the oceanic part from the AOD1B Release 4 product to the CSR Release 4 Level-2 data to restore the non-tidal ocean variability (which is not present in the Level-2 data). This oceanic part contains the inverted barometer effect. By adding this oceanic part back to the CSR Release 4 Stokes coefficients and afterwards computing the basin averages with the averaging kernel, more weight was given to the non-tidal variability in the middle of the basin than at the borders. Since this choice is not explained, the non-tidal variability in the next section will be added back in a different manner by giving equal weight to regions in the middle or at the borders of the Baltic Sea. In contrast to Virtanen et al. [69] no Gaussian filter will be used for the products representing tidal and non-tidal ocean variability. Furthermore, the GRACE derived mass-anomaly time-series were detrended using linear regression to remove the long-term variability due to for example post-glacial rebound or sea-level rise for the considered period April 2003 to December 2006.

The Baltic Sea shows mass variation due to both internal redistribution of water and water exchange with the North Sea which are both mainly driven by atmospheric pressure and wind. [69] Virtanen et al. [69] estimated sea-level anomalies from monthly tide-gauge data from the Permanent Service for Mean Sea Level (PSMSL). The sea-level anomalies were estimated from 22 to 26 tide-gauge stations available depending on the month. For each tide-gauge a reference value was defined as the intercept at $2000.0\ yr$ from a regression line through the whole length of the tide-gauge record (2003-2006). This reference value was subtracted from each tide-gauge time-series. Then a monthly time-series of sea surfaces over the entire Baltic Sea was constructed by fitting minimum-curvature-surface splines through the time-series at each tide-gauge. Consequently, spatial averages from these sea surfaces were computed by using an exact kernel (1 inside basin, 0 outside basin). These spatial averages were regarded as the basin averages derived from the PSMSL data. For the comparison to the GRACE-based time-series the linear trend for the period April 2003 - December 2006 was removed at the end.

The steric contribution to sea-level variation was estimated by using Ocean Model for Circulation and Tides (OMCT) [66] which includes variations in temperature and salinity. The steric anomalies were

obtained by computing differences between sea-level and the oceanic contribution to ocean bottom pressure. Virtanen et al. [69] consequently did not apply a steric correction to the PSMSL derived sea-level anomalies since the steric contribution showed a peak-to-peak amplitude of 8 cm and this was considered to be small. In contrast with them, the steric correction is applied in this research. For this, their reported time-series of the steric contribution to sea-level variations are considered.

Since the Baltic Sea is relatively small (area $390000\ km^2$ [69]) and a Gaussian filter of 400 km half-width is used, signal leakage will clearly be present in the basin averages derived from the GRACE Level-2 data. This signal leakage is both from land to sea and from sea to land.

The basin average mass-anomalies retrieved when using an averaging kernel can not directly be compared to mass-anomalies derived from the tide-gauges. The use of an averaging kernel causes a smaller basin average mass-anomaly due to sea-to-land signal leakage. By using the same averaging kernel to a uniform layer of water in the Baltic Sea, Virtanen et al. [69] derived a scaling factor of 4.0 by which the GRACE based mass-anomalies were multiplied to compare them to the tide-gauge mass-anomaly time-series.

To remove signal leakage from land to the Baltic sea, Virtanen et al. [69] derived estimates of surrounding mass variability by using the hydrological model GLDAS (Global Land Data Assimilation System [58]) is reported by them. The gridded mass anomalies of hydrological origin were converted to the spectral domain and consequently converted back to basin average mass-anomalies by using the same averaging kernel as for the GRACE Level-2 data. By using the averaging kernel a Gaussian filter of 400 km half-width is implicitly applied in the conversion from spectral to the spatial domain. Finally, this leakage signal from land was multiplied by the scaling factor 4.0, consistently with the scaling factor for the GRACE data. The maximum degree of the conversion to the spectral domain of the gridded mass anomalies of hydrological origin is not reported. It is assumed that this was 60 since the use of exactly the same scaling factors.

2.3.2. Comparison of several combined GRACE-based time-series to a tide-gauge based time-series

In this section the method to derive mass-anomaly GRACE-based time-series for the Baltic Sea (basin average time-series) in this research is explained. This method deviates on some aspects from the method described in the previous section. Similar to the above described method, tidal and non-tidal variability including the inverted barometer effect should be added back to the GRACE-based time-series to be able to make comparisons against the tide-gauge based mass-anomaly time-series. In this research, the basin-average mass-anomaly time-series are derived from the combined (and regularized) GRACE Release 5 solutions. GRACE Release 6 solutions are not considered since none of the AOD1B Release 6 products still included the inverted barometer effect. Therefore, it is for GRACE Release 6 solutions not possible to restore the total non-tidal variability including the inverted barometer effect.

The considered Release 5 GRACE Level-2 data are CSR Release 5, ITSG 2016 and GFZ Release 5. From these Level-2 data mass-anomaly time-series are computed on a 0.5 °equiangular grid in geodetic coordinates time-series. The exact description of this conversion can be found in section 3.2.1. A Gaussian filter of 400 km half-width is applied in this conversion and the total period under consideration is January 2003 - March 2016. Consequently, by VCE the combined mass-anomaly time-series are derived. The considered regularization techniques are Tikhonov first-order and MYDD minimization. Also a combined time-series is derived without regularization. Tikhonov zero-order and second-order are not considered since the numerical experiments (section 2.2) showed that these regularization techniques performed worse in the context of time-series containing predominantly a seasonal variability and linear trend. In the VCE the number of mass-anomaly time-series processed together is 3.

To compute the basin average of mass-anomaly at a certain time-step the following equation is used:

$$\overline{\Delta H_{w\,i}} = \frac{\sum_{j \in M_i} \Delta H_w\left(\vartheta_j, \lambda_j\right) \sin\left(\vartheta_j\right)}{\sum_{j \in M_i} \sin\left(\vartheta_j\right)}, \tag{2.24}$$

where $\overline{\Delta H_{w\,i}}$ is the basin average of mass-anomaly at a certain time-step for region i which is in this case the Baltic Sea. Furthermore, ϑ_j and λ_j are the geodetic colatitude and longitude of a point j which is contained in region i. Since in further chapters equation 2.24 is applied for different regions,

the indication with i is now introduced. First applying a Gaussian filter of $400\ km$ half-width in the computation of mass-anomalies from Stokes coefficients and then computing a basin average with equation 2.24 is the same as the application of an averaging kernel as done by Virtanen et al. [69] when:

- The definition of the borders of the ocean is exactly the same.
- The points (representing 1 inside and 0 outside the basin) are defined at the same equiangular grid.
- The distances between these points are approximated in the same manner by using the $\sin(\vartheta_j)$ term.

It is not known whether this is the case for Virtanen et al. [69]. It is likely that my way to compute basin averages is due to some of the differences itemized above not exactly similar to the computation of basin averages by them. It is assumed that these differences are that small that it is still justified to compare the GRACE-based time-series derived in this research to the tide-gauge derived time-series by Virtanen et al. [69].

The non-tidal and tidal products to restore the tidal and non-tidal ocean variability removed from GRACE Level-2 data are AOD1B GAB Release 5 and Ocean Tides Release 5. These tidal and non-tidal products are added to the combined (regularized) mass-anomaly time-series derived from the original GRACE Level-2 data and not to the GRACE Level-2 data themselves. The GAB coefficients of AOD1B Release 5 are used since these represent non-tidal ocean variability including the inverted barometer effect. In contrast to Virtanen et al. [69], also tidal variability for the ocean is added back because there might be some monthly mean tidal variability unequal to zero. This monthly mean tidal variability is also present in the monthly mean values of PSMSL. The GAB coefficients and monthly mean tidal variability are downloaded from `ftp://ftp.tugraz.at/outgoing/ITSG/GRACE/ITSG-Grace2016/monthly/monthly_background`. ITSG defines the monthly mean values independent of the length of the data acquisition for the GRACE Level-2 data. Missing days in the production of the GRACE Level-2 data are ignored. The monthly mean values of tidal and non-tidal variability provided by ITSG thus represent the total length of a month. The GAB coefficients are provided up to degree 100 and the monthly mean values of ocean tidal variability are provided up to degree 120. To add back the non-tidal and tidal ocean variability the Stokes coefficients are converted to mass-anomalies at the same 0.5°equiangular grid as for the GRACE Level-2 data but without applying a Gaussian filter. The low order Stokes coefficients for the tidal and non-tidal products are retained. Consequently, the basin averages are computed with equation 2.24. It is assumed that the computation of basin averages will compensate for the presence of the Gibbs phenomenon which arises when no Gaussian filter is used.

Since the maximum degree for the AOD1B GAB Release 5, Ocean tides Release 5 products and GRACE Release 5 data is different and no Gaussian filter is used in the computation of ocean tidal and non-tidal mass-anomaly time-series, different scaling factors have to be derived to compensate for the sea-to-land signal leakage. These scaling factors should be applied to the different mass-anomaly time-series prior to their summation. The scaling factors are derived by defining a uniform water-level for the Baltic Sea (1 inside the Baltic sea, 0 outside the Baltic Sea), converting this to Stokes coefficients and consequently recomputing mass-anomalies from these Stokes coefficients. The basin average of the uniform water-level (which is in this case 1) divided by the basin averages from the recomputed mass-anomalies gives the scaling factor. These scaling factors are computed for truncation to degree 120, truncation to degree 100, truncation to degree 60 and the combination of truncation to degree 60 and applying a Gaussian filter of 400 km half-width. These scaling factors are reported in section 2.4.2.

To remove the signal leakage from land to ocean from the GRACE-based mass-anomaly time-series the GLDAS derived leakage signal as reported by Virtanen et al. [69] is used. This reported time-series was by them constructed as described in section 2.3.1. In this study a scaling factor of 3.78 is derived for basin average mass-anomaly time-series for the Baltic Sea when the associated Stokes coefficients are truncated to degree 60 and a Gaussian filter of 400 km half-width is applied in the conversion (as shown in section 2.4.2). The signal leakage from land to ocean is subtracted from the GRACE-based mass-anomaly time-series by using this factor 3.78 (which is not exactly equal to 4.0 as reported by Virtanen et al. [69]). The difference in scaling factors can be due to a bit different definition of the borders of the Baltic sea or a different resolution of the grid of the spatial domain (in this study the distance between grid points is $0.5\ °$). When the definition of the borders of the Baltic Sea in this study is different with respect to the study of Virtanen et al. [69] other hydrological signals might leak into the

basin average mass-anomalies. Nevertheless, since the difference in scaling factors (4.0 and 3.78) is small, the GLDAS derived leakage signal (as reported by Virtanen et al. [69]) is multiplied by the factor 3.78 consistently with the GRACE derived mass-anomaly time-series.

For the comparison of the GRACE-based basin average mass-anomaly time-series to the tide-gauge time-series as reported by Virtanen et al. [69], the GRACE-based time-series are detrended for the period April 2003 - December 2006. The long-term mean and linear trend for this period are removed. If there is a linear trend in the non-tidal oceanic variability, this is also removed. While Virtanen et al. [69] did ignore the steric contribution to this tide-gauge derived time-series, in this study the steric contribution will be subtracted from the tide-gauge derived time-series. The steric contribution presented by Virtanen et al. [69] is used for this correction. The RMSE of the GRACE-based basin average mass-anomaly time-series are computed with respect to the tide-gauge based signal (including removal of the steric signal).

2.4. Results and discussion

2.4.1. Numerical study

In the following two figures (2.2 and 2.3) the estimates of the standard deviation (std) of random noise are shown. Each shown estimate is the mean of the 1000 realizations and is divided by the true noise standard deviation of the time-series to show how close the estimates are to the true values. The estimates are obtained by using the VCE method. Various setups in the VCE method are analyzed by using different numbers of time-series and different regularization techniques. The standard deviation of the estimated noise standard deviations as well as all other standard deviations of the reported results in this section can be found in appendix A.

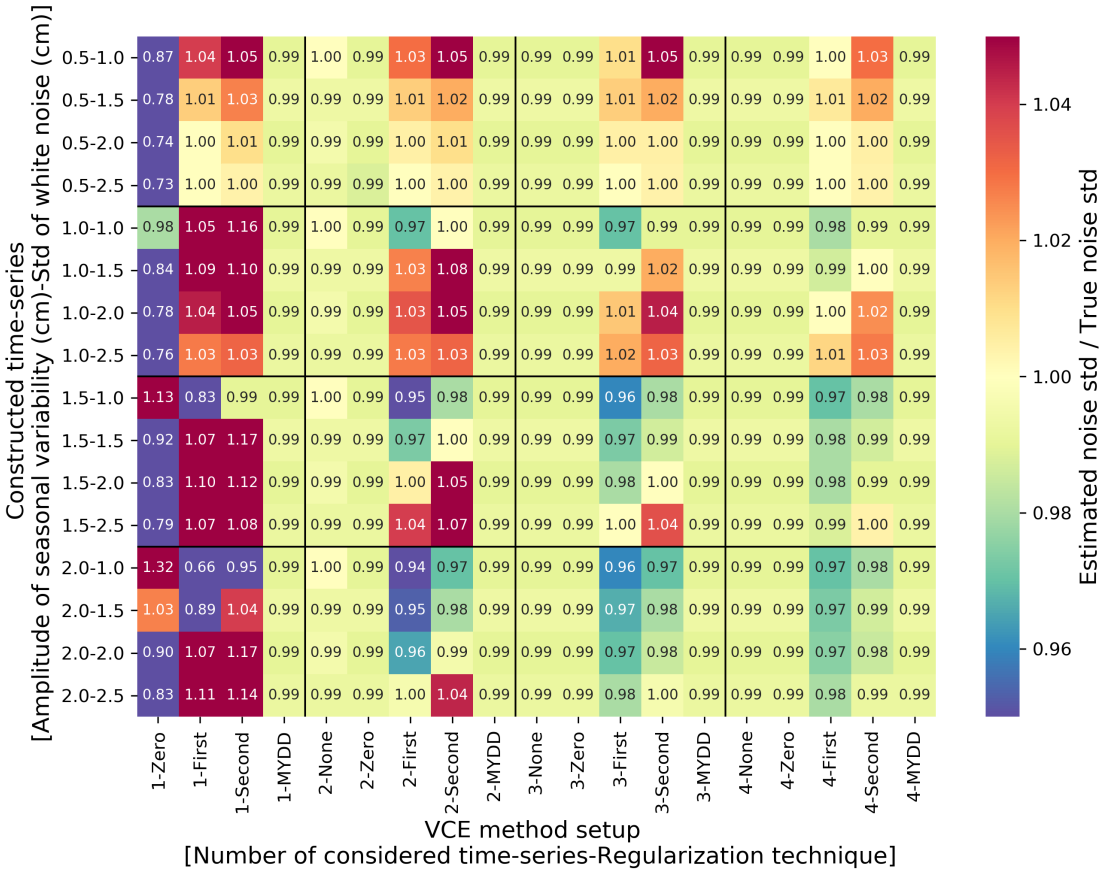

Figure 2.2: Estimated noise standard deviation divided by the true noise standard deviation of the time-series. Different combinations of signal and noise are shown in the y-direction. Different setups in the VCE method are shown in the x-direction. The signals differ in amplitude of the seasonal variability.

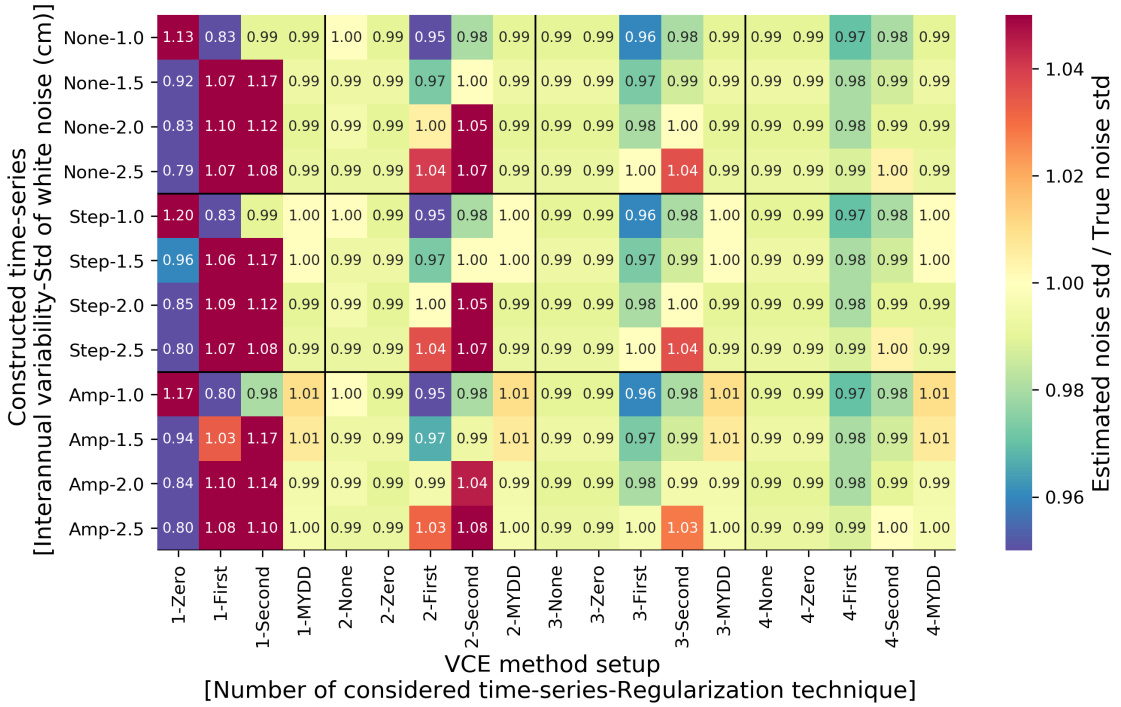

Figure 2.3: Estimated noise standard deviation divided by the true noise standard deviation of the time-series. Different combinations of signal and noise are shown in the y-direction. Different setups in the VCE method are shown in the x-direction. The signals contain the same linear trend and seasonal variability but differ in interannual variability (none, step function or amplified seasonal variability during half-year).

It can be observed that the noise standard deviation is estimated at almost equal quality when the MYDD minimization, zero-order Tikhonov or no regularization is used when 2 or more time-series are processed together in the VCE method. For MYDD minimization noise was equally well estimated when one time-series was used as input in the VCE method. It can be seen that for different signal to noise ratios and for different types of signal (with or without interannual variations) the noise is equally well estimated. The standard deviation of the estimated noise standard deviation (appendix A) shows no big difference for the different combinations of signal, true noise and VCE method setup and are $5 - 17$ % of the estimated noise standard deviation.

The RMSE of the combined and/or regularized solutions can be found in figures 2.4 and 2.5. The RMSE is divided by the true noise standard deviation of the time-series to have an estimate of the noise reduction after applying the VCE method.

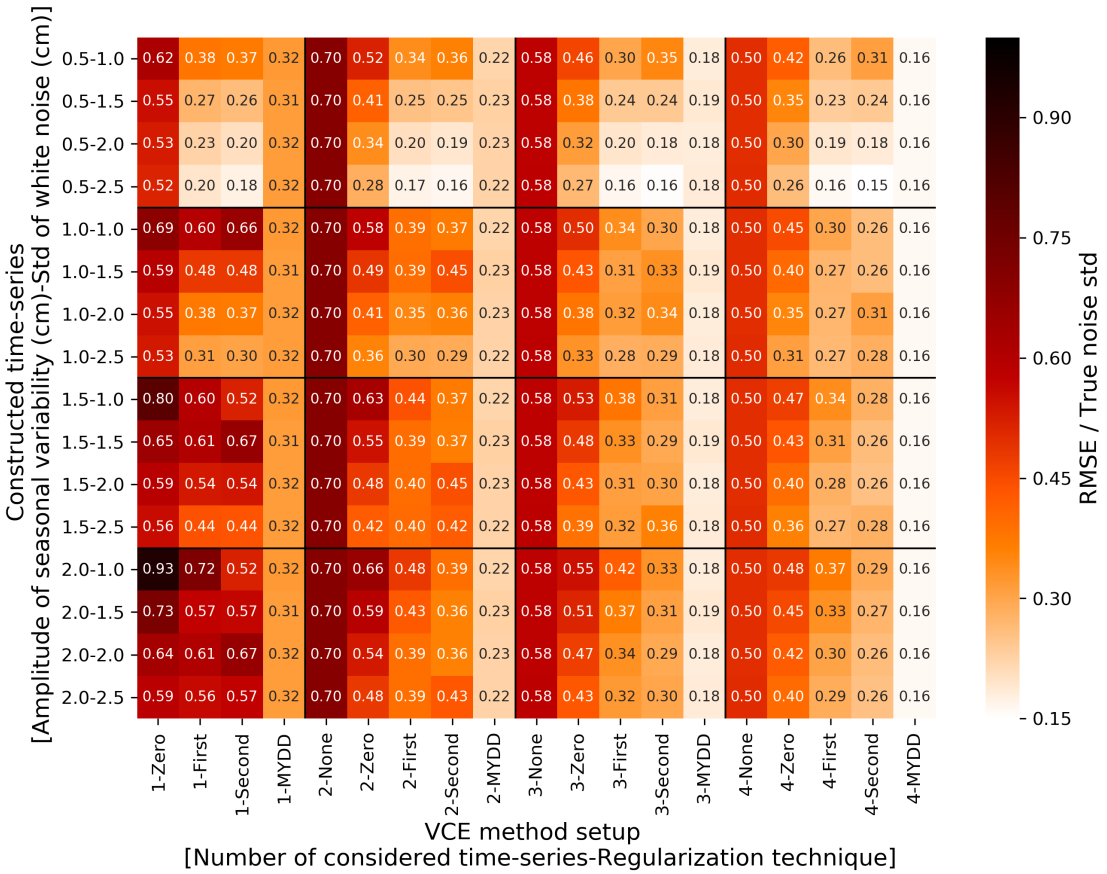

Figure 2.4: RMSE divided by the true noise standard deviation of the time-series. Different combinations of signal and noise are shown in the y-direction. Different setups in the VCE method are shown in the x-direction. The signals differ in amplitude of the seasonal variability.

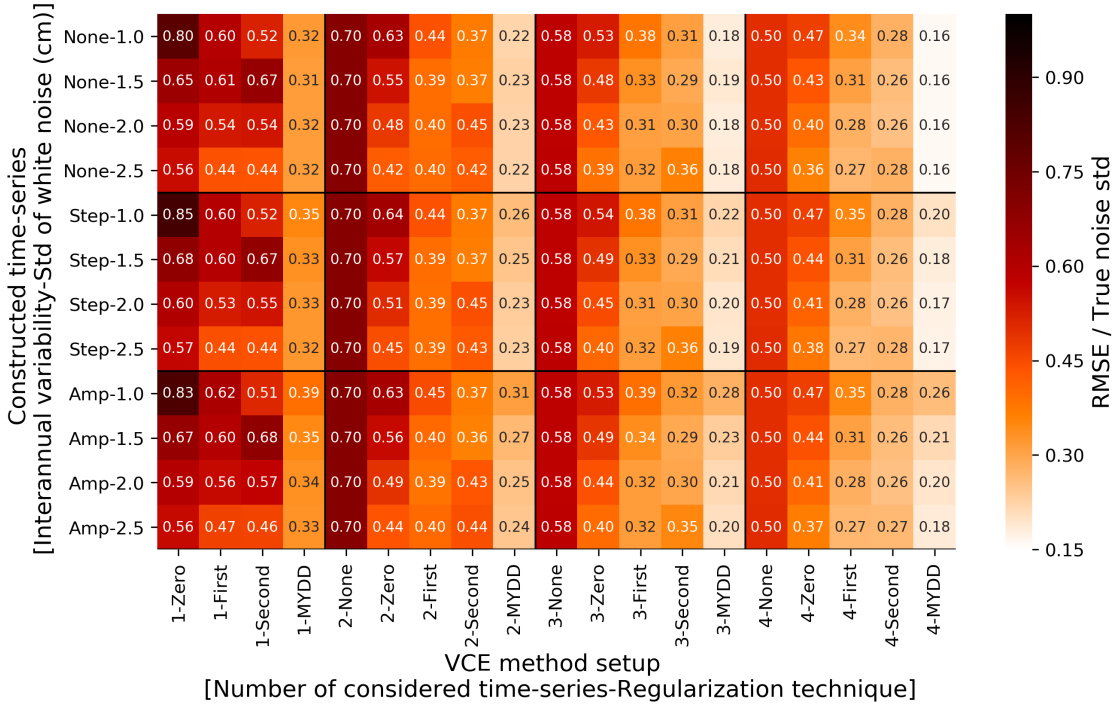

Figure 2.5: RMSE divided by the true noise standard deviation of the time-series. Different combinations of signal and noise are shown in the y-direction. Different setups in the VCE method are shown in the x-direction. The signals contain the same linear trend and seasonal variability but differ in interannual variability (none, step function or amplified seasonal variability during half-year).

In figures 2.4 and 2.5 it can be observed that the noise reduction (RMSE divided by the true noise std) is larger when more time-series are processed together in the VCE method. It can be expected that the combined and/or regularized time-series become more close to the true one when more noisy time-series are processed together. When more time-series are processed together the combination of the noise time-series (deviations from the true signal) might cancel out more since the combined solution is computed from more data vectors (equation 2.16). Furthermore, the lowest RMSE can be found when MYDD minimization is used as the regularization technique even when the signal contains interannual variability. From low to high RMSE the order in the regularization techniques is: MYDD minimization, Tikhonov second-order, Tikhonov first-order, Tikhonov zero-order, none. When there is no interannual variability, it seems logical that MYDD minimization shows the lowest RMSE since this regularization technique is tailored for time-series that contain only a linear trend and seasonal variations [25], which is exactly the case when there is no interannual variability. The other regularization techniques aim for a regularized solution that is either close to zero (Tikhonov zero-order), constant (Tikhonov first-order) or linear (Tikhonov second-order).

It cannot be excluded that the regularized solution retrieved with the MYDD minimization shows a low RMSE while ignoring the interannual variability. Therefore, it is important to look into the biases in the parameters of interannual variability. The biases in linear trend and in amplitude of seasonal variability are shown in figures 2.6, 2.7, 2.8 and 2.9. Again the mean biases of the 1000 realizations are shown and the standard deviations of the biases can be found in appendix A. In the case of signals containing interannual variability, the biases in the parameters of interannual variability (step function and amplified amplitude of seasonal variability during half-year period) can be found in figures 2.10 and 2.11.The bias in the amplitude of seasonal variability is divided by the true amplitude of the seasonal variability to compare the magnitude of the bias for signals with different amplitudes.

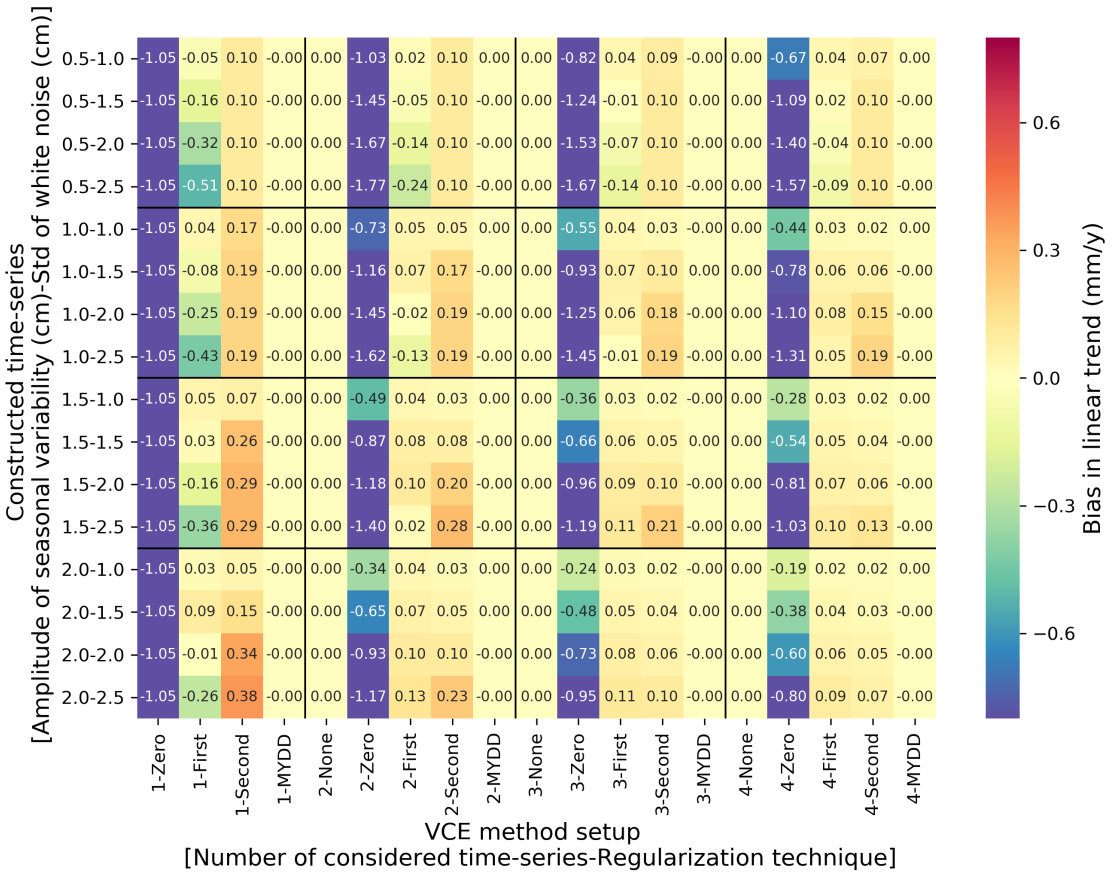

Figure 2.6: Bias in the linear trend of the combined and/or regularized solution. Different combinations of signal and noise are shown in the y-direction. Different setups in the VCE method are shown in the x-direction. The signals differ in amplitude of the seasonal variability.

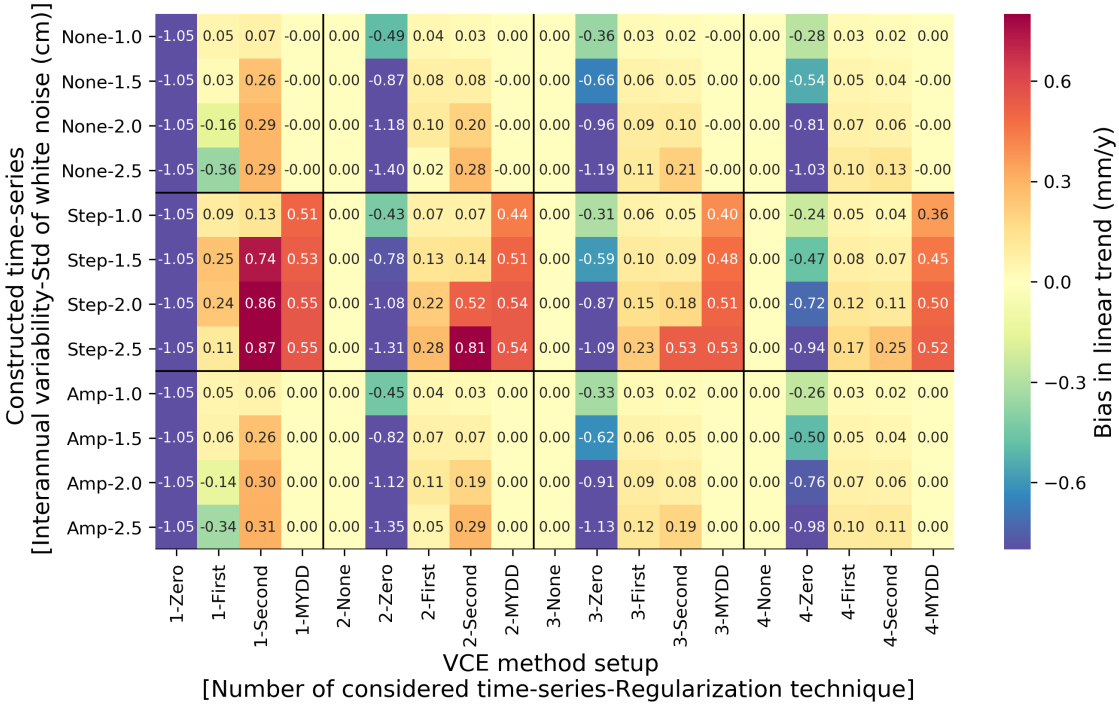

Figure 2.7: Bias in the linear trend of the combined and/or regularized solution. Different combinations of signal and noise are shown in the y-direction. Different setups in the VCE method are shown in the x-direction. The signals contain the same linear trend and seasonal variability but differ in interannual variability (none, step function or amplified seasonal variability during half-year).

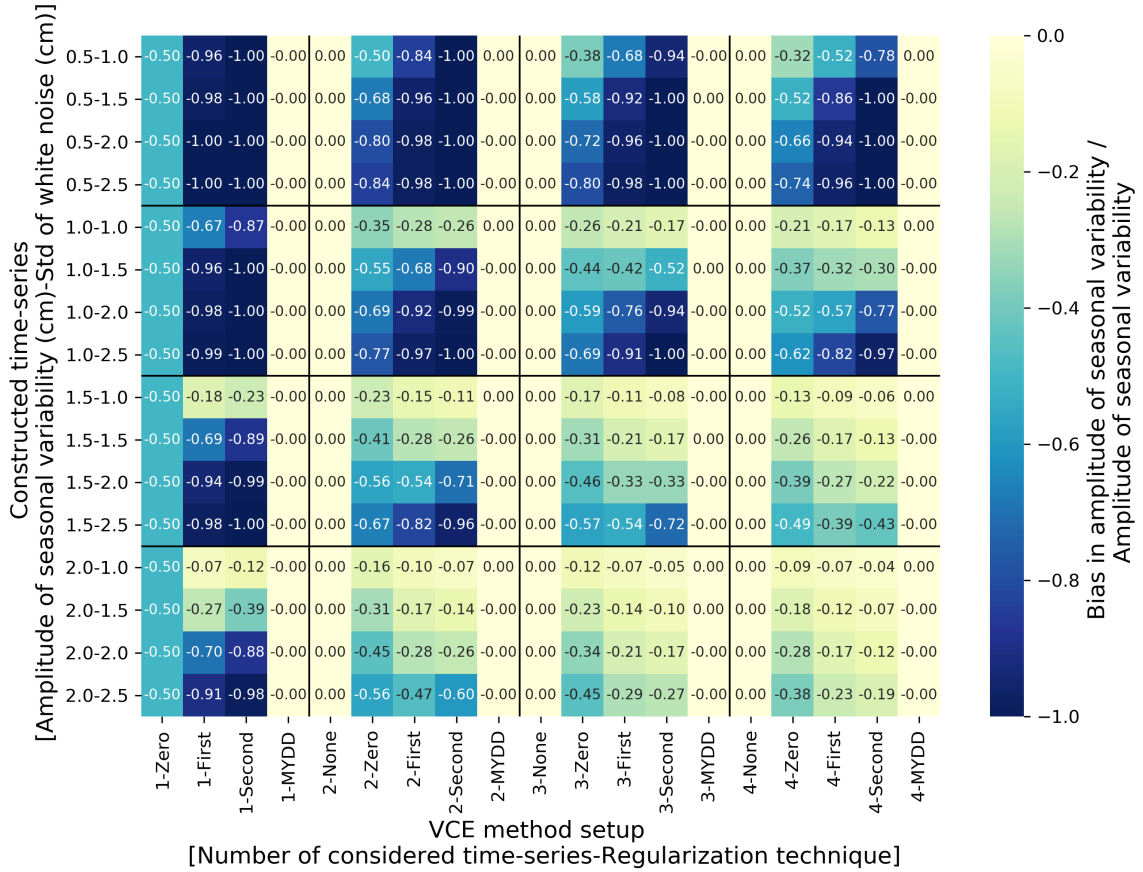

Figure 2.8: Bias in the amplitude of seasonal variability of the combined and/or regularized solution divided by the true amplitude of seasonal variability. Different combinations of signal and noise are shown in the y-direction. Different setups in the VCE method are shown in the x-direction. The signals differ in amplitude of the seasonal variability.

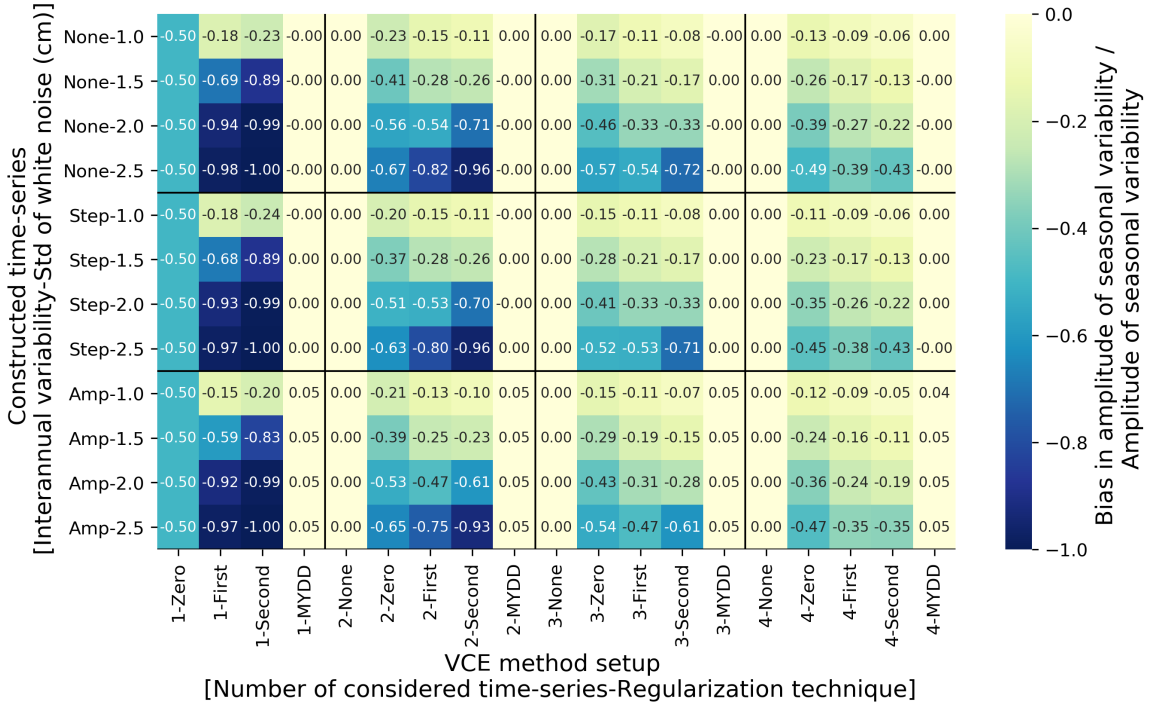

Figure 2.9: Bias in the amplitude of seasonal variability of the combined and/or regularized solution divided by the true amplitude of seasonal variability. Different combinations of signal and noise are shown in the y-direction. Different setups in the VCE method are shown in the x-direction. The signals contain the same linear trend and seasonal variability but differ in interannual variability (none, step function or amplified seasonal variability during half-year).

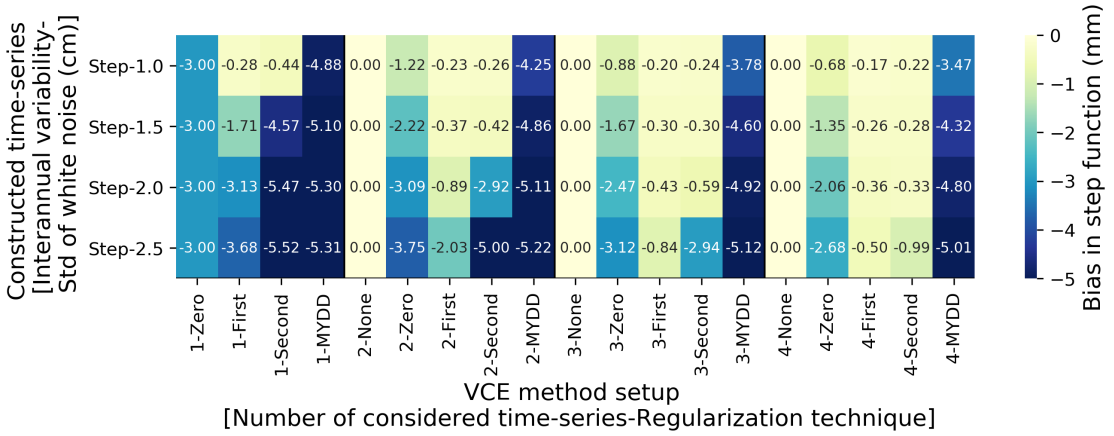

Figure 2.10: Bias in the step-wise increase in mass-anomaly of the regularized solution. Different combinations of signal and noise are shown in the y-direction. Different setups in the VCE method are shown in the x-direction.

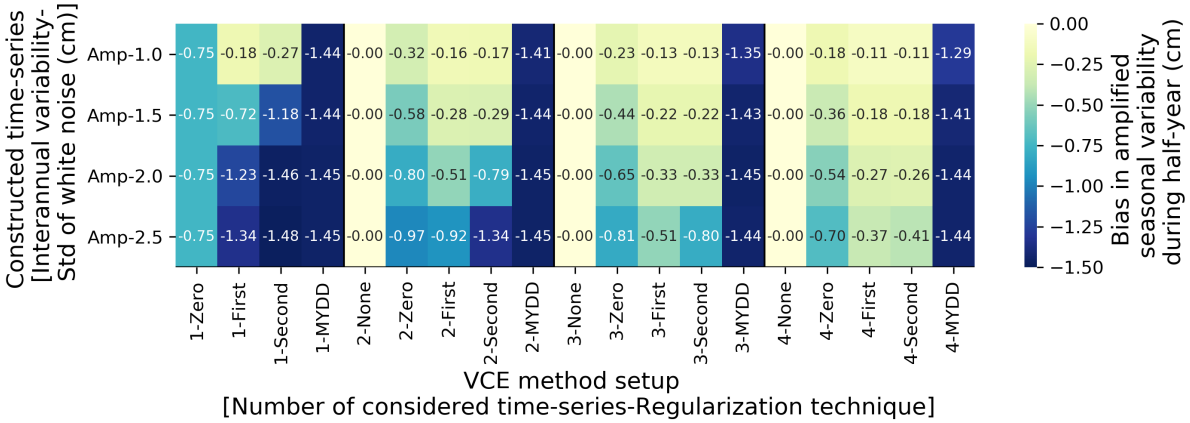

Figure 2.11: Bias in the amplified seasonal variability during half-year of the regularized solution. Different combinations of signal and noise are shown in the y-direction. Different setups in the VCE method are shown in the x-direction.

From figures 2.6, 2.7, 2.8, 2.9, 2.10 and 2.11 it can be observed that when no regularization is applied, no bias arises in the combined time-series. This is as expected. Therefore, when applying the VCE method to real mass anomaly time-series, it might be advisable to use multiple time-series and no regularization. Although, the noise reduction for this combined time-series is smaller than for regularized combined time-series (as observed in figures 2.4 and 2.5), the combined time-series will have no bias and might therefore be more realistic.

From the biases in figures 2.6, 2.7, 2.8 and 2.9, one can conclude that when no interannual variability is present, the MYDD-minimization is the best regularization technique in the VCE method by showing the smallest bias in linear trend and amplitude of seasonal variability. This is expected since MYDD minimization is tailored for a time-series which can have a seasonal variability and a linear trend. The other regularization functionals are not tailored for a time-series which include a seasonal variability. The general pattern which can be observed is that biases in amplitude of seasonal variability and linear trend increase for a smaller signal-to-noise ratio. This can be due to stronger regularization when the signal-to-noise ratio is smaller.

When a step function is present the linear trend is badly estimated when a step function is in the signal (figure 2.7) if MYDD is used as the regularization technique. Since MYDD minimization aims for a regularized solution with a linear trend, it is likely that this step function leaks into the regularized solution as increased linear trend. This could also cause the bias in linear trend when Tikhonov second-order regularization is used. These biases in linear trend increase with increasing noise level. This might be due to a larger weight of the regularization for a higher noise level, which leads to a regularized solution with less conservation of the step function and, therefore, a larger linear trend.

The bias in parameters of interannual variablity (figures 2.10 and 2.11) are the highest when MYDD minimization is used. In this case, the bias in amplified seasonal variability during half-year ranges

between 86% and 97% of the true signal for the considered scenario's. The bias in step function ranges between 58% and 88% of the true signal. Such high biases can be due to the fact that MYDD is tailored for a time-series without interannual variability by assuming consistency of variations in neighboring years. When the regularization is strong a regularized solution might arise which largely lacks the interannual variability. Especially when the interannual variability happens at the beginning or end of the time-series, the regularized solution might be quite close to the whole time-series expect for the first or last year and then the bias in a parameter of interannual variability might be almost equal to the true size of this parameter. The other regularization techniques are more general and do not aim to preserve seasonal variations and therefore might change less in quality when an interannual variability is present.

If substantial interannual variablity is present in the signal it might be better to use Tikhonov first-order as the regularization technique or no regularization at all. When Tikhonov first-order regularization is used, the noise reduction is larger (figures 2.4 and 2.5) with respect to the case without regularization. On the other hand, the Tikhonov first-order regularization shows a large bias in the amplitude of seasonal variability (almost equal to true seasonal variability) if noise is relatively large (figures 2.8 and 2.9). This can be expected since this regularization flat, which damps the seasonal variability. In any case, it is better to consider multiple time-series in the VCE to have lower biases (when a regularization is used) and larger noise reductions. It can still be doubted if it is better to use the Tikhonov first-order regularization instead of MYDD minimization if interannual variability is present since former shows lower biases in parameters of interannual variability but larger biases in the amplitude of seasonal variability and linear trend. The choice of the regularization functional thus depends on the expected or known signal in the time-series under consideration.

The RMSE and estimated noise standard deviation in the experiments of cross-correlated noise can be found in figures 2.12 and 2.13. The experiments performed with cross-correlated noise showed that when multiple time-series are used the cross-correlated noise is almost totally regarded as signal by the VCE technique. This can be concluded since the noise standard deviation is estimated as 0 m EWH or nearly 0 m EWH so a regularization is switched off and the RMSE of the combined and/or regularized solution is almost equal to the noise standard deviation. Only for the specific case of using two time-series as input for the VCE, a high noise level and using Tikhonov second-order regularization, the estimated noise level is not negligible (at most 10% of the actual one). Therefore, it might be advisable to estimate the noise in time-series by using only one time-series and MYDD minimization as the regularization technique because then cross-correlated noise can be identified as noise. When in real mass-anomaly time-series the noise level is estimated differently depending on whether one or more time-series are considered as input, one must be careful about cross-correlated noise which might be present to a high amount.

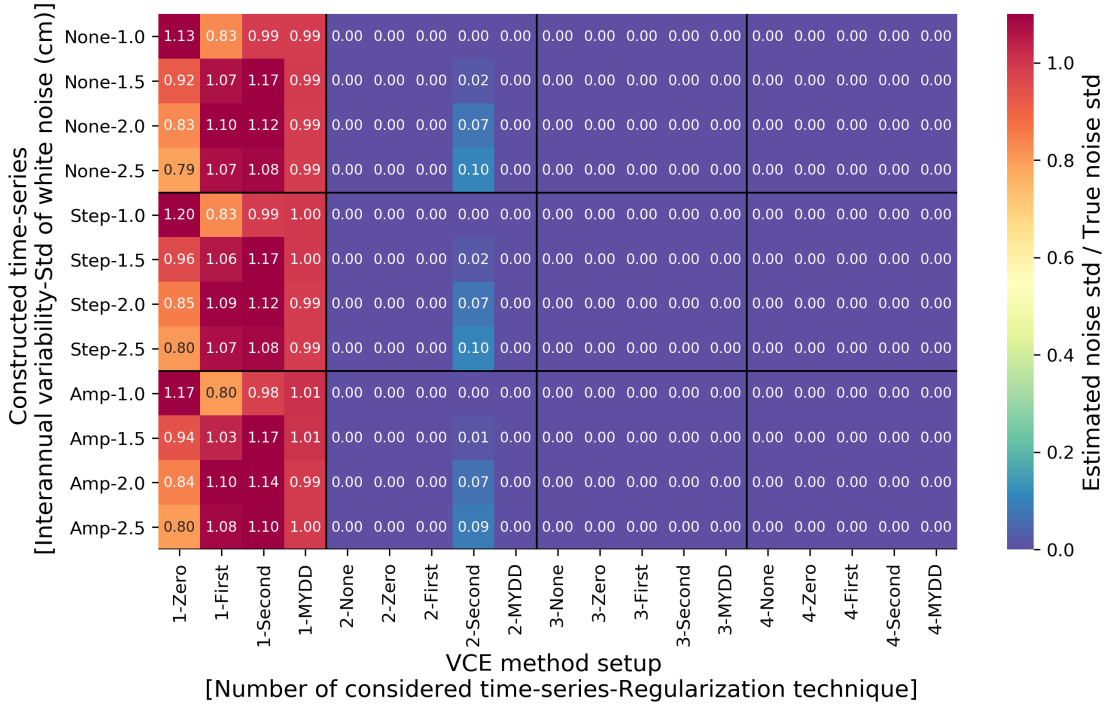

Figure 2.12: Estimated noise standard deviation divided by the true noise standard deviation of the time-series. Different combinations of signal and noise are shown in the y-direction. When multiple time-series are considered in the VCE the noise in the time-series is fully cross-correlated. Different setups in the VCE method are shown in the x-direction. The signals contain the same linear trend and seasonal variability but differ in interannual variability (none, step function or amplified seasonal variability during half-year).

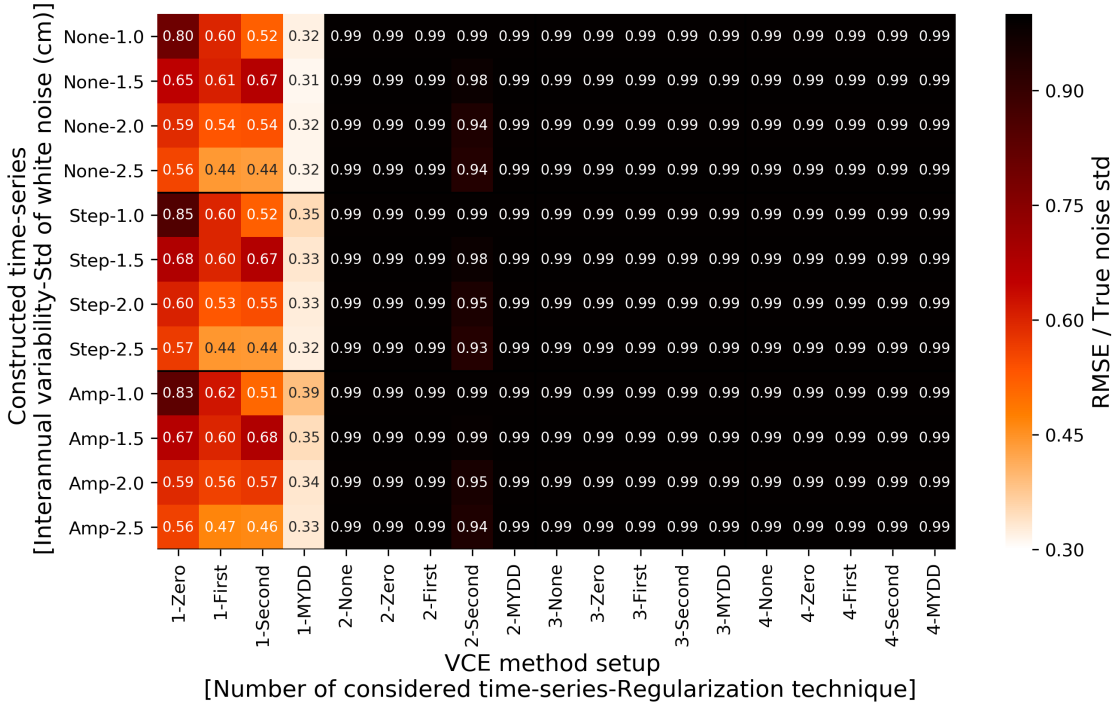

Figure 2.13: RMSE divided by the true noise standard deviation of the time-series. Different combinations of signal and noise are shown in the y-direction. When multiple time-series are considered in the VCE the noise in the time-series is fully cross-correlated. Different setups in the VCE method are shown in the x-direction. The signals contain the same linear trend and seasonal variability but differ in interannual variability (none, step function or amplified seasonal variability during half-year).

Now, a discussion about the estimated signal standard deviation when MYDD minimization is used as the regularization technique follows. The obtained results can be found in figures 2.14, 2.15 and 2.16. When there is no interannual variability, it would be expected that the signal standard deviation is zero since the signal is defined in terms of the pseudo-observations which are MYDDs. It can be observed that in practice this is not the case. When more time-series are considered in the VCE, the signal standard deviation becomes lower and for a higher noise level in the time-series the estimated signal standard deviation becomes higher. A lower signal standard deviation for more considered time-series seems logical since the noise reduction is better when more time-series are considered and the regularized signal will be closer to the true one, thus showing a smaller signal standard deviation. An increase in the signal standard deviation for higher noise levels can be the result of more leakage of the noise into the regularized solution. More noise leakage into the regularized solution results in a higher signal standard deviation. Although the signal standard deviation is not exactly zero, it is quite close to zero and the signal standard deviation divided by the noise standard deviation is at maximum 1.2% in these numerical experiments.

When an interannual variability is present in the time-series (figures 2.15 and 2.16), the estimated signal standard deviation is higher than in the absence of an interannual variability. This seems right. Nevertheless, when the estimated signal standard deviations are compared to the true ones, it can be observed that these are much smaller. Since the signal standard deviation represents how the combined regularized solution deviates from a signal containing only a linear trend and seasonal variability, this can be expected. In the regularized solution the interannual variability (present in the true signal) will be partly damped when MYDD minimization is applied. The influence of the number of considered time-series in the VCE is not clear. It can be observed that when one time-series is considered the signal standard deviation increases a bit for higher true noise levels which is similar to the observations made when signals without interannual variability were considered. When multiple time-series are considered in the VCE, it seems that there is a certain minimum in the estimated signal standard deviation for each number of considered time-series. This minimum can be the combination of two effects. An increase in estimated signal standard deviation for higher noise levels might be due to leakage of noise in the regularized time-series. A decrease in the estimated signal standard deviation for higher noise levels might be due to stronger regularization and thus more damping of the signal of interannual variability. This has to be taken into account when considering real mass-anomaly time-series since a similar signal of interannual variability might be estimated different when the noise level is different. When observing the 5 and 95 percent quantiles of the estimated signal standard deviation, the range seems quite large. For the lowest considered noise levels (noise standard deviation of 1 cm) it seems that considering more time-series gives a better estimate of the signal standard deviation. The regularized signal might contain more of the interannual variability and be more close to the true signal when more time-series are considered. Therefore it might be better to consider multiple time-series in the VCE.

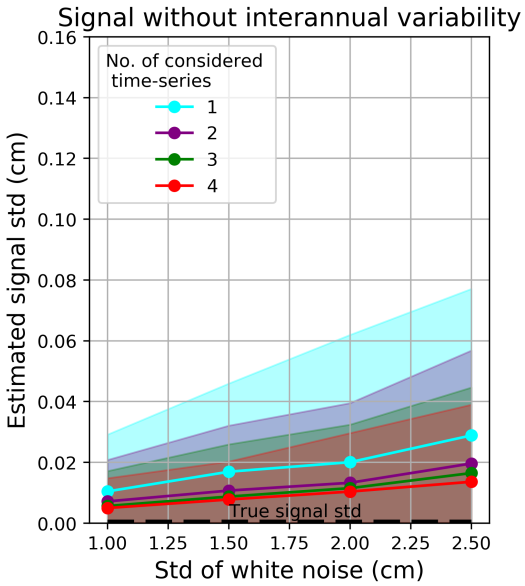

Figure 2.14: Estimated signal standard deviation for a signal without interannual variability by using MYDD minimization as the regularization technique in the VCE and different numbers of time-series. The true standard deviation of the white noise is shown in the x-direction. The shaded area is the region between the 5 percent and 95 percent quantiles of the estimated signal standard deviation.

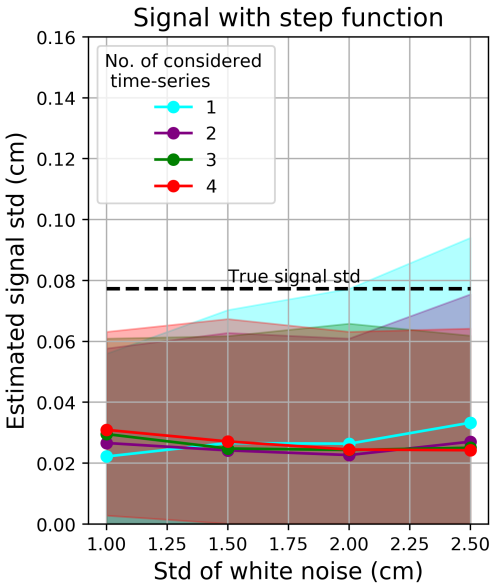

Figure 2.15: Estimated signal standard deviation for a signal with interannual variability (in this case a step function) by using MYDD minimization as the regularization technique in the VCE and different numbers of time-series. The true standard deviation of the white noise is shown in the x-direction. The shaded area is the region between the 5 percent and 95 percent quantiles of the estimated signal standard deviation.

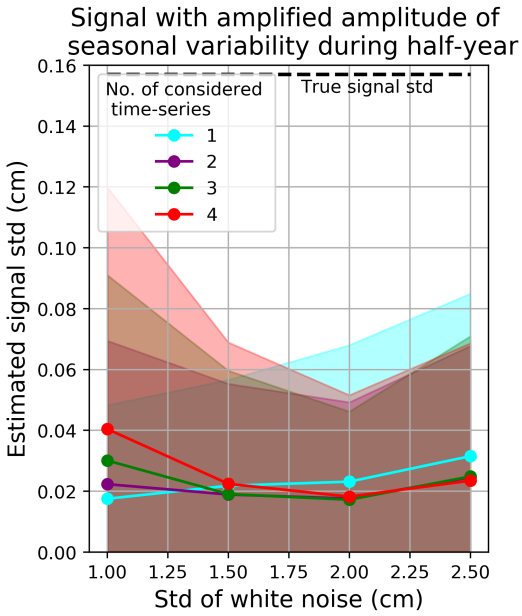

Figure 2.16: Estimated signal standard deviation for a signal with interannual variability (in this case an amplified amplitude of seasonal variability during half-year) by using MYDD minimization as the regularization technique in the VCE and different numbers of time-series. The true standard deviation of the white noise is shown in the x-direction. The shaded area is the region between the 5 percent and 95 percent quantiles of the estimated signal standard deviation.

In figure 2.17 the estimated standard deviation in the case of correlated noise and no interannual variability is shown. In appendix A the cases with interannual variability and correlated noise can be found. These are shown in the appendix since these are very similar to the figure 2.17. It can be observed that in the case of fully cross-correlated noise, the estimated signal standard deviation is two times the true noise standard deviation. Cross-correlated noise does thus show up as signal variance. When interpreting estimates of signal standard deviation, one must understand that these contain cross-correlated noise.

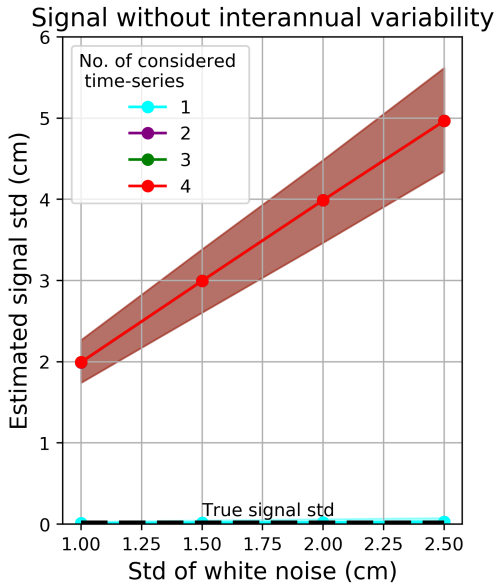

Figure 2.17: Estimated signal standard deviation for a signal without interannual variability by using MYDD minimization as the regularization technique in the VCE and different numbers of time-series. The true standard deviation of the white noise is shown in the x-direction. The shaded area is the region between the 5 percent and 95 percent quantiles of the estimated signal standard deviation. The noise in the considered time-series is fully cross-correlated.

2.4.2. Case study for the Baltic Sea

In this section the results with respect to the case study for the Baltic Sea are presented and discussed. The computed scaling factors for the Baltic Sea can be found in table 2.2:

Table 2.2: Computed scaling factors for the Baltic Sea for Stokes coefficients truncated at different degrees, with and without the use of a Gaussian filter.

Truncation to degree	Gaussian filter of 400 km half-width	Scaling factor
60	Yes	3.778
60	No	1.749
100	No	1.355
120	No	1.251

In figure 2.18 for the period January 2003 - March 2016 the basin average mass-anomaly time-series derived from the considered GRACE Level-2 are shown together with the mass-anomaly time-series regularized MYDD-minimization. From this figure you can get an idea of the influence of VCE with inclusion of a regularization functional for the Baltic Sea. It can be observed that the original mass-anomaly time-series are in the most extreme cases increased or reduced by about 15 cm. Furthermore, it can be observed that a linear trend and seasonal variability are clearly visible in these time-series. On the other hand, also interannual variability can be observed in the size of the seasonal variability for each year. The scaling factor of 3.78 is already applied in the time-series shown in figure 2.18 and 2.19. Without the scaling factor the amplitude in these time-series is about 5 cm. In section 3.3 the noise standard deviation for the Baltic Sea is estimated in the range 1-2.4 cm for GRACE Release 5 solutions. The signal-to-noise ratio in this time-series is thus quite larger than for the numerical experiments. This might explain why the MYDD-minimization retains the interannual variability which is present in the time-series. When the signal-to-noise ratio is larger less regularziation is expected. In figure 2.19 the combined (regularized) mass-anomaly time-series are shown which are obtained with the 3 considered VCE set-ups. It can be observed that different regularization techniques lead to differences in the basin average mass-anomaly time-series in the order of only a few centimeters. At the epochs when no GRACE Level-2 data are available the largest differences between the regularized solutions can be found. These epochs are visible in 2.18 as data gaps in the unregularized time-series.

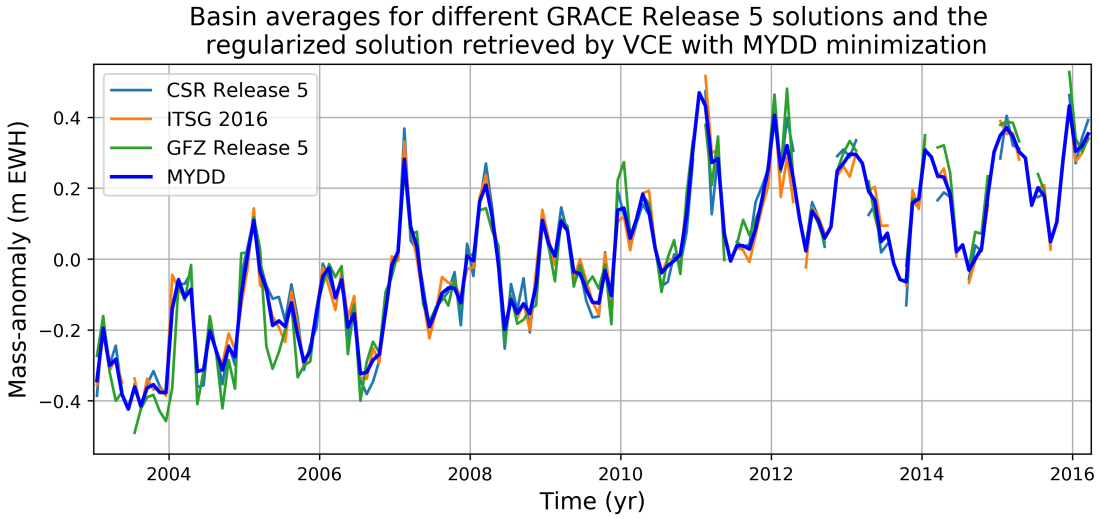

Figure 2.18: Basin averages for the Baltic Sea for different GRACE Release 5 solutions (CSR Release 5, ITSG 2016, GFZ Release 5) and the regularized time-series retrieved by VCE with MYDD-minimization as regularization technique. Note that the scaling factor of 3.78 is already applied.

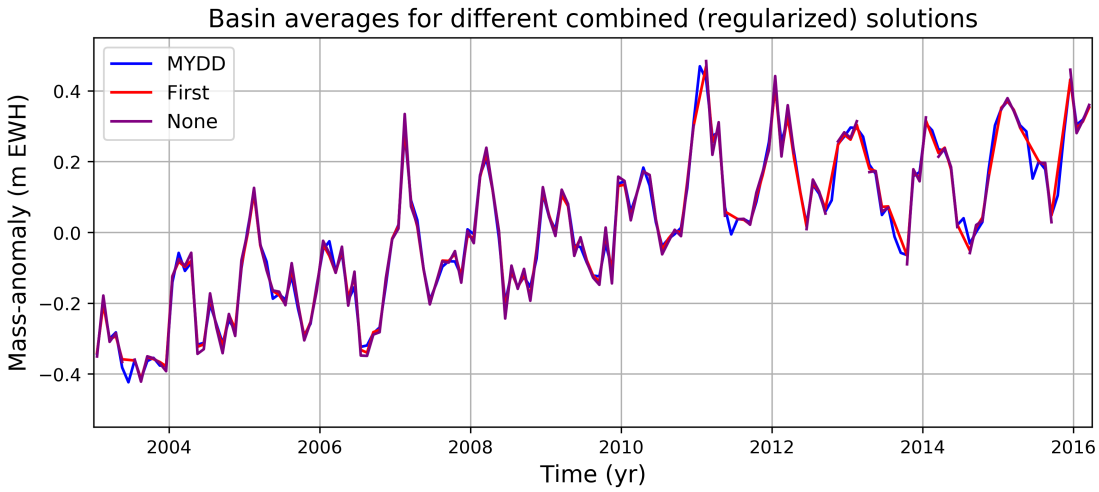

Figure 2.19: Basin averages for the Baltic Sea for different combined (regularized) time-series retrieved by VCE of GRACE Release 5 solutions (CSR Release 5, ITSG 2016, GFZ Release 5). VCE without regularization and with MYDD-minimazation and Tikhonov first-order regularization functionals are considered. Note that the scaling factor of 3.78 is already applied.

In figure 2.20 the combined (regularized) mass-anomaly time-series for the Baltic Sea are shown together with the tide-gauge based mass-anomaly time-series for the period April 2003 - December 2006. The signal leakage from the land to the ocean is removed by subtracting the GLDAS basin average time-series from the regularized solutions. The tidal and non-tidal ocean variability is added back by using the mass anomaly time-series derived from the AOD1B GAB Release 5 and Ocean tides Release 5 product. The steric signal is removed from the tide-gauge derived time-series. It can be observed that all three regularized solutions are quite close to the tide-gauge based mass-anomaly time-series. The RMSE with respect to the tide-gauge based time-series for the different regularization techniques can be found in table 2.3. Tikhonov first-order shows the smallest RMSE. You might that you can preliminary conclude that Tikhonov first-order regularization is the best regularization technique for the Baltic Sea. But, since the RMSE's corresponding to the different VCE-setups are quite close, it might be better to draw no conclusions about a better VCE set-up for the Baltic Sea. The errors in the tide-gauge based mass-anomaly time-series or in the modeled hydrological signal may be larger than the differences between the regularized mass-anomaly time-series. The differences between the different regularization techniques are also a lot smaller than the differences with respect to the tide-gauge derived mass-anomaly time-series. Furthermore, the considered period is quite short (shorter than 4 years) and it would be better to examine a longer period. It can only be concluded that the different combined (regularized) solutions are quite close (in the order of a few cm) to the tide-gauge based time-series including the irregular features. As it was already mentioned, the largest differences between the regularized solutions can be observed in the months when no GRACE data are available. In the period April 2003 - December 2006 only one data-gap for June 2003 is present. This is only one month of the in total 45 months of the considered period and therefore it is not right to draw conclusions about which regularization technique performs better at data gaps. For this specific data-gap June 2006 MYDD-minimization performs better than Tikhonov-first order with a deviation of 0.6 and 6.3 cm to the tide-gauge based value respectively.

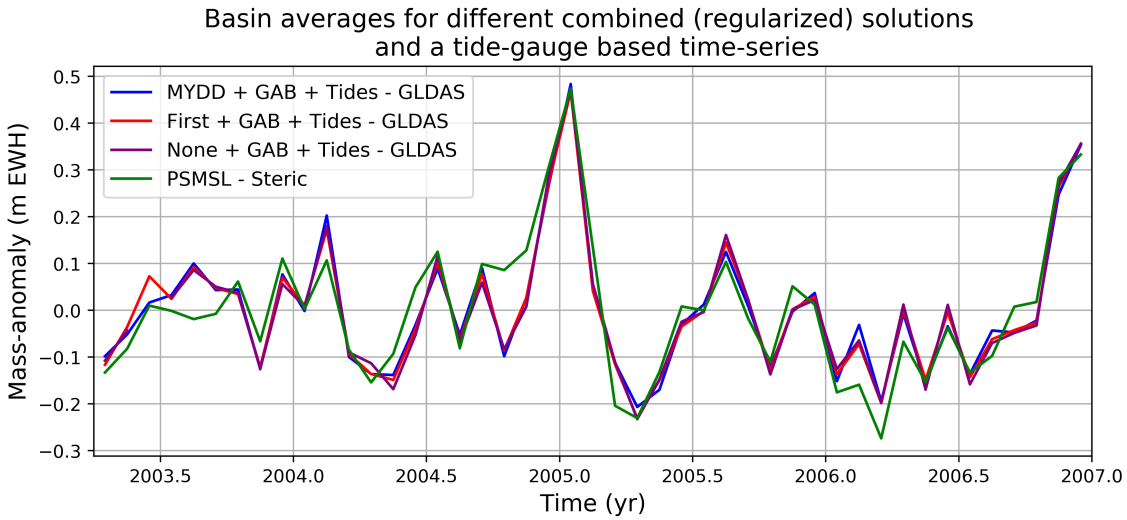

Figure 2.20: Basin averages for the Baltic Sea for different combined (regularized) time-series retrieved by VCE of GRACE Release 5 solutions. VCE without regularization and with MYDD-minimazation and Tikhonov first-order as regularization functionals are considered. Tidal and non-tidal variability is added back to the regularized solutions and the hydrological leakage signal from the surrounding land is subtracted (GLDAS). The tide-gauge based time-series is shown in green (PSMSL- Steric).

Table 2.3: RMSE with respect to a tide-gauge based mass-anomaly time-series for the Baltic Sea for various regularized solutions retrieved from GRACE Release 5 Level-2 data.

Monthly solutions	Regularization technique	RMSE w.r.t. tide-gauge based time-series
CSR Release 5, ITSG 2016, GFZ Release 5	None	5.862
	Tikhonov first-order	5.537
	MYDD-minimization	5.826

2.5. Summary and remarks

Based on the numerical study it seems that Tikhonov zero-order and Tikhonov second-order regularizations are not advisable in the analysis of real mass anomaly time-series. When the signal contains only a linear trend and seasonal variability and no interannual variability, it is best to use the MYDD minimization to identify the noise variance and signal best. When the signal contains beside a linear trend and seasonal variability also an interannual variability, it might be better to use Tikhonov first-order or no regularization. For the highest noise reduction and lowest biases it is advisable to consider more time-series. Cross-correlated noise is never identified as noise when multiple time-series are considered in the VCE. The use of one time-series and MYDD minimization as regularization technique is the best when you want to identify cross-correlated noise as noise although this cross-correlated noise might be signal in reality. For the estimation of signal standard deviation with MYDD minimization it seems better to use multiple time-series though the influence of (cross-correlated) noise in these estimates must not be neglected. Noise might leak in the estimated signal variance and cross-correlated noise shows itself almost fully up as signal variance instead of noise variance.

Real mass-anomaly time-series for the Baltic Sea show besides a linear trend and seasonal variability also a large amount of interannual variability. When comparing the real mass-anomaly time-series to a tide-gauge based time-series, it seems that Tikhonov first-order regularization, MYDD minimization and no regularization perform very similar. Even MYDD minimization seems to retain the interannual variability in the mass-anomaly time-series. This might be due to a higher signal-to-noise ratio for the Baltic Sea than in the numerical experiments.

Based on these results, Tikhonov zero-order and Tikhonov second-order regularizations will not be considered further in the next chapter. Furthermore, noise variance (and signal variance) will only be estimated by considering one or three mass-anomaly time-series. Consideration of two mass-anomaly time-series does not seem to give more insight. When MYDD minimization is applied, the estimated

signal variance represents interannual differences in the mass-derivative. Estimates of this signal variance seem interesting for the analysis of GRACE-based mass-anomaly time-series over the ocean. Therefore, it is advisable to consider MYDD minimization in the next chapter.

3

Quality of GRACE Release 5 and 6 monthly solutions

This chapter is about the second sub-question:

- What are the global distributions of signal and noise variance in GRACE Release 5 and 6 monthly solutions?

The quality of several GRACE monthly solutions is assessed by estimating signal and noise variance in the GRACE-based mass-anomaly time-series. These are estimated according to the method described in the previous chapter. Since this estimate of signal variance represents interannual differences in the mass-derivative this is used as estimate of the quality of GRACE monthly solutions over the ocean. For the GRACE monthly solutions which show the lowest estimated noise variance, the quality is even assessed in a different manner. For these solutions residuals are computed with respect to a low-pass filtered signal or analytical function. The low-pass filtered signal contains only periodical signals of frequencies lower than the semi-annual periodicity. The analytical function is a by least-squares estimated signal containing only a linear trend, semi-annual and annual periodicity. Therefore, the residuals can also give an indication of the quality of the GRACE monthly solutions over the ocean.

This chapter begins with a theoretical section which is mainly about Earth's gravitational potential and the conversion of Stokes coefficients to mass anomalies at the Earth's surface. Since this concept and conversion are basic knowledge needed to understand the available GRACE Level-2 data product and its use, this will be explained. Consequently, sets of Stokes coefficients of different research centers will be addressed. Thereafter the method to estimate the quality of these datasets is described in detail before analyzing the results.

3.1. Theory

In this section first the Earth's gravitational potential and its representation in spherical harmonics is explained. Then spherical and ellipsoidal coordinates are shortly reviewed. This description of the Earth's gravitational potential provides underlying knowledge which is needed to understand the GRACE Level-2 data product and the way how it is provided. Consequently, the method to convert time-series of Stokes coefficients to time-series of mass-anomalies is described. Then the sets of Stokes coefficients provided by different research centers which are analyzed in this research are discussed. Afterwards, degree-1 and C20 Stokes coefficients are shortly addressed because these coefficients are retrieved from a different source.

3.1.1. Earth's gravitational potential

A link between gravitational field and gravitational potential is given in equation 3.1:

$$\nabla V = \mathbf{g}, \tag{3.1}$$

where ∇ is the first-order vector differential operator, V in m^2/s^2 is the gravitational potential and $\mathbf{g}$ in $m/s^2$is the gravitational field. [23] Gravitational potential at a certain location represents the work done by gravitation in order to move a unit mass from infinity (where $V = 0$) to that location. [60] Gravitational potential is a harmonic function in vacuum since it satisfies Laplace equation there. The gravitational potential in a 3-D vacuum domain can thus be determined if the potential or its normal derivative is known at the boundary of this domain. [23] Now, the Earth and its exterior gravitational potential will be considered. When atmospheric mass is ignored [60] and the gravitational potential or its normal derivative is known at a closed surface enclosing the Earth, the gravitational potential can be computed at any point above this surface and between this surface and the Earth itself. [23]

Since it is assumed that Earth's gravitational potential satisfies Laplace equation outside the Earth's system, it can be described by a linear combination of harmonic base functions. These harmonic base functions can be defined in spherical coordinates and are called solid spherical harmonics [23]:

$$\begin{aligned} H_{l,m}(r,\theta,\lambda) &= \left(\frac{R}{r}\right)^{l+1} P_{l,|m|}(\cos(\theta)) \begin{cases} \cos(m\lambda) & \text{if } m \geq 0 \\ \sin(|m|\lambda) & \text{if } m < 0 \end{cases} \\ &= \left(\frac{R}{r}\right)^{l+1} Y_{l,m}(\theta,\lambda), \end{aligned} \tag{3.2}$$

where R is the Earth's mean equatorial radius ($6378137.0\ m$ [71]), λ (longitude), θ (geocentric co-latitude) and r (geocentric radius) are the spherical coordinates, l the degree and m the order of the solid spherical harmonic $H_{l,m}(r,\theta,\lambda)$, $P_{l,m}$ are the associated Legendre functions and $Y_{l,m}(\theta,\lambda)$ are the surface spherical harmonics. The explicit expression for the associated Legendre functions is [50]:

$$P_{l,m}(x) = 2^{-l}\left(1-x^2\right)^{\frac{m}{2}} \sum_{k=0}^{\left\lfloor \frac{l-m}{2} \right\rfloor} (-1)^k \frac{(2l-2k)!}{k!\,(1-k)!\,(l-m-2k)!} x^{l-m-2k}. \tag{3.3}$$

When the associated Legendre functions are scaled such that the norm of the corresponding surface spherical harmonics is 4π, the associated Legendre functions $P_{l,m}$ become fully-normalized associated Legendre functions $\bar{P}_{l,m}$. This scaling is applied as follows:

$$\bar{P}_{l,m}(\cos(\theta)) = P_{l,m}(\cos(\theta)) \begin{cases} \sqrt{2l+1} & \text{if } m = 0 \\ \sqrt{2\,(2l+1)\,\frac{(l-m)!}{(l+m)!}} & \text{if } m \neq 0 \end{cases} \tag{3.4}$$

In this way the solid spherical harmonics become scaled too, but they remain harmonic. [23] The fully-normalized associated Legendre functions can be computed by a recursive scheme [5]:

$$\bar{P}_{l,m}(t) = \begin{cases} 1 & \text{if } m = l = 0 \\ u\sqrt{3} & \text{if } m = l = 1 \\ u\sqrt{\frac{2l+1}{2l}}\,\bar{P}_{l-1,m-1}(t) & \text{if } m = l \geq 2 \\ a_{l,m}\frac{t}{u}\bar{P}_{l,m+1}(t) & \text{if } 0 \leq m = l-1 \\ a_{l,m}\frac{t}{u}\bar{P}_{l,m+1}(t) - b_{l,m}\frac{t}{u}\bar{P}_{l,m+2}(t) & \text{if } 0 \leq m \leq l-2 \end{cases} \tag{3.5}$$

where

$$\begin{aligned} u &= \sqrt{1-t^2} \\ a_{l,m} &= \frac{2}{\sqrt{1+\delta_{0,m}}} \frac{m+1}{\sqrt{(l-m)\,(l+m+1)}} \\ b_{l,m} &= \frac{1}{\sqrt{1+\delta_{0,m}}} \frac{\sqrt{(l+m+2)\,(l-m-1)}}{\sqrt{(l-m)\,(l+m+1)}} \end{aligned}$$

with $\delta_{i,j}$ is the Kronecker delta:

$$\delta_{i,j} = \begin{cases} 1 & \text{if } i = j \\ 0 & \text{if } i \neq j \end{cases} \tag{3.6}$$

Earth's exterior gravitational potential can now be described as a linear combination of the scaled solid spherical harmonics $\bar{H}_{l,m}(r,\theta,\lambda)$. When it is assumed that the Earth's gravitational potential approaches 0 when $r \to \infty$ [23], this combination is unique. This linear combination of the scaled solid spherical harmonics is:

$$V(r,\theta,\lambda) = \sum_{l=0}^{\infty}\sum_{m=-l}^{l} \bar{C}_{l,m}^{(V)} \bar{H}_{l,m}(r,\theta,\lambda) = \sum_{l=0}^{\infty}\sum_{m=-l}^{l} \bar{C}_{l,m}^{(V)} \left(\frac{R}{r}\right)^{l+1} \bar{Y}_{l,m}(\theta,\lambda) = \frac{GM_E}{R}\sum_{l=0}^{\infty}\sum_{m=-l}^{l} \bar{C}_{l,m} \left(\frac{R}{r}\right)^{l+1} \bar{Y}_{l,m}(\theta,\lambda) \tag{3.7}$$

with $\bar{Y}_{l,m}(\theta,\lambda)$ the 4π-normalized surface spherical harmonics and $\bar{C}_{l,m} = \frac{R}{GM_E}\bar{C}_{l,m}^{(V)}$ the fully-normalized spherical harmonic coefficients of Earth's exterior gravitational potential which are also called Stokes coefficients. The parameter M_E is the Earth's mass which is $5.9723 \cdot 10^{24}\, kg$ [76]. These coefficients are dimensionless. Earth's exterior gravitational potential and thus the Stokes coefficients are variable in time due to mass movement and exchange between Earth system components. [10] Monthly mean values of these Stokes coefficients up to a certain degree and order are provided as GRACE Level-2 product.

A surface spherical harmonic of order $m = 0$ is constant along a given latitude and called zonal. A surface spherical harmonic of order $m = \pm l$ is constant along a given longitude and called sectorial. [23]

3.1.2. Coordinate systems

Geocentric coordinates (also called spherical coordinates) are useful to represent the position of a point on a sphere [68]. In figure 3.1 the geocentric latitude ψ, longitude λ and *r* which is the geocentric radius of the point can be seen. When latitude is defined in degrees, geocentric co-latitude θ is defined as $90° - \psi$ [23]. For the Earth it is not practical to define heights with respect to a sphere [68].

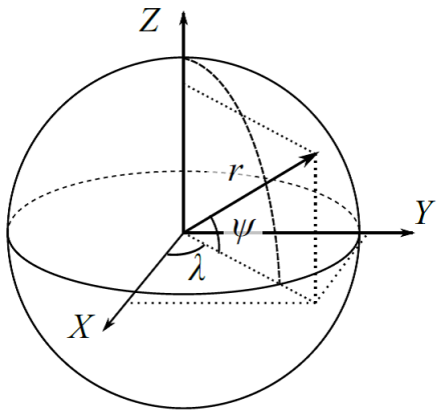

Figure 3.1: Geocentric coordinates ψ, λ and *r* [68].

An ellipsoid is a better approximation for the shape of the Earth than a sphere. Geodetic coordinates (also called ellipsoidal or geographic coordinates) are useful to represent the position of a point with respect to an ellipsoid. [68] In figure 3.2 the geodetic latitude ϕ, longitude λ and *h* which is the height of a point above a reference ellipsoid (ellipsoidal height) can be seen.

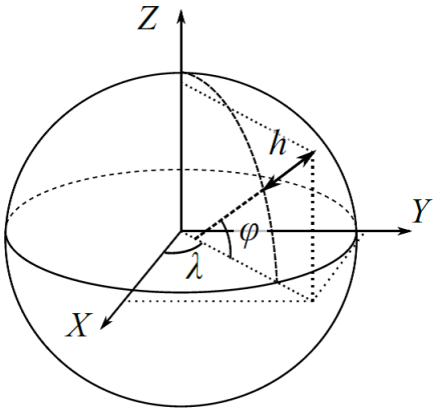

Figure 3.2: Geodetic coordinates ϕ, λ and h [68].

A commonly used coordinate reference system is the World Geodetic System 1984 (WGS84). The WGS84 is geocentric in the sense that the center of mass of the total Earth's system (including ocean and atmosphere) coincides with the center of WGS84. [38] The z-axis is defined in the direction of IERS Reference Pole (IRP). The x-axis is along the intersection of the IERS Reference Meridian (IRM) and the plane passing through the origin and normal to the Z-axis. The y-axis completes the right-handed, Earth-fixed orthogonal coordinate system. The WGS84 ellipsoid has the same origin and with respect to this ellipsoid longitude and geodetic latitude can be defined. The semi-major axis and flattening of (f) the WGS84 ellipsoid are defined as $a = 6378137.0\ m$ and $f = \frac{1}{298.257223563}$ respectively.

3.1.3. Conversion of Stokes coefficients to mass anomalies at the Earth's surface

Equation 3.7 shows the relation between the Earth's exterior gravitational potential and the Stokes coefficients. Accordingly, temporal variations in the Earth's gravitational potential can be related to temporal variations of the Stokes coefficients:

$$\Delta V\,(r,\theta,\lambda) = \frac{GM_E}{R}\sum_{l=0}^{\infty}\sum_{m=-l}^{l}\Delta\bar{C}_{l,m}\left(\frac{R}{r}\right)^{l+1}\bar{Y}_{l,m}\,(\theta,\lambda)\,. \tag{3.8}$$

The temporal variations of Stokes coefficients can be expressed as function of temporal variations of Earth's density distribution ($\Delta\rho\,(r,\theta,\lambda)$) [24]:

$$\Delta\bar{C}_{lm} = \frac{R^2}{M_E\,(2l+1)}\int_0^{2\pi}\int_0^{\pi}\int_0^{top\ of\ atmosphere}\left(\frac{r}{R}\right)^{l+2}\Delta\rho\,(r,\theta,\lambda)\;dr\,\bar{Y}_{lm}\,(\theta,\lambda)\sin(\theta)\;d\theta\,d\lambda. \tag{3.9}$$

This density ($\Delta\rho\,(r,\theta,\lambda)$) includes contributions from the atmosphere, solid Earth and water stored on land and in the ocean. [65] The load-induced deformation will be taken into account by load Love numbers [70]. When it is assumed that all mass transport takes place in a thin layer near the Earth surface and when it is assumed that this thin layer is a sphere of radius R', the inner integral of equation 3.9 can be rewritten [24]:

$$\int_0^{top\ of\ atmosphere}\left(\frac{r}{R}\right)^{l+2}\Delta\rho\,(r,\theta,\lambda)\;dr \approx \int_{thin\ layer}\left(\frac{r}{R}\right)^{l+2}\Delta\rho\,(r,\theta,\lambda)\;dr \approx \left(\frac{R'}{R}\right)^{l+2}\Delta\sigma\,(\theta,\lambda) \tag{3.10}$$

with $\Delta\sigma\,(\theta,\lambda)$ temporal variations in surface density (i.e., temporal variations in mass per unit area).

Since Earth is not a rigid body and hydrological and oceanic load deform the solid Earth [65], variations in gravitational potential are a combination of the direct effect of mass transport and the elastic deformation of the solid Earth [24]. To account for this effect, the load Love numbers (k_l) [70] are introduced. In this research, these load Love numbers are retrieved by linear interpolation of a set of

load Love numbers for $l = 0, 1, 2, 3, 4, 5, 6, 7, 8, 9, 10, 12, 15, 29, 30, 40, 50, 70, 100, 150, 200$ presented by them. The combination of equations 3.9 and 3.10 while including the load Love numbers is:

$$\begin{aligned}\Delta\bar{C}_{l,m} &= \frac{R^2}{M_E\,(2l+1)}\int_0^{2\pi}\int_0^{\pi}(1+k_l)\left(\frac{R'}{R}\right)^{l+2}\Delta\sigma\,(\theta,\lambda)\,\bar{Y}_{lm}\,(\theta,\lambda)\sin(\theta)\;d\theta\,d\lambda \\ &= \frac{R^2\,(1+k_l)}{M_E\,(2l+1)}\left(\frac{R'}{R}\right)^{l+2}\int_0^{2\pi}\int_0^{\pi}\Delta\sigma\,(\theta,\lambda)\,\bar{Y}_{lm}\,(\theta,\lambda)\sin(\theta)\;d\theta\,d\lambda,\end{aligned} \tag{3.11}$$

where k_l are the load Love numbers.

The temporal variations in surface density can also be expanded as a series of 4π-normalized surface spherical harmonics [23]:

$$\Delta\sigma\,(\theta,\lambda) = \sum_{l=0}^{\infty}\sum_{m=-l}^{l}\Delta\bar{C}_{l,m}^{(\Delta\sigma)}\bar{Y}_{l,m}\,(\theta,\lambda) \tag{3.12}$$

with $\bar{C}_{l,m}^{(\Delta\sigma)}$ appropriate Fourier coefficients defined as:

$$\bar{C}_{l,m}^{(\Delta\sigma)} = \frac{1}{4\pi}\int_0^{2\pi}\int_0^{\pi}\Delta\sigma\,(\theta,\lambda)\,\bar{Y}_{lm}\,(\theta,\lambda)\sin(\theta)\;d\theta\,d\lambda. \tag{3.13}$$

By combining equation 3.11 and 3.13 the following relation between the Stokes coefficients and the Fourier coefficients $\bar{C}_{l,m}^{(\Delta\sigma)}$:

$$\bar{C}_{l,m}^{(\Delta\sigma)} = \frac{M_E\,(2l+1)}{4\pi R^2\,(1+k_l)}\left(\frac{R}{R'}\right)^{l+2}\Delta\bar{C}_{l,m}. \tag{3.14}$$

The temporal variations in surface density can be related to mass anomalies in EWH by the following equation [43]:

$$\Delta H_w\,(\theta,\lambda) = \frac{\Delta\sigma\,(\theta,\lambda)}{\rho_w} \tag{3.15}$$

with ρ_w the density of water which is in the conversion from the temporal variations of Stokes coefficients to mass anomalies in EWH defined as $\rho_w = 1000\ kg/m^3$. Combining equation 3.12, 3.14 and 3.15 gives the following relation between the mass anomalies in EWH and the temporal variations of Stokes coefficients becomes:

$$\Delta H_w\,(\theta,\lambda) = \sum_{l=0}^{\infty}\sum_{m=-l}^{l}\frac{M_E\,(2l+1)}{4\pi R^2\,(1+k_l)\,\rho_w}\left(\frac{R}{R'}\right)^{l+2}\Delta\bar{C}_{l,m}\bar{Y}_{l,m}\,(\theta,\lambda)\,. \tag{3.16}$$

The radius of the thin layer sphere R' still has to be defined. Ditmar [24] recommends to use a locally spherical approximation. This means that that R' is chosen differently for each latitude and corresponds to the distance from the center of the Earth to the WGS84 reference ellipsoid. So it is still assumed that the mass transport takes place at a sphere but for each latitude a different sphere is considered. When this locally spherical approximation is used the ratio $\left(\frac{R}{R'}\right)$ becomes:

$$\left(\frac{R}{R'}\right) = \left(\frac{\sqrt{1-e^2\sin^2(\theta)}}{1-f}\right) \tag{3.17}$$

with $f = \frac{1}{298.2572}$ the flattening and $e = \sqrt{2f-f^2}$ the eccentricity of the WGS84 reference ellipsoid [38]. The relation by which in this chapter the temporal variations of the Stokes coefficients are converted to time-series of mass-anomalies is:

$$\Delta H_w\,(\theta,\lambda) = \sum_{l=0}^{\infty}\sum_{m=-l}^{l}\frac{M_E\,(2l+1)}{4\pi R^2\,(1+k_l)\,\rho_w}\left(\frac{\sqrt{1-e^2\sin^2(\theta)}}{1-f}\right)^{l+2}\Delta\bar{C}_{l,m}\bar{Y}_{l,m}\,(\theta,\lambda)\,. \tag{3.18}$$

Note that in equation 3.18 geocentric coordinates are present. If mass-anomalies at a grid in geodetic coordinates are calculated, the geodetic coordinates are first transformed to geocentric coordinates before applying equation 3.18. Furthermore, the degree l does in reality not to go until infinity. Stokes coefficients are always provided up to a certain maximum degree.

3.1.4. GRACE Release 5 and 6 Level-2 data

In this section first the method to produce Level-2 data is described. Several research centers produce these GRACE Level-2 data. A description of the GRACE Level-2 data which are considered in this research follows.

GRACE Level-2 data

GRACE Level-2 data considered in this research are addressed in this section. GRACE Level-2 data represent monthly average values of Earth's exterior gravitational potential and thus high-frequency geophysical signals have to be removed to prevent temporal aliasing of the high frequency signals in the monthly solutions. Various background models are used to model these high-frequency signals. The considered GRACE Level-2 data differ among others in the background models used in the production of these data. Also the considered days or part of days of which measurements are used to produce the monthly solutions differ for the different available GRACE Level-2 data.

In the processing of the GRACE, data estimates are made of updates to an in advance best-known model of Earth's exterior gravitational potential. [10] This in advance best-known model is also called the Background Model. This Background Model contains a set of background models among which the long-term mean Earth's exterior gravitational potential, background models for solid, ocean and pole tides and for atmospheric and non-tidal oceanic variability. The modeled geophysical phenomena are available at different and sometimes variable resolution in time and space. From this Background Model predictions of the difference in gravitational field between the two satellites are computed. Together with the difference in non-gravitational accelerations between the satellites [23] predictions of the observables which are first-derivatives or second-derivatives of the inter-satellite distance are made. These predictions of the observables differ from the true observables and this difference between the observed and predicted values is called the residual. This residual contains geophysical phenomena not modeled by the set of background models and model errors. [10] Furthermore, the residual also contains measurement errors.

From the residuals a residual gravitational field can be constructed. The update of the prior model of Earth's gravitational potential is made by least-squares fitting the gravitational field through the residuals for the time span of about a month. This update for a certain month indicates changes in the gravitational field which are not modeled. [10] The GRACE Level-2 data which are considered in this research are the sum of the described update and the long-term mean Earth's exterior gravitational potential (which is a part of the Background Model).

GRACE Release 5 and 6 solutions

Differences between GRACE Release 5 and 6 Level-2 data are related to differences in the data-processing among which the use of different background models. ITSG solutions are also considered in this research and they are not officially provided as Release 5 or 6 data. In this thesis ITSG solutions will be categorized as Release 5 and 6 according to the AOD1B product (Release 5 or 6) used in the data processing. In tables 3.1 and 3.2 the considered GRACE Level-2 data and the main background models used for the production of these data are shown.

Table 3.1: Considered Release 5 GRACE Level-2 data and the main background models used in the production of these data (long-term mean of Earth's exterior gravitational potential and background models for the solid Earth tides, ocean tides, pole tides, ocean pole tides, atmospheric tides and non-tidal atmosphere and ocean variability). [8] [54] [17]

Name	CSR Release 5	ITSG 2016	GFZ Release 5
Research institute	Center for Space Research, The University of Texas at Austin	Graz University of Technology	GFZ German Research Centre for Geosciences
Long-term mean gravity field model	GIF48	n/a	EIGEN-6C
Solid Earth tide	IERS 2010	IERS 2010	IERS 2010
Ocean tide	GOT4.8 and FES2004	EOT11a	EOT11a
Pole tide	IERS 2010	IERS 2010	IERS 2010
Ocean pole tide	Desai 2002 [21]	Desai 2004	Desai 2002 [21]
Atmospheric tide	Ray, Ponte 2003 [57]	van Dam, Ray 2010 [67]	Biancale, Bode 2006 [11]
Atmoshpere and ocean non-tidal variations	AOD1B RL05	AOD1B RL05	AOD1B RL05

Table 3.2: Considered Release 6 GRACE Level-2 data and the main background models used in the production of these data (long-term mean of Earth's exterior gravitational potential and background models for the solid Earth tides, ocean tides, pole tides, ocean pole tides, atmospheric tides and non-tidal atmosphere and ocean variability). [9] [55] [78]

Name	CSR Release 6	ITSG 2018	JPL Release 6
Research center	Center for Space Research, The University of Texas at Austin	Graz University of Technology	Jet Propulsion Laboratory, California Institute of Technology
Long-term mean gravity field model	GGM05C	n/a	GSM05C
Solid Earth tide	IERS 2010	IERS 2010	IERS 2010
Ocean tide	GOT4.8 and FES2004	FES2014b	Desai 2006 [22]
Pole tide	IERS 2010	IERS 2010	IERS 2010
Ocean pole tide	Desai 2002 [21]	Desai 2004	Desai 2002 [21]
Atmospheric tide	Ray, Ponte 2003 [57]	AOD1B RL06	Ray, Ponte 2003 [57]
Atmoshpere and ocean non-tidal variations	AOD1B RL06	AOD1B RL06	AOD1B RL06

3.1.5. Degree-1 and C20 coefficients

The center of mass of the Earth's system moves with respect to the center of its figure. [61] This process is known as geocenter motion. This geocenter motion is represented by time variations in the degree-1 Stokes coefficients. Since the GRACE satellites orbit the center of mass of the Earth's system [62], the GRACE Level-2 data product lacks these degree-1 Stokes coefficients.

The C20 coefficients also reflect large-scale mass redistribution within the Earth's system and these coefficients represent the its flattening [61] [63]. For example, the flattening is increased by ice sheet melt but decreased by the Glacial Isostatic Adjustment (GIA) [63]. Since the C20 coefficients show large uncertainties [16], it is a common practice to replace the GRACE-based C20 estimates with alternatives derived from a different technique.

The degree-1 and C20 Stokes coefficients which are used in this were produced by Y. Sun with the GRACE-OBP approach [62]. In that study data from the GRACE satellite mission, an Ocean Bottom Pressure model and a GIA model were combined. The GRACE monthly solutions of CSR were used

for this and thus different sets of degree-1 and C20 coefficients are produced for the different releases. The degree-1 and C20 coefficients where the Glacial Isostatic Adjustment (GIA) signal is restored are used for this research. This means that the coefficients represent total mass transport including the mass transport due to GIA. This is similar to the other degree Stokes coefficients used in this research. The degree-1 and C20 coefficients are produced by the use of CSR Release 5 and 6 GRACE solutions

3.2. Method

In this section the steps in the computation of mass-anomaly time-series from the available GRACE Level-2 is described as well as the set-up in the VCE to estimate the signal and noise in these mass-anomaly time-series. Furthermore, noise and signal are estimated for certain continental and oceanic regions. The definition of these regions is reported. Also the method to estimate non-seasonal signals and high-frequency signals in GRACE Level-2 data can be be found in this methodological section.

3.2.1. Computation of mass-anomaly time-series from different GRACE Level-2 data

The considered GRACE Level-2 data as described in section 3.1.4 are downloaded from the websites reported in table 3.3. The considered GRACE Level-2 data are those for the period January 2003 until March 2016. Some GRACE Level-2 data sets also contain a monthly solution for May 2015. Since for May 2015 only 11 days of data are used, the monthly solution of May 2015 is not considered for any set of GRACE Level-2 data.

Table 3.3: The source of the considered GRACE Level-2 data.

Name	GRACE Level-2 data retrieved from:
CSR Release 5	`ftp://podaac.jpl.nasa.gov/allData/grace/L2/CSR/RL05/`
ITSG 2016	`ftp://ftp.tugraz.at/outgoing/ITSG/GRACE/ITSG-Grace2016/monthly/monthly_n60`
GFZ Release 5	`ftp://icgem.gfz-potsdam.de/01_GRACE_monthly/GFZ%20Release%2005/unfiltered/`
CSR Release 6	`ftp://podaac.jpl.nasa.gov/allData/grace/L2/CSR/RL06/`
ITSG 2018	`ftp://ftp.tugraz.at/outgoing/ITSG/GRACE/ITSG-Grace2018/monthly/monthly_n60`
JPL Releae 6	`ftp://podaac.jpl.nasa.gov/allData/grace/L2/JPL/RL06/`

The Level-2 product is provided in the form of a set of Stokes coefficients up to a certain degree. Sets of Stokes coefficients up to degree 60 were downloaded. There is an exception for the GFZ Release 5 solutions. Since a variant of these solutions complete to degree 60 does not exist, the solutions complete to degree 90 were downloaded and truncated at degree 60. This approach might introduce extra errors as compared to the solutions complete to degree 60 from the very beginning.

The Release 5 GRACE Level-2 data have to be corrected for an inconsistency in the AOD1B product used for the generation of these data. The atmospheric part of the AOD1B Release 5 product is based on operational analysis data from the European Center for Medium-Range Weather Forecast (ECMWF) Integrated Forecast System (IFS). [30] This numerical weather prediction model is upgraded at specific moments to include improvements in the physical model, the numerics, the data assimilation scheme and to accommodate new observing technologies. [30] Such changes in the modeling process may lead to inconsistencies in the time-series of model states as for example surface pressure. Jumps in atmospheric surface pressure occurred at the following times:

- between 2006-01-29 18h and 2006-01-30 00h
- between 2010-01-26 00h and 2010-01-26 06h
- between 2015-05-12 00h and 2015-05-12 06h

These jumps in surface pressure propagate into the GRACE Level-2 data. Therefore, the monthly gravitational field solutions have to be corrected. This correction can be applied by using additional products

called GAE, GAF and GAG products (available from: `ftp://podaac.jpl.nasa.gov/allData/grace/docs/`). To correct the monthly gravity solutions the GAE, GAF or GAG products have to be subtracted from the available Release 5 GRACE Level-2 products.The GAE, GAF and GAG products have to be used for the following periods:

- GAE from February 2006 (included) till January 2010 (included).
- GAF from February 2010 (included) till May 2015 (included)
- GAG after May 2015

Afterwards the corrected Stokes coefficients can be turned to mass-anomaly time-series in the same manner as for the Release 6 GRACE Level-2 data. The AOD1B Release 6 product used in the production of Release 6 GRACE Level-2 data is already corrected for the jumps in atmospheric pressure.

In the processing of GRACE Level-2 data, first the Degree-1 and C20 coefficients are replaced by Degree-1 and C20 coefficients produced by Sun et al. [62] (as explained in section 3.1.5). Thereafter, the long-term mean (i.e. the mean in the period from January 2003 until March 2016) of each Stokes coefficient is subtracted.

Consequently, the Stokes coefficients are turned into GRACE-based mass-anomalies by using equation 3.18. To reduce the noise in the monthly solutions a Gaussian filter of $400\ km$ half-width is applied. Due to the filtering the accuracy of the derived mass-anomalies becomes higher, but the spatial resolution becomes lower. [65] Mass-anomaly time-series are calculated on a 0.5 °equiangular grid in geodetic coordinates.

3.2.2. Chosen set-up in the VCE and computation of regional estimates

In chapter 2 various VCE set-ups were tested. From the conclusions made in this chapter the following set-ups are considered for the analysis of the GRACE-based mass-anomaly time-series (table 3.4). Considering a different number of time-series is done because of the possible presence of cross-correlated noise.

Table 3.4: Various set-ups for the VCE to analyze GRACE-based mass-anomaly time-series.

Regularization technique	Number of considered time-series	Considered data
MYDD	3	CSR Release 5, ITSG 2016, GFZ Release 5
Tikhonov first-order	3	CSR Release 5, ITSG 2016, GFZ Release 5
None	3	CSR Release 5, ITSG 2016, GFZ Release 5
MYDD	1	CSR Release 5
MYDD	1	ITSG 2016
MYDD	1	GFZ Release 5
MYDD	3	CSR Release 6, ITSG 2018, JPL Release 6
MYDD	1	CSR Release 6
MYDD	1	ITSG 2018
MYDD	1	JPL Release 6

The standard deviations of the noise (and in the case of MYDD minimization also the signal standard deviations) are estimated for a 0.5 °equiangular grid in geodetic coordinates. From these estimates global mean values, mean values for only oceanic or continental regions and mean values for specific oceanic or continental parts are calculated. The mean noise or signal standard deviation for a certain

region is calculated as follows:

$$\overline{\sigma}_i = \sqrt{\frac{\sum_{j \in M_i} \left(\sigma\left(\vartheta_j, \lambda_j\right)\right)^2 \sin\left(\vartheta_j\right)}{\sum_{j \in M_i} \sin\left(\vartheta_j\right)}}, \tag{3.19}$$

where $\overline{\sigma_i}$ is the mean standard deviation for a certain region i. M_i is the set of points in region i and ϑ_j and λ_j are the geodetic colatitude and longitude of a point j. The definition of the considered regions follows in the next section.

Furthermore the estimated signal standard deviation will be shown versus bathymetry. The bathymetry is derived from GTSM 4.1.2. Ocean depths are categorized in bins of 100 m. Then each location of the ocean is assigned to a specific depth bin. For each bin the average signal standard deviation for that depth bin is calculated by taking into account the weight of a certain grid cell by the factor $\sin(\theta)$. This is similar to the use of equation 2.24 but then a bin is considered as a region. For each oceanic region (see 3.2.3), the estimated signal standard deviation is plotted versus bathymetry. To plot the standard deviation of the difference mass-anomaly time-series versus bathymetry buffer zones are incorporated in the analysis. This should reduce the signal leakage from land to ocean which is present in the estimated signal standard deviation. Two different buffer zones (200 and 400 km) are incorporated in the analysis to disregard the areas close to the coast where the signal leakage is the largest. The two buffer zones are shown in figures 3.3 and 3.4.

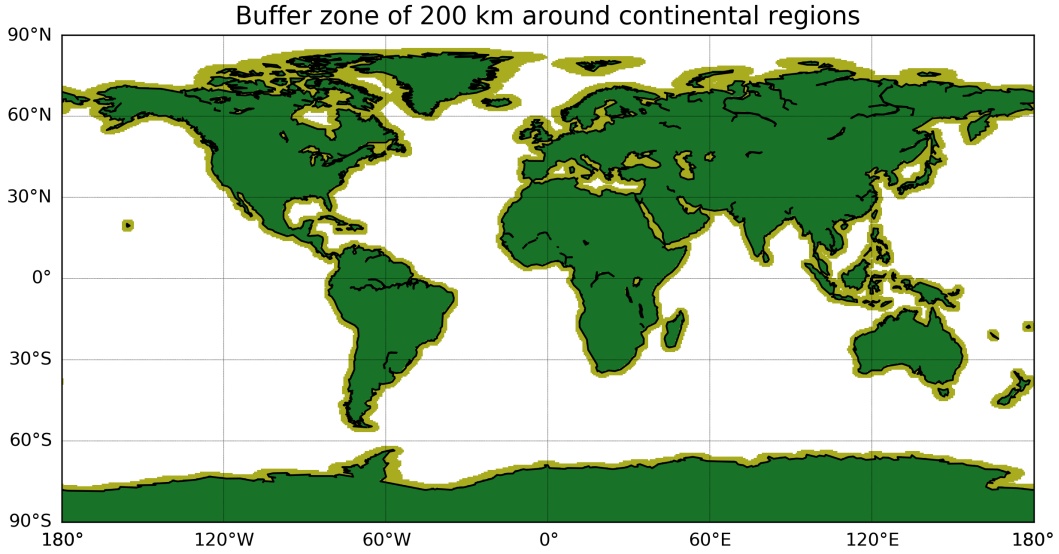

Figure 3.3: A 200 km buffer zone along the coast.

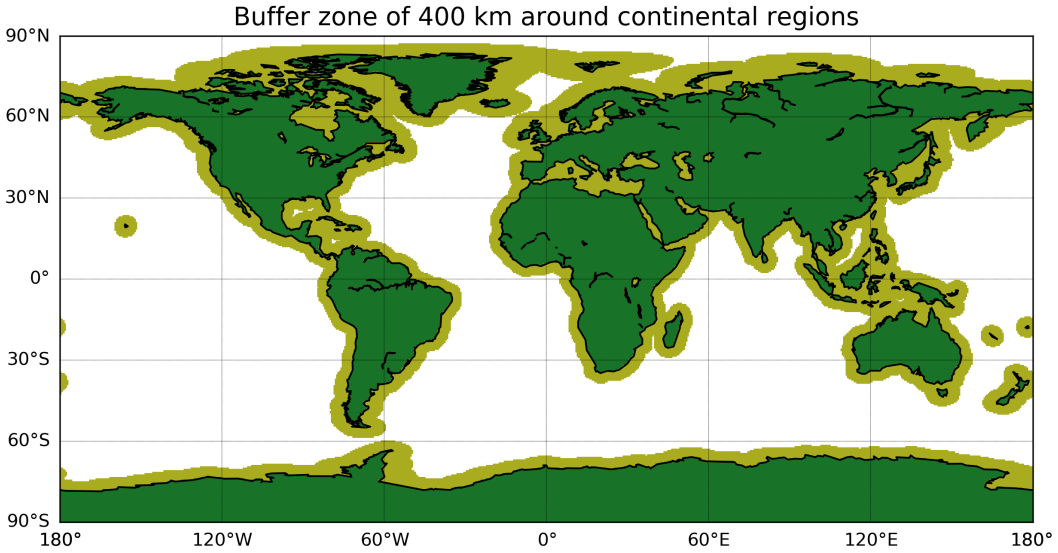

Figure 3.4: A 400 km buffer zone along the coast.

3.2.3. Definition of oceanic and continental regions

To compute the oceanic mean and continental mean of the estimated signal and noise standard deviation the function `is_land` from the Python module `mpl_toolkits.basemap` is used. This function is defined in line with coastline data from the Global Self-consistent, Hierarchical, High-resolution Shoreline Database (GSHHS) [74]. In this definition, points in lakes are also considered as being part of the oceanic and not the continental region.

When computing mean values for separate parts of the ocean and continental regions, a different source of coastline data is used. The definition of continental regions and oceanic parts is based on Natural Earth data [52]. For both land and ocean Natural Earth data the medium scale data (version 4.1.0) are considered. The 119 oceans and seas of the medium scale data are then categorized in oceanic parts described in Monaco [49]. Some small seas are categorized separately to be able to compute regional averages for specific regions where either high noise standard deviation is observed or which are close to Europe. In the analyses of this chapter these small oceanic regions are the Gulf of Thailand, Arafura Sea, Black Sea and Baltic Sea. In chapter 4 and 5 the North Sea is considered as a separate area of the North Atlantic Ocean because this area seemed specifically of interest in those chapters. In the definition of continental regions Greenland is considered as a separate region. Furthermore, Europe and Asia are considered as one continental region. The defined continental regions and oceanic parts (including the North Sea) can be found in figures 3.5 and 3.6 respectively.

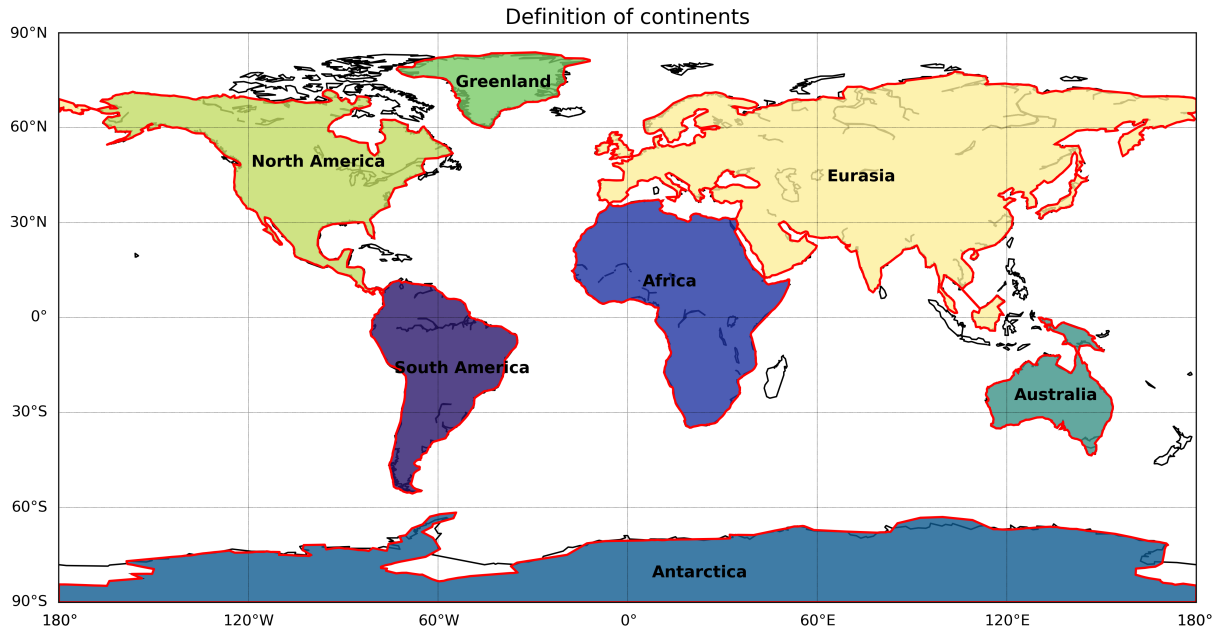

Figure 3.5: Polygons which define the continental regions for the computation of regional averages.

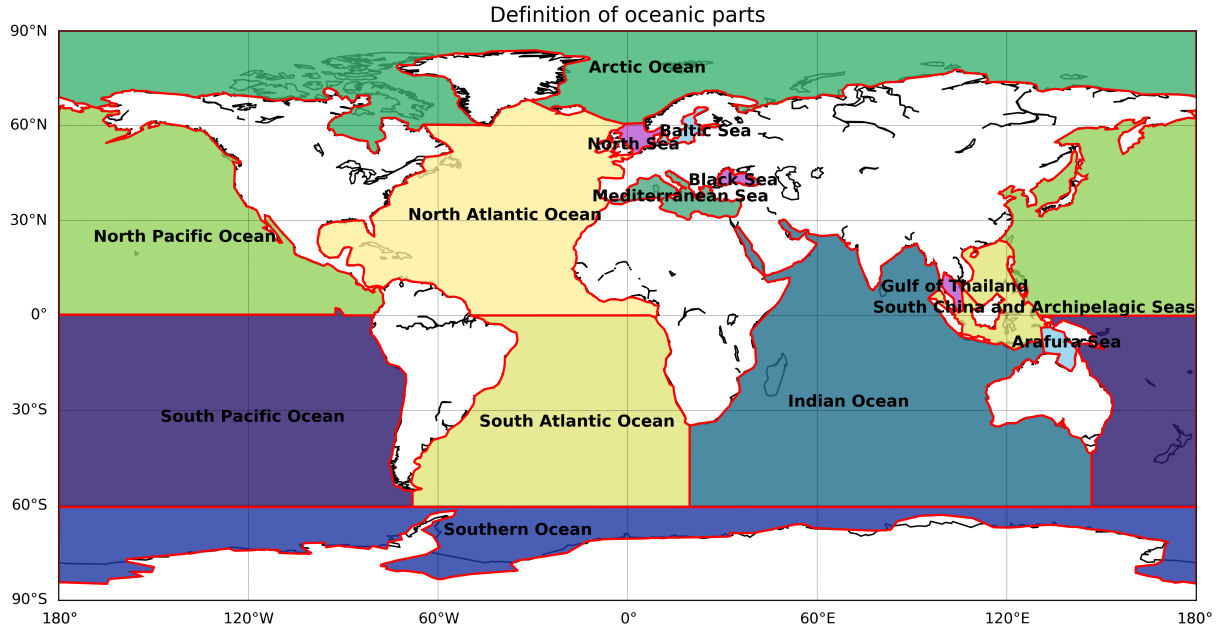

Figure 3.6: Polygons which define the oceanic parts (including the North Sea) for the computation of regional averages.

3.2.4. Estimation of non-seasonal and high-frequency residuals in ITSG monthly solutions

Since ITSG monthly solutions show a lower noise level with respect to CSR, GFZ and JPL solutions, the quality of these monthly solutions are separately assessed. This is done by estimating the RMSE with respect two types of signals. One type is a seasonal signal. The other type is a low-pass filtered signal. The two methods are considered below.

The first considered method makes use of least-squares estimation. By least-squares estimation a linear trend, annual and semi-annual signal are estimated for the ITSG monthly time-series at each

grid point. Consequently the Root Mean Square Error (RMSE) of the original monthly time-series is computed with respect to the by least-squares estimated signal. The Bessel's correction is not applied. This RMSE is visualized globally as well as versus bathymetry. Also regional average values for the ocean are computed in the same manner as for the estimated noise and signal standard deviation.

For the second considered method the monthly time-series are first interpolated to a monthly equal sampling to fill the data gaps. For this the Python function `scipy.interpolate.interp1d` is used. The chosen interpolation method is cubic spline interpolation. Consequently the Fourier transform is computed for the interpolated monthly time-series. All computed amplitudes belonging to frequencies larger than 2 cycles per year are put to zero before applying the inverse Fourier transform. In this way the interpolated monthly time-series are low-pass filtered. Then the RMSE is computed with respect to the low-pass filtered monthly time-series. This RMSE is visualized globally as well as versus bathymetry. Also regional average values for the ocean are computed. In this context the term high-frequency is related to frequencies higher than the semi-annual cycle.

3.3. Results and discussion

In this section the noise and signal standard deviation estimated by VCE are shown for different GRACE solutions. For GRACE Release 5 solutions different regularization techniques in the VCE are considered. For both GRACE Release 5 and GRACE Release 6 the noise and signal are also estimated by considering only one time-series in the VCE with MYDD minimization as regularization technique. Finally, the estimated residuals for ITSG monthly solutions as described in section 3.2.4 are shown and discussed.

Estimates of signal and noise standard deviation for GRACE Release 5 solutions

A selection of the estimates of signal and noise standard deviation for different GRACE Release 5 solutions and different VCE set-ups can be found in figures 3.7, 3.8, 3.9, 3.10, 3.11 and 3.12. A total set of figures containing all estimates can be found in Appendix B. In tables 3.5 and 3.6 regional averages of the estimates of signal and noise standard deviation can be found.

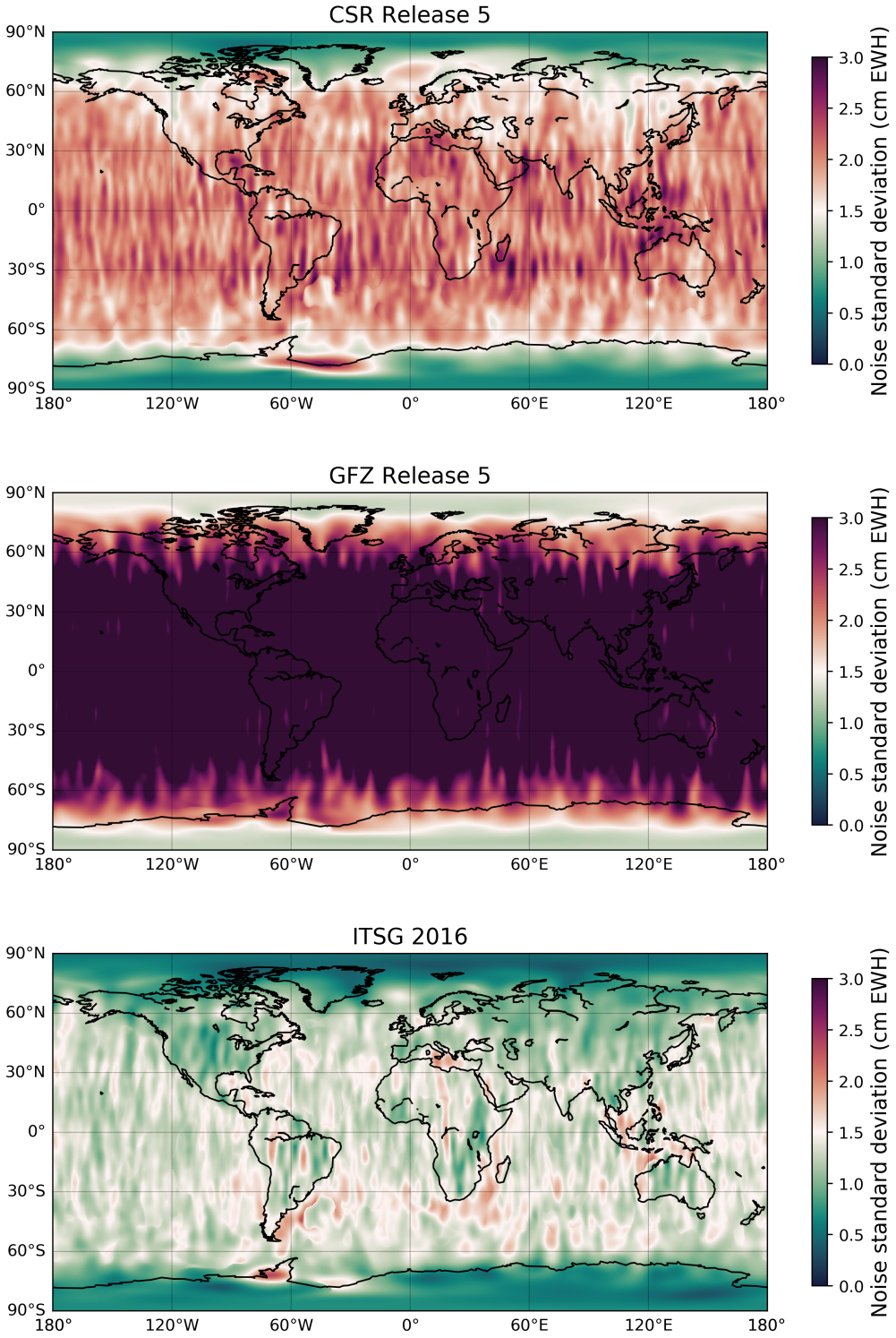

Figure 3.7: Estimated noise standard deviation for GRACE Release 5 solutions (CSR Release 5, GFZ Release 5, ITSG 2016) by considering three mass-anomaly time-series in the VCE and MYDD minimization as regularization technique.

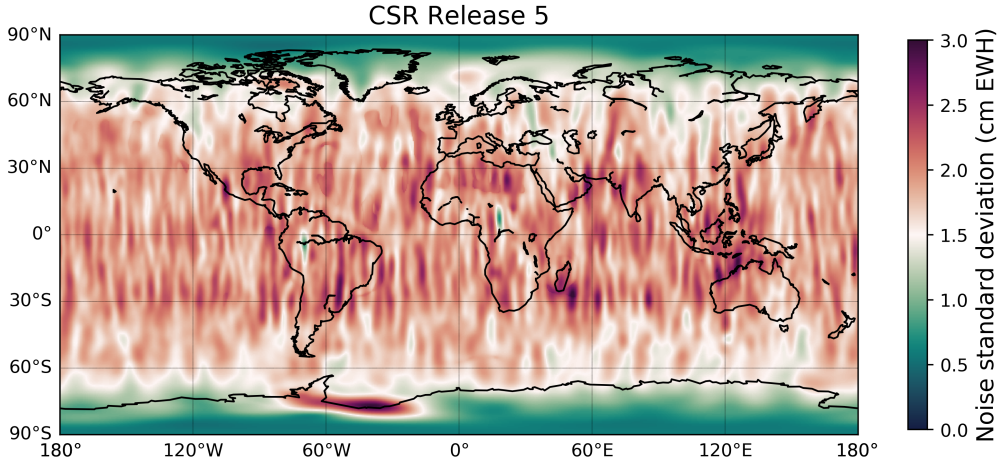

Figure 3.8: Estimated noise standard deviation for GRACE solution CSR Release 5 by considering three mass-anomaly time-series (CSR Release 5, ITSG 2016, GFZ Release 5) in the VCE and Tikhonov first-order as regularization technique.

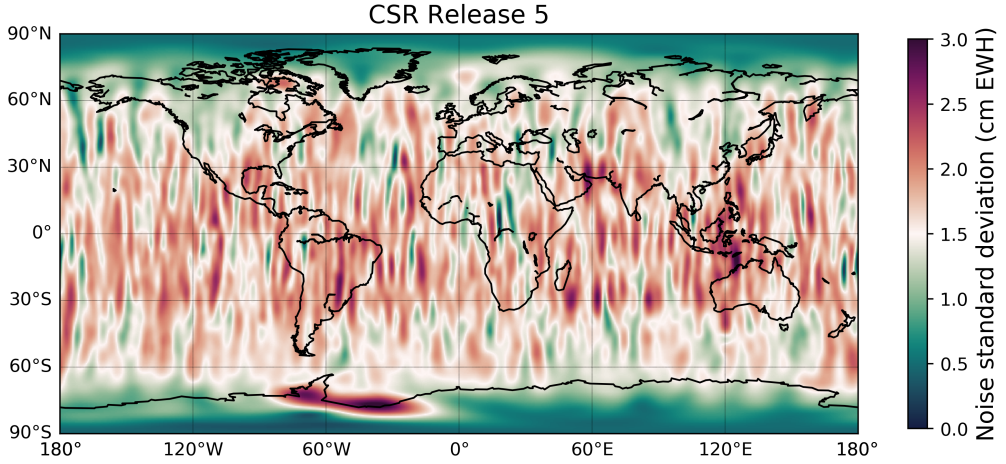

Figure 3.9: Estimated noise standard deviation for GRACE solution CSR Release 5 by considering three mass-anomaly time-series (CSR Release 5, GFZ Release 5, ITSG 2016) in the VCE and applying no regularization.

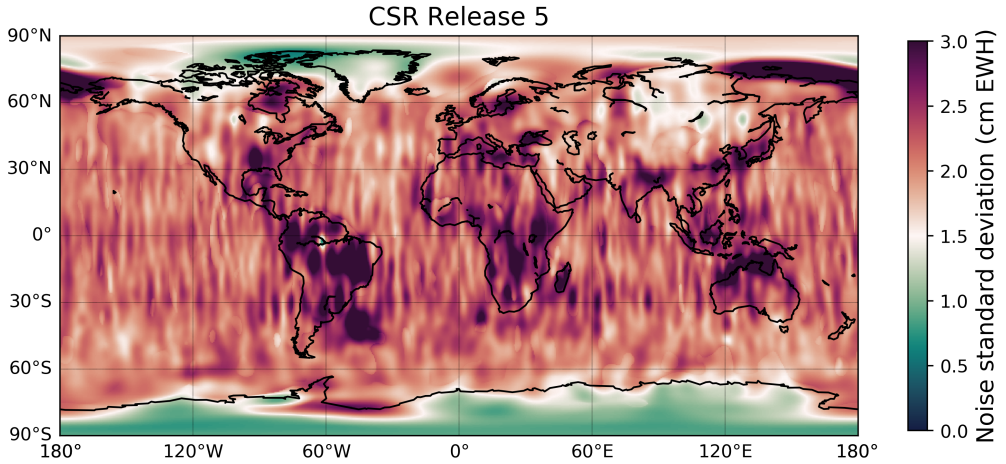

Figure 3.10: Estimated noise standard deviation for GRACE solution CSR Release 5 by considering one mass-anomaly time-series in the VCE and MYDD minimization as regularization technique.

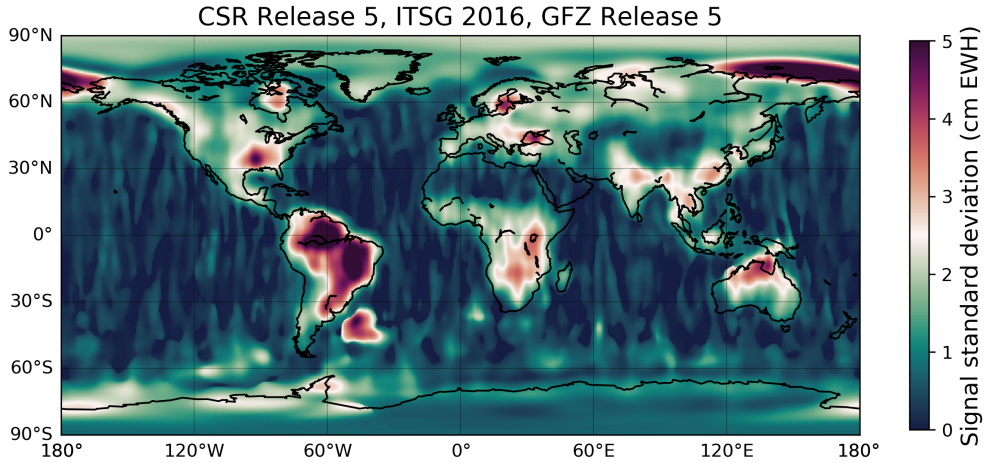

Figure 3.11: Estimated signal standard deviation for GRACE Release 5 solutions by considering three mass-anomaly time-series (CSR Release 5, GFZ Release 5, ITSG 2016) in the VCE and MYDD minimization as regularization technique.

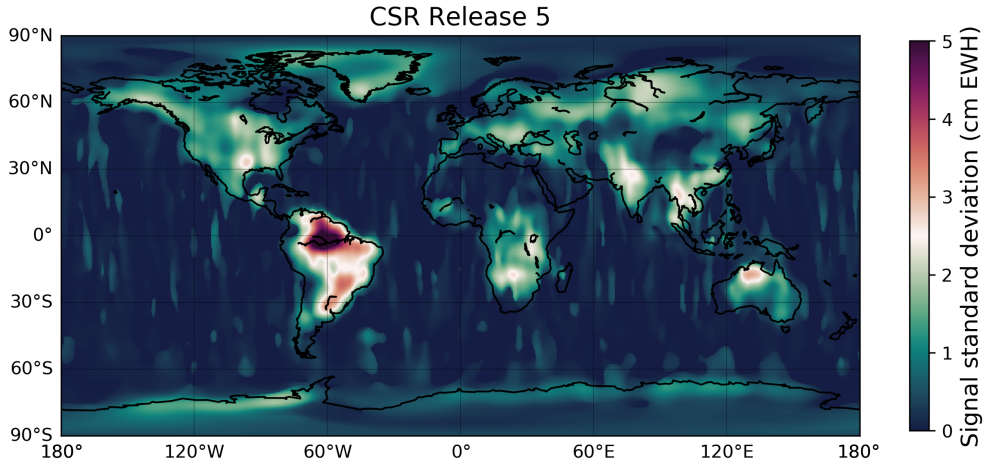

Figure 3.12: Estimated signal standard deviation for GRACE solution CSR Release 5 by considering one mass-anomaly time-series in the VCE and MYDD minimization as regularization technique.

Table 3.5: Regional averages of estimated noise standard deviation in cm EWH for different GRACE Level-2 data and different VCE setups. The VCE setups differ in the number of considered time-series and applied regularization technique in the estimation process.

GRACE Level-2 data	CSR Release 5				GFZ Release 5				ITSG 2016			
No. of considered time-series	3			1	3			1	3			1
Regularization technique	MYDD	Tikhonov first-order	None	MYDD	MYDD	Tikhonov first-order	None	MYDD	MYDD	Tikhonov first-order	None	MYDD
Total area	1.946	1.838	1.661	2.207	3.392	3.333	3.266	3.533	1.303	1.077	1.240	1.549
Only ocean	1.992	1.858	1.685	2.181	3.459	3.384	3.317	3.547	1.347	1.110	1.230	1.536
Only land	1.827	1.786	1.600	2.272	3.217	3.203	3.138	3.498	1.187	0.992	1.263	1.579
Arafura Sea	2.265	2.160	1.967	3.408	3.730	3.615	3.532	4.608	1.624	1.389	1.669	2.748
Arctic Ocean	1.245	1.186	1.112	2.049	1.922	1.911	1.892	2.430	0.891	0.733	0.833	1.720
Baltic Sea	1.650	1.573	1.405	2.704	2.386	2.399	2.381	3.028	1.307	1.073	1.247	2.464
Black Sea	1.582	1.493	1.437	2.830	3.128	3.138	3.132	3.569	1.433	1.272	1.356	2.593
Gulf of Thailand	1.982	1.948	1.799	2.307	3.700	3.601	3.567	4.207	1.577	1.126	1.405	1.975
Indian Ocean	2.070	1.922	1.741	2.209	3.498	3.411	3.353	3.571	1.413	1.165	1.296	1.544
Mediterranean Sea	2.073	1.872	1.591	2.602	3.691	3.615	3.542	3.948	1.515	1.133	1.439	1.902
North Atlantic Ocean	1.989	1.905	1.700	2.134	3.651	3.613	3.520	3.718	1.354	1.156	1.189	1.478
North Pacific Ocean	2.011	1.881	1.685	2.152	3.573	3.506	3.435	3.613	1.325	1.103	1.241	1.461
South Atlantic Ocean	2.089	1.895	1.711	2.304	3.535	3.435	3.361	3.652	1.433	1.154	1.300	1.650
South China and Archipelagic Seas	2.167	2.075	1.978	2.433	3.585	3.520	3.449	3.717	1.436	1.207	1.365	1.669
South Pacific Ocean	2.043	1.896	1.732	2.151	3.597	3.506	3.438	3.632	1.358	1.116	1.248	1.463
Southern Ocean	1.630	1.549	1.487	1.986	2.385	2.310	2.269	2.646	1.153	0.877	0.926	1.548
Africa	2.056	1.975	1.662	2.528	3.604	3.574	3.479	3.903	1.313	1.144	1.472	1.658
Antarctica	1.140	1.165	1.136	1.350	1.837	1.817	1.778	1.953	0.811	0.643	0.717	1.066
Australia	2.012	1.950	1.817	2.558	3.306	3.280	3.230	3.679	1.323	1.111	1.312	1.796
Eurasia	1.765	1.728	1.565	2.130	3.139	3.130	3.071	3.360	1.168	0.949	1.212	1.506
Greenland	1.108	1.126	0.980	1.331	1.888	1.933	1.882	1.883	0.754	0.619	0.855	0.898
North America	1.727	1.742	1.509	2.159	3.241	3.248	3.156	3.562	1.088	0.820	1.238	1.452
South America	2.074	2.018	1.901	2.785	3.680	3.666	3.635	4.107	1.332	1.207	1.404	2.012

Table 3.6: Regional averages of estimated signal standard deviation in cm EWH for different GRACE Level-2 data and different VCE setups. The VCE setups differ in the number of considered time-series (one or three) in the estimation process.

GRACE Level-2 data	CSR Release 5, GFZ Release 5, ITSG 2016	CSR Release 5	GFZ Release 5	ITSG 2016
Total area	1.338	0.791	0.750	0.844
Only ocean	0.864	0.313	0.335	0.315
Only land	2.096	1.393	1.297	1.497
Arafura Sea	2.837	0.513	0.591	0.738
Arctic Ocean	2.236	0.513	0.523	0.502
Baltic Sea	3.210	0.616	0.474	0.506
Black Sea	3.518	1.297	1.478	1.274
Gulf of Thailand	1.661	1.160	0.484	1.024
Indian Ocean	0.576	0.270	0.283	0.256
Mediterranean Sea	1.431	0.583	0.511	0.689
North Atlantic Ocean	0.614	0.310	0.313	0.343
North Pacific Ocean	0.602	0.263	0.319	0.254
South Atlantic Ocean	0.953	0.244	0.204	0.254
South China and Archipelagic Seas	1.023	0.574	0.687	0.641
South Pacific Ocean	0.434	0.158	0.242	0.125
Southern Ocean	1.218	0.345	0.378	0.338
Africa	1.764	0.963	0.930	1.189
Antarctica	1.140	0.737	0.727	0.747
Australia	2.147	1.262	1.195	1.442
Eurasia	1.790	1.153	1.040	1.199
Greenland	1.672	1.377	1.417	1.436
North America	2.009	1.332	1.178	1.457
South America	3.655	2.684	2.530	2.807

From these figures and tables several observations can be made. Firstly, the noise level in GRACE solution GFZ Release 5 is a lot larger than for GRACE solutions CSR Release 5 and ITSG 2016. This is observed for the different regularization techniques in the VCE and also when considering only one or three mass-anomaly time-series in the VCE with MYDD minimization as regularization technique. For example, the global mean noise standard deviation is 1.7 times larger w.r.t. CSR Release 5 and 2.6 times larger w.r.t. ITSG 2016 when three time-series and MYDD-minimization are considered in the VCE.

As previously told, the GRACE Level-2 data are produced by different research centers. Which part in the processing is the cause of these large differences in estimated noise in these GRACE Level-2 data is difficult to say. The different GRACE solutions were made by making use of different background models (see table 3.2). Besides that, the non-gravitational forces which influence the inter-satellite distance and the measurements of the satellite orientation and position are incorporated in a different way into the production of the monthly mean solutions. [47] Also the considered measurements of inter-satellite distance are different. Differences in time epochs where the inter-satellite distance measurements are considered might arise by a different way of selecting the measurements of sufficient quality. Furthermore, there are differences in the computational procedures.

A second observation which can be made is that the noise level in general is lower near the poles and increases towards the equator. Effectively, when one considers an area of a certain size near the equator or near the poles, the GRACE satellites fly over the area near the poles more often than over the one near the equator. Also the angle between the flight paths near the poles is larger than near the equator. Both reasons induce a lower noise level near the poles than near the equator.

Furthermore, a striping pattern in North-South direction in the estimated noise standard deviation can be observed in the figures of estimated noise standard deviation (figures 3.7, 3.8, 3.9, 3.10). In section 1.3 it was already stated that the zonal Stokes coefficients are more accurate than the sectorial ones due to the nearly polar orbit of the GRACE satellites. For the production of monthly mean solutions measurements along certain longitudes might be considered more often during a month. This might arise biases in the estimated sectorial Stokes coefficients. Less accurate sectorial Stokes coefficients for certain orders might produce this striping pattern in noise standard deviation. But one should also keep in mind in mind that the estimates of noise might deviate from the true noise. According to Dobslaw et al. [26] and Nie et al. [53] the temporal aliasing by inaccurately taking into account high-frequency variations by using inaccurate background models in the Level-2 data production is partly responsible for the meridional stripes in GRACE gravity field solutions. The striping pattern in these solutions might result in more constant estimated noise standard deviation along a certain longitude and more rapid variations in the estimated noise standard deviation along a certain latitude.

Now different VCE setups are compared in the estimation of signal and noise. When a different number of mass-anomaly time-series considered in the VCE with MYDD minimization as regularization technique, it can be observed that when only one solution solution is considered the signal standard deviation becomes lower whereas noise standard deviation increases. When only one solution is considered all deviations from the regularized solution (which consists predominantly of a seasonal and linear trend) are estimated as noise. When multiple solutions are considered and there is cross-correlation in the deviations from a seasonal and linear trend between these solutions, this shows up predominantly as signal variance. This was observed in section 2.4. Cross-correlated noise or signal can not be separated by the VCE with MYDD minimization as regularization technique. So when mass-anomaly time-series contain cross-correlated noise, it is expected that a high signal standard deviation would be estimated when three mass-anomaly time-series are considered and a high noise standard deviation would be estimated when one mass-anomaly time-series is considered in the VCE. Therefore, the difference between figures 3.11 and 3.12 is interesting since it gives an indication of cross-correlated noise which might be caused by inaccurate background models.

When comparing the estimates of noise standard deviation by considering different regularization techniques it can be observed that in general the noise standard deviation is estimated a bit lower when Tikhonov first-order instead of MYDD minimization is used. When considering the CSR Release 5 solutions the global mean noise standard deviation goes down by 5.7%. A smaller noise estimation by Tikhonov first-order with respect to MYDD was also observed in section 2.4 for the numerical experiments when the signal-to-noise ratio (amplitude of seasonal variability divided by true noise standard deviation) increased. In turn, applying no regularization gives lower estimates of noise standard deviation than Tikhonov first-order (on a global mean basis by 11%). The mass-anomaly time-series considered in the VCE might all differ more from a regularized solution than from the combined solution when no regularization was applied. This could explain why the estimated noise for certain locations is estimated smaller the case when no regularization is applied compared to the cases where regularization is applied.

An exception can be observed in the mass-anomaly time-series derived from ITSG 2016 where no regularization leads to lower noise estimates than Tikhonov first-order regularization. When Tikhonov first-order is used as regularization technique the estimated noise is 13% lower than the case where no regularization is applied in the VCE (on the basis of the global mean). It might be the case that the ITSG 2016 solutions are in time more constant than CSR Release 5 and GFZ Release 5 (i.e. show little fluctuations in mass-anomaly over time). When Tikhonov first-order is used as regularization technique the regularized solution is aimed to become close to a constant value since the slope of the mass-anomaly time-series at every moment is minimized. When ITSG 2016 shows less fluctuations in mass-anomaly over time compared to CSR Release 5 and GFZ Release 5, ITSG 2016 could be closer to the regularized solution and the estimated noise standard deviation for this solution can become very small. For ITSG 2016 it could thus be the case that this solution is more close to the regularized solution (obtained by using Tikhonov first-order) than to only a combined solution of ITSG 2016, GFZ

Release 5 and CSR Release 5. The Tikhonov first-order regularization might thus favor the quality of ITSG 2016 data.

When looking at the estimates of signal standard deviation for certain regions it can be identified where the signal standard deviation is relatively large. These are:

- South America
- The Southern part of Africa
- The area around the river Mississippi
- Baltic Sea
- Black Sea
- Arafura Sea (including Gulf of Carpentaria)
- East Siberian Arctic Shelf
- Argentine Basin
- Hudson Bay

For the region near the Mississippi river and also for South America it might be that a signal of interannual variability is present since the river basins in those areas might contain interannual variability in water mass. High signal standard deviations for the regions Baltic Sea, Black Sea, Arafura Sea, East Siberian Arctic Shelf and Argentine Basin might indicate that the oceanic background models for those regions are in need for improvement. When the oceanic background models would perform very well, the signal standard deviation over the ocean would be almost 0 since the oceanic signals (when cleaned from high-frequency variations due to atmospheric and tidal forcing) should then contain almost only a linear trend and seasonal variability. Ideally, the GRACE-based time-series over the oceans only show changes of mass between the ocean and land and effects of self-attraction and loading which would both result in predominantly a linear trend and seasonal variability. When oceanic background models make wrong predictions, these wrong predictions might alias into the GRACE-based mass-anomaly time-series. Also, when the oceanic background models for these regions are of insufficient quality, a part of the ocean variability due to wind, atmospheric pressure and tidal forcing might still be in the GRACE monthly solutions because it is not or only partly removed. These predominantly high-frequency oceanic variabilities (periods smaller than a month) then also alias in the mass-anomaly time-series. The aliasing can cause a higher estimated signal standard deviation since the aliasing can result in interannual differences in the mass-derivative in the time-series. For the Hudson Bay, it might be the case that the presence of sea ice during a part of the year is not good enough taken into account in the oceanic background models. This might be a reason for less accurateness of the considered oceanic background model in the Hudson Bay. The regions of large signal standard deviation might indicate areas for improvement in the oceanic background models.

The figure of signal standard deviation (figure 3.11) can also be compared to results presented by Dobslaw et al. [27]. A by them presented figure (fig. 8) reflects the impact of physical processes currently not included in the AOD1B Release 5 product. A high impact can be observed for the Argentina Basin, Hudson Bay, Sargasso Sea, Baltic Sea, a part of the East Siberian Arctic Shelf, Bering Strait and several areas around Antarctica. Since the AOD1B Release 5 product is produced by using a global ocean circulation model which excludes meso-scale variability and small-scale eddies the product is particularly inaccurate in energy-rich areas of the ocean. [27] The excluded physical processes might explain the high signal standard deviation observed in figure 3.11 for the Argentina Basin, Hudson Bay, Baltic Sea and East Siberian Arctic Shelf. This contributes to the reasoning that high signal standard deviations show up in regions where the de-aliasing product is inaccurate.

Another figure shown by Dobslaw et al. [27] (fig. 6b) indicated areas of lower accuracy of AOD1B Release 5. This figure showed an exceptionally low accuracy for the Arctic ocean. The Arctic Ocean also does show a high signal standard deviation compared to the open ocean (figure 3.11). One reason of inaccuracy is the incorrect practice of the inverse barometric correction for this area. Due to the narrow straits to the Atlantic and Pacific Ocean the reaction of the ocean to the changes in atmospheric pressure might be later or smaller. Also high inaccuracies are shown for the Arafura Sea, the Gulf of Thailand, the East China Sea, the Hudson Bay, the Baltic Sea, the Black Sea, the North sea and several regions near Antarctica (in the vicinity of the Antarctic Circumpolar Current). Again, many areas of high inaccuracy for the AOD1B Release 5 product are similar to regions of high signal standard deviation estimated in this research. Inaccuracies in the AOD1B Release 5 product for certain regions cause inaccuracies in the GRACE-based mass-anomaly time-series. When the same de-aliasing product is used, these inaccuracies show up as the same residual signal. Therefore it seems logical that

the regions presented by Dobslaw et al. [27] are similar to regions of high signal standard deviation presented in this research.

Estimates of noise and signal standard deviation for GRACE Release 6 solutions

A selection of the estimates of signal and noise standard deviation for different GRACE Release 6 solutions and different VCE set-ups can be found in figures 3.13 and 3.14. A total set of figures containing all estimates can be found in Appendix B. Figure 3.15 shows the differences in estimated signal standard deviation for GRACE Release 5 and GRACE Release 6 solutions. In tables 3.7 and 3.8 regional averages of the estimates of signal and noise standard deviation can be found.

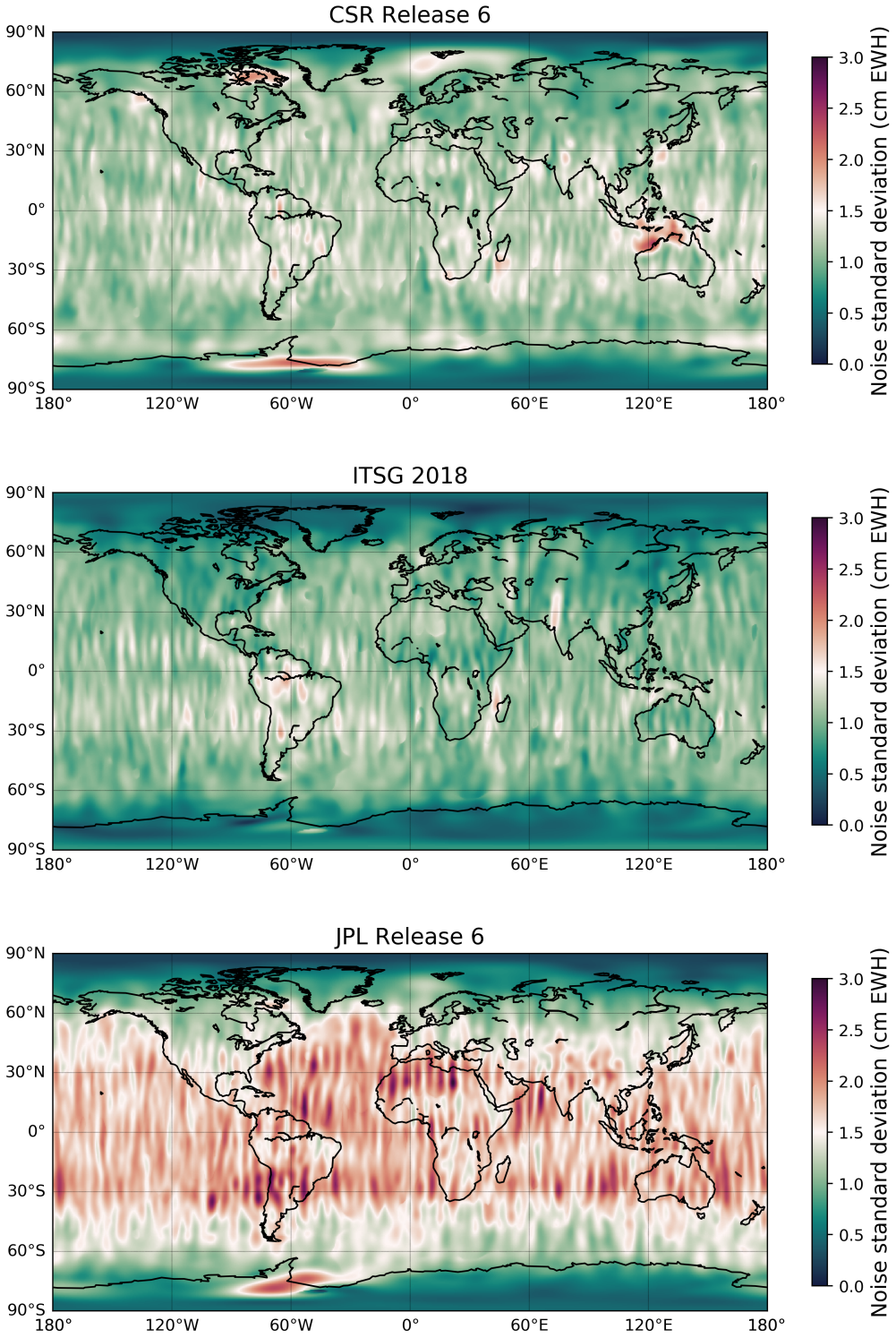

Figure 3.13: Estimated noise standard deviation for GRACE Release 6 solutions (CSR Release 6, ITSG 2018, JPL Release 6) by considering three mass-anomaly time-series in the VCE and MYDD minimization as regularization technique.

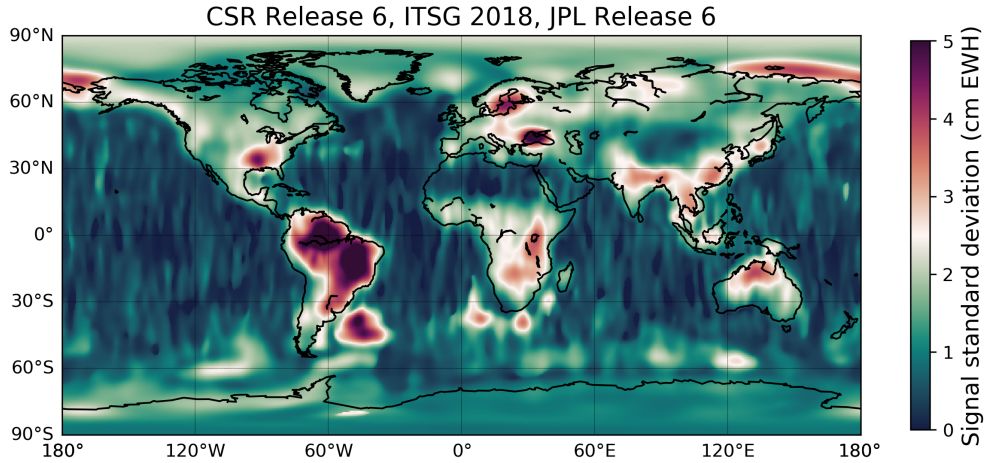

Figure 3.14: Estimated signal standard deviation for GRACE Release 6 solutions by considering three mass-anomaly time-series (CSR Release 6, ITSG 2018, JPL Release 6) in the VCE and MYDD minimization as regularization technique.

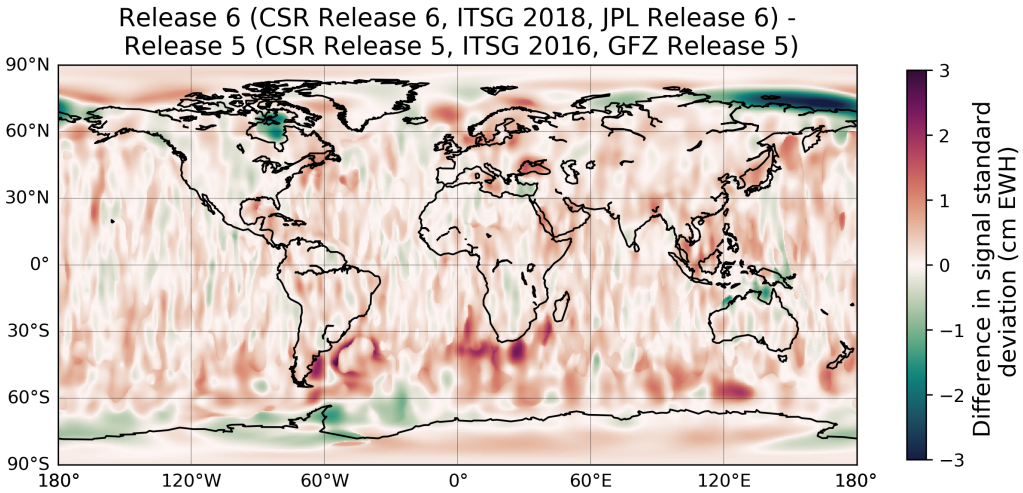

Figure 3.15: Difference in estimated signal standard deviation for GRACE Release 6 (CSR Release 6, ITSG 2018, JPL Release 6) solutions and GRACE Release 5 solutions (CSR Release 5, ITSG 2016, GFZ Release 5).

Table 3.7: Regional averages of estimated noise standard deviation in cm EWH for different GRACE Level-2 data and different VCE setups. The VCE setups differ in the number of considered time-series (one or three) in the estimation process.

GRACE Level-2 data	CSR Release 6		ITSG 2018		JPL Release 6	
No. of considered time-series	3	1	3	1	3	1
Regularization technique	MYDD		MYDD		MYDD	
Total area	1.188	1.501	1.047	1.314	1.618	1.961
Only ocean	1.200	1.448	1.071	1.298	1.654	1.919
Only land	1.156	1.628	0.982	1.353	1.524	2.060
Arafura Sea	1.707	2.543	1.162	1.860	1.702	2.509
Arctic Ocean	0.990	1.555	0.639	1.235	0.828	1.453
Baltic Sea	0.995	2.441	0.956	2.315	1.165	2.429
Black Sea	1.097	2.969	0.999	2.772	1.463	3.197
Gulf of Thailand	1.330	2.011	1.102	1.763	1.792	2.435
Indian Ocean	1.243	1.466	1.094	1.303	1.663	1.917
Mediterranean Sea	1.205	1.643	1.070	1.484	1.762	2.268
North Atlantic Ocean	1.211	1.384	1.094	1.265	1.810	2.009
North Pacific Ocean	1.180	1.363	1.064	1.238	1.650	1.869
South Atlantic Ocean	1.192	1.574	1.143	1.494	1.707	2.082
South China and Archipelagic Seas	1.311	1.692	1.061	1.397	1.773	2.213
South Pacific Ocean	1.207	1.361	1.128	1.263	1.738	1.929
Southern Ocean	1.201	1.544	0.807	1.115	1.212	1.568
Africa	1.233	1.672	1.054	1.369	1.793	2.297
Antarctica	0.905	1.138	0.557	0.782	0.797	1.082
Australia	1.317	1.818	1.023	1.445	1.790	2.264
Eurasia	1.091	1.540	0.954	1.330	1.428	1.897
Greenland	0.927	1.062	0.586	0.773	0.828	1.112
North America	1.126	1.462	0.866	1.175	1.341	1.801
South America	1.306	2.153	1.302	1.858	1.819	2.812

Table 3.8: Regional averages of estimated signal standard deviation in cm EWH for different GRACE Level-2 data and different VCE setups. The VCE setups differ in the number of considered time-series (one or three) in the estimation process.

GRACE Level-2 data	CSR Release 5, GFZ Release 5, ITSG 2016	CSR Release 6, ITSG 2018, JPL Release 6	CSR Release 6	ITSG 2018	JPL Release 6
Total area	1.338	1.442	0.821	0.864	0.787
Only ocean	0.864	0.994	0.321	0.361	0.302
Only land	2.096	2.190	1.449	1.512	1.391
Arafura Sea	2.837	2.195	0.572	0.794	0.665
Arctic Ocean	2.236	1.843	0.474	0.525	0.488
Baltic Sea	3.210	3.666	0.617	0.566	0.559
Black Sea	3.518	4.690	1.159	1.169	1.170
Gulf of Thailand	1.661	2.455	1.158	1.082	1.190
Indian Ocean	0.576	0.871	0.275	0.311	0.265
Mediterranean Sea	1.431	1.541	0.610	0.673	0.635
North Atlantic Ocean	0.614	0.781	0.357	0.387	0.337
North Pacific Ocean	0.602	0.753	0.266	0.304	0.238
South Atlantic Ocean	0.953	1.352	0.276	0.306	0.244
South China and Archipelagic Seas	1.023	1.326	0.571	0.686	0.509
South Pacific Ocean	0.434	0.609	0.160	0.211	0.123
Southern Ocean	1.218	1.112	0.359	0.414	0.352
Africa	1.764	1.860	1.117	1.278	1.048
Antarctica	1.140	1.168	0.709	0.741	0.699
Australia	2.147	2.135	1.362	1.444	1.355
Eurasia	1.790	1.943	1.155	1.204	1.122
Greenland	1.672	1.650	1.385	1.362	1.319
North America	2.009	2.001	1.392	1.487	1.349
South America	3.655	3.809	2.767	2.787	2.636

Again it can be observed that the noise standard deviation decreases towards the poles. The estimated noise in Release 6 solutions is in general estimated lower than for the Release 5 solutions. This might be due to a better performance of the background models or improved data processing techniques. From the three considered GRACE Release 6 solutions, the estimated noise is again the lowest for CSR and ITSG.

When looking at the signal standard deviation for Release 6 (figure 3.14) and the difference in signal standard deviation between Release 5 and 6 (figure 3.15), it can be observed that the signal standard deviation goes down for the Hudson Bay, the East Siberian Arctic Shelf, the Gulf of Carpentaria and parts of the Arctic and Southern Ocean. In other regions no improvements can be observed. The region south to Africa shows a clear increase of the signal of interannual variability compared to the Release 5 solutions. One could think that the oceanic background models considered for Release 6 perform worse in this area. Since the estimated signal standard deviation is influenced by the noise level, comparing the estimated signal standard deviations for Release 5 to Release 6 is not totally correct. A larger cross-correlation between different products (which can also be a cross-correlation in noise) will result in less applied regularization and thus a higher signal standard deviation. It could

be that the three Release 6 solutions are more cross-correlated and that less regularization is applied for these solutions which causes higher values of signal standard deviation. But regions which show a very strong sign of reduction or increase of the signal standard deviation might still give an indication where the different Releases are better or worse. When even correlations can be found to a different type of unexpected signals (as will be done in the section which is about residuals in ITSG solutions), the distribution of estimated signal standard deviation can become more reliable. When considering one instead of three mass-anomaly time-series in the VCE a similar observation can be made that a large part of the estimated signal standard deviation then shows up increased noise.

In figure 3.16 the signal standard deviation is shown versus bathymetry. It can be observed that the patterns of signal standard deviation versus bathymetry are very similar for release 5 and 6 but that the estimated signal standard deviation for Release 6 is in general higher. A larger signal standard deviation can be observed for the shallowest regions. Also when a buffer zone is included the signal standard deviation is larger for the shallow regions. A larger signal standard deviation in shallow regions might thus not only be due to leakage signals from the continents. It must be kept in mind that these estimated signal standard deviations are influenced by the noise level. Therefore, no strong conclusions can be made with just these estimated signal variances.

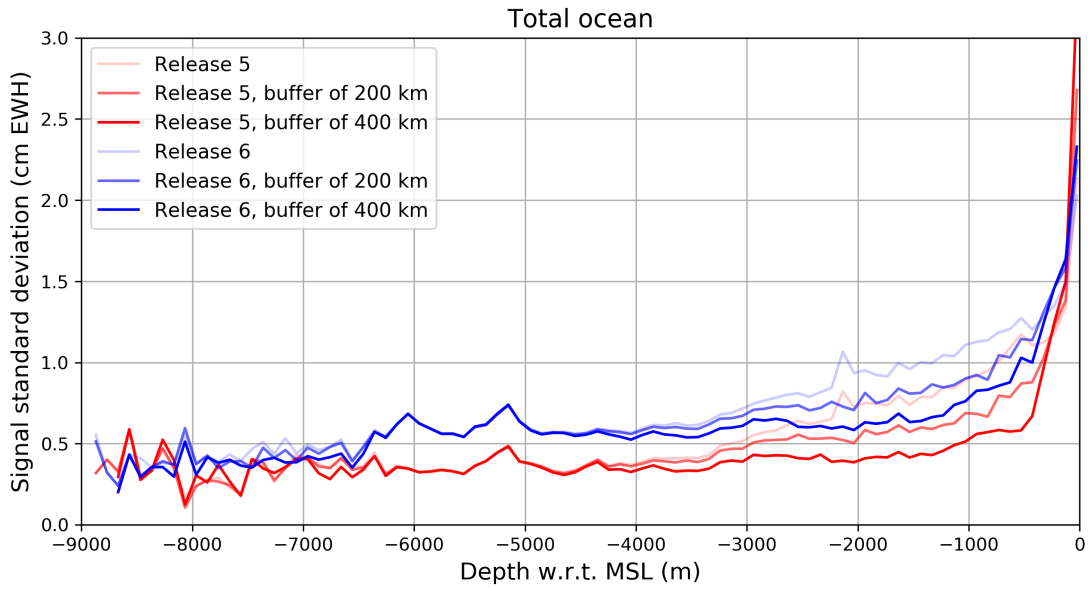

Figure 3.16: Estimated signal standard deviation for GRACE Release 6 (CSR Release 6, ITSG 2018, JPL Release 6) solutions and GRACE Release 5 solutions (CSR Release 5, ITSG 2016, GFZ Release 5). The estimated signal standard deviation for Release 5 (red) and Release 6 (blue) are shown versus bathymetry for the total ocean.

Estimation of non-seasonal residuals in ITSG solutions

In figures 3.17 and 3.18 the RMSE for the ITSG monthly solutions (ITSG-2016 and ITSG-2018) is shown. This is the RMSE of the monthly time-series with respect to a seasonal signal. This seasonal signal is estimated by least-squares estimated and a combination of a linear trend and a semi-annual and annual variability. Figure 3.19 shows the difference between figures 3.17 and 3.18. In table 3.9 regional average RMSE's for the considered oceanic regions can be found. By comparing the global plots of estimated signal standard deviation with the global plots of RMSE for the ITSG solutions similar global patterns are observed. The East Siberian Arctic Shelf, Baltic Sea, Black Sea, Argentine Basin, Hudson Bay, Gulf of Thailand and Argentine Basin show both a high RMSE as well as a high signal standard deviaton for Release 5. For Release 6, both the signal standard deviation as well as the RMSE decrease clearly for the regions Hudson Bay, the East Siberian Arctic Shelf and Arafura Sea with respect to Release 5. It is not strange that there is much correlation between regions of high/low RMSE and signal standard deviation. The signal standard deviation gives an indication of the amount of interannual differences in the mass-derivative and the RMSE gives an indication of the size of the residuals w.r.t. a seasonal signal. The non-seasonal residuals are likely varying over the years although this does not have to be the case. The other way around, areas of larger estimated signal variance

should (if correctly estimated) show up as residuals with respect to a seasonal signal. If the estimated signal variance are primary due to non-ITSG monthly solutions this correlation does not hold.

Except for the Black Sea the RMSE goes down for ITSG 2018 with respect to ITSG 2016. For a large extent this can be due to a decrease of the noise in Release 6 solutions with respect to Release 5 solutions. The regions of extreme improvement over the oceans (Hudson Bay, East Siberian Arctic Shelf and Arafura Sea) seem likely due to a change of oceanic background models.

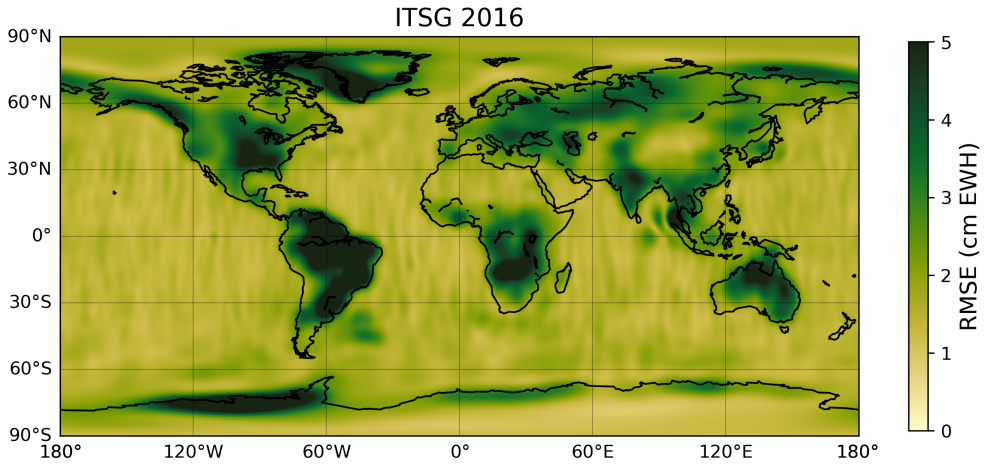

Figure 3.17: Estimated RMSE for ITSG 2016. The RMSE is estimated with respect to a by least-squares estimated signal containing only a linear trend and annual and semi-annual periodicity.

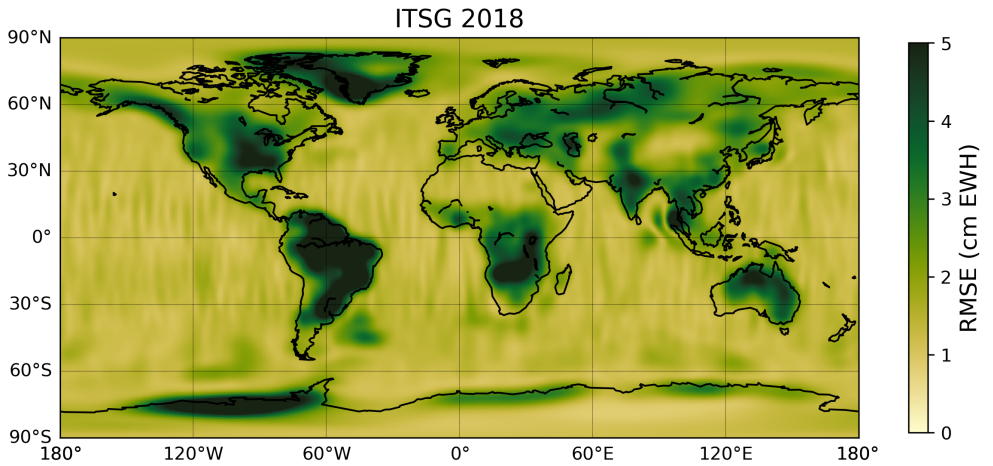

Figure 3.18: Estimated RMSE for ITSG 2018. The RMSE is estimated with respect to a by least-squares estimated signal containing only a linear trend and annual and semi-annual periodicity.

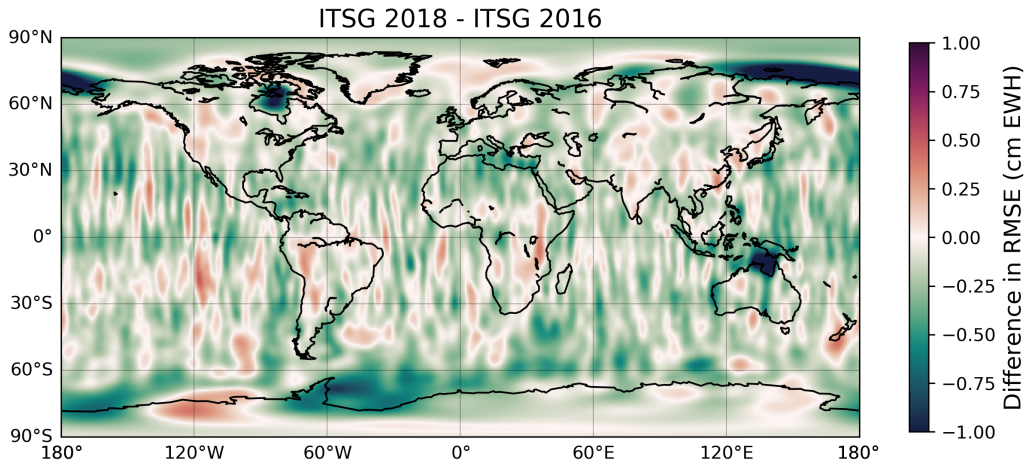

Figure 3.19: Difference in estimated RMSE between ITSG 2018 and ITSG 2016. The RMSE is estimated with respect to a by least-squares estimated signal containing only a linear trend and annual and semi-annual periodicity.

In figures 3.20 the estimated RMSE for ITSG 2016 and ITSG 2018 are shown versus bathymetry for the total ocean. As for the estimates of signal standard deviation, the RMSE patterns versus bathymetry are quite similar for the different releases and only of different magnitude. Also an increase of RMSE in shallow regions can be observed. When observing figures of RMSE versus bathymetry for specific regions, the South Pacific Ocean (figure 3.21) shows a clear difference between ITSG 2016 and ITSG 2018. For the shallow regions up to about 750 m the non-seasonal residuals are larger for ITSG 2018 with respect to ITSG 2016. This might be the region below New Zealand which corresponds to this depth and shows a larger non-seasonal residuals for ITSG 2018.

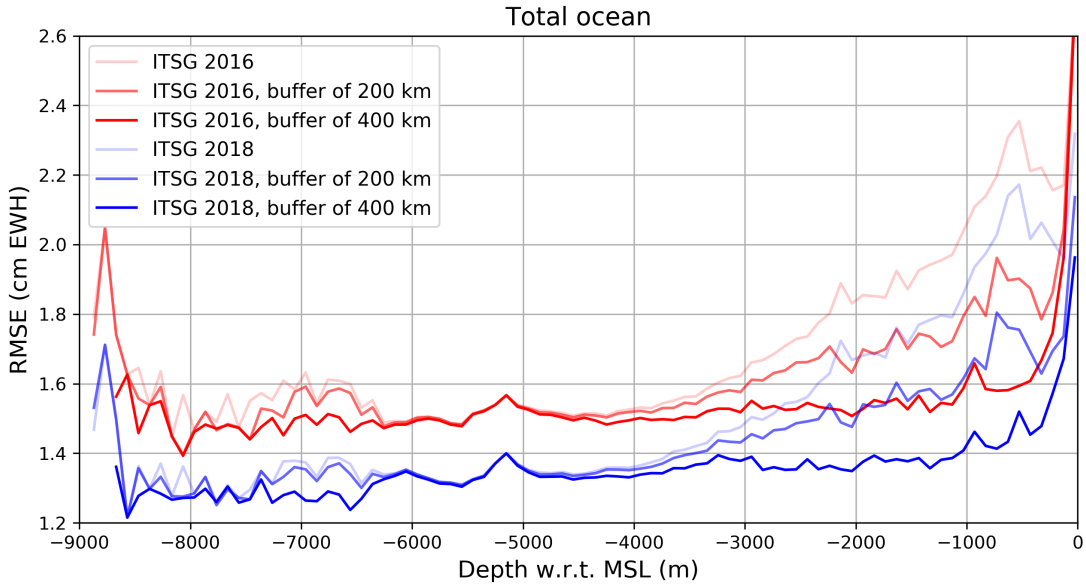

Figure 3.20: Estimated RMSE for ITSG solutions versus bathymetry for the total ocean. The RMSE is estimated with respect to a by least-squares estimated signal containing only a linear trend and annual and semi-annual periodicity.

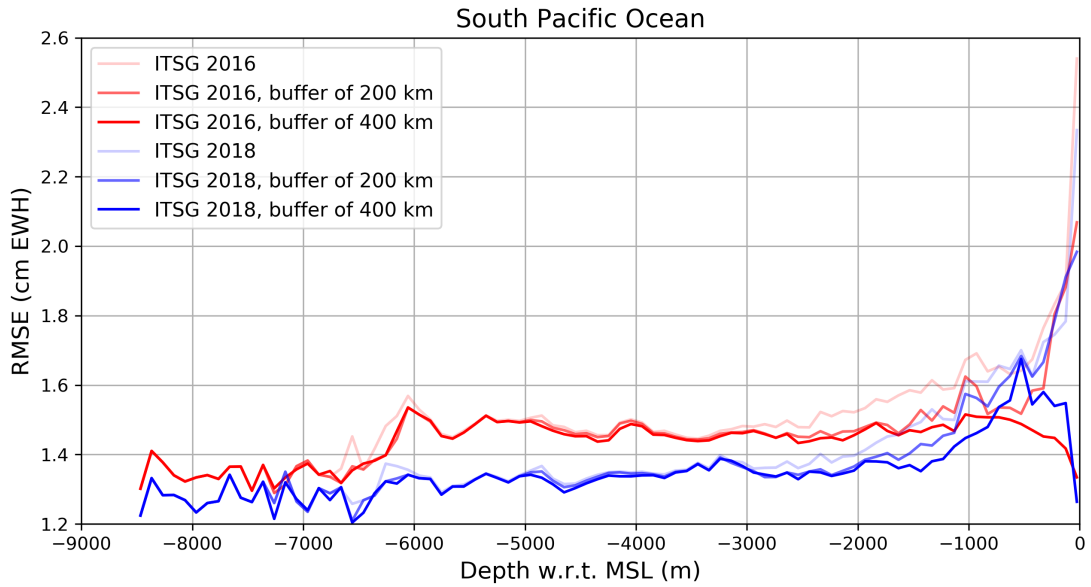

Figure 3.21: Estimated RMSE for ITSG solutions versus bathymetry for the South Pacific Ocean. The RMSE is estimated with respect to a by least-squares estimated signal containing only a linear trend and annual and semi-annual periodicity.

Regarding the estimation of signal standard deviation and computation of RMSE for ITSG solutions it must be said these quantities do not always indicate regions of lower or higher quality. First of all the estimates of signal variance might not correlate to the true signals variance. Furthermore, a part of these estimates (signal standard deviation and RMSE w.r.t. a seasonal signal) might be a true mass-anomaly signal. For example, the seasonal periodicity might be shifted in time between the years and might be of different size for different size due to for example an increased melt for a certain year. Periodicities of more than a year will show up in the true signal standard deviation and non-seasonal residuals. It might be better not to categorize these long-term patterns as an unexpected signal/residual over the oceans.

Estimation of high-frequency residuals in ITSG solutions

In this section again RMSE values for ITSG are shown. Now the RMSE is computed with respect to a low-passed monthly time-series. By this, regions of high-frequency residuals (frequencies larger than 2 cycles per year) can be identified. With respect to the previous two sections this might give different results since now signals of a periodicity larger than a year will not show up as an unexpected residual.

In figures 3.22,3.23,3.24 the RMSE values with respect to the low-pass filtered signal can be observed. The regional values of RMSE for oceanic regions can be found in table 3.9. Most regions of high non-seasonal residuals and high-frequency residuals are similar. Therefore, also the regions of large high-frequency residuals correlate with the global patterns of signal variance. The size of the unexpected residuals is reduced when changing from non-seasonal to high-frequency residuals. This is logical since all low-frequency signals of a periodicity larger than a half year are no part of the residuals w.r.t. the low-pass filtered signal.

The the Arafura Sea seems an exemption in the correlation between non-seasonal and high-frequency residuals. For the Arafura Sea, the non-seasonal residuals dropped down by 33% while the high-frequency residuals dropped down by only 15%. This might indicate a reduction of low-frequency signal over the Arafura Sea for ITSG-2018 w.r.t. ITSG-2016.

Table 3.9: Regional averages of the RMSE in cm EWH for ITSG monthly solutions. The RMSE in column 2 and 3 is estimated with respect to a by least-squares estimated signal containing only a linear trend and annual and semi-annual periodicity. The RMSE in column 4 and 5 is estimated with respect to a low-pass filtered signal (frequencies smaller than or equal to the semi-annual cycle are retained).

	RMSE w.r.t. seasonal signal		RMSE w.r.t. low-pass filtered signal	
	ITSG 2016	ITSG 2018	ITSG 2016	ITSG 2018
Total Ocean	1.745	1.577	1.248	1.076
Arafura Sea	3.523	2.437	2.169	1.854
Arctic Ocean	2.430	2.159	1.811	1.567
Baltic Sea	2.819	2.748	2.011	1.933
Black Sea	3.878	3.869	1.922	1.973
Gulf of Thailand	3.742	3.691	2.036	1.792
Indian Ocean	1.684	1.506	1.206	1.014
Mediterranean Sea	2.309	2.012	1.444	1.172
North Atlantic Ocean	1.689	1.539	1.221	1.075
North Pacific Ocean	1.583	1.415	1.180	1.003
South Atlantic Ocean	1.744	1.627	1.274	1.152
South China and Archipelagic Seas	2.280	2.091	1.351	1.126
South Pacific Ocean	1.504	1.378	1.130	0.989
Southern Ocean	1.969	1.705	1.334	1.057

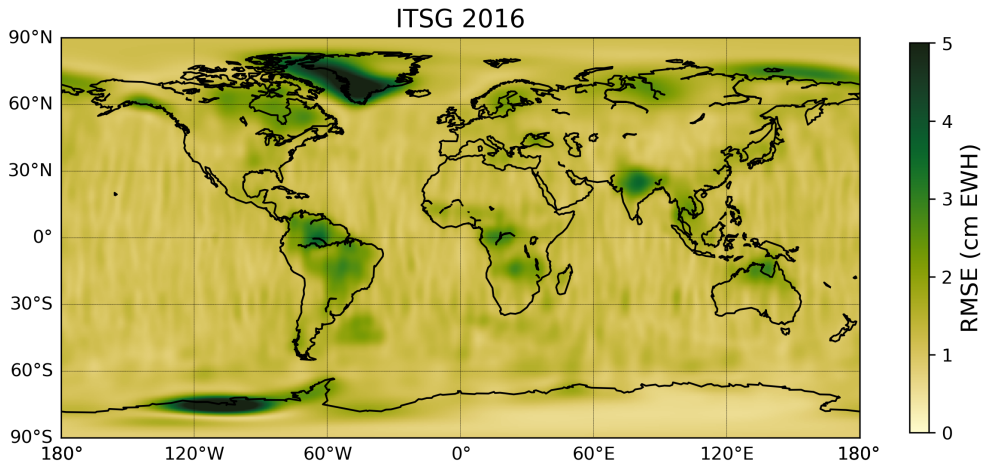

Figure 3.22: Estimated RMSE for ITSG 2016. The RMSE is estimated with respect to a low-pass filtered signal (frequencies smaller than or equal to the semi-annual cycle are retained in the low-pass filtered signal).

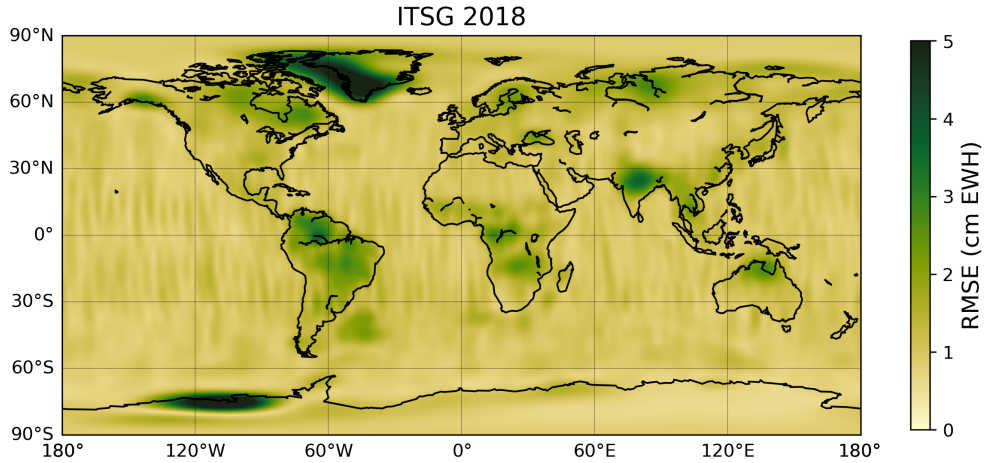

Figure 3.23: Estimated RMSE for ITSG 2018. The RMSE is estimated with respect to a low-pass filtered signal (frequencies smaller than or equal to the semi-annual cycle are retained in the low-pass filtered signal).

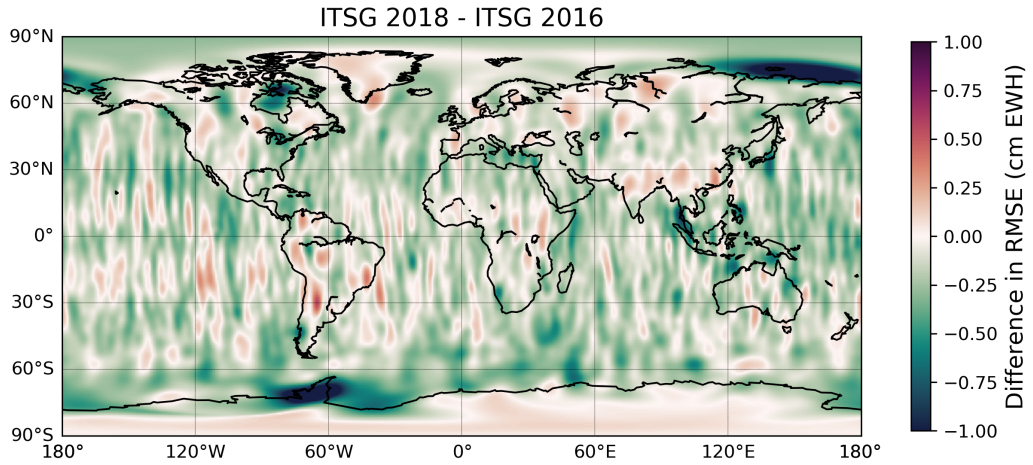

Figure 3.24: Difference in estimated RMSE between ITSG 2018 and ITSG 2016. The RMSE is estimated with respect to a low-pass filtered signal (frequencies smaller than or equal to the semi-annual cycle are retained in the low-pass filtered signal).

In figures 3.25 and 3.26 the estimated RMSE for ITSG 2016 and ITSG 2018 are shown versus bathymetry for the total ocean and Southern Ocean. It can also be observed that the computed RMSE's for ITSG 2018 are in general lower than for ITSG 2016 over the whole range of depths. From both the figures of RMSE versus bathymetry and global plotted RMSE it can be seen that in general the high-frequency signal is lower for Release 6 than for Release 5. Since this is a general pattern over almost the whole ocean it seems that this is largely due to a general noise reduction for Release 6 with respect to Release 5.

Again the RMSE does increase for the shallow regions when observing the RMSE versus bathymetry for the total ocean. For the South Pacific Ocean an exception can be observed. The shallow regions (respectively up to 1 km and 500 m) of the South Pacific Ocean seem to contain less high-frequency residuals than the deeper regions for ITSG 2016 and ITSG 2018.

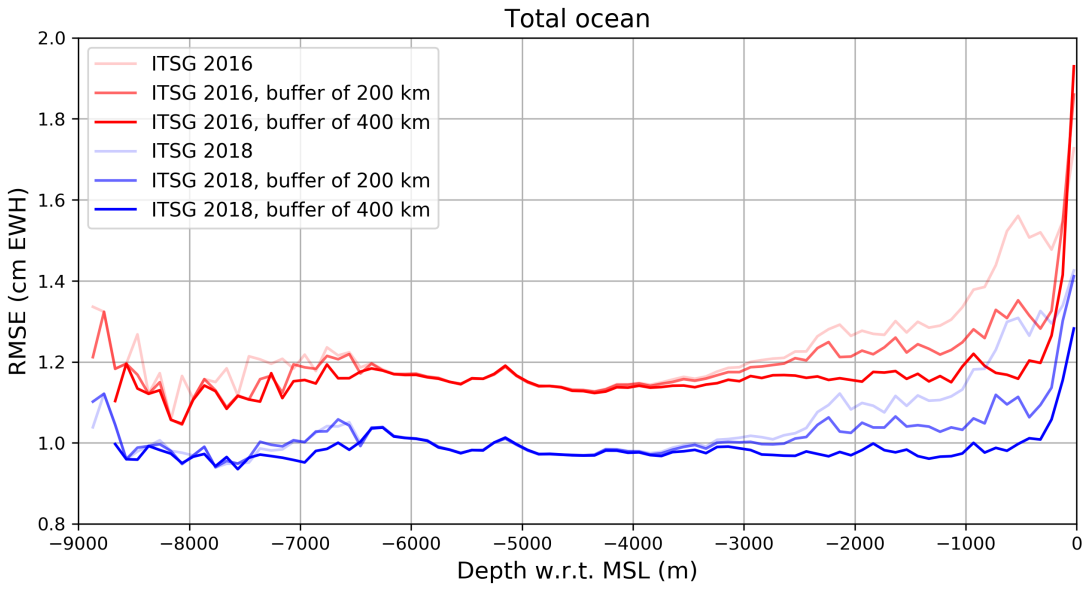

Figure 3.25: Estimated RMSE for ITSG solutions versus bathymetry for the total ocean. The RMSE is estimated with respect to a low-pass filtered signal (frequencies smaller than or equal to the semi-annual cycle are retained).

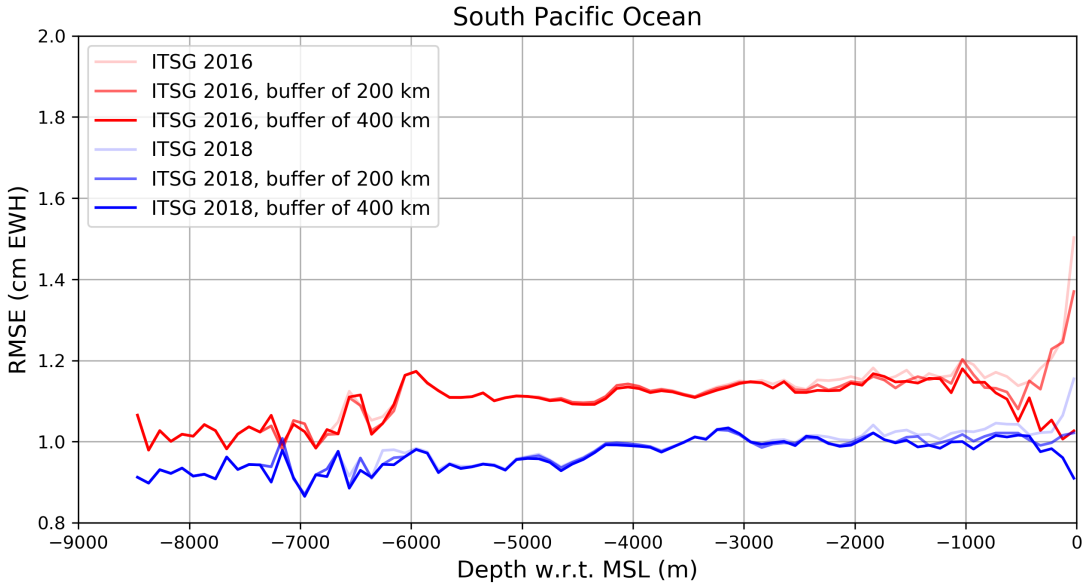

Figure 3.26: Estimated RMSE for ITSG solutions versus bathymetry for the South Pacific Ocean. The RMSE is estimated with respect to a low-pass filtered signal (frequencies smaller than or equal to the semi-annual cycle are retained).

3.4. Summary and remarks

For GRACE Release 5 solutions the estimated noise is the lowest for ITSG 2016 after which CSR Release 5 and GFZ Release 5 follow. For GRACE Release 6 solutions the estimated noise is the lowest for ITSG 2018 after which CSR Release 6 and JPL Release 6 follow. The estimated noise generally reduces towards the poles. When one instead of three mass-anomaly time-series is considered in the VCE global patterns of estimated signal standard deviation show up as global patterns in the estimated noise standard deviation.

Over the oceans, the signal standard deviation is largest for the regions: Baltic Sea, Black Sea, Arafura Sea (including Gulf of Carpentaria), East Siberian Arctic Shelf, Argentine Basin and Hudson Bay. Although the estimates of signal standard deviation are influenced by the noise level (as observed in the previous chapter), areas of large signal standard deviation might indicate oceanic regions where the quality of the GRACE monthly solutions is lower. Especially, because the global patterns of estimated signal standard deviation correlate with the global patterns of the residuals w.r.t. to a low-pass

filtered signal and seasonal signal for ITSG solutions. GRACE Release 6 solutions show with respect to Release 5 a significant decrease in signal standard deviation over for the Hudson Bay and East Siberian Arctic Shelf. These areas also show a significant decrease in both types of residuals.

Since the estimated signal standard deviation and RMSE's are non-zero over the oceans, the GRACE Level-2 data products are still in need for improvement over the oceanic regions and especially in the shallow regions (up to 200 m, which include the Baltic Sea, East Siberian Arctic Shelf, Gulf of Thailand and Arafura Sea), the Argentine Basin and the Black Sea. Signal leakage from land to ocean might cause an increase of the estimated signal standard deviation and residuals in the coastal areas.

4

Comparison of GTSM to oceanic background models currently used in GRACE data processing

This chapter is about the third sub-question:

- Which regions show significant differences between 3-hourly, 6-hourly and monthly mass-anomaly time-series generated by GTSM and those generated by the oceanic background models currently used in GRACE data processing?

This question is assessed because this gives an indication of the regions where GTSM performs significantly differently from the currently used oceanic background models. These regions are the ones where the use of GTSM can potentially alter GRACE monthly solutions. After a short introduction about oceanic processes, GTSM will be introduced. Thereafter which theoretical differences between GTSM and the currently used oceanic background models are listed. Then the method to create mass-anomaly time-series (3-hourly, 6-hourly and monthly) from raw GTSM output is described. For the monthly time-series also the method to convert the mass-anomaly time-series to the spherical domain is described. Finally, the time-series comparison is performed and regions of large differences are identified.

4.1. Theory

In this theoretical section first some basic knowledge about ocean variability is provided. After this, GTSM will be described. Then the currently used oceanic background models are described and differences in the modeling strategy are listed.

4.1.1. Ocean variability

In GRACE data processing oceanic background models are used to remove rapid oceanic signals from the measurements. As a result the oceanic signal observed in GRACE monthly solutions would ideally only contain mass exchange between continents and ocean and self-attraction and loading effects. Each ocean variability which should be removed is listed below [42]:

- Tides. Tides of many frequencies exist due to the combined gravitational forces of the Sun and Moon. The tidal constituents can be categorized in semidiurnal, diurnal and long-period. Although the tide generating forces are well known, the tidal ranges and phases depend on location. The shape, size and depth of a sea or ocean basin determines to a high extent the tidal range at a certain location.
- Storm surges. Storm surges are pressure and wind driven changes of the water elevation with a spatial scale similar to the storm which generates the surge. The wind for a storm surge is

sustained and has a constant direction [2]. Compared to tides, the characteristic time is generally shorter and the area smaller.

- Density-driven currents. When density-driven currents induce changes in the oceanic bottom pressure these should be removed from GRACE data. An example of a large-scale density-driven current is the thermohaline circulation.

Furthermore, all processes listed above influence each other and non-linear interaction between these effects exists. For GRACE Release 5 and Release 6 monthly solutions separate oceanic background models are used to model the tidal and non-tidal part of ocean currents. In GTSM storm surges and tides are modeled at the same time by which non-linear interaction between these two processes is taken into account. On the other hand, in GTSM density-driven currents are not modeled since the water density in GTSM is constant.

4.1.2. Global Tide and Surge Model

The Global Tide and Surge Model (GTSM) simulates 2D hydrodynamics on a global scale as it is a global application of Delft3D-FM [44] [6]. The Delft3D Flexible Mesh software is developed by Deltares. GTSM is a 2-dimensional application of this software. By this 2D model water depth is calculated for each grid cell [6]. The variables in the governing equations are depth-averaged [6]. Since GTSM is a 2-dimensional model and thus the density for a water column is constant, it is categorized as a barotropic model. GTSM models flow and transport phenomena due to tidal and meteorological forcing.

Governing equations

In GTSM the governing equations are [41] [19] [44]:

$$\frac{\partial h}{\partial t} + \nabla \cdot (h\mathbf{u}) = 0 \tag{4.1}$$

$$\begin{aligned} &\frac{\partial \mathbf{u}}{\partial t} + \mathbf{f} \times \mathbf{u} + \frac{1}{h}\left(\nabla \cdot (h\mathbf{u}\mathbf{u}) - \mathbf{u}\nabla \cdot (h\mathbf{u})\right) = \\ &- g\nabla\left(\xi - \xi_{EQ} - \xi_{SAL}\right) + \nabla \cdot \left(\nu\left(\nabla\mathbf{u} + \nabla\mathbf{u}^T\right)\right) + \frac{\tau_B}{h} + \frac{\tau_{IT}}{h} + \frac{\tau_w}{\rho_w h} - \frac{1}{\rho_w}\nabla p_{atm} \end{aligned} \tag{4.2}$$

Equation 4.1 is the conservation equation for mass. Since the water mass is constant in GTSM (there are no sources of addition or removal of water), the right term in equation 4.1 is 0. Equation 4.2 is the conservation equation for momentum. The term h is the instantaneous water depth (the water column height). The velocity vector is represented by $\mathbf{u}$, the time by t, the horizontal viscosity by ν, gravity (which is constant in the model) by g, the *water level* (which is the water column minus the bathymetry) by ξ, the water density by ρ_w and the effect of the Coriolis force by $\mathbf{f}\times\mathbf{u}$ where $\mathbf{f} = 2\Omega$ with Ω the Earth rotation vector. When $\mathbf{u}$ is represented as a combination of a velocity in the East and North direction, the term $\mathbf{f}\times\mathbf{u}$ becomes $\mathbf{f}\times\mathbf{u} = 2\omega\sin(\phi)\begin{bmatrix}0 & -1\\ 1 & 0\end{bmatrix}\mathbf{u}$. When no forcing is applied the *water level* ξ is at each location 0. Therefore the internal vertical reference for the model is an equipotential surface.

The dissipation terms are τ_B and τ_{IT}. The term τ_B represents dissipation through bottom friction which is the main mechanism of dissipation in shallow waters. [41] The term τ_{IT} represents dissipation through internal tides. This dissipation mechanism is dominant in deep waters where tides travel across a steep topography and where the water is stratified. [41] The tidal period oscillations which arise in the surfaces of equal density induce flow in different directions at different depths. [2] So it can be clear that the internal tidal currents and the associated dissipation is parametrized.

The term ξ_{EQ} represents the equilibrium tide which can be computed from the tide generating forces. The term ξ_{SAL} is related to self-attraction and loading (SAL). In the model the self-attraction is related to the gravitational attraction of the water on itself. The loading is the deformation of the ocean floor due to the weight of the ocean column. In GTSM the SAL effects are modeled by implementing the SAL equations as published by Kuhlmann et al. [46]. [18] No actual deformation of the ocean bottom floor is modeled and the bathymetry is kept constant in the model. The *water level* output of GTSM thus represents the decrease/increase of the total water column (h) and does not include changes in

ocean bottom floor (the loading effect). SAL effects like the attraction of water to large mass changes like those due to ice sheet melting are not included in the model.

Two terms $\frac{\tau_w}{\rho_w h}$ and $-\frac{1}{\rho_w}\nabla p_{atm}$ in the momentum equation represent the effect of the wind and atmospheric pressure. These terms will be discussed in the next section. Of course equation 4.2 is limited and much more terms are present there. These are for now neglected because their role is considered minor.

Meteorological forcing

The meteorological forcing in GTSM is derived from the ERA5 meteorological reanalysis product [36] of the European Center for Medium-range Weather Forecast (ECMWF). This product is available at hourly sampling and 31 km resolution. The ERA5 meteorological data are interpolated to a 0.3° grid. This 0.3° grid of wind and pressure data is applied as meteorological forcing in GTSM.

The influence of the wind on the flow is implemented as a shear stress (τ_w). [20] This shear stress is computed from the wind speed at 10 m above the surface, density of air and a wind drag coefficient. This wind drag coefficient is computed computed according to the Charnock formulation [14] and for this a Charnock coefficient should be implemented in GTSM. The Charnock coefficient used in this model is 0.041. The term $-\frac{1}{\rho_w}\nabla p_{atm}$ represents the influence of the atmospheric pressure. [19] Because of the minus term in from to the gradient in atmospheric pressure (p_{atm}), a locally high pressure region will lead to a flow away from this region.

Bathymetry and computational grid

The bathymetry in GTSM is implemented as the depth with respect to mean sea level. The bathymetry data are a combination of different sources. The General Bathymetric Chart of the Ocean 2014 (GEBCO 2014) [73] is used as main data source. For Europe and the region around Australia the EMODnet bathymetry [1] and a dataset of Whiteway [75] are implemented. [6] For regions to the south of -60° latitude the Bedmap2 dataset [31] is used to incorporate regions below the permanent ice shelves near Antarctica. These regions are considered as ocean in the modeling. The bathymetric data are consequently interpolated onto the computational grid. [51] The bathymetry implemented in GTSM can be found in figure 4.1. This figure is made by subtracting for a certain time-step the *water level* from the instantaneous water column height.

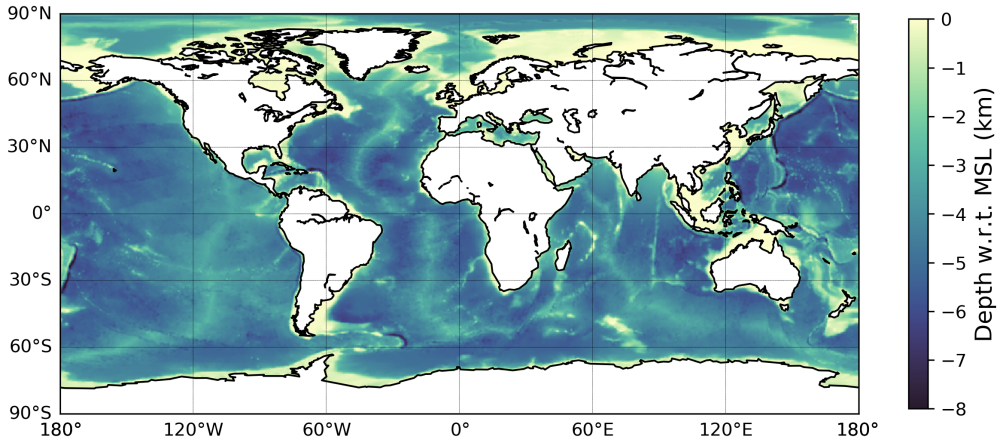

Figure 4.1: Bathymetry in GTSM.

The Delft3D-FM software allows for a flexible and unstructured grid. The grid cells are of different size for different areas. The size of the grid cells depends on the bathymetry. For deep regions the grid cells have a resolution of about 50 km and for shallow regions the grid cells have resolution of about 5 km. [51] Furthermore, for regions where the gradient of the topography is large the grid cells are also refined. [41] This improves the modeling of dissipation due to internal tides. The combination of small grid cells in shallow and topographically complex regions and larger grid cells for the deep ocean gives a good combination of computational time and accurate modeling. The unstructured grid is built up of

triangles and quadrangles. In figure 4.2 the refinement towards the shallow regions can be seen. The coordinate reference system for GTSM is WGS84 and the latitude in GTSM is thus a geodetic latitude.

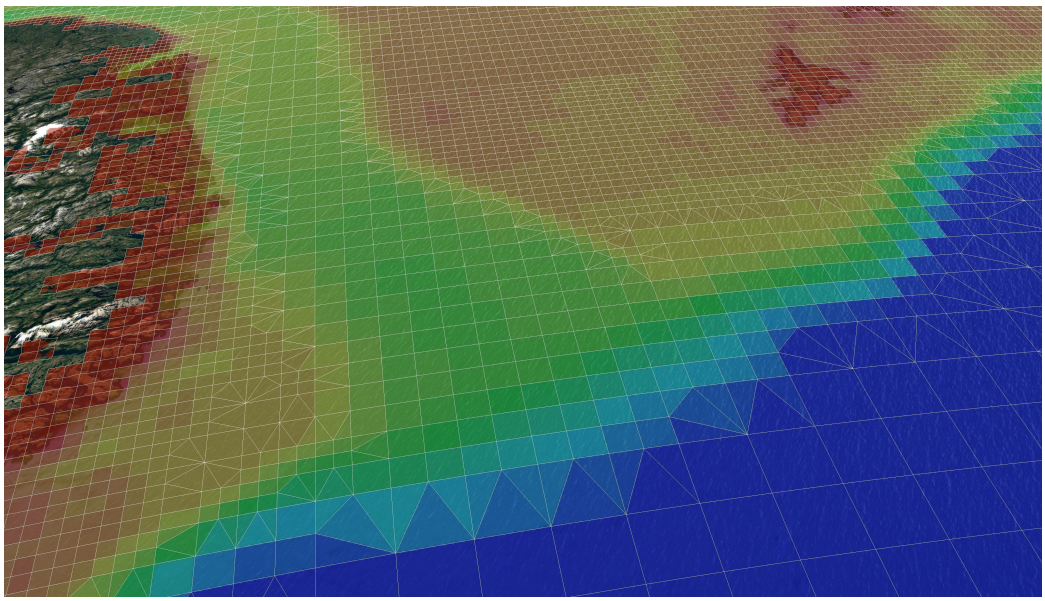

Figure 4.2: Grid densification in shallow regions in GTSM (blue represents deep regions, red represents shallow regions).

4.1.3. Atmosphere and Ocean non-tidal De-aliasing product

The Atmosphere and Ocean non-tidal De-aliasing product (AOD1B) product contains an oceanic and atmospheric part. Only the oceanic part is considered in this research. The oceanic part is constructed by the use of an oceanic background model which is different for the different for AOD1B Release 5 and 6. These oceanic background models which model the non-tidal changes in oceanic bottom pressure are discussed in this section.

For the AOD1B Release 5 product the Ocean Model for Circulation and Tides (OMCT) is used [30]. OMCT is a baroclinic model [79]. For the AOD1B Release 6 product the Max-Planck-Institute for Meteorology Ocean Model (MPIOM) is used [26]. This model is also a baroclinic ocean circulation model. In a baroclinic ocean model the density can be different for different water depths. The changes in vertical density distribution and their influences on the flow are included in the model. [29] In MIPIOM also precipitation and radiation are included to account for thermodynamic processes. An example of a primarily baroclinic phenomenon is an El Niño. In table 4.1 differences between the three models (GTSM, OMCT and MPIOM) are listed.

Table 4.1: Differences between the ocean models OMCT, MPIOM and GTSM [30] [26] [56] [6] [41] [51] [35].

Ocean model	OMCT	MPIOM	GTSM
Dimensions	3D	3D	2DH
Spatial resolution	1.0° x 1.0° grid, 20 vertical layers	1.0° tri-polar grid, 40 vertical layers	Locally refined grid: 5-50 km
Temporal resolution	20 minutes	90 minutes	Up to 2.5 minutes
Topography	ETOPO5	ETOPO5	Combination of GEBCO 2014, EMODnet, dataset of Whiteway [75] and Bedmap2
Spin-up time	265 years followed by real-time simution of 12 years	499 years followed by real-time simulation of 21 years	real-time simulation of 16 days
Atmospheric data for the period 2001-2016	Operational analysis data from ECMWF Integrated Forcast System (IFS) (data extracted every 6 hours at 0.5° grid)	2001-2006: ECMWF ERA-Interim re-analysis data (3-hourly available from short-term forecasts from the reanalysis at 0.75° grid)	ECMWF ERA5 reanalysis data (available every hour at a spatial resolution of 31 km)
		2007-2016: Operational analysis data from ECMWF IFS	
Atmospheric forcing	Atmospheric surface pressure	Atsmospheric surface pressure	Atmospheric pressure
	Horizontal wind speed and direction at 10 m	Horizontal wind speed and direction at 10 m	Horizontal wind speed and direction at 10 m
	Temperature at 2 m	Temperature at 2 m	
	Temperature at 10 m	Dew point at 2 m	
	Sea surface temperature	Short-wave incoming radiation at the surface	
	Freshwater fluxes (precipitation minus evaporation)	Precipitation	
	Specific humidity	Cloud cover	
Includes a dynamic-thermodynamic sea ice model	Yes	Yes	No
Simulation of ocean dynamics under the Antarctic ice -shelves	Yes	No	Yes (considered as ocean)
Conservation equations for heat and salt	Yes	Yes	No
Includes SAL effects (self-attraction of the water column on itself and deformations of the sea-floor)	Yes	No	Yes

The method to compute the AOD1B product from the ocean model output is now described in order to be able to compute a similar product from the model output of GTSM. Two types of AOD1B products are produced. One at an hourly time-scale and one of monthly mean values. The months over which averages are taken to compute the monthly means are determined in according to the days

considered to create the GRACE Level-2 data product. Therefore, every research center provides their own monthly de-aliasing products since the considered days for each month to produce the GRACE Level-2 data product differs for each research center. The monthly AOD1B products are thus based on the same time-series but the considered days in a month to compute the monthly mean is different for each research center.

To create the AOD1B Release 5 product OMCT is run without taking into account tidal induced ocean dynamics. The OMCT is thus run to simulate oceanic mass-redistribution's due to thermohaline and wind- and pressure driven circulation. To create the AOD1B OBA Release 5 product (6-hourly) and AOD1B GAD Release 5 product (monthly) the following steps are followed [30]:

- Running the model and storing the atmospheric and water column contribution to the oceanic bottom pressure (OBP) separately and 6-hourly at the 1° grid of the model. The epochs are 0h, 6h, 12h, 18h.
- Computation of block mean values of the water column contribution to the OBP.
- Interpolation of the water column contribution to OBP to a 0.5° grid.
- Removal of the long-term mean (the mean of the years 2001-2002) for each location.
- Removal of the ocean mean water column contribution to the OBP at each time. This is the mean in space.
- Computation of block mean values of the atmospheric surface pressure (the input) at the 0.5° grid.
- Removal of the long-term mean (the mean of the years 2001-2002) of the atmospheric surface pressure time-series at each location.
- Removal of the mean atmospheric pressure for the whole Earth at each time step.
- Combination of the residual water column contribution to the OBP and the residual atmospheric surface pressure. This combination represents the inverse barometric correction.
- Removal of the S2 tide from the 6-hourly time-series at each location.
- Land regions are assigned 0 Pa.
- Conversion of the total OBP fields at every time step to Stokes coefficients up to d/o 100. These are the OBA coefficients of AOD1B Release 5.
- Computation of the monthly mean values from the OBA coefficients. This is the AOD1B GAD Release 5 product.

The AOD1B GAD Release 5 product does thus contain a static residual pressure field of the atmosphere over the ocean for each time step. This static residual pressure over the oceans is equal to the mean atmospheric pressure over the ocean minus the mean atmospheric pressure for the whole Earth. A reported deficiency of the OMCT is that it does not include barystatic sea-level changes (which are present due to changes of the total mass of the ocean) and small-scale eddies which have an important contribution to the OBP changes in energy rich areas of the ocean[27]. Dobslaw et al. [27] also reports that over the Arctic Ocean the inverse barometric correction might be inaccurate since the adjustment to the changes in pressure might be slower or less due to the narrow straits through which water can flow to the Pacific or Atlantic Ocean. This inaccurate inverse barometric correction might also be an inaccuracy for AOD1B Release 6 and the products derived from GTSM which are created in this research.

When creating the AOD1B Release 6 product MPIOM is run by applying atmospheric forcing only. Therefore, no luni-solar induced tides of the ocean are modeled. The tidal patterns which can be observed in the model output of MPIOM are due to atmospheric tides. To create the AOD1B OCN Release 6 product (3-hourly) and AOD1B GAB Release 6 product (monthly) the following steps are followed [26]:

- Running the model and storing the total OBP 6-hourly. The epochs are 0h, 3h, 6h, 9h, 12h, 15h, 18h, 21h.
- Removal of the atmospheric surface pressure forcing from the total OBP.
- Removal of the ocean mean water column contribution to the OBP at each time.
- Removal of 12 tidal constituents from the 3-hourly time-series at each location. The removal of the tidal constituents is done for each year separately. The 12 tidal constituents can be found in table 4.2.
- Removal of the long-term mean (2003-2014) for each location.
- Removal of 12 tidal constituents from the 3-hourly atmospheric surface pressure time-series at each location.
- Removal of the long-term mean (2003-2014) of the atmospheric surface pressure at each location.
- Applying inverse-barometric correction to the OBP values by adding the local atmospheric pressure minus the ocean mean atmospheric pressure at each location.
- Conversion of the total OBP fields at every time step to Stokes coefficients up to d/o 180. These are the OCN coefficients of AOD1B Release 6. This conversion is applied by assuming that all mass variability takes place at the reference ellipsoid described in the IERS conventions 2010.
- Computation of the monthly mean values from the OCN coefficients. This is the AOD1B GAB Release 6 product.

Table 4.2: 12 tidal constituents removed from AOD1B OCN Release 6 product.

Tidal constituent	Frequency (°/h)
P1	14.9589314
S1	15.0000000
K1	14.0410686
N2	28.4397295
M2	28.9831042
L2	29.5284789
T2	29.9589333
S2	30.0000000
R2	30.0410667
T3	44.9589300
S3	45.0000000
R3	45.0410700

The AOD1B GAB Release 6 product does not contain a static residual pressure field of the atmosphere over the ocean. The AOD1B GAB Release 6 product represents monthly means of the ocean dynamic contribution to the OBP.

4.2. Method

In this section first some details about the conversion of the AOD1B and ocean tide products to mass-anomaly time-series is provided. Afterwards, configurations in GTSM are listed like the spin-up period and the type of output requested. Then the method to make the model output similar to the AOD1B product is described. A separate section about the conversion of the mass-anomaly time-series to Stokes coefficients follows. After this, the analysis techniques to compare the separate products are described.

4.2.1. Computation of mass-anomaly time-series from ocean tide and AOD1B products

The ocean tide and AOD1B products are provided up to a different degree. The Release 5 ocean tide product is provided up to degree 120, the Release 6 ocean tide product up to degree 180, the AOD1B Release 5 GAD product up to degree 100 and the AOD1B Release 6 GAB product up to degree 180. For consistency, all products are truncated at degree 100. This is at the cost of the spatial resolution of certain products. To convert the truncated products to mass-anomaly time-series a method similar to the method described in section 3.1.3 is applied (see equation 3.18). In contrast to the method described in section 3.1.3 no long-term is subtracted from the Stokes coefficients before the conversion into mass-anomaly time-series. The mass-anomaly time-series are computed at a 0.5° equiangular grid. For the AOD1B OBP Release 5 coefficients, the ocean mean is not zero. Therefore, for each epoch the ocean mean is subtracted from the grid of mass-anomalies at that epoch. The ocean mean is computed similarly to equation 2.24 with as region the total ocean.

4.2.2. Configurations in GTSM

The version of Delft3D-FM which is run is 1.1.270.54102. For each year GTSM is run separately. Every year has a spin-up period of 16 days so each run starts at the year before 16 December at 0:00h. For each year GTSM is run twice: one time with only meteorological forcing and one time with both meteorological and tidal forcing. The type of output which is requested is *water level*. This *water level* represents the difference between the instantaneous water column height and the predefined bathymetry. Two types of output are created: monthly mean output for each grid cell and 3-hourly output at a 0.5° equiangular grid. The 3-hourly output at a 0.5° equiangular grid consists of both values for the *water level* and the atmospheric surface pressure. This 3-hourly output is stored for the run of GTSM with only meteorological forcing. Since the ocean tide products are only available as monthly means, the 3-hourly output of the run of GTSM with both meteorological and tidal forcing is not considered. The monthly mean output at the computation grid is stored for both runs of GTSM (with only meteorological forcing and with the total forcing). The stored parameter at the computation grid is in this case only *water level*. The monthly mean output is created according to the length of a calendar month. This choice is made since the products are compared against de-aliasing products and ocean-tidal products provided by the Graz University of Technology and they use the length of a calendar month to compute their monthly mean products. GTSM is run for the years 2001 until 2016.

4.2.3. Creation of GTSM products comparable to the AOD1B products

To create a 6-hourly product comparable to the AOD1B OBA Release 5 product the following calculations are performed:

- For each epoch of the years 2003, 2004, 2005, 2006 and 2007 the *water level* and atmospheric surface pressure values are converted to block mean values at a 0.5° equiangular grid by computing the average of the four corner points at each location.
- For each of the following years 2003, 2004, 2005, 2006 and 2007 time-series of *water level* and atmospheric surface pressure are summed for each location of the newly created 0.5° equiangular grid. This summation is performed after dividing the atmospheric surface pressure by the gravitational acceleration and density of water as defined in GTSM. The predefined gravitational attraction and density of water in GTSM are $9.81\ m/s^2$ and $1024\ kg/m^3$.
- For each epoch the ocean mean is computed and consequently removed.
- For each location the yearly mean is subtracted. (Later on, for each year separately comparisons are made between the GTSM and AOD1B products in the hourly scale.)
- The time-series are then multiplied by $1024\ kg/m^3$ and divided by $1000\ kg/m^3$ to convert the time-series in mass-anomaly time-series in EWH.
- For each location the linear trend, annual cycle and the 12 tidal constituents listed in table 4.2 are estimated by least-squares. Consequently the periodic signal of the S2 tide is removed from the mass-anomaly time-series.

To create a 3-hourly product comparable to the AOD1B OCN Release 6 product the same steps are followed as for the creation of 6-hourly product comparable to the AOD1B OBA Release 5 product. The only difference is that now all calculations are performed for 3-hourly output and not 6-hourly output. Furthermore, the last step of the removal of tidal constituents due to the atmospheric tides is different. Instead of only removing the S2 tide, all 12 tidal constituents listed in table 4.2 are removed from the mass-anomaly time-series.

The created 3/6-hourly product from GTSM is not converted into Stokes coefficients. In the comparison of the monthly time-series it was observed that the conversion of GTSM output into Stokes coefficients and back did not give new insights about regions where the different models are more different/similar. Only the small scale features disappeared. When the product derived from GTSM is directly compared to an AOD1B which is truncated at degree 100, incorrectly small scale differences between the products can be observed. When GTSM output is converted to the spherical domain and back these small scale differences disappear. Since the conclusions about the regions where the different models are more different/similar did not change by the conversion to the spherical domain and back, it did not seem needed to convert the 3/6-hourly created product of GTSM to the spherical domain and back. This also saved computation time.

To create a monthly product comparable to the AOD1B GAD Release 5 product the following calculations are performed:

- For each epoch the *water level* values are converted to block mean values at a 0.5° equiangular grid by computing the average of all computational grid cells present in a certain region of 0.5°x0.5°.
- Since certain regions of 0.5°x0.5° size did not contain a computational grid cell (in the Arctic region) or did only contain grid cells representing land areas during the time of computation, interpolation is needed. In the predefined 0.5° equiangular grid containing the block mean values, first land regions are given value 0. Then linear barycentric interpolation is applied to fill all locations in the 0.5° equiangular grid. For this the Python function `scipy.interpolate.griddata` is used.
- The time-series are multiplied by the density predefined in GTSM and consequently divided by $1000\ kg/m^3$ in order to get mass-anomaly time-series in m EWH.
- From the hourly atmospheric forcing data a monthly mean atmospheric pressure time-series is computed for each location of the 0.3° equiangular grid.
- Linear barycentric interpolation is applied to the atmospheric forcing data to interpolate to a 0.5° equiangular grid. For this again the Python function `scipy.interpolate.griddata` is used.
- At each monthly epoch the mean oceanic atmospheric surface pressure is removed from the interpolated atmospheric surface pressure time-series and the residual pressure is consequently divided by the gravitational acceleration of $9.81\ m/s^2$ and density of $1000 kg m^{-3}$. The resulting product is the monthly time-series of the inverse-barometric correction in m EWH.
- For each location and at each time the inverse-barometric correction is applied to the monthly *water level* time-series at the 0.5°x0.5° grid.
- For each location the long-term mean (2001-2002) of the monthly time-series is removed. The long-term mean is computed by weighting the different months according to their length.
- For each monthly epoch the ocean mean of the mass-anomaly field is removed. Then for each monthly epoch the ocean mean of the AOD1B GAD Release 5 product is added. As previously stated, this ocean mean represents the residual atmospheric pressure over the ocean (ocean mean atmospheric pressure minus global mean atmospheric pressure).

The same steps as above are followed when creating a monthly product comparable to the combination of the products AOD1B GAD Release 5 and ocean tide Release 5. This monthly product is computed from GTSM output when it is forced with both atmospheric and tidal forcing. No separate ocean tide product was computed from GTSM. This is not done because when GTSM was run with only tidal forcing strange features were observed in the Arctic Ocean, Southern Ocean and South Atlantic

Ocean. These strange features were locally very large mass-anomalies of about half a meter EWH which build up during each year. When GTSM is run with only tidal forcing and the monthly means are stored as output these signals are unexpected. Likely these strange features arise due to errors in the models which should be solved. For the year 2003, global plots of monthly mean values for the cases where GTSM is run with only meteorological forcing, only tidal forcing and total forcing are made. These figures can be found in appendix D. These are just raw output data of *water level*. Locations which are non-flooded land areas are still present in these figures as positive values of *water level*.

To create a monthly product comparable to the AOD1B GAB Release 6 product the same steps as for the monthly product comparable to the AOD1B GAD Release 5 are applied. The only differences are in the last two steps. Instead of removing a long-term mean computed from the years 2001-2002, a long-term mean computed from the years 2003-2014 is removed. Furthermore, for each monthly epoch the ocean mean of the mass-anomaly field is removed and no ocean mean from an AOD1B product is consequently added.

The same steps as for the creation of a monthly product similar to the AOD1B GAB Release 6 product are followed when creating a monthly product comparable to the combination of the products AOD1B GAB Release 6 and ocean tide Release 6. This monthly product is computed from GTSM output when it is forced with both atmospheric and tidal forcing.

To compare the GTSM-based monthly time-series to the AOD1B monthly products the time-series are converted to Stokes coefficients up to degree 100 and consequently converted back to mass-anomalies in the spatial domain. These steps reduce the spatial resolution of the mass-anomaly time-series created from GTSM and makes the spatial resolution of the GTSM-based monthly time-series similar to the AOD1B products (which are truncated at degree 100). The conversion of mass-anomalies to Stokes coefficients is described in the next section. The conversion back to the spatial domain is again performed with equation 3.18.

4.2.4. Conversion of mass-anomaly time-series at a structured grid to Stokes coefficients

This section is about the conversion of temporal variations of mass in EWH at a structured grid to temporal variations of Stokes coefficients. The temporal variations in mass are always 0 at gridpoints which are at land.

Coordinate conversion of gridpoints in structured grid

When the structured grid is defined in geodetic coordinates (which is for example the case for output retrieved from GTSM which uses WGS84 as coordinate reference system) the geodetic colatitudes first have to be converted to geocentric colatitudes since for all equations in the sections 4.2.4 and 4.2.4 the colatitude is the geocentric colatitude. With the following equation geodetic colatitudes can be converted to geocentric colatitudes [24]:

$$\theta_c = ATAN2\left(\sin\left(\theta_g\right), (1-f)^2 \cos\left(\theta_g\right)\right) \tag{4.3}$$

where θ_c is the geocentric colatitude, θ_g is the geodetic colatitude, $f = \frac{1}{298.2572}$ is the Earth's flattening according to WGS84 [59] and where:

$$ATAN2\,(y,x) = \begin{cases} \arctan\left(\frac{y}{x}\right) & \text{if } x > 0 \\ \arctan\left(\frac{y}{x}\right) + \pi & \text{if } x < 0 \\ \frac{\pi}{2} & \text{if } x = 0 \end{cases}$$

In equation 4.3 it is assumed that $0 < \theta_g < 2\pi$ (i.e., the structured grid of geodetic coordinates has no grid points at the poles). By using equation 4.3 a structured grid of geodetic coordinates can be turned into a structured grid of geocentric coordinates. In the following sections θ always refers to the geocentric colatitude.

Relation between Stokes coefficients and mass anomalies in EWH
The temporal variations of Stokes coefficients can be expressed as function of temporal variations of mass in EWH ($\Delta H_w\,(\theta,\lambda)$) as explained in section 3.1.3:

$$\Delta C_{lm} = \frac{R^2}{M_E\,(2l+1)} \int_0^{2\pi} \int_0^{\pi} (1+k_l) \left(\frac{1-f}{\sqrt{1-e^2 \sin^2(\theta)}} \right)^{l+2} \rho_w \Delta H_w\,(\theta,\lambda)\, \bar{Y}_{lm}\,(\theta,\lambda) \sin(\theta)\; d\theta\, d\lambda \tag{4.4}$$

For this equation it is assumed that all mass transport takes place in a thin layer at the surface of the Earth and that this surface is the WGS84 reference ellipsoid.

Computation of Stokes coefficients from mass anomalies in EWH at structured grid
The integrals in equation 4.4 can be numerically approximated:

$$\begin{aligned} &\int_0^{2\pi} \int_0^{\pi} (1+k_l) \left(\frac{1-f}{\sqrt{1-e^2 \sin^2(\theta)}} \right)^{l+2} \rho_w \Delta H_w\,(\theta,\lambda)\, \bar{Y}_{lm}\,(\theta,\lambda) \sin(\theta)\; d\theta\, d\lambda \\ &\approx \sum_{i=1}^{i_{max}} \sum_{j=1}^{j_{max}} (1+k_l) \left(\frac{1-f}{\sqrt{1-e^2 \sin^2(\theta_j)}} \right)^{l+2} \rho_w \Delta H_w\,(\theta_j,\lambda_i)\, \bar{Y}_{lm}\,(\theta_j,\lambda_i) \sin(\theta_j)\, \Delta\theta_j \Delta\lambda_i \end{aligned} \tag{4.5}$$

where θ_j is the series of in value increasing colatitudes of the structured grid, λ_i is the series of in value increasing longitudes of the structured grid and where:

$$\Delta\theta_j = \begin{cases} (\theta_{j+1} - \theta_j)/2 + \theta_j & \text{if } j = 1 \\ (\theta_j - \theta_{j-1})/2 + \pi - \theta_j & \text{if } j = j_{max} \\ (\theta_{j+1} - \theta_{j-1})/2 & \text{if } 1 < j < j_{max} \end{cases} \tag{4.6}$$

$$\Delta\lambda_i = \begin{cases} (\lambda_{i+1} - (\lambda_{i_{max}} - 2\pi))/2 & \text{if } i = 1 \\ ((\lambda_1 + 2\pi) - \lambda_{i-1})/2 & \text{if } i = i_{max} \\ (\lambda_{i+1} - \lambda_{i-1})/2 & \text{if } 1 < i < i_{max} \end{cases} \tag{4.7}$$

If the set of longitudes is equidistant (which is the case in the considered structured grids), equation 4.7 reduces to:

$$\Delta\lambda_i = \frac{2\pi}{i_{max}} \tag{4.8}$$

To compute the temporal variations of Stokes coefficients from temporal variations of mass-anomaly in EWH at a structured grid in geocentric coordinates the numerical approximation shown in equation 4.5 is used. The resulting equation to compute the Stokes coefficients becomes:

$$\Delta C_{lm} = \frac{R^2}{M_E\,(2l+1)} \sum_{i=1}^{i_{max}} \sum_{j=1}^{j_{max}} (1+k_l) \left(\frac{1-f}{\sqrt{1-e^2 \sin^2(\theta_j)}} \right)^{l+2} \rho_w \Delta H_w\,(\theta_j,\lambda_i)\, \bar{Y}_{lm}\,(\theta_j,\lambda_i) \sin(\theta_j)\, \Delta\theta_j \Delta\lambda_i \tag{4.9}$$

with θ_j and λ_i in value increasing series and $\Delta\theta_j$ and $\Delta\lambda_i$ defined as in equations 4.6 and 4.7.

4.2.5. 3/6-hourly time-series comparison between GTSM and AOD1B products

To compare the 3/6-hourly GTSM product to the 3/6-hourly AOD1B products the yearly mean is subtracted from the mass-anomaly grids computed from the AOD1B products. This is done for each of the considered years 2003, 2004, 2005, 2006 and 2007 separately. For each locations at the 0.5° equiangular grid a difference time-series is computed by subtracting the mass-anomaly time-series derived

from GTSM from the mass-anomaly time-series of AOD1B. From this difference time-series the standard deviation is computed. Since the mean difference is 0, the computed values are equal to RMS differences. Consequently, for each year the standard deviation of the difference in mass-anomaly is plotted globally. Besides this, regional average std's of the differences in mass-anomaly time-series are reported. These are computed by using equation 3.19. Furthermore the std's of the differences in mass-anomaly are shown versus bathymetry to see whether differences between the models are larger for certain ocean depths. For this, all locations are categorized in depths of bin width 100 m. Consequently the average standard deviation for each bin is computed according to equation 2.24 by considering a bin as an area.

Again buffer zones are incorporated in the analysis when the standard deviation of the difference mass-anomaly time-series are plotted versus bathymetry. Although the buffer zones are in the previous chapter introduced because of signal leakage from land to ocean, still buffer zones are included in this analysis. The Gibbs phenomenon, which is present due to the large changes in mass-anomaly at the coast (land is always defined as 0 m EWH) for the AOD1B products, could result in large differences close to the coast with respect to the GTSM time-series. Although, the Gibbs phenomenon is present over large areas, it is the largest close the coast so a buffer zone might partly reduce the differences caused by the Gibbs phenomenon. Furthermore, since the AOD1B products are truncated to degree 100 a part of the oceanic signal leaks into the land by the reduction of the spatial resolution. Therefore, it is not a good idea to incorporate the regions close to the coast in the analysis of the difference mass-anomaly time-series. Therefore, again two different buffer zones (200 and 400 km) are incorporated in the analysis to disregard the areas close to the coast.

Besides an analysis of the differences between GTSM and the AOD1B products at the hourly scale, AOD1B Release 5 OBP and AOD1B Release 6 OCN are compared directly. Besides the removal of the yearly mean for both products and the removal of the ocean mean for AOD1B Release 5 removal, two additional adaptations have to be performed to make the comparison. AOD1B Release 6 OCN time-series must be reduced to a 6-hourly time-series. For AOD1B Release 5 OBP all 12 tidal constituents as observed in table 4.2 should be removed since these are also removed from AOD1B Release 6 OCN. Furthermore, to observe for which area which of the models (OMCT, MPIOM and GTSM) are more close in performance, distance plots will be constructed where distances represent differences between certain models. To make these distance plots, normalization of the standard deviations is needed. Therefore, for each region the standard deviations of the difference time-series are divided by the standard deviation of the difference time-series between AOD1B Release 5 OBP and AOD1B Release 6 OCN. For consistency, a new difference time-series is computed between AOD1B Release 5 OBP and GTSM where all 12 tidal constituents according to table 4.2 are removed in both time-series. In the distance plot the standard deviation of this difference mass-anomaly time-series will be used instead of the standard deviation of the difference time-series between AOD1B Release 5 OBP and GTSM where only the S2 tidal constituent was removed. In this way, the distances in the distance plot represent differences between the different models without differences which are due to atmospheric tides.

Apart of the above described comparison of 3/6-hourly time-series a Fourier analysis is performed to see whether the GTSM showed signals of different frequency than the currently considered oceanic background models in GRACE data processing. The Fourier analysis is performed for separate oceanic regions. For this, first the mean time-series for each region is calculated with equation 2.24. Consequently the Fourier analysis is performed and amplitude spectra are made. The shown amplitudes are harmonic coefficients. It is also analyzed if the models are more different in the low or high frequencies. For this the standard deviation of the differences in amplitude are computed for certain frequency ranges. Low frequencies are defined as being lower than 1/31 cycles per day and high frequencies higher than this value. This choice is made to observe whether the time-series differ more in the sub-monthly frequencies or in frequencies with a period larger than a month. Since the AOD1B Release 6 product is 3-hourly the maximum frequency for this time-series is 4 cycles per day instead of 2 cycles per day for the AOD1B Release 5 product. For consistency, the frequency range between 1/31 and 2 cycles per day is also analyzed for the differences in amplitude between AOD1B Release 6 and GTSM. The standard deviations of the difference in amplitudes (AOD1B product minus GTSM) for a certain frequency range is reported. Also the ratio of the standard deviation of the difference in amplitudes for the low and high frequency is reported.

4.2.6. Monthly time-series comparison between GTSM and AOD1B products

For the monthly time-series comparison the time span of the considered monthly time-series is January 2003 - March 2016. For each locations at the 0.5° equiangular grid a difference time-series is computed by subtracting the mass-anomaly time-series deduced from GTSM from the mass-anomaly time-series of AOD1B. Four GTSM derived mass-anomaly time-series are considered which were made in order to compare GTSM against AOD1B GAD Release 5, AOD1B GAD Release 5 + Ocean tides Release 5, AOD1B GAB Release 6 and AOD1B GAB Release 6 + Ocean tides Release 6. From this difference time-series the standard deviation is computed. The standard deviation of the difference in mass-anomaly is plotted globally. Besides this, regional average std's of the differences in mass-anomaly time-series are reported. Also the std's of the differences in mass-anomaly are shown versus bathymetry. A similar distance plot as described in section 4.2.5 is constructed for the monthly time-series by normalizing to the standard deviation of differences between AOD1B GAD Release 5 and AOD1B GAB Release 6. To compute monthly difference mass-anomaly time-series between AOD1B GAD Release 5 and AOD1B GAB Release 6, the AOD1B GAD Release 5 time-series are adapted to make those consistent to the AOD1B GAB Release 6 time-series. For this, for each epoch the ocean mean is subtracted from the AOD1B GAD Release 5 time-series. Furthermore, for both time-series (AOD1B GAD Release 5 and AOD1B GAB Release 6) the same long-term mean (January 2003 - March 2016) is subtracted.

4.3. Results and discussion

This section is about the comparison of time-series computed by the currently used oceanic background models in GRACE data processing and time-series computed by GTSM. First the 3/6-hourly time-series are compared. Thereafter, the frequency analysis of the 3/6-hourly time-series follows. Afterwards, the monthly time-series are discussed.

4.3.1. 3/6-hourly time-series comparison

Since the results for the years 2003, 2004, 2005, 2006, 2007 are very similar. Therefore, figures for only the year 2003 are shown in this section.

In figures 4.3, 4.4 and 4.5 the standard deviations of the difference mass-anomaly time-series are shown globally. In table 4.3 and 4.4 regional average standard deviations are shown. In general it can be observed that GTSM does differ more from AOD1B Release 5 OBP than from AOD1B Release 6 OCN. From the globally plotted standard deviations it can be observed that GTSM clearly differs more from AOD1B Release 5 OBP than from AOD1B Release 6 OCN for the regions:

- Hudson Bay
- East Siberian Antarctic Shelf
- Arctic Ocean
- Southern Ocean
- Arafura Sea
- Baltic Sea

Except for the Baltic Sea, the list above shows regions where GRACE Release 6 solutions showed a smaller signal variance than GRACE Release 5 solutions. In the regions (Hudson Bay and East Siberian Antarctic Shelf) where it seems that GRACE Release 6 solutions are better than GRACE Release 5 solutions, GTSM is more close to the AOD1B Release 6 than AOD1B Release 5 product. For these regions it is thus also expected that GTSM can improve the GRACE Level-2 data of Release 5. From the globally plotted standard deviations and table 4.3 it can be clearly observed that GTSM differs less from AOD1B Release 5 OBP than from AOD1B Release 6 OCN for the Gulf of Thailand and the North Sea. The regions where a clear difference in quality between Release 5 and Release 6 GRACE Level-2 data is observed (Hudson Bay and East Siberian Arctic Shelf, see figures 3.15, 3.19 and 3.24) correlate to regions where the AOD1B products differ significantly (see figure 4.5). This makes it likely that the oceanic background models do significantly influence the quality of GRACE Level-2 data. When observing

Regions which show in general large differences between GTSM and the AOD1B products are:

- Arctic Ocean
- Baltic Sea
- Black Sea

- North Sea
- Gulf of Thailand
- Arafura Sea
- Bering Strait
- Hudson Bay
- Red Sea
- Coastal regions around Eurasia in general

The list above goes along with mostly shallow regions (see figure 4.1). In figure 4.7 where the standard deviation of the difference time-series is plotted versus bathymetry it can also be observed that differences are larger for shallow regions. The regions where no differences are observed between mass-anomaly time-series computed by GTSM and mass-anomaly time-series of the AOD1B products are regions where no improvement can be made by switching to GTSM in GRACE data processing. For the large open oceans (Atlantic, Pacific) less potential improvements are expected since the standard deviation of the difference mass-anomaly time-series is only 1.8-2.0 cm EWH. When comparing figure 4.5 with figures 4.3 and 4.4, it can be observed that in general the regions of large differences are similar for the three considered models. These differences might also be due to differences in phase of similar signals. In table 4.4 it can be observed that the differences between AOD1B OBP Release 5 and GTSM are smaller when from both time-series all 12 tidal constituents (table 4.2) are removed. A part of the differences between AOD1B OBP Release 5 and GTSM are thus due to differences in the response to atmospheric tides. In figure 4.6 a distance plot is shown for the monthly time-series to visualize table 4.4. From this figure it can be easily observed that for most regions GTSM is closer to AOD1B OCN Release 6 than AOD1B OBP Release 5.

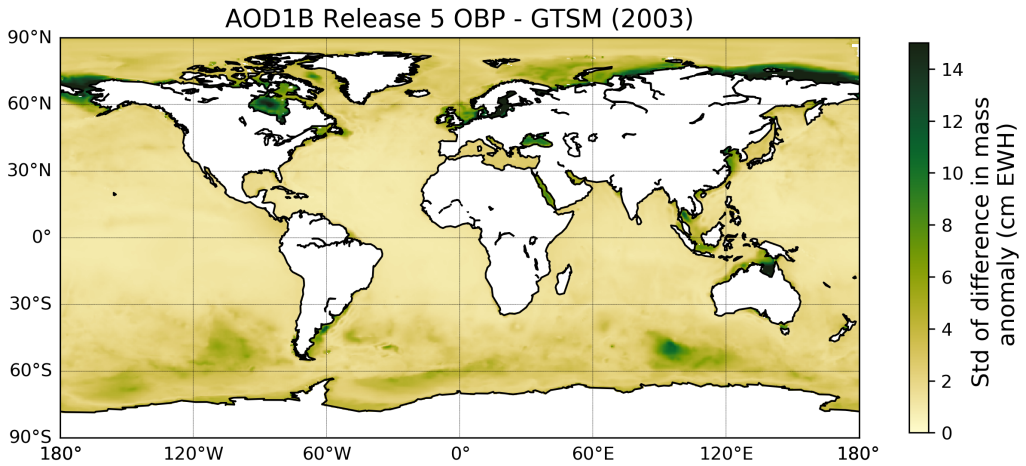

Figure 4.3: Standard deviation of the 6-hourly difference mass-anomaly time-series for the year 2003. This difference mass-anomaly time-series is computed by subtracting GTSM from AOD1B OBP Release 5.

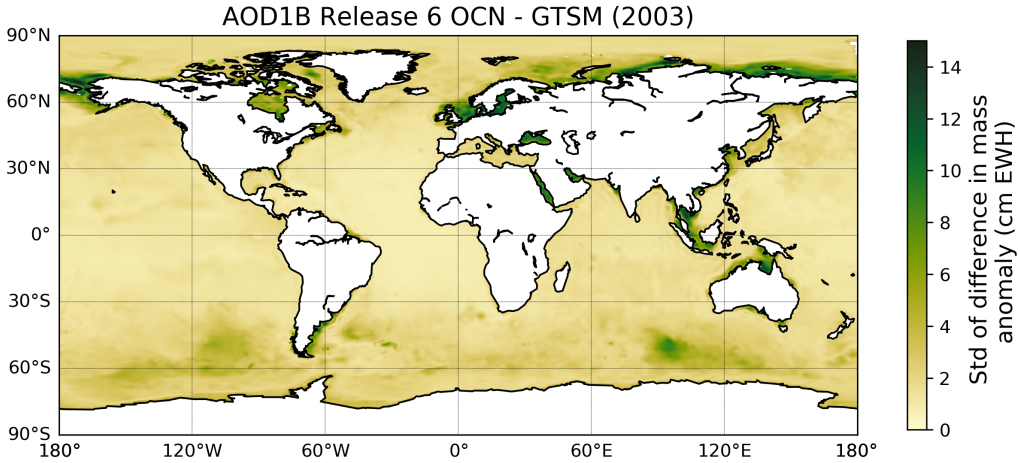

Figure 4.4: Standard deviation of the 6-hourly difference mass-anomaly time-series for the year 2003. This difference mass-anomaly time-series is computed by subtracting GTSM from AOD1B OCN Release 6.

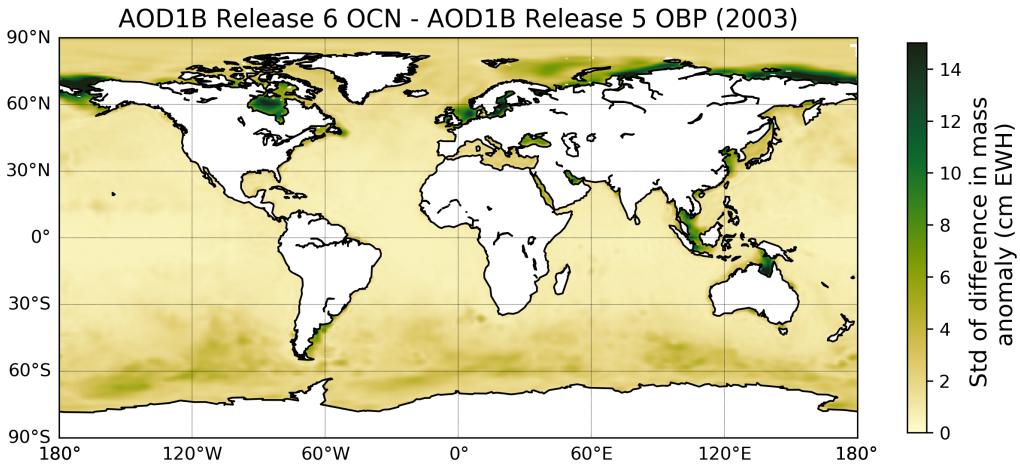

Figure 4.5: Standard deviation of the 6-hourly difference mass-anomaly time-series for the year 2003. This difference mass-anomaly time-series is computed by subtracting AOD1B OBP Release 5 (after removal of 12 tidal constituents) from AOD1B OCN Release 6.

Table 4.3: Regional averages of the standard deviation in cm EWH of the difference mass-anomaly times-series at the hourly scale. The results for the difference mass-anomaly time-series for the years 2003, 2004, 2005, 2006 and 2007 are shown.

	AOD1B Release 5 OBP - GTSM					AOD1B Release 6 OCN - GTSM				
Year	2003	2004	2005	2006	2007	2003	2004	2005	2006	2007
Total ocean	2.565	2.525	2.559	2.540	2.587	2.276	2.235	2.257	2.290	2.282
Arafura Sea	8.773	7.976	7.884	8.555	8.734	6.451	5.935	5.630	6.959	6.077
Arctic Ocean	5.763	5.637	5.744	5.624	5.991	4.077	3.999	4.407	4.338	4.260
Baltic Sea	14.671	15.477	15.925	13.202	18.417	9.828	10.227	10.426	9.401	11.727
Black Sea	8.379	8.801	9.123	9.328	8.520	8.791	7.360	8.872	8.989	7.562
Gulf of Thailand	6.136	5.201	6.409	5.068	5.907	8.509	7.274	8.257	7.259	9.376
Indian Ocean	2.387	2.226	2.233	2.410	2.274	2.345	2.292	2.180	2.347	2.303
Mediterranean Sea	2.496	2.696	2.495	2.563	2.366	2.169	2.103	2.152	2.086	2.283
North Atlantic Ocean	1.623	1.559	1.628	1.540	1.613	1.518	1.512	1.570	1.508	1.572
North Pacific Ocean	1.846	1.984	1.919	1.885	1.856	1.816	1.857	1.783	1.772	1.762
North Sea	6.863	7.307	8.349	7.693	8.388	8.429	8.605	8.862	8.592	9.396
South Atlantic Ocean	2.068	1.955	2.026	2.051	2.064	1.877	1.842	1.817	1.989	1.898
South China and Archipelagic Seas	2.681	2.515	2.691	2.704	2.745	3.139	3.058	3.209	3.173	3.415
South Pacific Ocean	1.933	1.944	1.947	1.890	1.831	1.764	1.716	1.685	1.684	1.657
Southern Ocean	2.988	2.964	3.009	3.032	3.002	2.557	2.523	2.620	2.658	2.544

Table 4.4: Regional averages of the standard deviation in cm EWH of difference mass-anomaly times-series at the hourly scale. Results for the difference mass-anomaly time-series for the year 2003 are shown. Note that a distinction is made between AOD1B OBP time-series where only the S2 tide is removed and where all 12 tidal constituents according to table 4.2 are removed. In all cases the GTSM time-series are made consistently to the specific AOD1B products (by removal of specific atmospheric tides).

	AOD1B OBP Release 5 - GTSM	AOD1B OBP Release 5 (12 tidal constituents removed) - GTSM	AOD1B OCN Release 6 - GTSM	AOD1B OCN Release 6 - AOD1B OBP Release 5 (12 tidal constituents removed)
Total ocean	2.565	2.495	2.276	2.143
Arafura Sea	8.773	8.485	6.451	8.236
Arctic Ocean	5.763	5.723	4.077	5.328
Baltic Sea	14.671	14.665	9.828	10.610
Black Sea	8.379	8.378	8.791	6.018
Gulf of Thailand	6.136	6.085	8.509	8.250
Indian Ocean	2.387	2.330	2.345	1.657
Mediterranean Sea	2.496	2.479	2.169	2.157
North Atlantic Ocean	1.623	1.549	1.518	1.229
North Pacific Ocean	1.846	1.746	1.816	1.451
North Sea	6.863	6.794	8.429	8.122
South Atlantic Ocean	2.068	2.000	1.877	1.723
South China and Archipelagic Seas	2.681	2.510	3.139	3.102
South Pacific Ocean	1.933	1.835	1.764	1.428
Southern Ocean	2.988	2.936	2.557	2.652

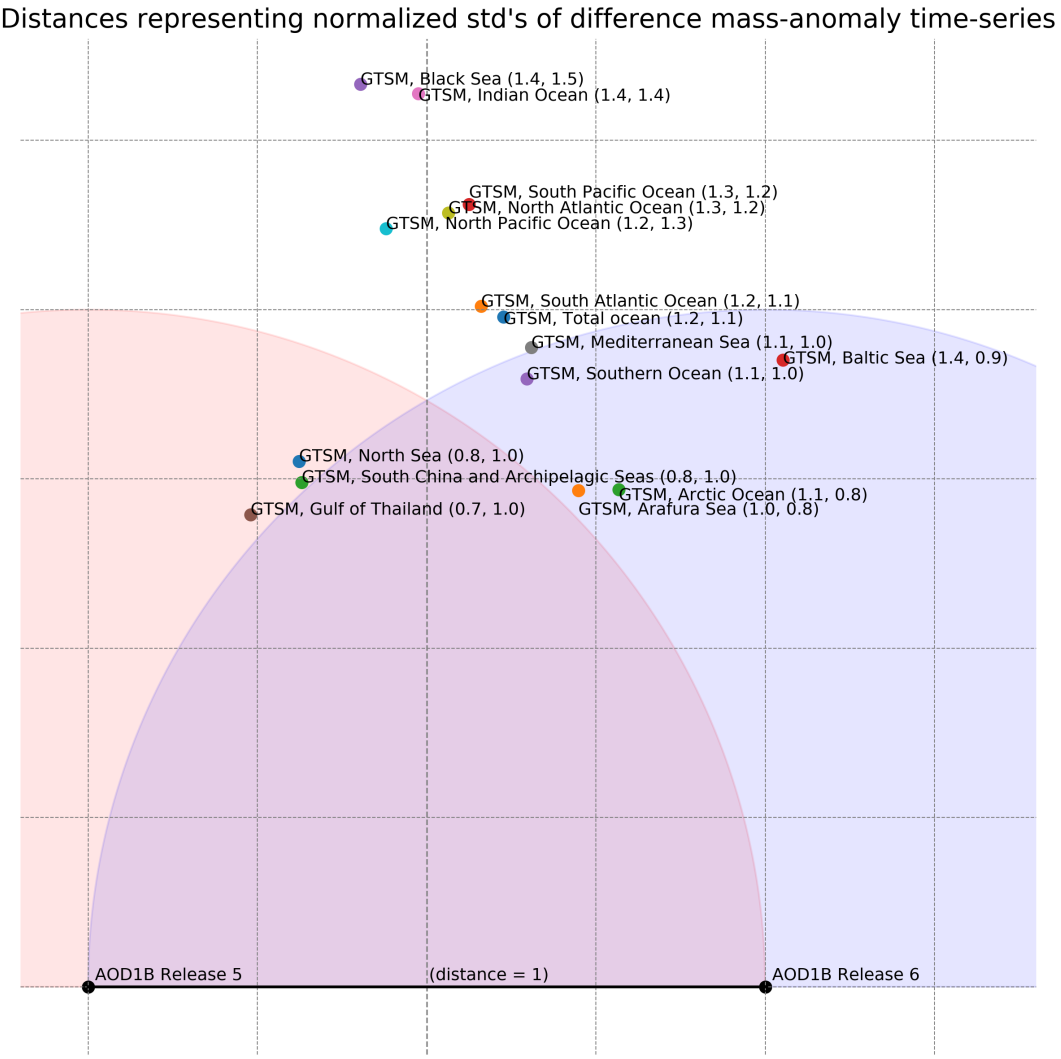

Figure 4.6: Distance plot where distances represent normalized differences between different ocean models. For each region the regional average std (as reported in table 4.4) is divided by the regional average std of difference time-series between AOD1B OBP Release 5 and AOD1B OCN Release 6. The considered time-series are at the hourly scale and are those where all 12 tidal constituents are removed according to table 4.2.

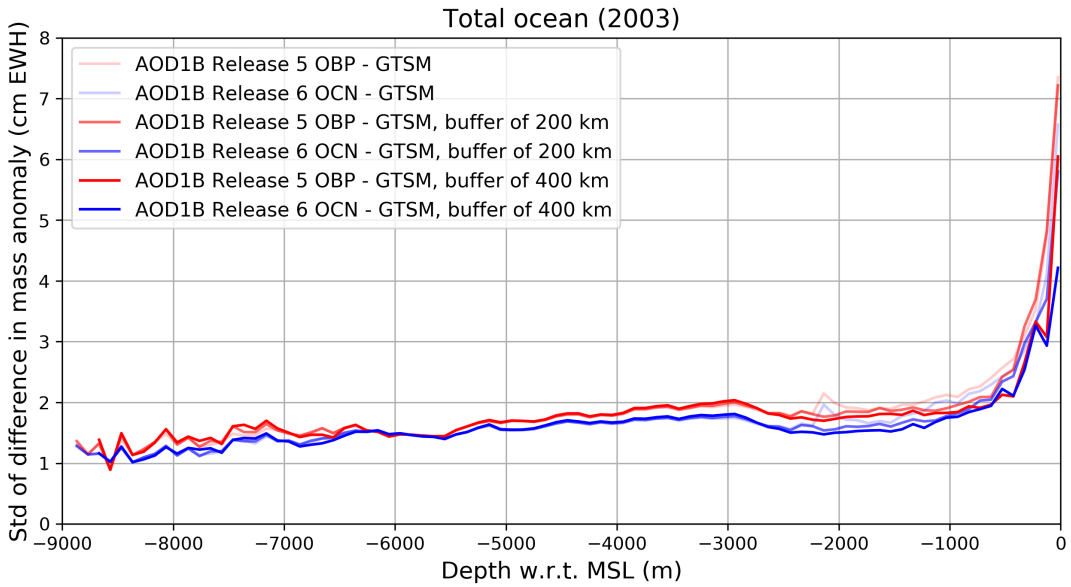

Figure 4.7: Standard deviation of the 3/6-hourly difference mass-anomaly time-series versus bathymetry for the year 2003. These difference mass-anomaly time-series are computed by subtracting GTSM from AOD1B OBP Release 5 (red) and subtracting GTSM from AOD1B OCN Release 6 (blue).

The standard deviation of the difference time-series versus bathymetry are also plotted for each region separately. Three regions (Southern Ocean, Indian Ocean and South Atlantic Ocean) are shown in figures 4.8, 4.9 and 4.10. These three regions show not such a clear sign of larger standard deviation for shallow regions. So there are also some deep regions where GTSM significantly differs from the currently used oceanic background models. A full list of standard deviation versus bathymetry for the considered oceanic regions can be found in Appendix C. Since GTSM has a grid densification in shallow regions it is expected that GTSM performs better in shallow regions and thus differ more from the currently used oceanic background models. It could be that the deeper areas in the Southern Ocean, South Atlantic Ocean and Indian Ocean are in steep regions where also grid densification in GTSM is present. It could be that because of this grid densification in GTSM in these regions, GTSM performs better than the currently used oceanic background models. Other reasons are also be possible for differences in performance. For example, it could be that in these areas pressure-induced currents are present which are not modeled by GTSM or that dissipation mechanisms are modeled differently which also influence the (remaining) flow. Differences in the models indicate that it is expected that one of the models is better, but this does not have to be the case. When models differ significantly it is also possible that both models are inaccurate but for different reasons. For the South Atlantic Ocean (figure 4.10) it an increase of the difference can be observed around 6000 m depth. In figures 4.3 and 4.4 it can be observed that in the Argentine Basin the differences between the models are large and according to figure 4.1 the depth is also reaching 6000 m in this area. So the increase of differences around 6000 m might correlate to the Argentine Basin. In general, it must be mentioned that sometimes the amount of locations per bin can be very small (for example for the bins of large depth). It could be that the bins to which a small amount of locations is categorized are more erroneous. A large standard deviation for one location will not be averaged out by the other locations categorized in the same bin when there are only a few locations categorized in a certain bin.

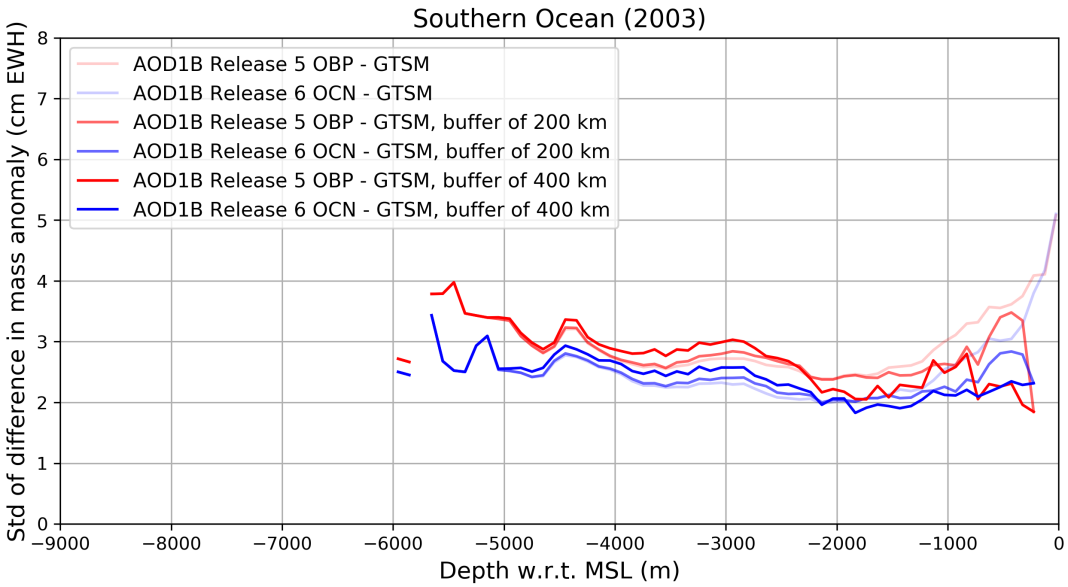

Figure 4.8: Standard deviation of the 3/6-hourly difference mass-anomaly time-series (year 2003) versus bathymetry for the Southern Ocean. These difference mass-anomaly time-series are computed by subtracting GTSM from AOD1B OBP Release 5 (red) and subtracting GTSM from AOD1B OCN Release 6 (blue).

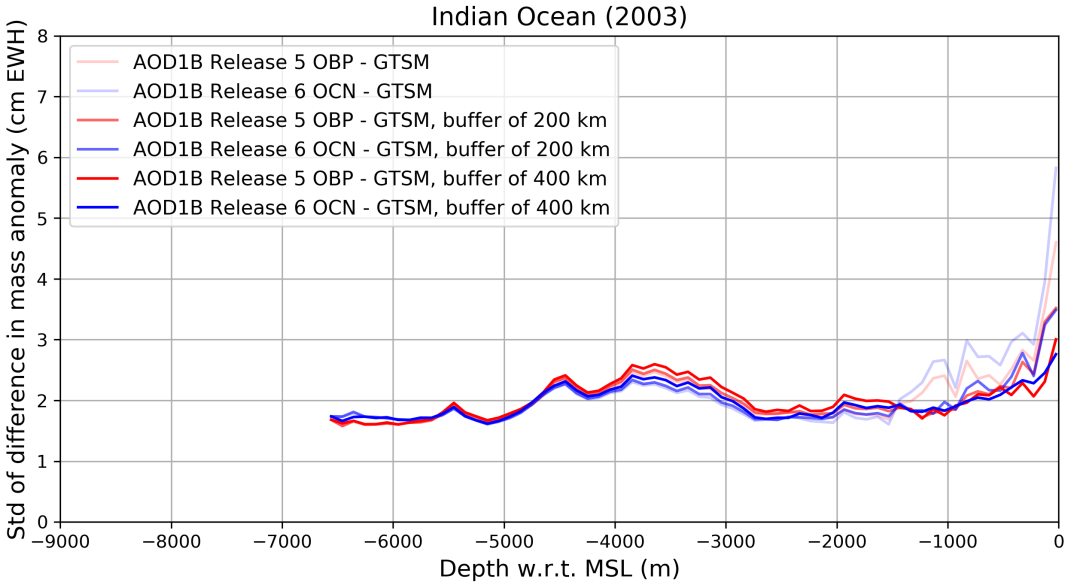

Figure 4.9: Standard deviation of the 3/6-hourly difference mass-anomaly time-series (year 2003) versus bathymetry for the Indian Ocean. These difference mass-anomaly time-series are computed by subtracting GTSM from AOD1B OBP Release 5 (red) and subtracting GTSM from AOD1B OCN Release 6 (blue).

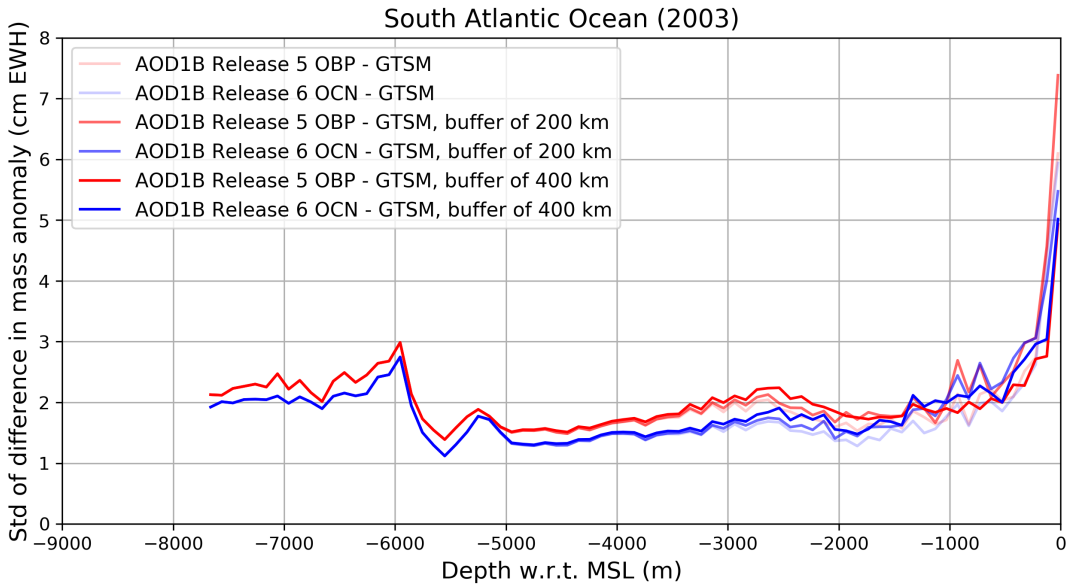

Figure 4.10: Standard deviation of the 3/6-hourly difference mass-anomaly time-series (year 2003) versus bathymetry for the South Atlantic Ocean. These difference mass-anomaly time-series are computed by subtracting GTSM from AOD1B OBP Release 5 (red) and subtracting GTSM from AOD1B OCN Release 6 (blue).

4.3.2. Fourier analysis of basin average 3/6-hourly time-series

After performing a frequency analysis to the basin average mass-anomaly time-series for each region, differences in the amplitude spectra of the different models are calculated. The standard deviation of the differences in amplitudes for the low and high frequency regions are consequently separately calculated. In table 4.5 the standard deviation of the differences in amplitudes for different oceanic regions are shown. It can be observed that for the large oceanic regions (Arctic Ocean, Indian Ocean, South Atlantic Ocean, Pacific Ocean) except the North Atlantic Ocean and Southern Ocean the standard deviation of differences in amplitude for the frequencies lower than 1/31 cycles per day are larger for AOD1B Release 6 than for AOD1B Release 5. Also the ratio's of std's (low/high (limited)) are larger for AOD1B Release 6 than for AOD1B Release 5 for these regions. Also for some other regions (Gulf of Thailand, Mediterranean Sea, North Sea, South China and Archipelagic Seas) this is the case. It seems that for most regions AOD1B Release 5 (compared to AOD1B Release 6) differs more from GTSM in the low frequencies. This can explain why GTSM is in general more close to AOD1B Release 5 than to AOD1B Release 6 for monthly time-series (which is discussed in section 4.3.3). In the high frequency range (1/31 - 2 cycles per day) GTSM differs more from AOD1B Release 5 than AOD1B Release 6 expect for the regions Black Sea, Gulf of Thailand, North Sea and Southern Ocean. From table 4.5 it can also be observed that the ratio of std's goes up for AOD1B Release 6 when the high frequencies are not limited to a maximum frequency of 2 cycles per day. This implies that there are less differences in the high frequencies range of 2-4 cycles per day than in the range 1/31-2 cycles per day.

Table 4.5: Standard deviation in cm EWH of the differences in amplitudes after performing a frequency analysis to basin average mass-anomaly time-series. The low frequencies have as maximum 1/31 cycles per day. The high frequencies are unlimited or limited to a maximum frequency of 2 cycles per day.

	AOD1B RI 5 OBP - GTSM			AOD1B RI 6 OCN - GTSM				
	Std for low frequencies	Std for high frequencies	Ratio of std's (low/high)	Std for low frequencies	Std for high frequencies (limited)	Ratio of std's (low/high (limited))	Std for high frequencies	Ratio of std's (low/high)
Arafura Sea	0.969	0.146	6.653	0.505	0.107	4.728	0.077	6.530
Arctic Ocean	0.260	0.034	7.752	0.377	0.027	14.208	0.019	20.110
Baltic Sea	1.156	0.245	4.716	0.817	0.237	3.450	0.174	4.682
Black Sea	0.995	0.147	6.748	0.894	0.151	5.932	0.107	8.327
Gulf of Thailand	0.704	0.134	5.242	2.477	0.156	15.839	0.113	21.918
Indian Ocean	0.111	0.019	5.871	0.130	0.017	7.508	0.012	10.608
Mediterranean Sea	0.225	0.079	2.841	0.349	0.043	8.176	0.030	11.528
North Atlantic Ocean	0.086	0.016	5.418	0.058	0.015	3.992	0.010	5.616
North Pacific Ocean	0.082	0.013	6.457	0.159	0.011	15.064	0.008	21.071
North Sea	0.431	0.118	3.642	1.151	0.175	6.583	0.123	9.335
South Atlantic Ocean	0.070	0.016	4.358	0.077	0.014	5.491	0.010	7.718
South China and Archipelagic Seas	0.115	0.027	4.302	0.252	0.026	9.888	0.018	13.964
South Pacific Ocean	0.067	0.013	5.288	0.086	0.010	8.998	0.007	12.629
Southern Ocean	0.144	0.028	5.180	0.143	0.029	4.876	0.021	6.803

In figures 4.11, 4.12, 4.13 and 4.14 frequency analyses for the North Pacific Ocean and the Mediterranean Sea are shown. In general, it can be observed that the amplitudes for the lower frequencies are larger for all considered ocean models than for the higher frequencies. The energy distribution over high and low frequencies is thus quite similar for the different ocean models. Since a frequency analysis is performed for basin average mass-anomaly time-series, it is expected that signals of smaller wavelength are more damped than signals of larger wavelength. Especially for the large ocean basins as for example the North Pacific Ocean it can be that signals of small wavelength are averaged out since similar signals with a different phase are present in the same ocean basin.

When comparing the amplitude spectra for the North Pacific Ocean, it can be observed that AOD1B Release 5 OBP product indeed contains the S1 tide (due to atmospheric tidal forcing). To make GTSM output comparable to the AOD1B Release 6 OCN product the tidal signals of frequencies of table 4.2 were removed. It seems that the method to remove the tides from GTSM output by least-squares estimation works well since for example the S1 and M2 tides are clearly removed from the signal for the North Pacific Ocean. For the lowest frequencies (up to 1/31 cycles per day) it seems that GTSM is more different from AOD1B Release 6 OCN than from AOD1B Release 5 OBP which corresponds to the results presented in table 4.5. When comparing the amlitude spectra for the Mediterranean Sea it can be observed that the differences in amplitudes for the frequency range 0.04-0.5 cycles per day is quite large for AOD1B Release 5 OBP and GTSM. These are differences in the high frequencies and

thus contributes to the observation that AOD1B Releaes 5 OBP differs more from GTSM in the higher frequencies than AOD1B Release 6.

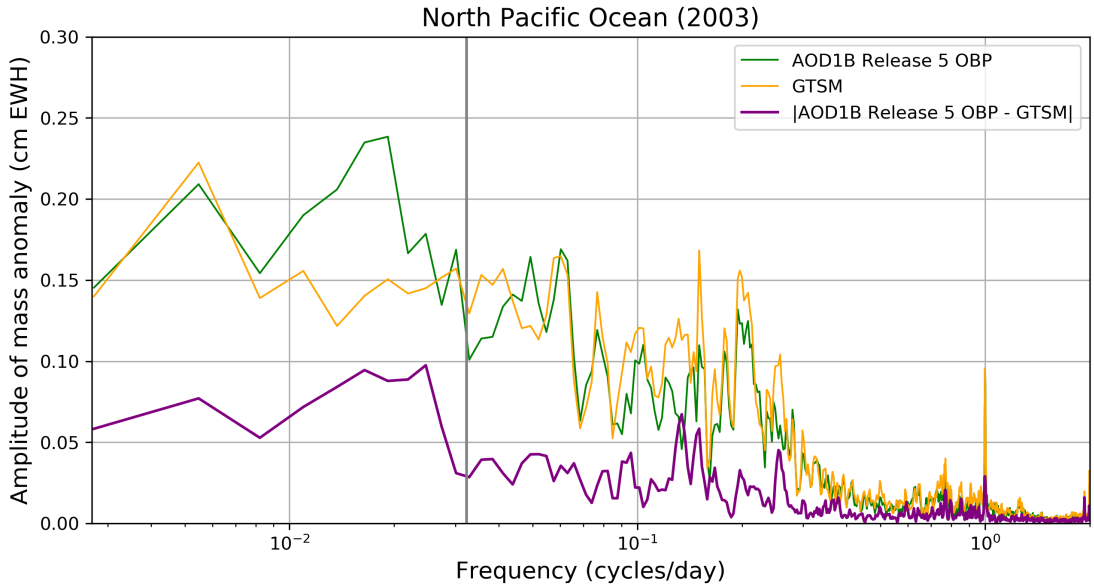

Figure 4.11: Frequency analysis of basin-average mass-anomaly time-series (year 2003) for the North Pacific Ocean. The considered time-series are derived from the AOD1B Release 5 OBP product and GTSM forced by only meteorological forcing. For all frequencies the amplitudes (harmonic coefficients). The absolute difference of the amplitudes is shown in purple. A moving average of 3 elements is applied to the amplitude spectra. The gray vertical line is at 1/31 cycles per day.

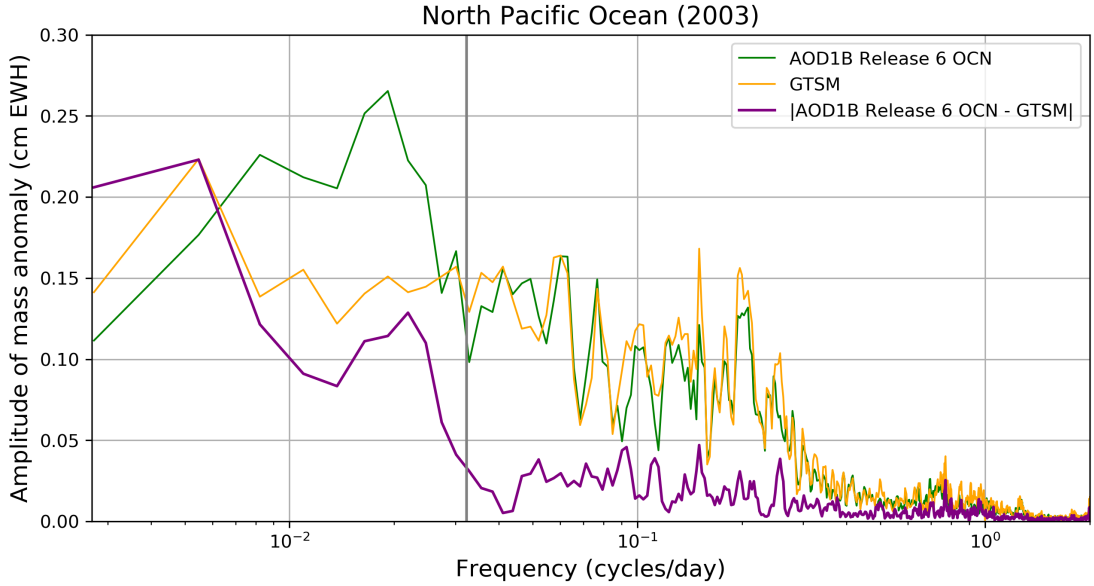

Figure 4.12: Frequency analysis of basin-average mass-anomaly time-series (year 2003) for the North Pacific Ocean. The considered time-series are derived from the AOD1B Release 6 OCN product and GTSM forced by only meteorological forcing. For all frequencies the amplitudes (harmonic coefficients). The absolute difference of the amplitudes is shown in purple. A moving average of 3 elements is applied to the amplitude spectra. The gray vertical line is at 1/31 cycles per day.

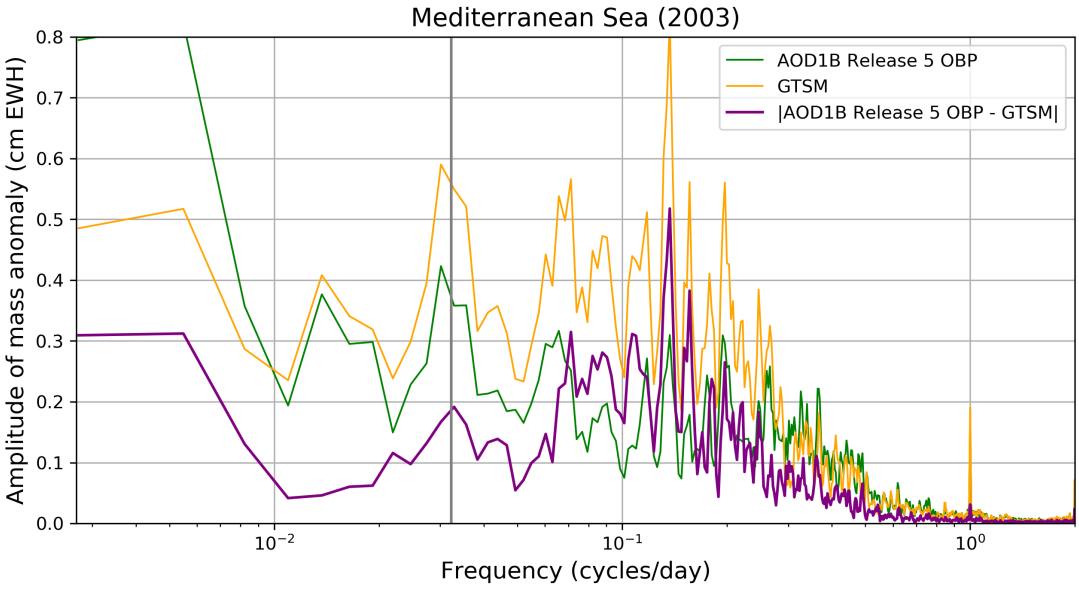

Figure 4.13: Frequency analysis of basin-average mass-anomaly time-series (year 2003) for the Mediterranean Sea. The considered time-series are derived from the AOD1B Release 5 OBP product and GTSM forced by only meteorological forcing. For all frequencies the amplitudes (harmonic coefficients). The absolute difference of the amplitudes is shown in purple. A moving average of 3 elements is applied to the amplitude spectra. The gray vertical line is at 1/31 cycles per day.

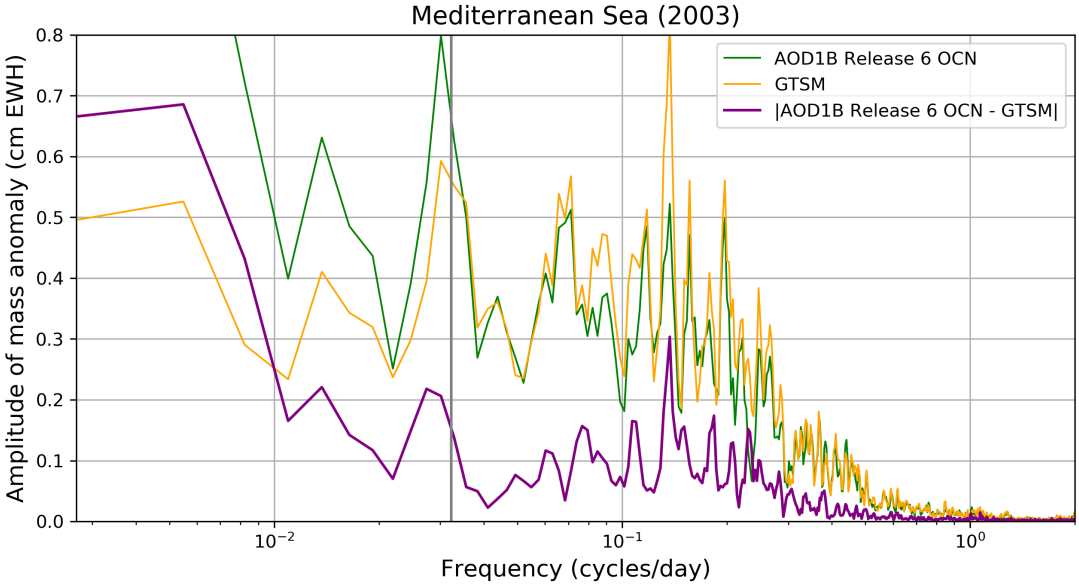

Figure 4.14: Frequency analysis of basin-average mass-anomaly time-series (year 2003) for the Mediterranean Sea. The considered time-series are derived from the AOD1B Release 6 OCN product and GTSM forced by only meteorological forcing. For all frequencies the amplitudes (harmonic coefficients). The absolute difference of the amplitudes is shown in purple. A moving average of 3 elements is applied to the amplitude spectra. The gray vertical line is at 1/31 cycles per day.

4.3.3. Monthly time-series comparison

In figures 4.15 and 4.16 the standard deviations of the monthly difference mass-anomaly time-series are shown globally. The monthly mass-anomaly time-series for these figures are a combination of both tidal and meteorological-forced dynamics. The global pattern of the calculated standard deviations was similar for the monthly mass-anomaly time-series of only meteorological-forced dynamics. The globally calculated standard deviations for these time-series can be found in Appendix C. In Appendix C also a global plot of the standard deviations of the monthly difference mass-anomaly time-series between AOD1B GAB Release 6 and AOD1B GAD Release 5 can be found. The monthly time-series have as duration January 2003 until March 2016. In table 4.6 the regional average standard deviations are shown. Again a distance plot is made to visualize the regional differences between GTSM, AOD1B

GAD Release 5 and AOD1B GAB Release 6. This distance plot can be found in figure 4.17. In figures 4.18 and 4.19 the standard deviations are plotted versus bathymetry for the whole ocean.

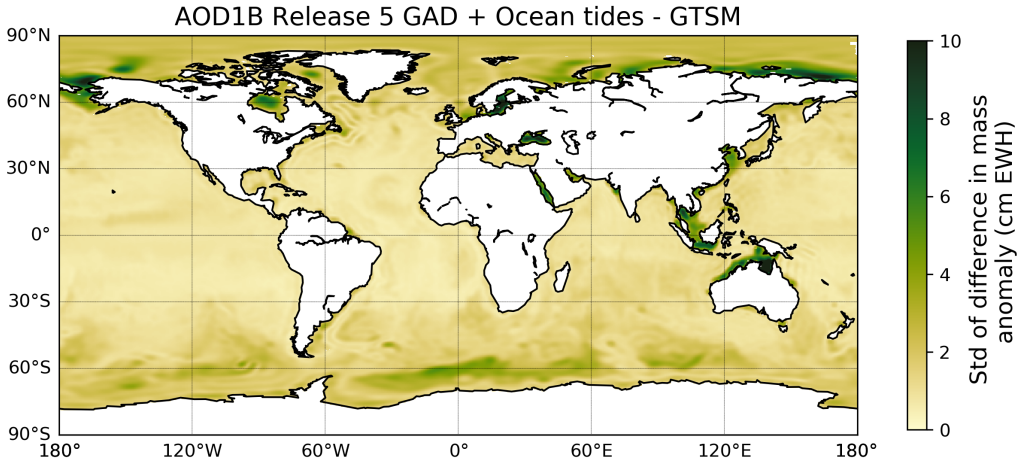

Figure 4.15: Standard deviation of the monthly difference mass-anomaly time-series. This difference mass-anomaly time-series is computed by subtracting GTSM (run with both tidal and meteorological forcing) from the AOD1B GAD Release 5 product plus the ocean tide Release 5 product.

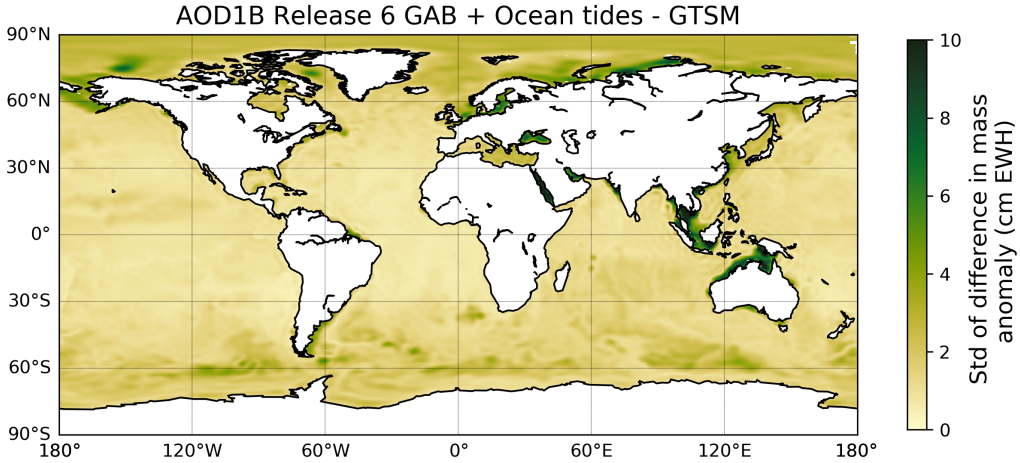

Figure 4.16: Standard deviation of the monthly difference mass-anomaly time-series. This difference mass-anomaly time-series is computed by subtracting GTSM (run with both tidal and meteorological forcing) from the AOD1B GAB Release 6 product plus the ocean tide Release 6 product.

Table 4.6: Regional averages of the standard deviation in cm EWH of the difference mass-anomaly times-series. The results for the difference mass-anomaly time-series for the hourly time-series (for the year 2003) and the monthly time-series are shown. For the monthly difference time-series only meteorological-forced dynamics and the combination of tidal and meteorological-forced dynamics are considered.

	Std of hourly time-series differences		Std of monthly time-series differences				
	AOD1B Release 5 OBP - GTSM	AOD1B Release 6 OCN - GTSM	AOD1B Release 5 GAD - GTSM	AOD1B Release 6 GAB - GTSM	AOD1B Release 5 GAD + Ocean tides - GTSM	AOD1B Release 6 GAB + Ocean tides - GTSM	AOD1B GAB Release 6 - AOD1B GAD Release 5
Total ocean	2.565	2.276	1.430	1.505	1.595	1.672	1.340
Arafura Sea	8.773	6.451	7.034	6.553	7.822	6.847	5.472
Arctic Ocean	5.763	4.077	3.142	2.383	3.101	2.648	2.803
Baltic Sea	14.671	9.828	6.834	4.438	7.029	4.809	4.372
Black Sea	8.379	8.791	6.791	5.603	6.934	5.618	6.158
Gulf of Thailand	6.136	8.509	4.391	8.242	5.328	9.412	6.287
Indian Ocean	2.387	2.345	1.309	1.640	1.502	1.791	1.194
Mediterranean Sea	2.496	2.169	1.158	1.944	1.354	2.066	1.594
North Atlantic Ocean	1.623	1.518	0.860	0.916	1.043	1.091	0.841
North Pacific Ocean	1.846	1.816	0.957	1.133	1.173	1.311	0.897
North Sea	6.863	8.429	2.603	3.489	2.805	3.530	3.332
South Atlantic Ocean	2.068	1.877	1.057	1.191	1.249	1.378	1.193
South China and Archipelagic Seas	2.681	3.139	2.294	3.097	2.563	3.368	2.432
South Pacific Ocean	1.933	1.764	0.908	0.990	1.061	1.126	0.917
Southern Ocean	2.988	2.557	1.951	1.645	2.231	1.819	1.833

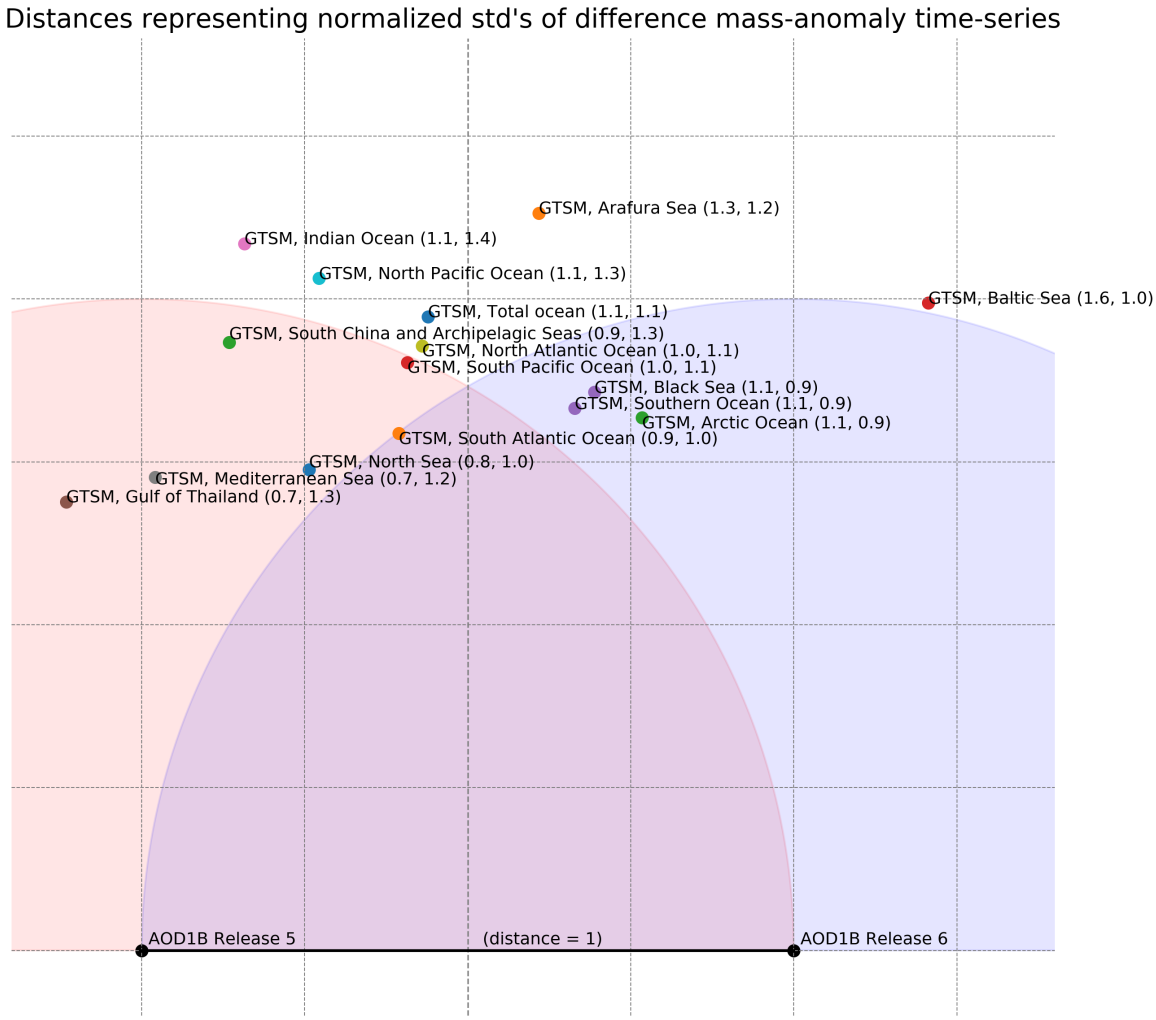

Figure 4.17: Distance plot where distances represent normalized differences between different ocean models. For each region the regional average std (as reported in table 4.6) is divided by the regional average std of difference time-series between AOD1B GAD Release 5 and AOD1B GAB Release 6. The considered time-series are at the monthly scale.

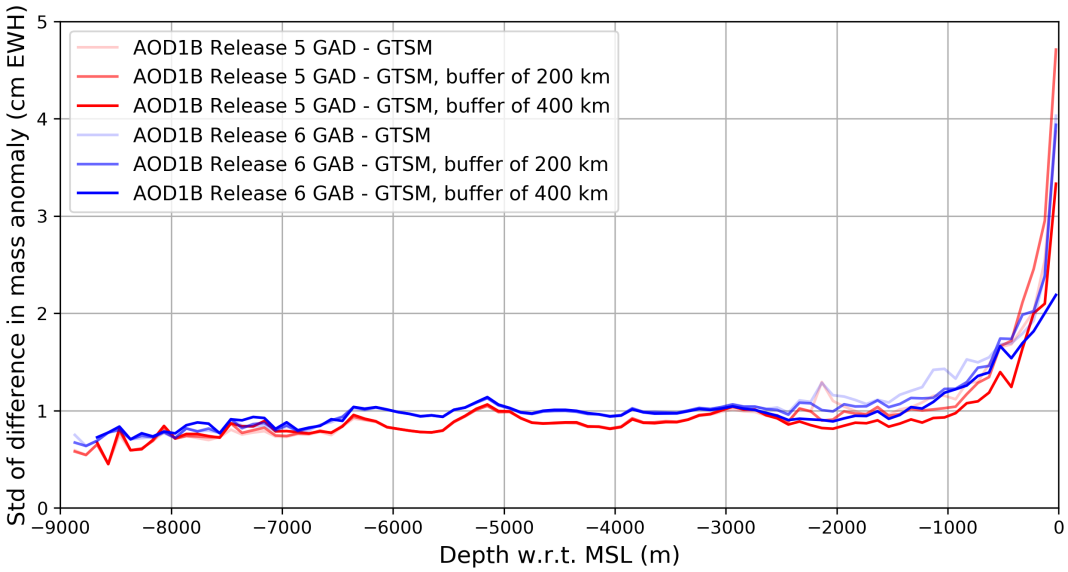

Figure 4.18: Standard deviation of the monthly difference mass-anomaly time-series versus bathymetry for the total ocean. These difference mass-anomaly time-series are computed by subtracting GTSM (run with only meteorological forcing) from AOD1B GAD Release 5 (red) and subtracting GTSM (run with only meteorological forcing) from AOD1B GAB Release 6 (blue).

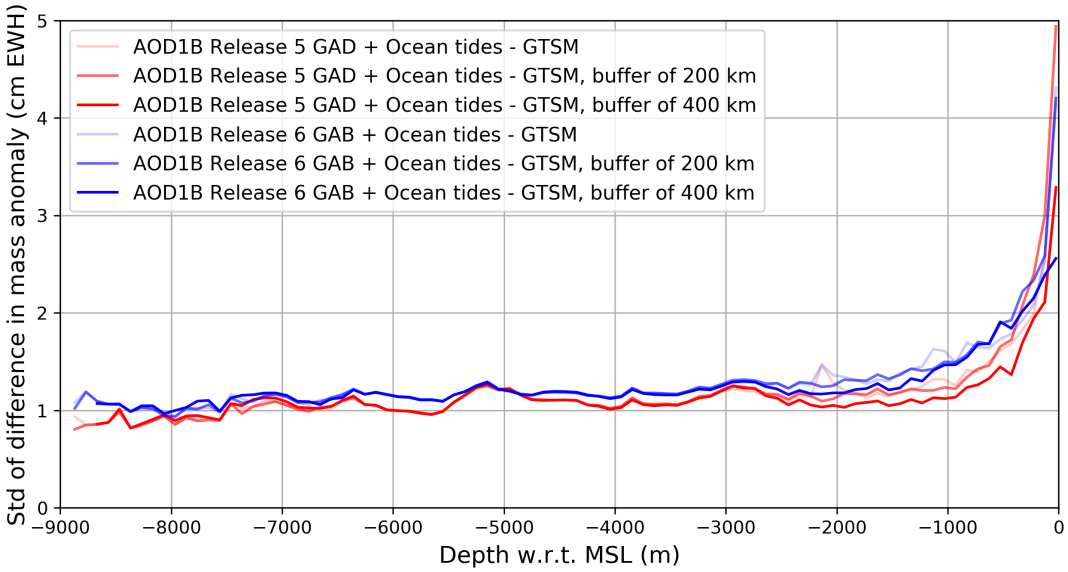

Figure 4.19: Standard deviation of the monthly difference mass-anomaly time-series versus bathymetry for the total ocean. These difference mass-anomaly time-series are computed by subtracting GTSM (run with both tidal and meteorological forcing) from AOD1B GAD Release 5 + ocean tide Release 5 (red) and subtracting GTSM (run with both tidal and meteorological forcing) from AOD1B GAB Release 6 + ocean tide Release 6 (blue).

It can be observed that the global patterns of small and large differences between GTSM and the AOD1B products are similar for the 3/6-hourly time-series and monthly time-series (see figures 4.3, 4.4, C.8 and C.9 and table 4.6). The largest differences are thus observed for shallow regions up to 200 m and the Red Sea, Black Sea and Arctic Ocean. The magnitude of the differences is smaller for the monthly time-series than for the hourly time-series. When considering monthly time-series the standard deviation is calculated from the differences of monthly mean values. In the monthly mean values high frequency signals (frequencies of a period smaller than a month) are largely (or totally) averaged out. Therefore, it is logical that the standard deviation of the difference mass-anomaly time-series are smaller for the monthly than the 3/6-hourly time-series.

For the regions where GRACE Level-2 data product for Release 6 seems better than for Release 5 (Hudson Bay and East Siberian Antarctic Shelf) the monthly time-series of GTSM are more close to AOD1B GAB Release 6 than to AOD1B GAD Release 5. For most regions (except Baltic Sea,

Black Sea, Arctic Ocean, Southern Ocean and Arafura Sea) GTSM shows on the monthly scale more agreement with AOD1B GAD Release 5. This can also be observed in figure 4.17. In section 4.3.2 it was already observed that GTSM differed in general less from AOD1B OBP Release 5 than from AOD1B OCN Release 6 for the frequencies smaller than 1/31 cycles per day. So it seems that GTSM is in the low frequencies more close to AOD1B GAD Release 5 and in the high frequencies more close to AOD1B GAB Release 6. Also from the plotted signal standard deviations versus bathymetry (figures 4.18 and 4.19) it can be observed that the monthly GTSM time-series are on the monthly scale close to AOD1B Release GAD 5 than AOD1B GAB Release 6 except for swallow regions up to a depth of approximately 350 m.

From table 4.6 it can also be observed that when GTSM is run with both tidal and meteorological forcing, it differs more from the AOD1B product + ocean tide product than when it is only run with meteorological forcing and compared to the AOD1B product only. Clearly the ocean tides are modeled differently by the currently used ocean tide background models and GTSM. It is also possible that non-linear interactions between tides and meteorological-forced dynamics in GTSM are a part of these differences since the GTSM time-series is compared against a combination time-series of a separately modeled ocean tide and meteorological-forced signal. Also from figures 4.18 and 4.19 it can be observed that for all depths the differences become larger when the tidal signals are included. Since non-linear interaction is more dominant in the swallow regions, it seems that the large differences arising when tidal signals are included are mostly due to a different way of tidal modeling (and not predominantly due to the non-linear interaction present in GTSM).

4.4. Summary and remarks

For both 3/6-hourly time-series and monthly time-series the largest differences between the considered oceanic models (GTSM, OMCT and MPIOM) can be found in shallow areas up to 200 m, Red Sea, Black Sea and Arctic Ocean. Differences in computed mass-anomaly time-series by the different models can have a large variety of reasons. For example, especially in shallow regions, the bathymetry has a large influence on the velocity and the bathymetry in the models might be quite different. Furthermore, the discretization in space is very different and GTSM has significantly finer grid cells in the shallow areas. A different parametrization of turbulence might cause large differences in energy rich parts of the ocean. In general, the differences between the models can also be due to the different applied meteorological forcing to the models or a different method to model dissipation mechanisms. Differences in dissipation due to bottom friction might also result in larger differences between the models in predominantly shallow areas. The inclusion of a sea ice model in the ocean model and the inclusion of pressure-driven flows (when the ocean model contains variations in water density) might be contributing to the differences in and near the Arctic Ocean. It is difficult to state which reasons are dominant.

It seems that GTSM is more close to AOD1B Release 5 than AOD1B Release 6 for the low frequencies (up to 1/31 cycles per day). This can be both observed in the frequency analysis of the 3/6-hourly time-series as well as in the differences in observations for the time-series at the hourly and monthly time-scale. The monthly time-series show in general smaller differences than the 3/6 hourly time-series. For monthly time-series, the ocean mean std's are 1.4 and 1.5 cm for respectively AOD1B Release 5 and AOD1B Release 6. For 3/6-hourly time-series these std's 2.6 and 2.3 cm.

The regions where significant differences between GTSM and currently used oceanic background models are observed are an indication of regions where improvements or deteriorations to the GRACE Level-2 data product can occur when changing to GTSM in GRACE data processing. Therefore, in predominantly the shallow regions up to 200 m, Black Sea, Red Sea and Arctic Ocean changes in the GRACE Level-2 data product are most expected when changing to GTSM. Significant differences between the AOD1B Release 5 and AOD1B Release 6 products can be observed for the regions where the quality of GRACE Release 6 solutions is clearly higher than the quality of GRACE Release 5 solutions (Hudson Bay and East Siberian Arctic Shelf). This indicates that the oceanic background models do influence the quality of GRACE Level-2 data.

5

Potential improvements to GRACE monthly solutions by the use of GTSM

This chapter is about the identification of regions where it is expected that GRACE monthly solutions will be improved by changing to GTSM as oceanic background model in GRACE data processing. The sub-question for this section is:

- For which regions does the quality of GRACE monthly solutions increase by the use of monthly mass-anomaly time-series generated by GTSM?

No new theory will be covered in this chapter. Only the method to identify regions of expected improvements or detoriations is explained. In this method monthly time-series are used which are generated by GTSM. From chapter 4 it seems that tides are modeled differently by GTSM and the current applied oceanic background models. These differences could also be due to non-linear interaction between tidal and meteorological forced dynamics which are present in GTSM. Therefore, two types of monthly mass-anomaly time-series are considered. The first type is retrieved by applying both tidal and meteorological forcing to GTSM. The second type is retrieved by applying only meteorological forcing to GTSM. After the explanation of the method, the results are presented and discussed.

5.1. Method

In this section it is explained how GRACE Level-2 data are modified to estimate which oceanic regions are expected to be improved by considering GTSM as oceanic background model in GRACE data processing. Monthly time-series from GTSM are produced according to the method described in section 4.2.3. Both versions (with and without tidal forcing) are considered in this chapter. Version 1 relates to the version where GTSM is forced by both meteorological and tidal forcing. Version 2 relates to the version where GTSM is forced by only meteorological forcing. The GTSM-based monthly time-series are turned into Stokes coefficients up to degree and order 60 according to the method described in section 4.2.4.

The GRACE Level-2 data CSR Release 5, CSR Release 6, ITSG 2016, ITSG 2018, GFZ Release 5 and JPL Release 6 are turned to mass-anamolies at a 0.5° equiangular grid using the method described in section 3.2.1. Also the considered period (2003-2016), removal of long-term mean and the use of a Gaussian filter (400 km half-width) are similar. The monthly ocean tide and monthly AOD1B product provided by ITSG are the considered data-sets to be add back to the GRACE Level-2 data. The AOD1B products at the hourly scale are provided by GFZ, but ITSG provides their own monthly mean products of these AOD1B products at the hourly scale. The tidal and non-tidal products are also provided as a set of Stokes coefficients. These are truncated to degree 60 before the conversion into to mass-anomaly time-series. This conversion is applied using a method similar to that described in section 3.2.1. In contrast to section 3.2.1, the low-degree Stokes coefficients are retained and not replaced or removed for these tidal and non-tidal products. The GTSM-based Stokes coefficients are converted back to mass-anomaly time-series in a similar way. This includes the use of the Gaussian filter of 400

km half-width, retaining low-degree Stokes coefficients and removal of the long-term mean (January 2003-March 2016) for each particular Stokes coefficient.

For each grid point of the 0.5° equiangular grid the mass-anomaly time-series retrieved from the AOD1B (and tidal) products are added to mass-anomaly time-series retrieved from the GRACE Level-2 data. Consequently the mass-anomaly time-series retrieved from the created GTSM products are removed. When both the AOD1B and tidal product are added back the GTSM-based version 1 product is removed. When only the AOD1B product is added back the GTSM-based version 2 product is removed. This addition and subtraction of time-series gives (apart from rounding errors) edited mass-anomaly time-series exactly similar to time-series computed from edited Stokes coefficients (computed by addition and subtraction of Stokes coefficients of the different products). This will be named the method of addition and subtraction (MAS). For the GRACE Level-2 data CSR Release 5, GFZ Release 5 and ITSG 2016 the considered non-tidal and tidal products to be added back are AOD1B GAD Release 5 and ocean tide Release 5 as provided by ITSG. For the GRACE Level-2 data CSR Release 6, JPL Release 6 and ITSG 2018 the considered non-tidal and tidal products to be added back are AOD1B GAB Release 6 and ocean tide Release 6 as provided by ITSG. The GTSM product which is added back depends on both the consideration of the tidal product or not and on the consideration of Release 5 or 6 GRACE Level-2 data. The Release 5 and 6 variants of GTSM vary by the removal of a different long-term mean and inclusion or not of a residual mean atmospheric pressure over the ocean. Version 1 and 2 relate to GTSM monthly time-series where GTSM is run with both tidal and meteorological forcing (version 1) or with only meteorological forcing (version 2). In table 5.1 an overview of the added products can be found. The GTSM-based product which is consequently removed is always the product which is constructed similarly to the added products.

Table 5.1: Overview of the products which are added back to GRACE monthly solutions in the addition part of the MAS to create edited GRACE monthly solutions.

GRACE monthly solution	Release 5 (edited version 1)	Release 5 (edited version 2)	Release 6 (edited version 1)	Release 6 (edited version 2)
Added products	AOD1B GAD Release 5 and ocean tide Release 5	AOD1B GAD Release 5	AOD1B GAB Release 6 and ocean tide Release 6	AOD1B GAB Release 6

For all edited mass-anomaly time-series the signal variance is estimated by VCE while considering three mass-anomaly time-series in the VCE and using MYDD-minimization as regularization technique. For edited ITSG solutions, the residuals with respect to a low-pass filtered signal and analytical function are similarly estimated as described in section 3.2.4. Again all types of unexpected signals and residuals are shown globally as well as versus bathymetry. Regional average values are reported too.

5.2. Results and discussion

In figures 5.1, 5.4, 5.7, 5.10 the changes in signal standard deviation due to the application of the MAS to GRACE Release 5 and GRACE Release 6 solutions are shown globally. In figures 5.2, 5.5, 5.3, 5.6,5.8, 5.11, 5.9 and 5.12 the changes in the residuals (with respect to a low-pass filtered signal or analytical function) due to the application of the MAS to ITSG 2016 and ITSG 2018 are shown globally. In tables 5.2, 5.3 and 5.4 regional averages of the changes in the unexpected signals and residuals are shown.

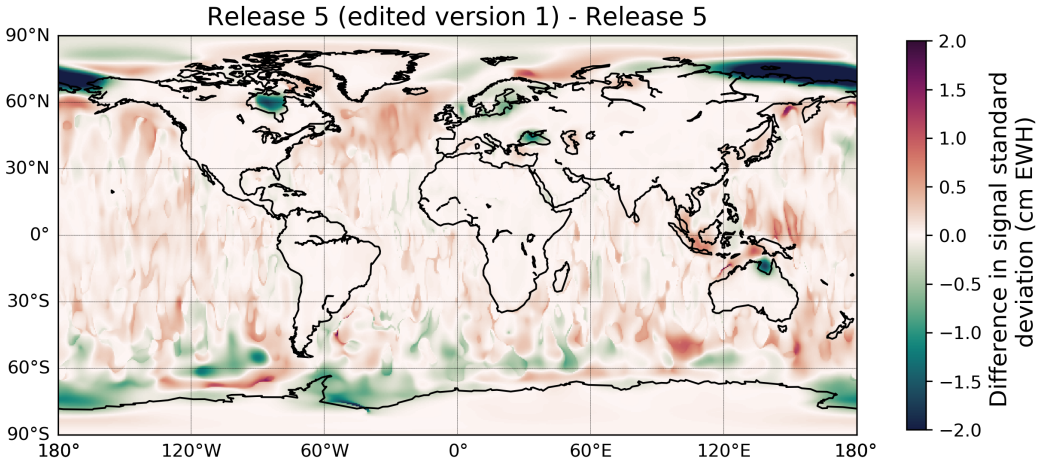

Figure 5.1: Difference in estimated signal standard deviation between edited GRACE Release 5 solutions (CSR Release 5 (edited version 1), ITSG 2016 (edited version 1), GFZ Release 5 (edited version 1)) and original GRACE Release 5 solutions (CSR Release 5, ITSG 2016, GFZ Release 5).

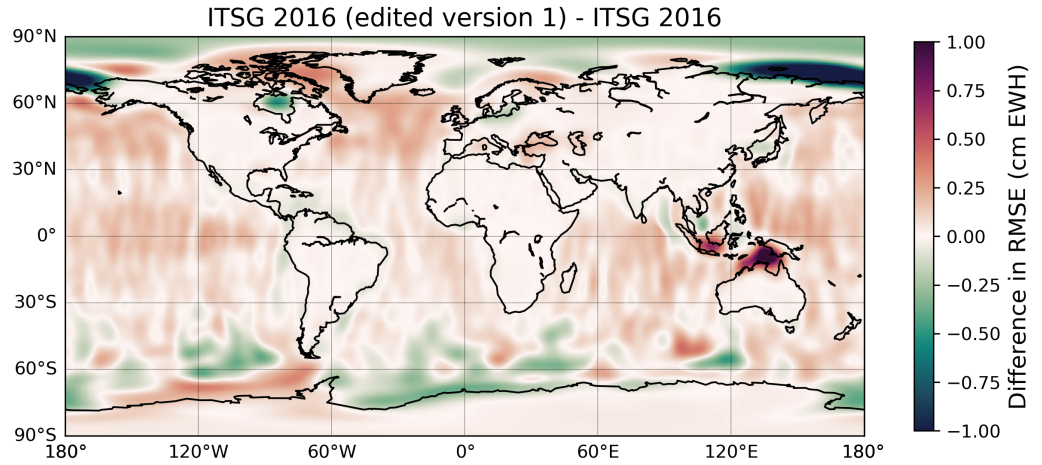

Figure 5.2: Difference in estimated RMSE between ITSG 2016 (edited version 1) and ITSG 2016. The RMSE is estimated with respect to a by least-squares estimated signal containing only a linear trend and annual and semi-annual periodicity.

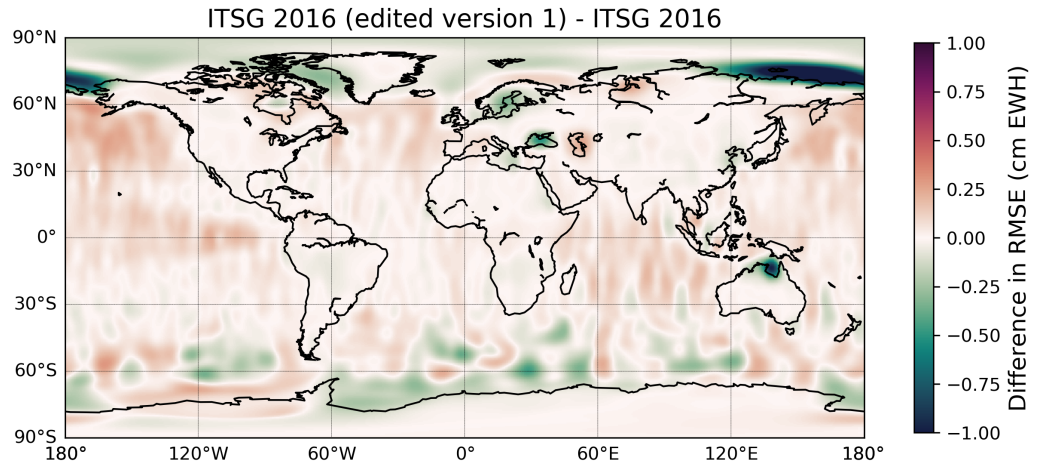

Figure 5.3: Difference in estimated RMSE between ITSG 2016 (edited version 1) and ITSG 2016. The RMSE is estimated with respect to a low-pass filtered signal (frequencies smaller than or equal to the semi-annual cycle are retained in the low-pass filtered signal).

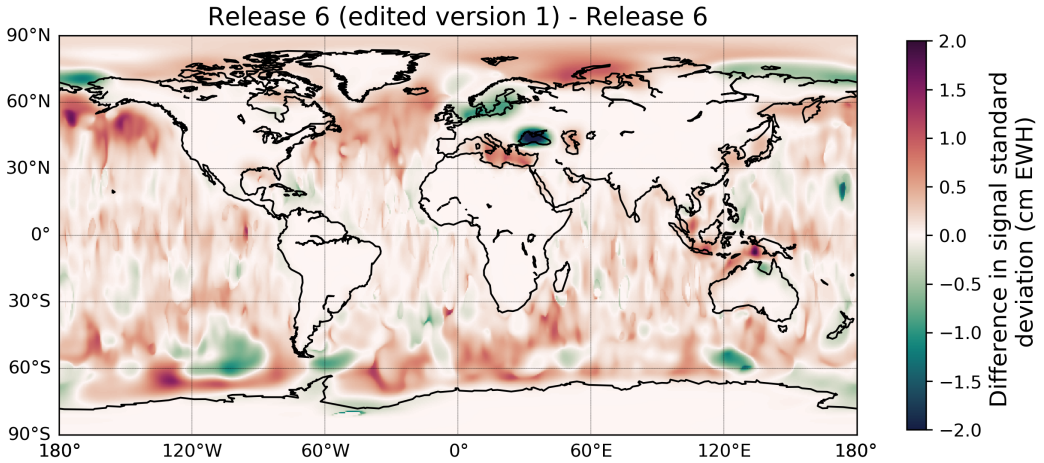

Figure 5.4: Difference in estimated signal standard deviation between edited GRACE Release 6 (CSR Release 6 (edited version 1), ITSG 2018 (edited version 1), JPL Release 6 (edited version 1)) solutions and original GRACE Release 6 solutions (CSR Release 6, ITSG 2018, JPL Release 6).

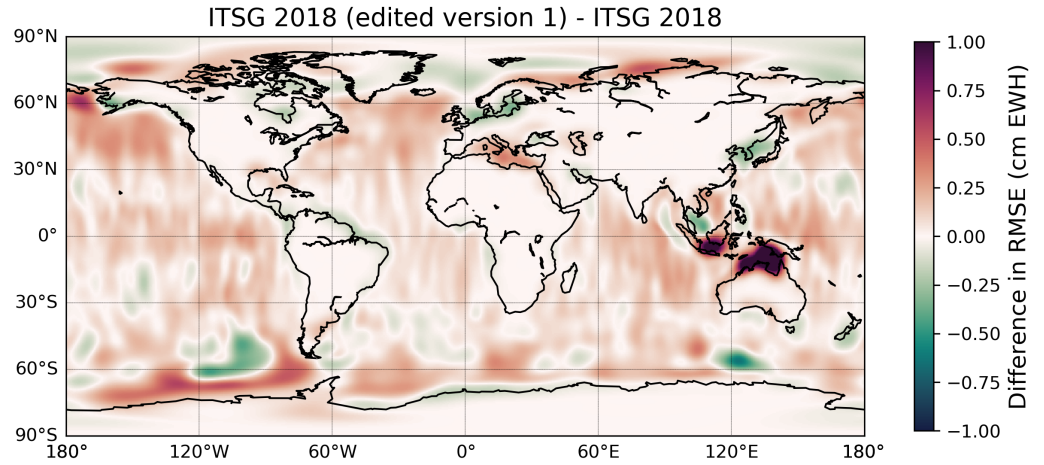

Figure 5.5: Difference in estimated RMSE between ITSG 2018 (edited version 1) and ITSG 2018. The RMSE is estimated with respect to a by least-squares estimated signal containing only a linear trend and annual and semi-annual periodicity.

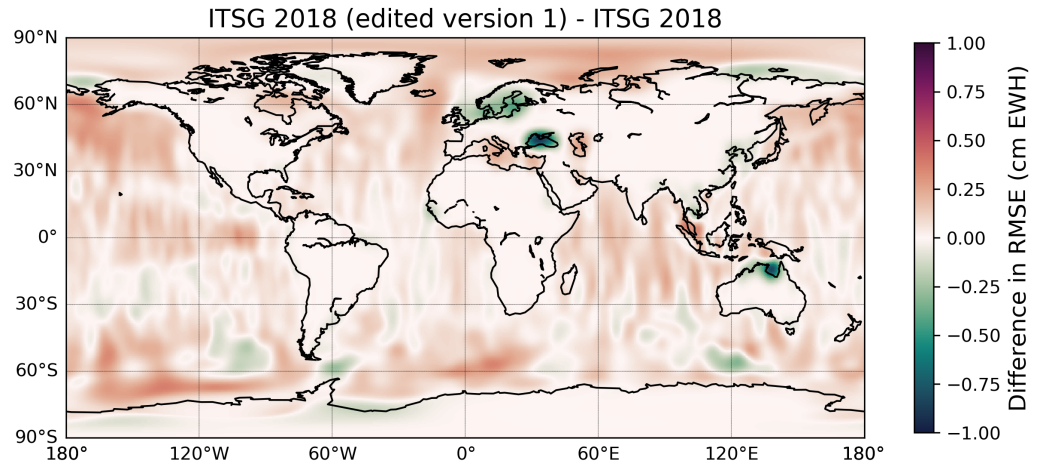

Figure 5.6: Difference in estimated RMSE between ITSG 2018 (edited version 1) and ITSG 2018. The RMSE is estimated with respect to a low-pass filtered signal (frequencies smaller than or equal to the semi-annual cycle are retained in the low-pass filtered signal).

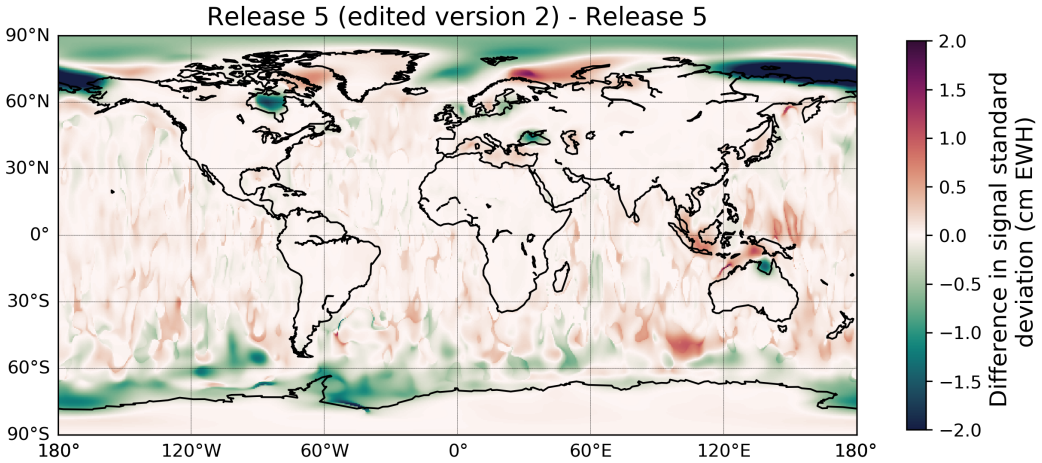

Figure 5.7: Difference in estimated signal standard deviation between edited GRACE Release 5 solutions (CSR Release 5 (edited version 2), ITSG 2016 (edited version 2), GFZ Release 5 (edited version 2)) and original GRACE Release 5 solutions (CSR Release 5, ITSG 2016, GFZ Release 5).

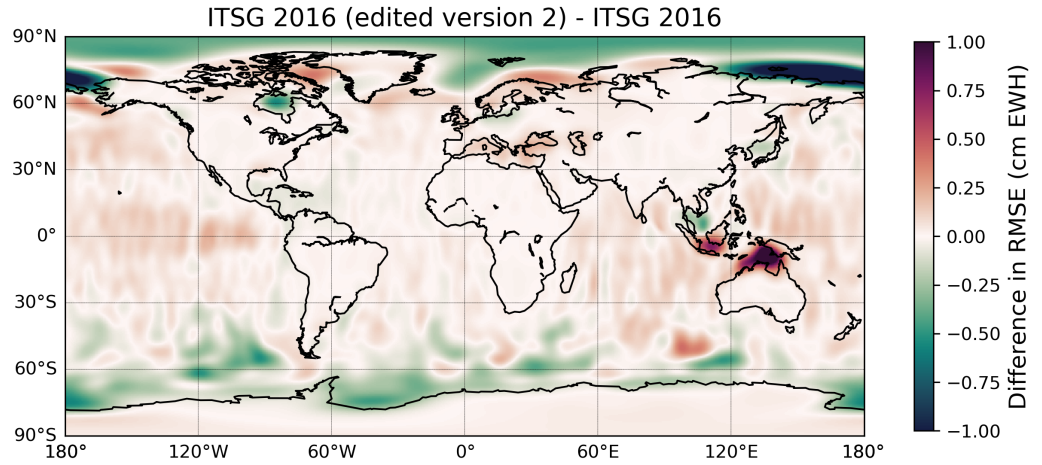

Figure 5.8: Difference in estimated RMSE between ITSG 2016 (edited version 2) and ITSG 2016. The RMSE is estimated with respect to a by least-squares estimated signal containing only a linear trend and annual and semi-annual periodicity.

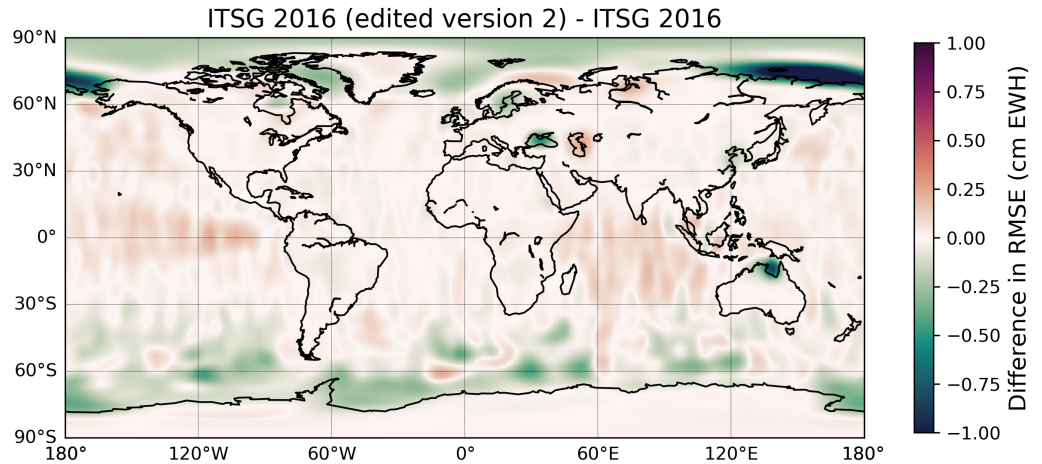

Figure 5.9: Difference in estimated RMSE between ITSG 2016 (edited version 2) and ITSG 2016. The RMSE is estimated with respect to a low-pass filtered signal (frequencies smaller than or equal to the semi-annual cycle are retained in the low-pass filtered signal).

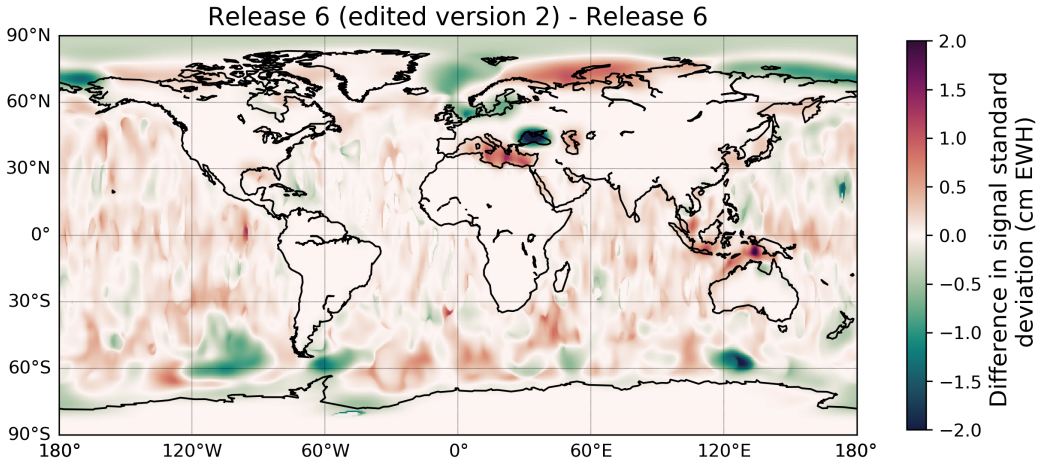

Figure 5.10: Difference in estimated signal standard deviation between edited GRACE Release 6 (CSR Release 6 (edited version 2), ITSG 2018 (edited version 2), JPL Release 6 (edited version 2)) solutions and original GRACE Release 6 solutions (CSR Release 6, ITSG 2018, JPL Release 6).

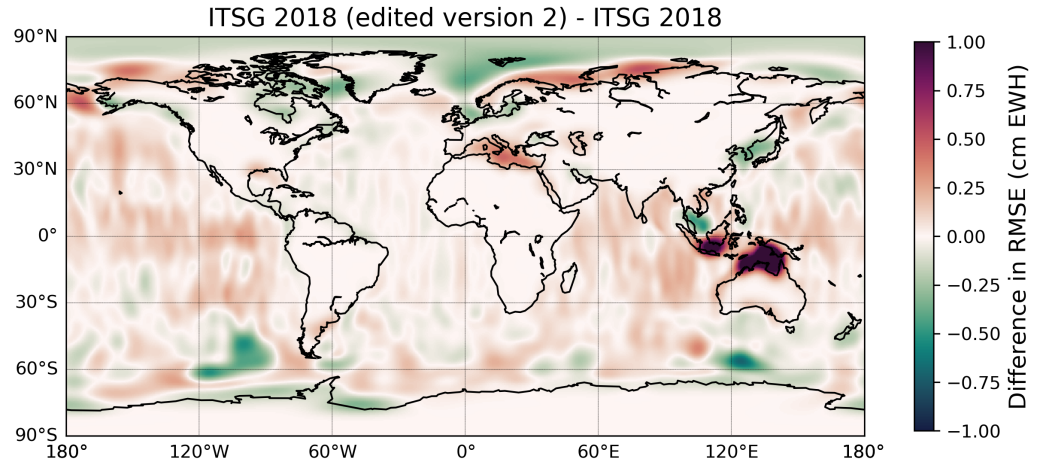

Figure 5.11: Difference in estimated RMSE between ITSG 2018 (edited version 2) and ITSG 2018. The RMSE is estimated with respect to a by least-squares estimated signal containing only a linear trend and annual and semi-annual periodicity.

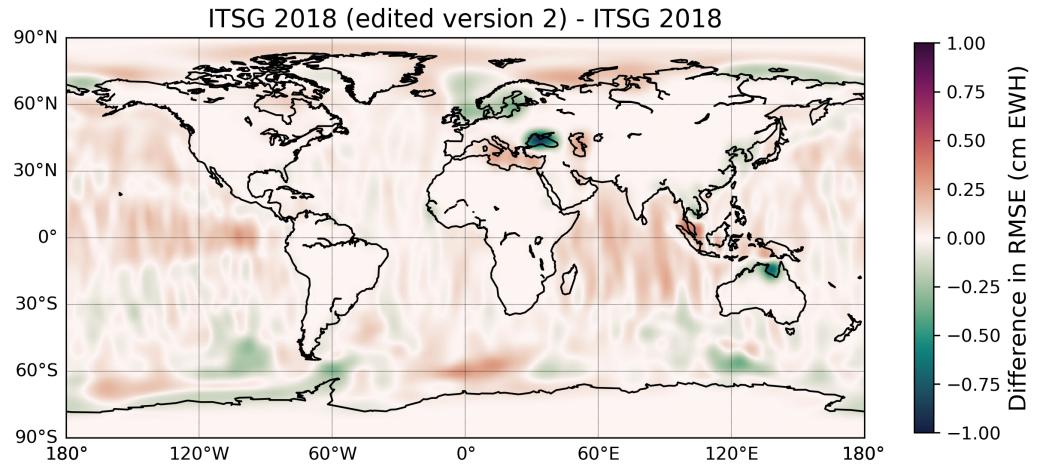

Figure 5.12: Difference in estimated RMSE between ITSG 2018 (edited version 2) and ITSG 2018. The RMSE is estimated with respect to a low-pass filtered signal (frequencies smaller than or equal to the semi-annual cycle are retained in the low-pass filtered signal).

Table 5.2: Regional averages of estimated signal standard deviation in cm EWH for different GRACE Level-2 data before and after the MAS. For Release 5 the signal standard deviation is determined by considering CSR Release 5, GFZ Release 5 and ITSG 2016 time-series together in the VCE. For Release 6 the signal standard deviation is determined by considering CSR Release 6, JPL Release 6 and ITSG 2018 time-series together in the VCE.

	Signal standard deviation					
	Release 5	Release 6	Release 5 (edited version 1)	Release 6 (edited version 1)	Release 5 (edited version 2)	Release 6 (edited version 2)
Total Ocean	0.864	0.994	0.811	1.100	0.772	1.003
Arafura Sea	2.837	2.195	2.474	2.497	2.618	2.651
Arctic Ocean	2.236	1.843	1.643	1.975	1.537	1.720
Baltic Sea	3.210	3.666	2.798	2.960	2.955	3.127
Black Sea	3.518	4.690	2.829	2.836	2.828	2.834
Gulf of Thailand	1.661	2.455	1.921	2.594	1.913	2.564
Indian Ocean	0.576	0.871	0.626	0.996	0.615	0.923
Mediterranean Sea	1.431	1.541	1.466	1.993	1.559	2.094
North Atlantic Ocean	0.605	0.761	0.659	0.878	0.610	0.764
North Pacific Ocean	0.602	0.753	0.673	0.919	0.617	0.801
North Sea	1.154	1.742	0.929	1.284	0.912	1.194
South Atlantic Ocean	0.953	1.352	0.973	1.417	0.952	1.361
South China and Archipelagic Seas	1.023	1.326	1.125	1.520	1.151	1.525
South Pacific Ocean	0.434	0.609	0.467	0.696	0.432	0.615
Southern Ocean	1.218	1.112	1.022	1.307	0.862	1.034

Table 5.3: Regional averages of the RMSE in cm EWH for ITSG monthly solutions before and after applying the MAS. The RMSE is estimated with respect to a by least-squares estimated signal containing only a linear trend and annual and semi-annual periodicity.

	RMSE w.r.t. seasonal signal					
	ITSG 2016	ITSG 2018	ITSG 2016 (edited version 1)	ITSG 2018 (edited version 1)	ITSG 2016 (edited version 2)	ITSG 2018 (edited version 2)
Total Ocean	1.745	1.577	1.789	1.656	1.750	1.613
Arafura Sea	3.523	2.437	4.325	4.047	4.480	4.207
Arctic Ocean	2.430	2.159	2.306	2.175	2.239	2.098
Baltic Sea	2.819	2.748	2.738	2.537	2.814	2.625
Black Sea	3.878	3.869	4.035	3.791	4.036	3.794
Gulf of Thailand	3.742	3.691	3.682	3.493	3.559	3.380
Indian Ocean	1.684	1.506	1.738	1.591	1.714	1.571
Mediterranean Sea	2.309	2.012	2.357	2.202	2.404	2.248
North Atlantic Ocean	1.688	1.536	1.746	1.600	1.688	1.529
North Pacific Ocean	1.583	1.415	1.674	1.506	1.627	1.453
North Sea	1.782	1.758	1.825	1.629	1.826	1.590
South Atlantic Ocean	1.744	1.627	1.760	1.658	1.744	1.632
South China and Archipelagic Seas	2.280	2.091	2.358	2.278	2.344	2.256
South Pacific Ocean	1.504	1.378	1.553	1.438	1.515	1.404
Southern Ocean	1.969	1.705	1.949	1.821	1.824	1.681

Table 5.4: Regional averages of the RMSE in cm EWH for ITSG monthly solutions before and after applying the MAS. The RMSE is estimated with respect to a low-pass filtered signal (frequencies smaller than or equal to the semi-annual cycle are retained in the low-pass filtered signal).

	RMSE w.r.t. low-pass filtered signal					
	ITSG 2016	ITSG 2018	ITSG 2016 (edited version 1)	ITSG 2018 (edited version 1)	ITSG 2016 (edited version 2)	ITSG 2018 (edited version 2)
Total Ocean	1.248	1.076	1.259	1.132	1.232	1.098
Arafura Sea	2.169	1.854	1.788	1.618	1.831	1.691
Arctic Ocean	1.811	1.567	1.637	1.629	1.621	1.592
Baltic Sea	2.011	1.933	1.785	1.630	1.847	1.698
Black Sea	1.922	1.973	1.579	1.308	1.572	1.300
Gulf of Thailand	2.036	1.792	2.140	1.849	2.129	1.834
Indian Ocean	1.206	1.014	1.225	1.072	1.215	1.055
Mediterranean Sea	1.444	1.172	1.427	1.294	1.445	1.313
North Atlantic Ocean	1.219	1.071	1.245	1.123	1.214	1.079
North Pacific Ocean	1.180	1.003	1.251	1.093	1.207	1.048
North Sea	1.358	1.345	1.323	1.155	1.318	1.131
South Atlantic Ocean	1.274	1.152	1.283	1.190	1.265	1.171
South China and Archipelagic Seas	1.351	1.126	1.365	1.181	1.368	1.177
South Pacific Ocean	1.130	0.989	1.151	1.031	1.123	0.996
Southern Ocean	1.334	1.057	1.297	1.141	1.209	1.045

In figures 5.1, 5.4, 5.7, 5.10, 5.3, 5.6, 5.9 and 5.12 it can be observed that the regions where the signal standard deviation changes due to the MAS are similar to the regions where the residual with respect to a low-pass filtered signal for ITSG solutions changes (in direction, not in size). This is not surprising since the signal standard deviation is a measure for interannual differences in the mass-derivative. Therefore high-frequency signals (which do not repeat yearly) will also show up in this estimate of signal standard deviation. For GRACE Release 5 solutions the MAS decreases the signal standard deviation and the residual w.r.t. a low-pass filtered signal for the regions Gulf of Carpentaria, Baltic Sea, Black Sea, North Sea, East Siberian Arctic Shelf, Hudson Bay and parts of the Arctic and Southern Ocean. For GRACE Release 6 solutions the MAS decreases this signal standard deviation and the residual w.r.t. a low-pass filtered signal for the regions Gulf of Carpentaria, Baltic Sea, Black Sea, East Siberian Arctic Shelf and North Sea. These regions where the signal standard deviation and the residuals w.r.t. low-pass filtered signal become lower indicate regions where improvements are most expected when applying GTSM in GRACE data processing.

When the types of MAS (version 1 and version 2) are compared it can be observed that the estimates of signal standard devation and residuals for both Release 5 and Release 6 solutions decrease for especially the regions in and close to the Arctic and Southern Ocean for version 2. In general, it seems that most regions (except the Arafura Sea, Baltic Sea, Mediterranean Sea, South China and Archipelagic Seas) improve more when the tidal forced dynamics are not taken into account. This might indicate that the monthly mean values of the tides are worse modeled by GTSM than by the currently used ocean tide models. This might also indicate that there is some non-linear interaction showing up in the monthly means. Since the monthly means contain predominantly the lowest tidal frequencies (solar semiannual, solar annual) actually not so much differences in the estimated standard deviation and residuals are expected when comparing version 1 with version 2. The tidal forcing of these low frequencies should be exactly similar for each year. Maybe these differences in estimated signal standard deviation and residuals are caused by differences in the modeled tides of frequencies of roughly a month or half a month (like the lunar monthly). The effect of these tides is partly present in the monthly means since the length of the month over which an average is computed is not exactly

equal to the period or a multiple of the period of these tides.

Most regions where the signal standard deviation and the residual w.r.t. low-pass filtered signal change correlate to regions where also the non-seasonal variability changes. But there are some regions (for example Black Sea and Arafura Sea/Gulf of Carpentaria) where this correlation is not present. It seems that there are after the MAS some yearly repeating patterns in the Arafura Sea/Gulf of Carpentaria which cannot be described by sine and cosine functions representing only an annual and semi-annual periodicity. In figure 5.13 as ITSG time-series before and after the MAS for a location in the Gulf of Carpentaria are shown. It can be observed that the MAS introduces more interannual variability on the long-term while high-frequency irregularities are reduced. These signals show up as residuals w.r.t. the seasonal signal but not as residuals w.r.t. the low-pass filtered signal because long-term signals cause the interannual variability. It seems that the signal standard deviation is also more sensitive to interannual differences of high-frequency than low-frequency because the signal standard deviation decreases for the Arafura Sea. For this, you can also observe the regularized solutions for the same location in the Gulf of Carpentaria in figure 5.14. Since some long-term variability might be true-signal, it might be possible that also for the Gulf of Carpentina (Arafura Sea) the GRACE Level-2 data can be improved when changing to GTSM.

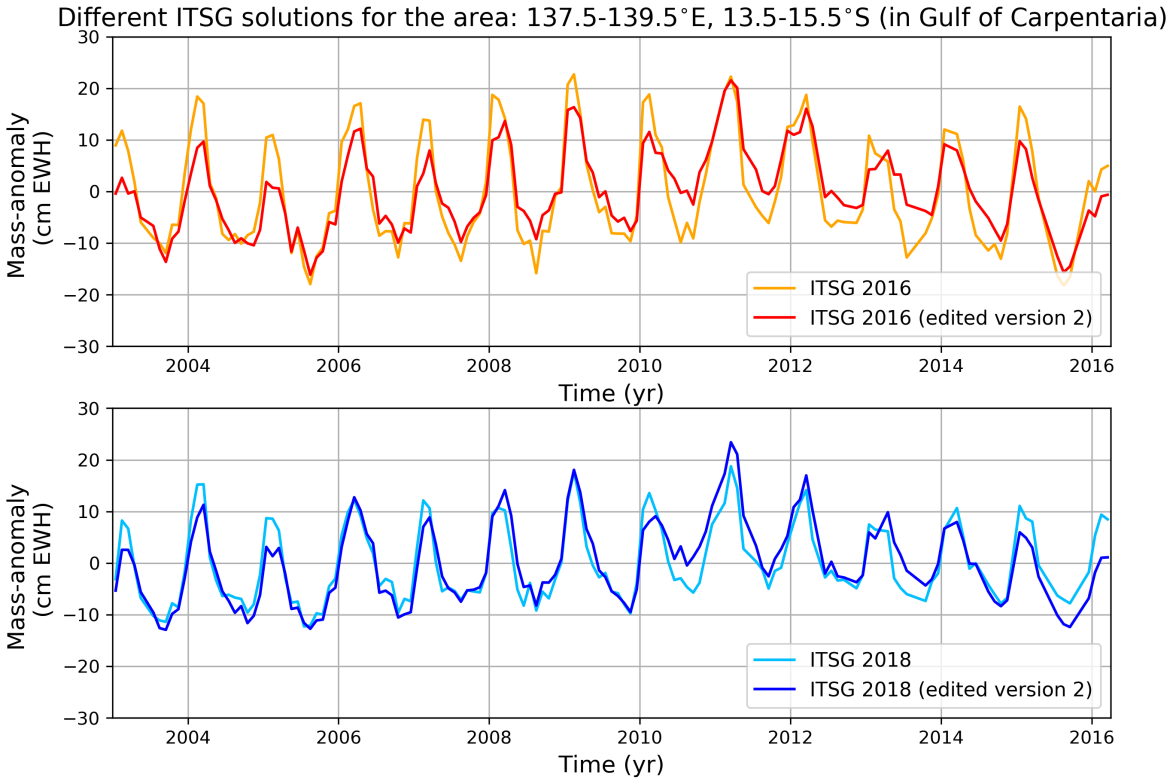

Figure 5.13: Time-series of ITSG solutions before and after the MAS. The average mass-anomaly time-series for a square region in the Gulf of Carpentina are shown.

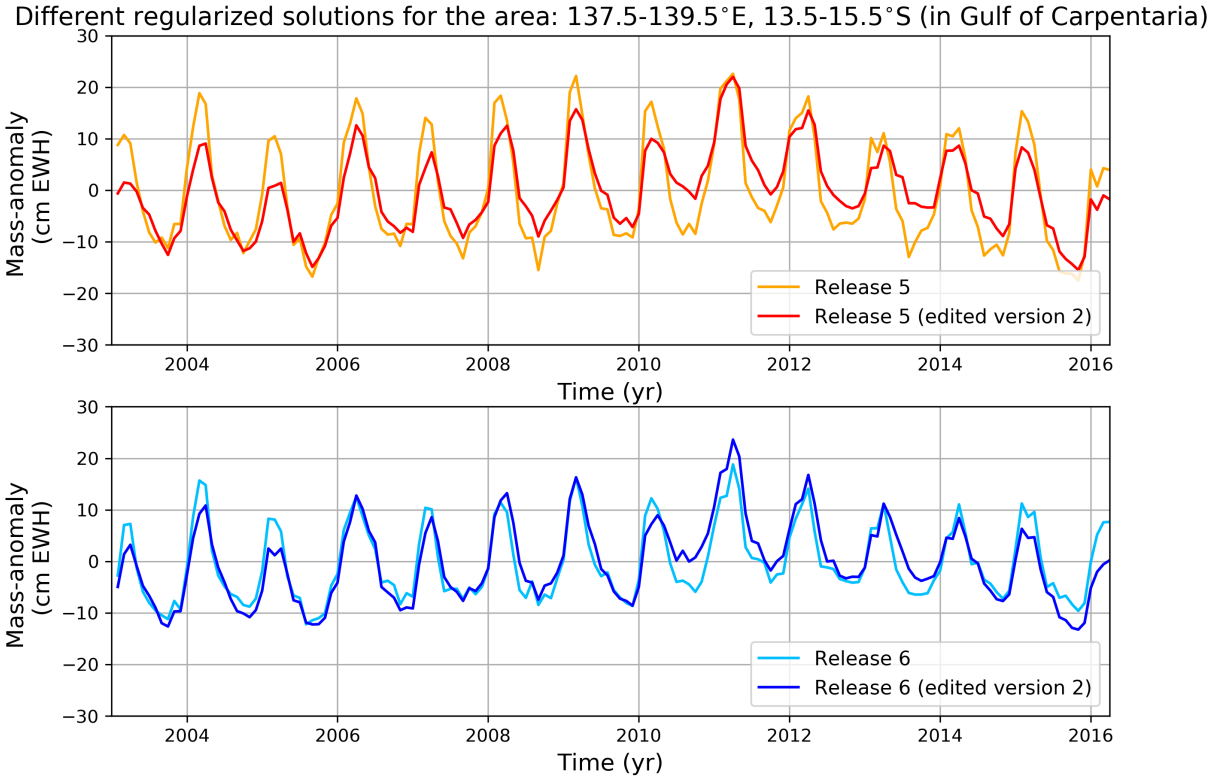

Figure 5.14: Time-series of regularized solutions estimated from GRACE monthly solutions before and after the MAS. The average mass-anomaly time-series for a square region in the Gulf of Carpentina are shown.

For the North Sea, Baltic Sea and Black Sea, both GRACE Release 5 and 6 monthly solutions improve due to the MAS by showing a decrease in the signal standard deviation and the residual w.r.t. low-pass filtered signal for those areas. In general it can be expected that GTSM might perform better than the currently applied oceanic background models for the regions around Europe. Since GTSM is developed by a Dutch company, it seems logical that more validation of the model has been performed for regions near The Netherlands and around Europe (also because of the available verification data). Maybe GTSM could be used in GRACE data-processing for the regions around Europe (except Mediterranean Sea) and currently used oceanic background models still for the other regions.

To observe the influence of the MAS for some other locations the regularized time-series are shown before and after applying the MAS to GRACE monthly solutions. This is done for a location in the North Sea (figure 5.15), Black Sea (figure 5.16) and Indian Ocean (figure 5.17). For the North Sea and Black Sea clearly a reduction in the high-frequency variability can be observed. For the North Sea it can be observed that also a long-term trend is altered for Release 5. A change in phase of the seasonal signal can be observed for Release 6. The time-series for the Indian Ocean are shown since the amplitude of the seasonal variability increases due to the MAS. These figures show that the MAS can change the seasonal variability and long-term trend in the mass-anomaly time-series.

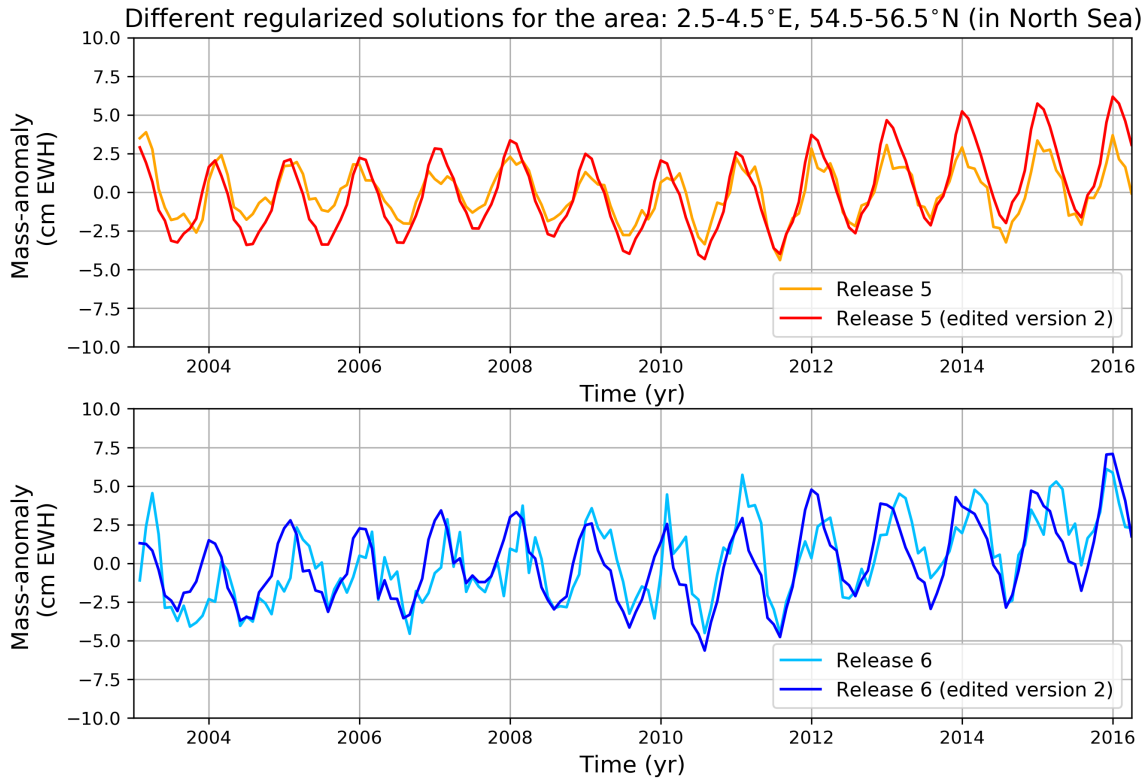

Figure 5.15: Time-series of regularized solutions estimated from GRACE monthly solutions before and after the MAS. The average mass-anomaly time-series for a square region in the North Sea are shown.

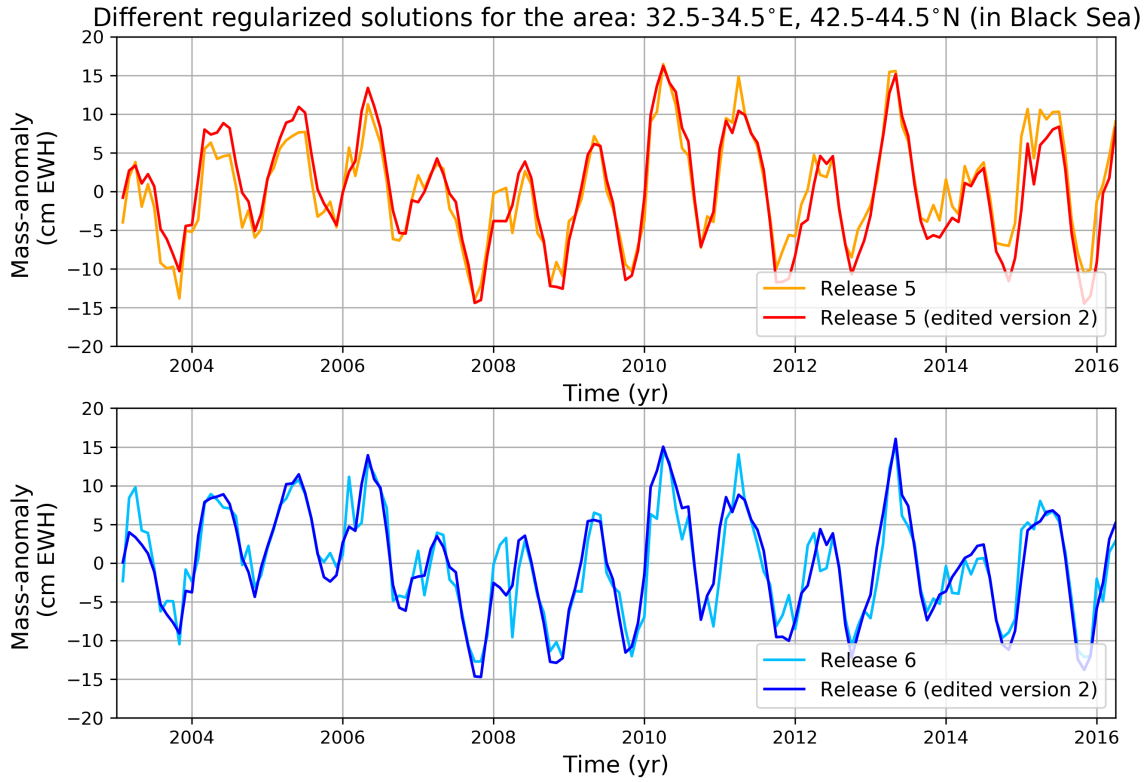

Figure 5.16: Time-series of regularized solutions estimated from GRACE monthly solutions before and after the MAS. The average mass-anomaly time-series for a square region in the Black Sea are shown.

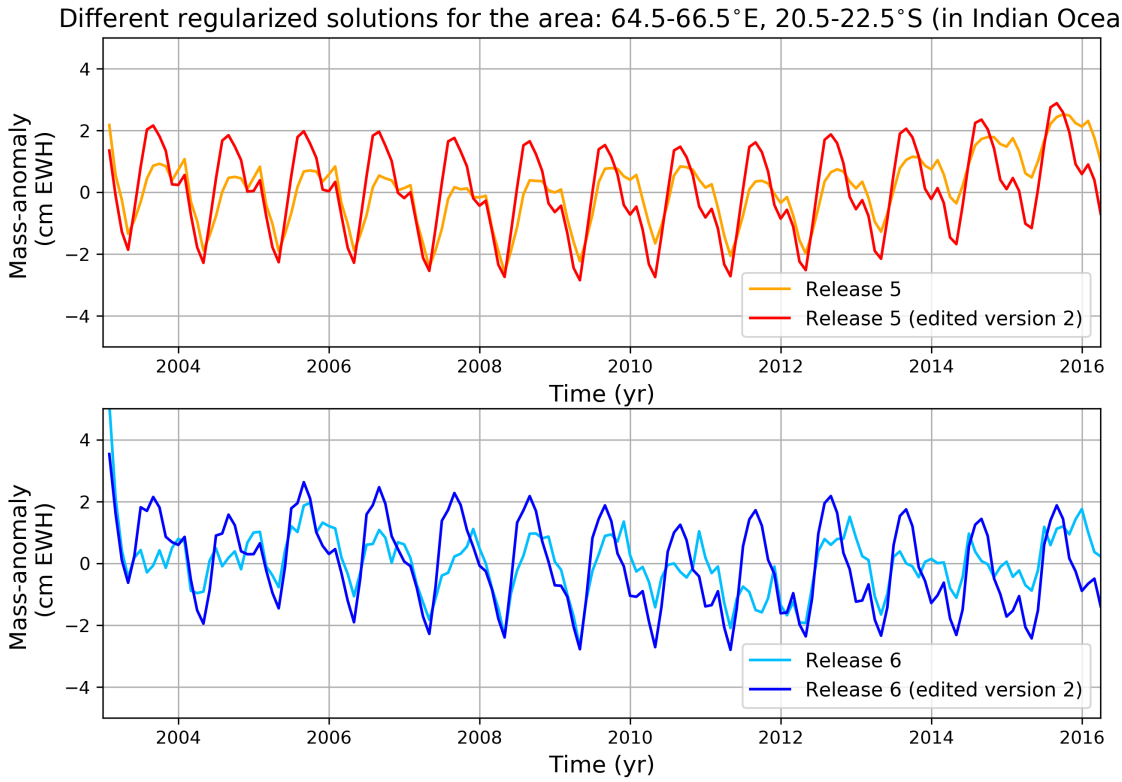

Figure 5.17: Time-series of regularized solutions estimated from GRACE monthly solutions before and after the MAS. The average mass-anomaly time-series for a square region in the Indian Ocean are shown.

Changes of the unexpected signals and residuals versus bathymetry can be observed in figures 5.18, 5.19, 5.20 (for the Total Ocean), 5.21, 5.22, 5.23 (for the Arctic Ocean), and 5.24, 5.25, 5.26 (for the South Atlantic Ocean). When observing these figures, it can be observed that on a global mean basis the unexpected signals decrease up to a depth of about 450 m. For the Arctic Ocean GTSM seems improve the GRACE Release 5 Level-2 data over the whole ocean basin when the buffer zones are not considerd. Actually, it is not expected that GTSM would perform better in the Arctic Ocean since no dynamic sea-ice model is included in GTSM (which is included in OMCT and MPIOM). It could be that (the implementation of) the dynamic sea-ice model in OMCT and MPIOM is not that good. For the shallow regions in the South Atlantic Ocean (up to about 2000 m depth) GRACE 6 solutions seem to improve by GTSM (figures 5.24 and 5.26). When looking at figures 5.10 and 5.12 these improvements might correlate to the region just below the Argentine Basin. There can be various regions why GTSM performs better than OMCT and MPIOM for this area. Maybe it is due grid densification.

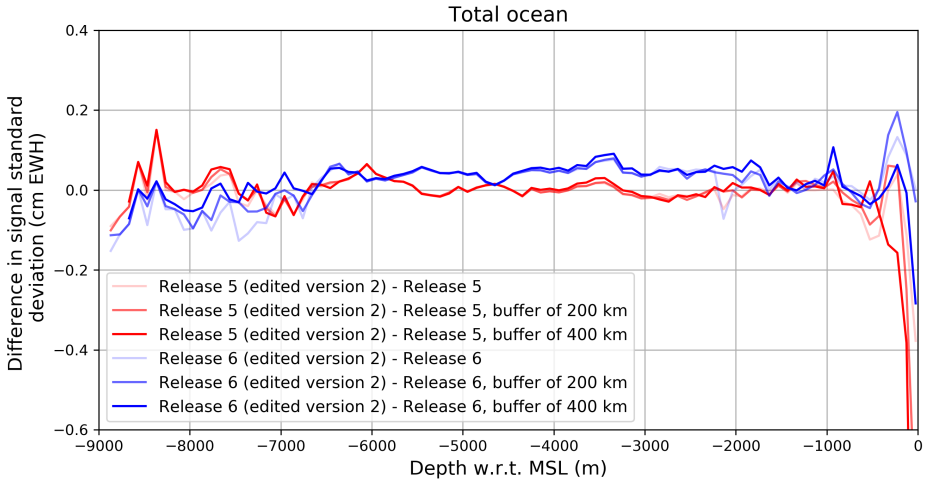

Figure 5.18: Difference in estimated signal standard deviation versus bathymetry for the total ocean. The differences in estimated signal standard deviation for edited (version 2) GRACE Release 5 and original GRACE Release 5 solutions are shown in red and for edited GRACE Release 6 and original GRACE Release 6 solutions in blue.

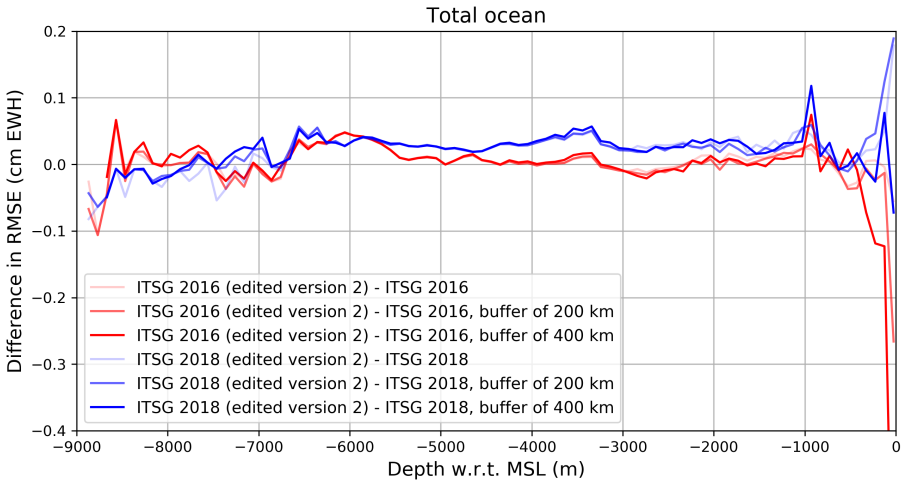

Figure 5.19: Difference in estimated RMSE for ITSG solutions versus bathymetry for the total ocean. The RMSE is estimated with respect to a by least-squares estimated signal containing only a linear trend and annual and semi-annual periodicity. The differences in RMSE for ITSG 2016 (edited version 2) and ITSG 2016 are shown in red and for ITSG 2018 (edited version 2) and ITSG 2018 in blue.

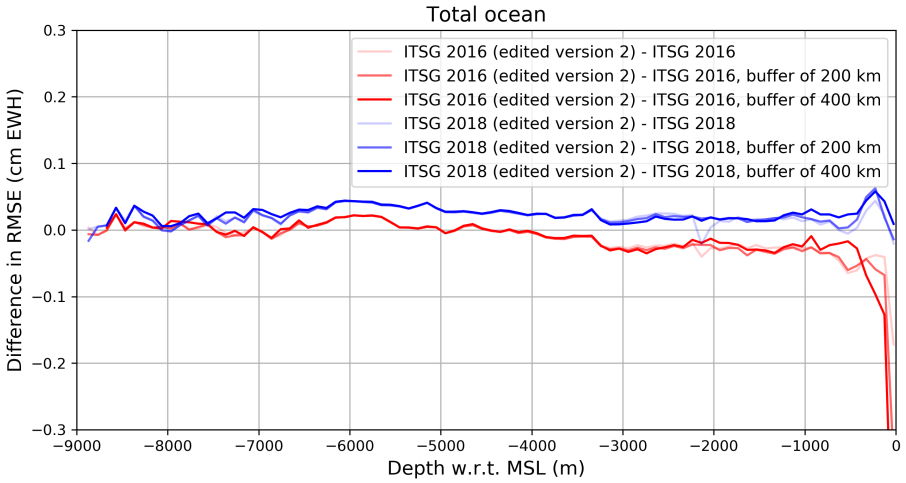

Figure 5.20: Difference in estimated RMSE for ITSG solutions versus bathymetry for the total ocean. The RMSE is estimated with respect to a low-pass filtered signal (frequencies smaller than or equal to the semi-annual cycle are retained in the low-pass filtered signal). The differences in RMSE for ITSG 2016 (edited version 2) and ITSG 2016 are shown in red and for ITSG 2018 (edited version 2) and ITSG 2018 in blue.

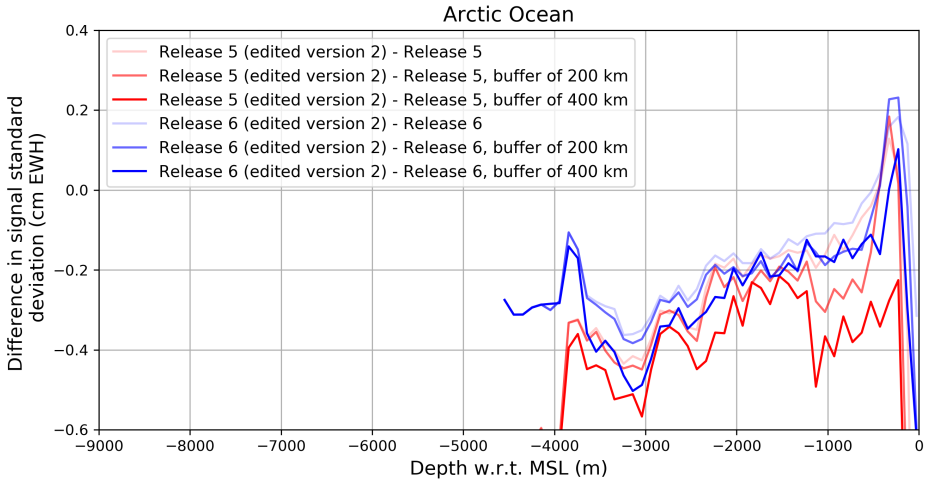

Figure 5.21: Difference in estimated signal standard deviation versus bathymetry for the Arctic Ocean. The differences in estimated signal standard deviation for edited (version 2) GRACE Release 5 and original GRACE Release 5 solutions are shown in red and for edited GRACE Release 6 and original GRACE Release 6 solutions in blue.

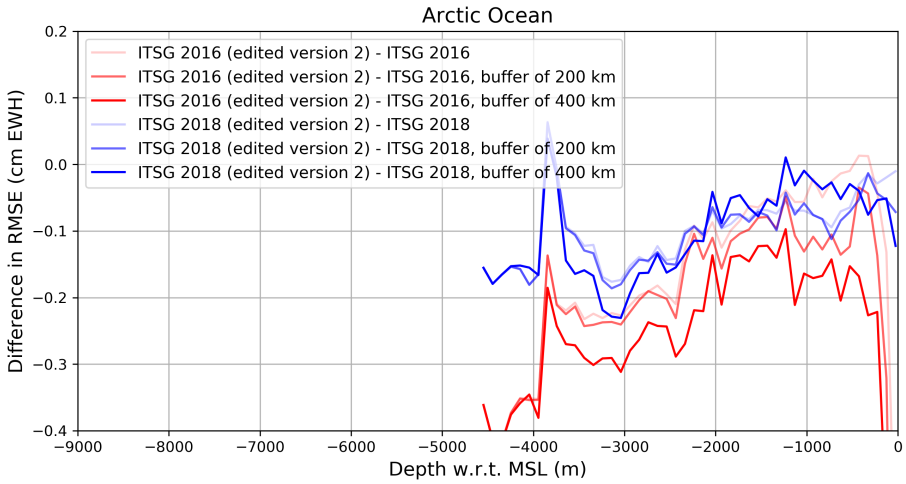

Figure 5.22: Difference in estimated RMSE for ITSG solutions versus bathymetry for the Arctic Ocean. The RMSE is estimated with respect to a by least-squares estimated signal containing only a linear trend and annual and semi-annual periodicity. The differences in RMSE for ITSG 2016 (edited version 2) and ITSG 2016 are shown in red and for ITSG 2018 (edited version 2) and ITSG 2018 in blue.

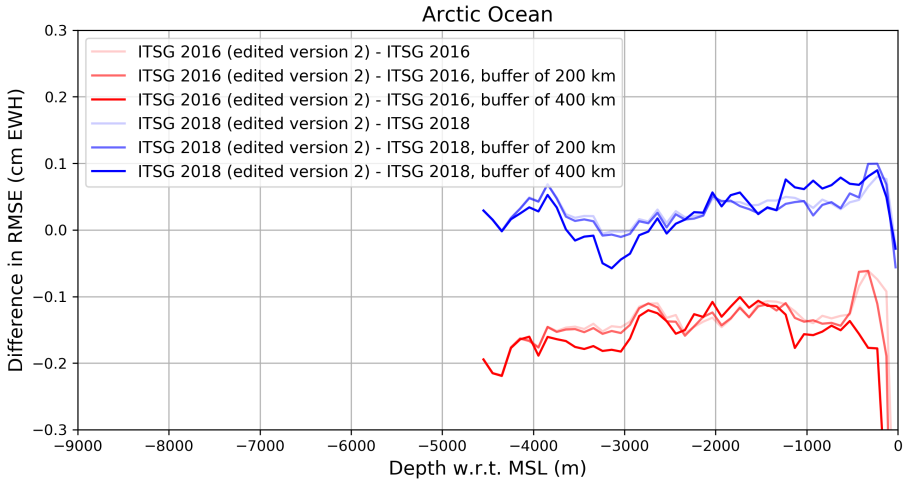

Figure 5.23: Difference in estimated RMSE for ITSG solutions versus bathymetry for the Arctic Ocean. The RMSE is estimated with respect to a low-pass filtered signal (frequencies smaller than or equal to the semi-annual cycle are retained in the low-pass filtered signal). The differences in RMSE for ITSG 2016 (edited version 2) and ITSG 2016 are shown in red and for ITSG 2018 (edited version 2) and ITSG 2018 in blue.

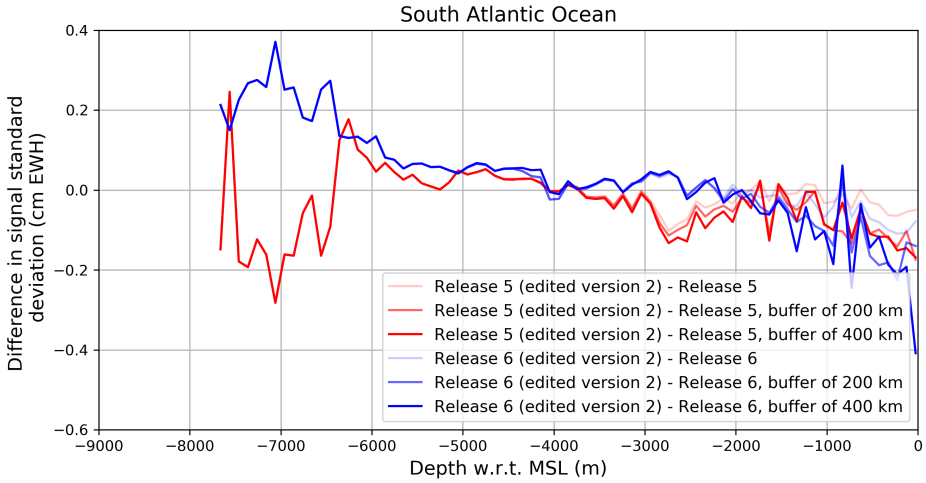

Figure 5.24: Difference in estimated signal standard deviation versus bathymetry for the South Atlantic Ocean. The differences in estimated signal standard deviation for edited (version 2) GRACE Release 5 and original GRACE Release 5 solutions are shown in red and for edited GRACE Release 6 and original GRACE Release 6 solutions in blue.

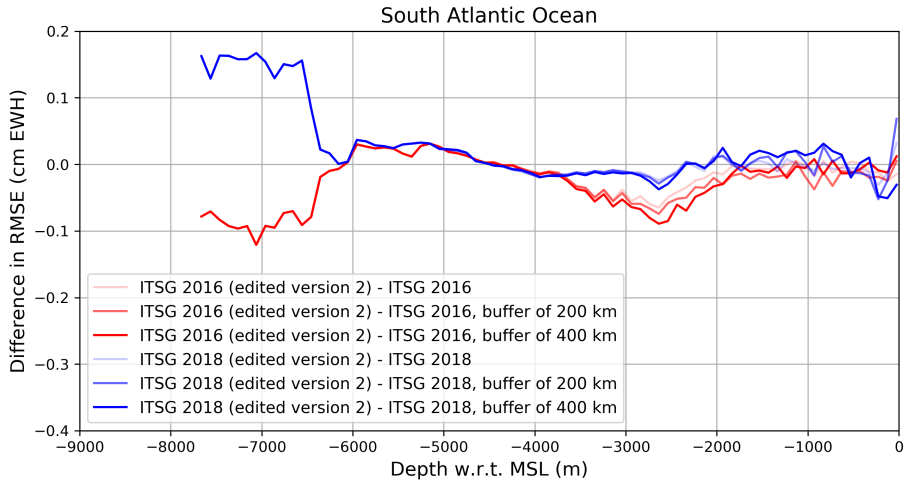

Figure 5.25: Difference in estimated RMSE for ITSG solutions versus bathymetry for the South Atlantic Ocean. The RMSE is estimated with respect to a by least-squares estimated signal containing only a linear trend and annual and semi-annual periodicity. The differences in RMSE for ITSG 2016 (edited version 2) and ITSG 2016 are shown in red and for ITSG 2018 (edited version 2) and ITSG 2018 in blue.

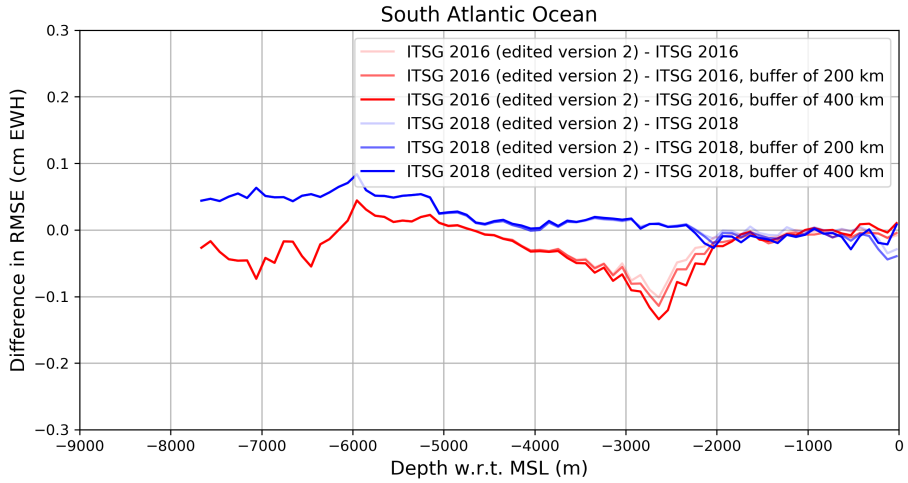

Figure 5.26: Difference in estimated RMSE for ITSG solutions versus bathymetry for the South Atlantic Ocean. The RMSE is estimated with respect to a low-pass filtered signal (frequencies smaller than or equal to the semi-annual cycle are retained in the low-pass filtered signal). The differences in RMSE for ITSG 2016 (edited version 2) and ITSG 2016 are shown in red and for ITSG 2018 (edited version 2) and ITSG 2018 in blue.

5.3. Summary and remarks

The method of addition and subtraction (MAS) to GRACE monthly solutions by the use of monthly time-series generated by GTSM is a first step in the assesment whether GTSM can improve GRACE monthly solutions. On the basis of the MAS it seems that GRACE Release 5 solutions can improve by GTSM for the regions: Gulf of Carpentina, Baltic Sea, Black Sea, North Sea, East Siberian Arctic Shelf, Hudson Bay and parts of the Arctic and Southern Ocean. On the basis of the MAS it seems that GRACE Release 6 solutions can improve by GTSM for the regions: Gulf of Carpentina, Baltic Sea, Black Sea, East Siberian Arctic Shelf and North Sea. The results of the MAS are different when also the tidal dynamics are included or not. This might indicate that tides are modeled significantly different or that a significant amount of non-linear interaction is present in GTSM. The regions where the monthly mean time-series of one model seem to be better than another in the context of GRACE Level-2 data are also an indication of regions where a certain model can potentially be improved. For this improvement it must be known why the models compute different time-series for those areas. Then it can be known what could be changed in the set-up of the model.

Most clear improvements to both GRACE Release 5 and Release 6 monthly solutions can be observed for some regions around Europe: Baltic Sea, Black Sea and North Sea. These shallow areas correspond to areas of large grid densification in GTSM. This could be a possible reason why GTSM performs better in these areas. A better observed performance could also be due to a possibly better implemented bathymetry in GTSM. More general reasons might also be possible like for example differences in the applied meteorological forcing. GRACE Release 5 monthly solutions are by the MAS clearly improved for the Hudson Bay and East Siberian Arctic Shelf. These areas correlate to regions where GTSM was more similar to AOD1B Release 6 than AOD1B Release 5 products (both on the hourly and monthly scale).

Figures of monthly (regularized) times-series show that phase and the amplitude of the seasonal variability as well as long-term trends can be significantly altered by the MAS. This can be observed beside a diminution of high-frequency fluctuations (periods smaller than the semi-annual cycle). It is remarkable that changes in the quality of GRACE Level-2 data are already observable on the basis of GTSM-based monthly mean time-series. This indicates that GRACE Level-2 data can be significantly altered (and possibly improved) when considering GTSM as oceanic background model in GRACE data processing for several regions. It is expected that the consideration of GTSM time-series at the hourly scale can result in even larger alterations in the GRACE Level-2 data.

6

Conclusions and recommendations

In this chapter first all sub-questions are answered before answering the main question. Thereafter, recommendations regarding future research follow.

6.1. Conclusions regarding the sub-questions

The sub-questions will be answered one by one.

- Which regularization functional should be used in Variance Component Estimation to identify the noise variance and signal in time-series which consist predominantly of a seasonal variability and linear trend?

  In a numerical study, four regularization functionals (Tikhonov zero-order, Tikhonov first-order, Tikhonov second-order and MYDD minimization) are considered besides applying no regularization in the VCE. In this numerical study, time-series are constructed as a combination of a signal and noise realization. When the signal in the time-series does only contain a seasonal variability and linear trend the MYDD minimization is the regularization technique which restores the true signal best (and thus identifies the true signal best). When a larger number of time-series is considered in the VCE, the true signal is restored better. When signals also contain a signal of interannual variability like a step function or an amplified amplitude of the annual signal during half a year, Tikhonov first-order regularization or signal retrieval without a regularization show better results by yielding no or smaller biases in the signal of interannual variability. Noise variance is best estimated by MYDD minimization for both time-series containing signals with and without an interannual variability. When multiple time-series are considered as input, cross-correlated noise is identified as signal variance. The estimated signal variance is also influenced by the magnitude of uncorrelated noise.

  A case study for the Baltic Sea is performed where GRACE-based mass-anomaly time-series are compared against a tide-gauge based mass-anomaly time-series. These GRACE-based basin-average mass-anomaly time-series contain interannual variability beside an evident linear trend and seasonal variability. For the period April 2003 to December 2007 time-series retrieved by applying Tikhonov first-order regularization, MYDD minimization, and no regularization in the VCE are compared against the tide-gauge based time-series. The Tikhonov regularization technique results in a mass-anomaly time-series closest to the tide-gauge based mass-anomaly time-series and thus seems to identify the true signal in mass-anomaly time-series best. This can be because of the presence of interannual variability in the water level variations in the Baltic Sea. The differences between Tikhonov first-order, MYDD minimization and applying no regularization are very small (in the order of a few millimeters EWH) compared to the difference between the GRACE-based and tide-gauge based time-series which are in the order of 5-6 cm. Since the precision and accuracy of the tide-gauge based time-series is unknown and the differences between the considered regularization functionals are very small, the results of this experiment are preliminary.

- What are the global distributions of signal and noise variance in GRACE Release 5 and 6 monthly solutions?

To identify regions of smaller or higher quality in GRACE monthly solutions signal and noise variance are estimated for these solutions. This is done for three Release 5 GRACE monthly solutions (CSR Release 5, GFZ Release 5 and ITSG 2016) and three Release 6 GRACE monthly solutions (CSR Release 6, JPL Release 6 and ITSG 2018). The estimated noise variance for Release 6 solutions is generally lower than for Release 5 solutions. For both releases ITSG solutions show the lowest estimated noise variance. In general the estimated noise variance is smaller over the poles compared to lower latitudes. This is due to a higher sampling frequency over the poles and a larger angle between ascending and descending satellite tracks over the polar areas. The consideration of MYDD-minimization, Tikhonov first-order and no regularization in the VCE give similar conclusions about the global distribution of the noise. When only one time-series is considered in the VCE instead of three, global patterns of estimated signal variance (which were estimated when three time-series were used as input) show up in the global patterns of estimated noise variance.

For GRACE Release 5 solutions large signal variances are observed for the Baltic Sea, Black Sea, Arafura Sea (including Gulf of Carpentaria), East Siberian Arctic Shelf, Argentine Basin and Hudson Bay. For these areas the signal standard deviation is about 3-5 cm EWH w.r.t. the global mean of 0.86 cm EWH. GRACE Release 6 solutions show a clear decrease in this signal standard deviation for the Hudson Bay and East Siberian Arctic Shelf. For most other regions, the signal standard deviation increases for GRACE Release 6 solutions. For both GRACE Release 5 and 6 solutions, the signal standard deviation increases for shallow regions. For the shallow coastal regions, this might be (partly) due to signal leakage from land to ocean. Since the estimated signal standard deviation is influenced by the magnitude of the noise it is not totally fair to compare the absolute values of signal standard deviation.

Since ITSG solutions show the lowest noise, two extra methods are applied to assess the quality of these solutions. Firstly, the RMSE is estimated w.r.t. an analytical function. This analytical function is a by least-squares estimated signal containing a linear trend and seasonal variability. Secondly, the RMSE is estimated w.r.t. a low-pass filtered signal. In the low-pass filtered signal only signals of frequency lower than the semi-annual cycle are retained. The non-seasonal and high-frequency residuals decrease in general for Release 6 compared to Release 5. This reduction can be due to an improvement of the oceanic background models or due to a decrease in noise in general for Release 6 compared to Release 5. Large non-seasonal and high-frequency residuals are observed for for the Baltic Sea, Black Sea, Hudson Bay, Arafura Sea, Gulf of Thailand, Argentine Basin and East Siberian Arctic Shelf, which are similar to the regions of large signal standard deviation. For Release 6 the non-seasonal and high-frequencies residuals do clearly decrease for the Hudson Bay and East Siberian Arctic Shelf. The correlation between the estimates of signal variance and residuals makes it likely that the estimates of signal variance indicate regions of lower quality in GRACE Level-2 data. The presence of strong non-seasonal and high-frequency residuals and signal variance in certain oceanic regions show that GRACE Level-2 data are still in need of improvement for these areas.

- Which regions show significant differences between 3-hourly, 6-hourly and monthly mass-anomaly time-series generated by GTSM and those generated by the oceanic background models currently used in GRACE data processing?

  Generally the 3/6-hourly time-series computed by the Global Tide and Surge Model (GTSM) are more similar to the MPIOM model used for Release 6, than the OMCT model used for Release 5. Regions where GTSM is significantly closer to MPIOM than OMCT are the Hudson Bay, East Siberian Arctic Shelf, Arctic Ocean, Southern Ocean, Arafura Sea and Baltic Sea. For the Hudson Bay and East Siberian Arctic Shelf, these regions are consistent with regions where the GRACE Release 6 solutions showed better results than GRACE Release 5 solutions. Since also the differences between the time-series of MPIOM and OMCT are significantly different for these two areas, it seems that the oceanic background models do significantly influence the quality of GRACE Level-2 data. Regions where in general the differences between GTSM and the currently used oceanic background models are large are the shallow regions (up to about 200 m depth), the Red Sea and the Black Sea. This is both the case for the 3/6-hourly time-series and monthly time-series. Regions of large differences are the regions where significant improvements or detoriations of the GRACE Level-2 data product can be expected.

When considering the monthly time-series, it is observed that GTSM is closer to OMCT than to MPIOM except the following regions: Baltic Sea, Arafura Sea, Black Sea, Southern Ocean and Arctic Ocean. At the monthly time-scale, GTSM is in general closer to OMCT than MPIOM which is in contrast to the short-term scale. A frequency analysis of the 3/6-hourly time-series supports this finding. On the monthly scale, the differences between GTSM (containing both meteorological-forced and tidal dynamics) and the combination of currently used tidal and non-tidal oceanic background models are larger than the differences between GTSM (containing only meteorogical-forced dynamics) and the non-tidal oceanic background model. Because these differences already arise in the monthly means, it seems that the tides are modeled significantly differently by GTSM and the currently used oceanic tidal background models.

- For which regions does the quality of GRACE monthly solutions increase by the use of monthly mass-anomaly time-series generated by GTSM?

  As a first attempt to identify regions where GTSM might improve GRACE monthly soutions, monthly time-series of the currently used oceanic background models are added to GRACE monthly solutions after which GTSM-based time-series are subtracted. This addition should restore the ocean variability which is primarily removed in the production of GRACE monthly solutions. This method of addition and subtraction (MAS) is both performed with and without taking the tidal dynamics into account. The GRACE solutions show after the MAS in general a smaller signal variance and smaller non-seasonal and hih-frequency residuals when the tidal dynamics are not taken into account. Therfore, the rest of this paragraph is about the results obtained by the MAS with only non-tidal variability.

  After applying the MAS to GRACE Release 5 solutions it can be observed that the estimated signal variance decreases significantly for the Hudson Bay, East Siberian Arctic Shelf, Gulf of Carpentaria, Black Sea, Baltic Sea, North Sea and certain parts of the Arctic and Southern Ocean. The signal variance decreased in general for shallow regions up to a depth of about 450 m. These regions and depths are similar to those where the high-frequency residuals of ITSG 2016 decrease by the MAS. These regions which show both a reduction in signal variance and high-frequency residuals indicate regions where it is expected that GTSM will improve the GRACE Level-2 data.

  After applying the MAS to GRACE Release 6 solutions, the signal variance increased in general except for the Baltic Sea, Black Sea, North Sea, Gulf of Carpentaria, the East Siberian Arctic Shelf and some parts in and close to the Arctic and Southern Ocean. For ITSG 2018 high-frequency signals decreased after the MAS for the same regions except the regions in and close to the Arctic and Southern Ocean. Therefore, it is expected that GTSM will improve GRACE Release 6 monthly solutions for the Baltic Sea, Black Sea, North Sea, Gulf of Carpentaria and the East Siberian Arctic Shelf.

  When observing time-series before and after the MAS it can be observed that GTSM can, beside reducing some of the high-frequency variability, change long-term patterns and change the size and phase of the seasonal variability in certain areas.

6.2. Main conclusions

The main question for this research is:

(i) What is the global distribution of the quality of GRACE Release 5 and 6 monthly solutions and (ii) is it expected that these solutions will be improved by the use of the Global Tide and Surge Model as oceanic background model?

The GRACE monthly solutions which are accessed are CSR Release 5, ITSG 2016, GFZ Release 5, CSR Release 6, ITSG Release 2018 and JPL Release 6. The estimated noise variances for all these solutions decrease towards the poles. In several oceanic regions unexpected signal and residuals are present which indicate a lower quality of the GRACE monthly solutions for these areas. Unexpected signal is estimated as a signal variance which represents interannual differences of the mass-derivative. For Release 5, this estimated signal variance is the largest for the oceanic regions Hudson Bay, East Siberian Arctic Shelf, Baltic Sea, Black Sea, Argentine Basin, Gulf of Carpentaria and Arctic Ocean.

These regions correlate to regions of large high-frequency and non-seasonal residuals in ITSG 2016 solutions. Although the signal variance reduce for the Hudson Bay, East Siberian Arctic Shelf and Gulf of Carpentaria for GRACE Release 6 solutions, the ocean is far from being free from the unexpected oceanic signals. Also for GRACE Release 6 solutions the global patterns of signal variance correlate to the global patterns of high-frequency and non-seasonal residuals in ITSG 2018 solutions. The presence of unexpected signal and residuals in oceanic regions indicates that both GRACE Release 5 and 6 solutions are still in need for improvement over the ocean.

The Hudson Bay and East Siberian Arctic Shelf are areas where large reductions in unexpected signal and residuals can be observed. These areas correlate to areas where the differences between currently applied oceanic background is significant. The MAS also influences the quality of the GRACE monthly solutions. Both these observations suggest that the quality of GRACE Level-2 data is significantly influenced by the oceanic background models. When applying the MAS, GTSM shows improvements with respect to GRACE Release 5 monthly solutions for the regions: Hudson Bay, East Siberian Arctic Shelf, Arafura Sea, Black Sea, Baltic Sea, North Sea and parts of the Southern and Arctic Ocean. With respect to GRACE Release 6 solutions improvements are observed for the regions: Black Sea, Baltic Sea, North Sea, Arafura Sea and East Siberian Arctic Shelf. Since for some regions GRACE monthly solutions are already positively influenced by differences in the oceanic background models on the monthly mean basis, it is expected that for these regions GRACE Level-2 data will be improved when GTSM is considered in the GRACE data processing. The areas where the 3/6-hourly time-series between GTSM and currently applied oceanic background models differ in the order of a decimeter are the swallow regions up to 200 m, Black Sea and Red Sea. For these regions it is expected that the quality of the GRACE Level-2 data will be altered most. To test whether GTSM may indeed improve the GRACE Level-2 data over the ocean the model has to be included directly in the GRACE data processing.

6.3. Recommendations

Regarding the numerical experiments performed in order to identify the best regularization technique, it has to be said that the performed numerical experiments are limited in scope. More combinations of signal and noise could be investigated. Especially different forms of interannual variability should be exploited to have better knowledge of how the estimated signal standard deviation depends on noise. For the noise realization, it would be better to include the possibility of different noise levels for different solutions. Since in reality different GRACE monthly solutions contain a different amount of random noise, it would be good to include these differences in noise level in the construction of synthetic data.

The best way to identify which regularization technique is the best to use in the VCE, is to compare GRACE Level-2 data against mass-anomaly time-series retrieved by other measurement techniques. Then it can be observed how the regularization techniques perform in the context of real mass-anomaly time-series. These mass-anomaly time-series can contain a wide range of types of interannual variability which might easily be oversimplified in the construction of synthetic data. Therefore, experiments similar to the comparison against the tide-gauge based mass-anomaly time-series for the Baltic Sea are recommended to perform for different oceanic regions and for longer time intervals. It is also recommended to compare GRACE Level-2 data against by altimetry determined (and steric corrected) time-series. This will make the analysis of different regularization techniques more representative.

Regarding the comparison against the tide-gauge based time-series for the Baltic Sea a reduction of the errors in the tide-gauge time-series could be considered to make a comparison of higher quality. This could be achieved by re-processing the tide-gauge data and by modeling the steric effect yourself. Also better hydrological modeling is recommended since the currently used hydrological model lacks mass variations assocaited with groundwater and open water bodies.

Testing even more regularization functionals, like a functional which minimizes the differences in the second time-derivatives between consecutive years, would also be interesting since the minimization of the differences in first time-derivatives penalizes acceleration in the mass-anomaly time-series. Since sea-level rise is accelerating, it could be better to apply a regularization functional which will retain this type of signal.

Regarding the quality estimation of GRACE Level-2 data the following improvements could be implemented. It would be better to exactly compute the correlation between the estimated signal variance and residuals. At the moment, global maps are visually compared and regional mean values are com-

pared. Based on mostly a visual inspection of the global maps, it is concluded that the regions of large signal variance and large residuals correlate. This should be made more exact by computing the correlation for each grid point. Furthermore, when observing the estimated parameters versus bathymetry the largest considered buffer zone is 400 km. Since a Gaussian filter of 400 km half-width is applied also areas which are further than 400 km away from the coast still contain signal leakage from the land. It would be better to consider larger buffer zones too.

The comparison of oceanic background models (both 3/6-hourly and monthly times-series) has been done quite thoroughly. Nevertheless, the frequency analysis could be improved. It would be better to perform a frequency analysis for each grid point in an ocean basin. Consequently, an average amplitude spectra for several area's could be computed. This would overcome the problem of averaging out signals of short wavelength.

A more in-depth analysis of the modeling process of the different models is advisable. This may explain the differences between the models present at certain locations, which is still not known well. If it is better understood why the models are performing differently in specific regions, it might be possible to improve the models over these areas. By this, both the currently used oceanic background models and GTSM might be improved by incorporating certain features of the best performing model into the other.

Furthermore, GTSM with only tidal dynamics was not compared to the currently used oceanic tide models due to several strange features of the former model. These features were observed in the Arctic Ocean, Southern Ocean and South Atlantic Ocean. This might be an evidence of errors in GTSM which should be fixed. Since the differences between GTSM (meteorological-forced) and the non-tidal background models are smaller than the differences between GTSM (tidal and meteorological-forced) and the combination of the non-tidal and tidal background models it would be interesting to identify the differences in tidal modeling separately. Also, when the issue of GTSM run with only tidal forcing is solved, estimates of the non-linear interaction between tidal and meteorological forced dynamics in GTSM can be made and analyzed. This can improve the understanding of the observed differences between GTSM and the currently applied oceanic background models.

The most important recommendation is to incorporate the GTSM-based 3-hourly time-series (similar to the 3-hourly time-series made in this research) in GRACE data processing, to create a new Level-2 data product, and assess the quality of this Level-2 data product. Only then the real improvements or deteriorations by using GTSM instead of the currently applied oceanic background models can be accessed. Now, only monthly means are added and subtracted from the GRACE Level-2 data for the whole Earth. Firstly, this does not take into account high-frequency differences between the models. Secondly, in GRACE data processing the predictions of the oceanic background models are used in combination with the satellites location. Therefore, to compare monthly mean values for each location is incorrect, since only the predictions of the ocean model in the moment where the satellites are overflying are taken into account in the data processing. Differences in the models occurring at locations and times when the satellites are not in the neighborhood are not important differences in the context of GRACE Level-2 data. Of course, differences in the models are roughly similar over time, but for a precise investigation whether GRACE Level-2 data can be improved by GTSM, the location of the satellites at each specific time should be taken into account.

A

Standard deviations of reported results in section 2.4

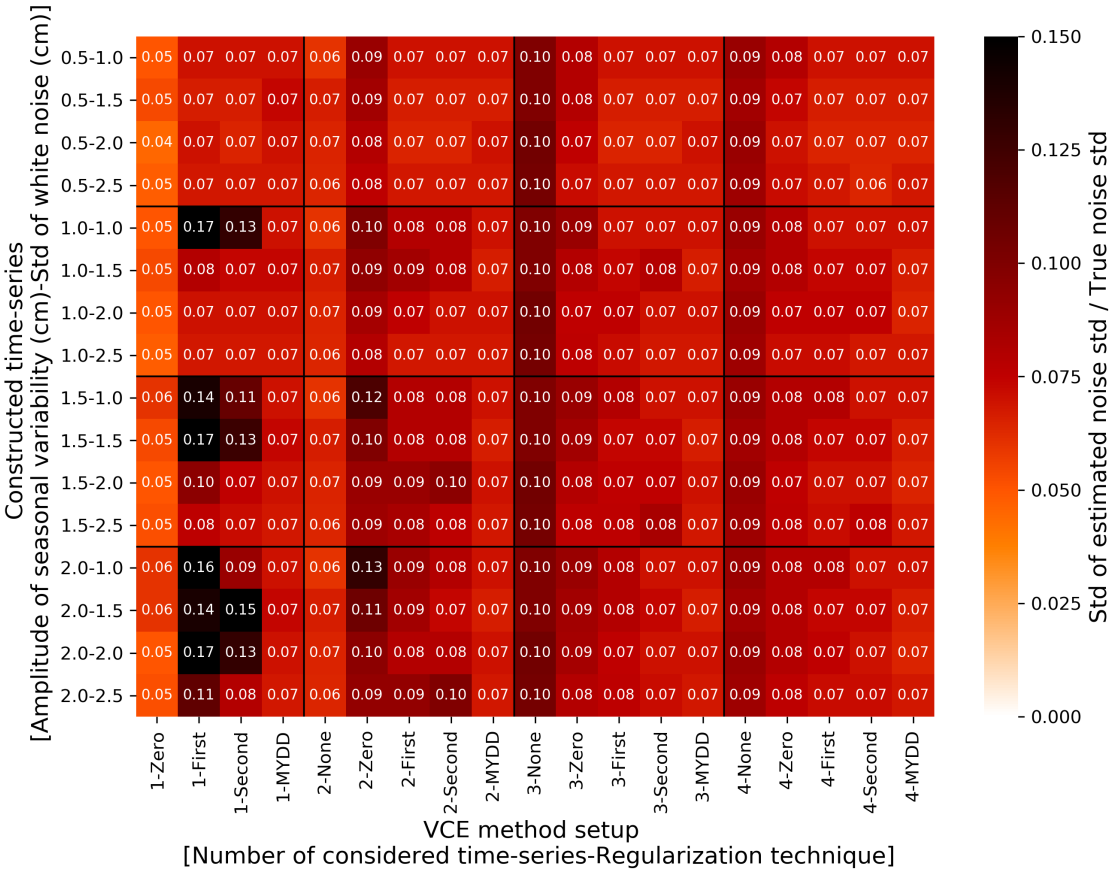

Figure A.1: Standard deviation of estimated noise standard deviation divided by the true noise standard deviation of the time-series. Different combinations of signal and noise are shown in the y-direction. Different setups in the VCE method are shown in the x-direction. The signals differ in amplitude of the seasonal variability.

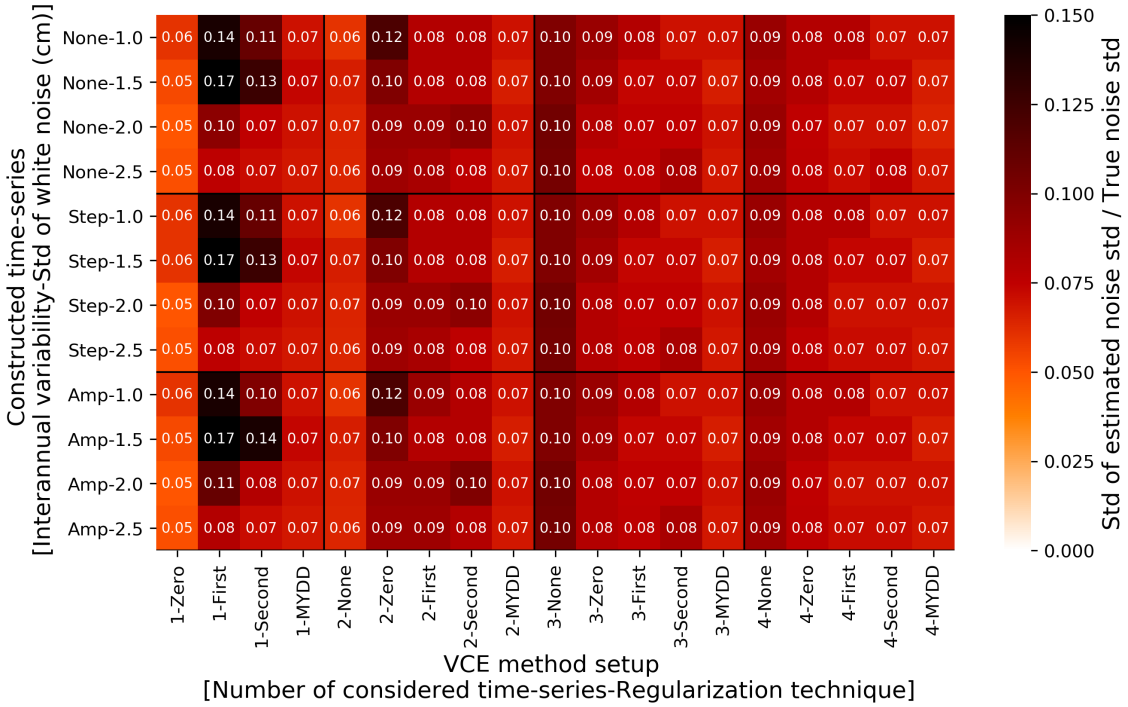

Figure A.2: Standard deviation of estimated noise standard deviation divided by the true noise standard deviation of the time-series. Different combinations of signal and noise are shown in the y-direction. Different setups in the VCE method are shown in the x-direction. The signals contain the same linear trend and seasonal variability but differ in interannual variability (none, step function or amplified seasonal variability during half-year).

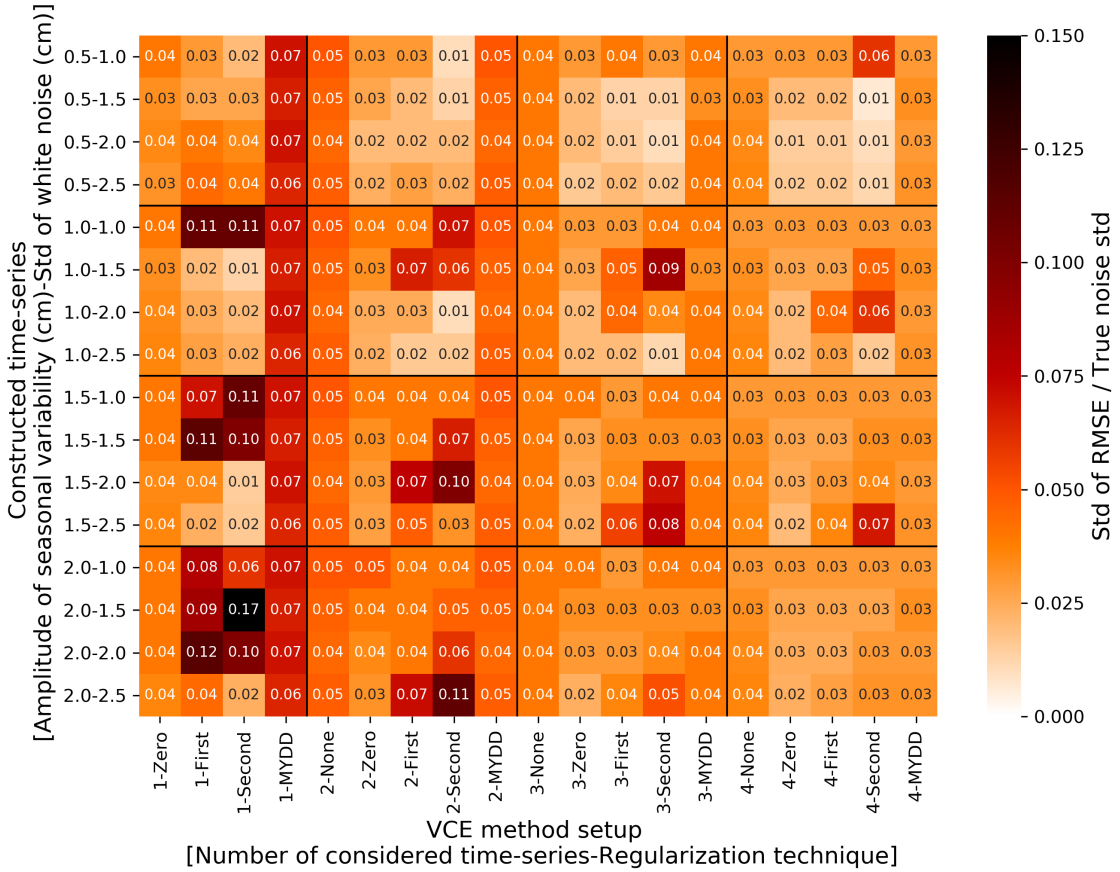

Figure A.3: Standard deviation of RMSE divided by the true noise standard deviation of the time-series. Different combinations of signal and noise are shown in the y-direction. Different setups in the VCE method are shown in the x-direction. The signals differ in amplitude of the seasonal variability.

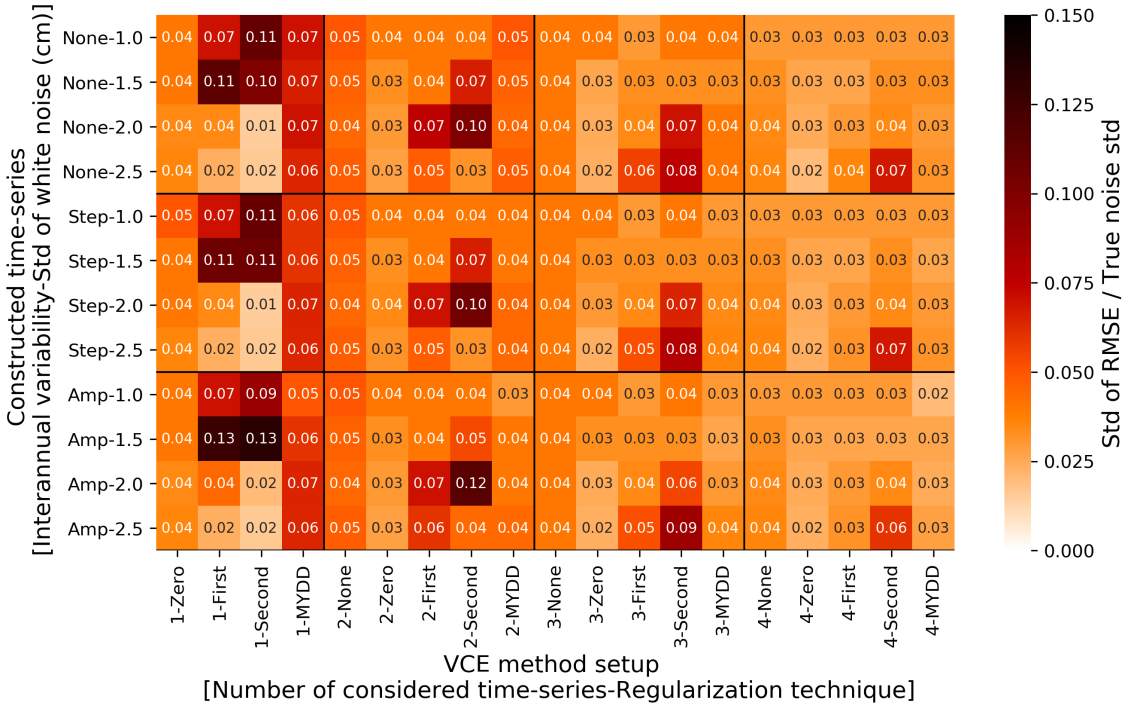

Figure A.4: Standard deviation of RMSE divided by the true noise standard deviation of the time-series. Different combinations of signal and noise are shown in the y-direction. Different setups in the VCE method are shown in the x-direction. The signals contain the same linear trend and seasonal variability but differ in interannual variability (none, step function or amplified seasonal variability during half-year).

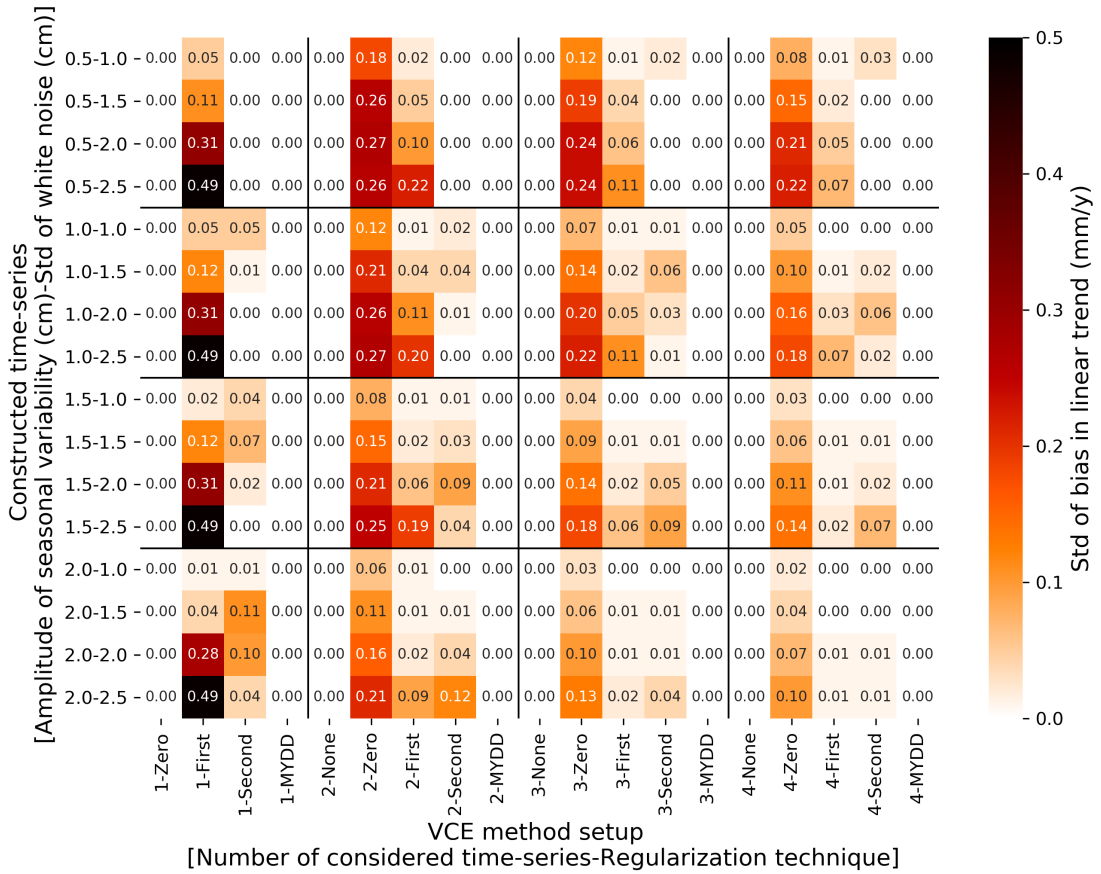

Figure A.5: Standard deviation of the bias in the linear trend of the combined and/or regularized solution. Different combinations of signal and noise are shown in the y-direction. Different setups in the VCE method are shown in the x-direction. The signals differ in amplitude of the seasonal variability.

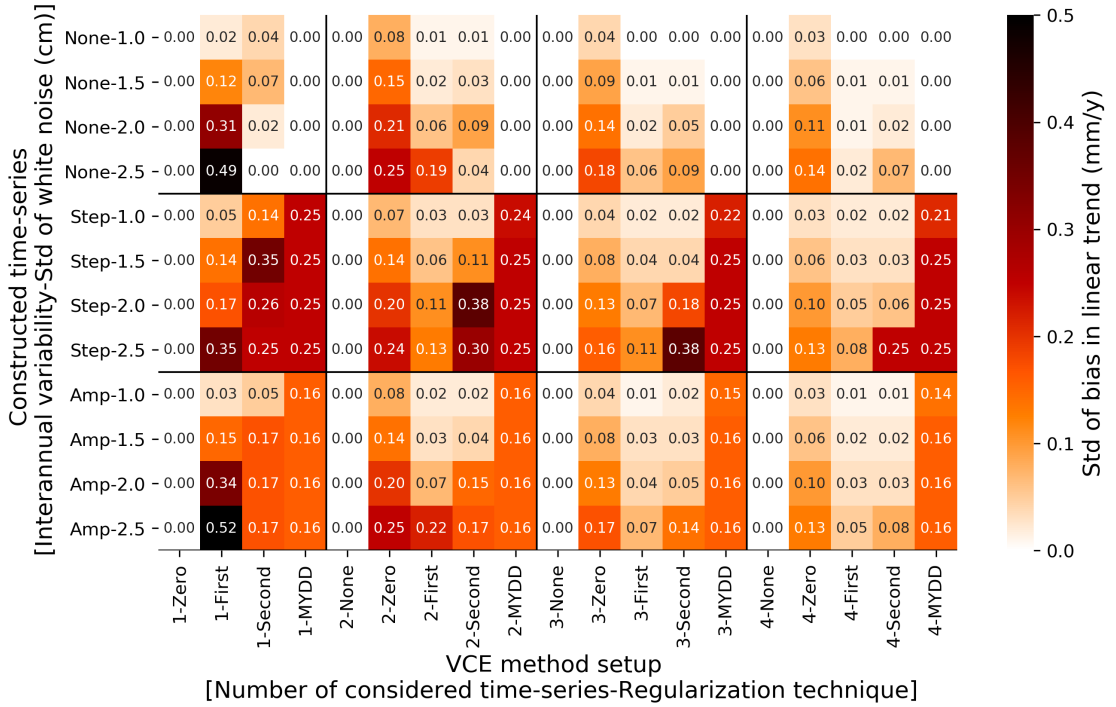

Figure A.6: Standard deviation of the bias in the linear trend of the combined and/or regularized solution. Different combinations of signal and noise are shown in the y-direction. Different setups in the VCE method are shown in the x-direction. The signals contain the same linear trend and seasonal variability but differ in interannual variability (none, step function or amplified seasonal variability during half-year).

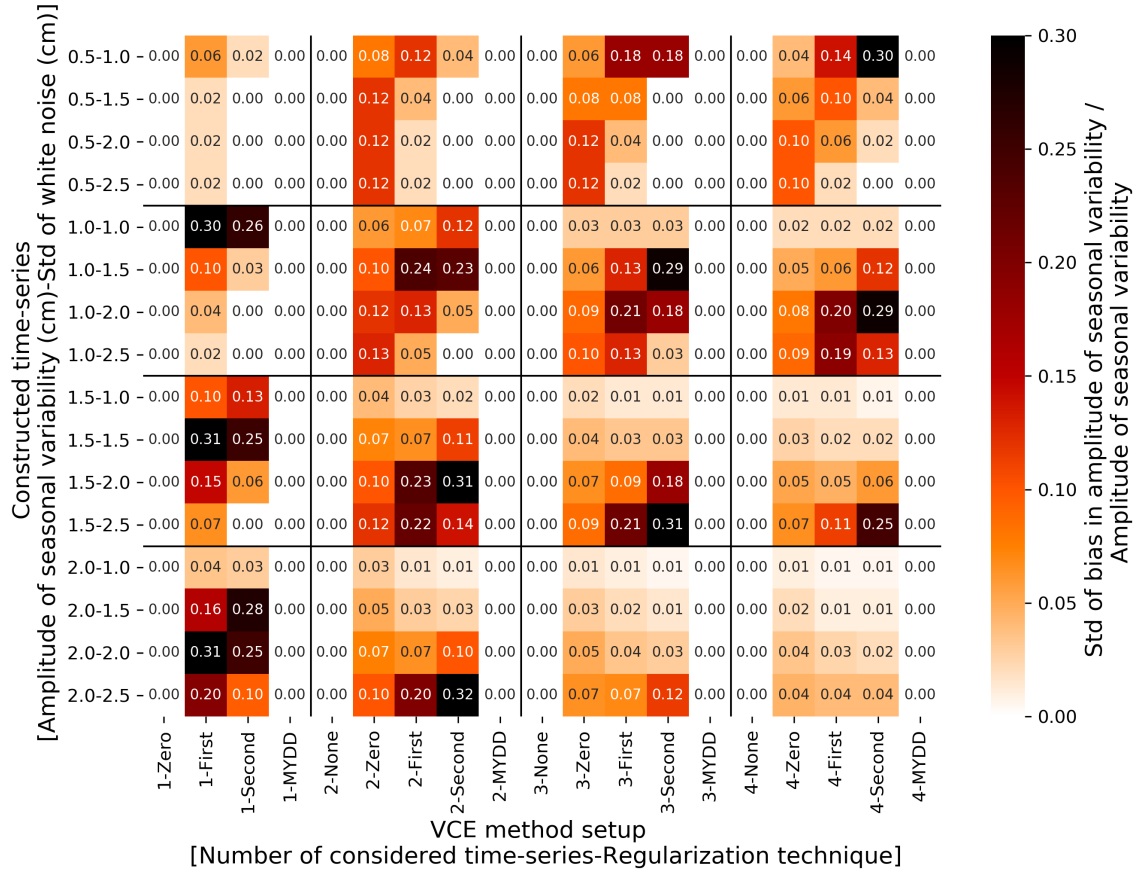

Figure A.7: Standard deviation of the bias in the amplitude of seasonal variability of the combined and/or regularized solution divided by the true amplitude of seasonal variability. Different combinations of signal and noise are shown in the y-direction. Different setups in the VCE method are shown in the x-direction. The signals differ in amplitude of the seasonal variability.

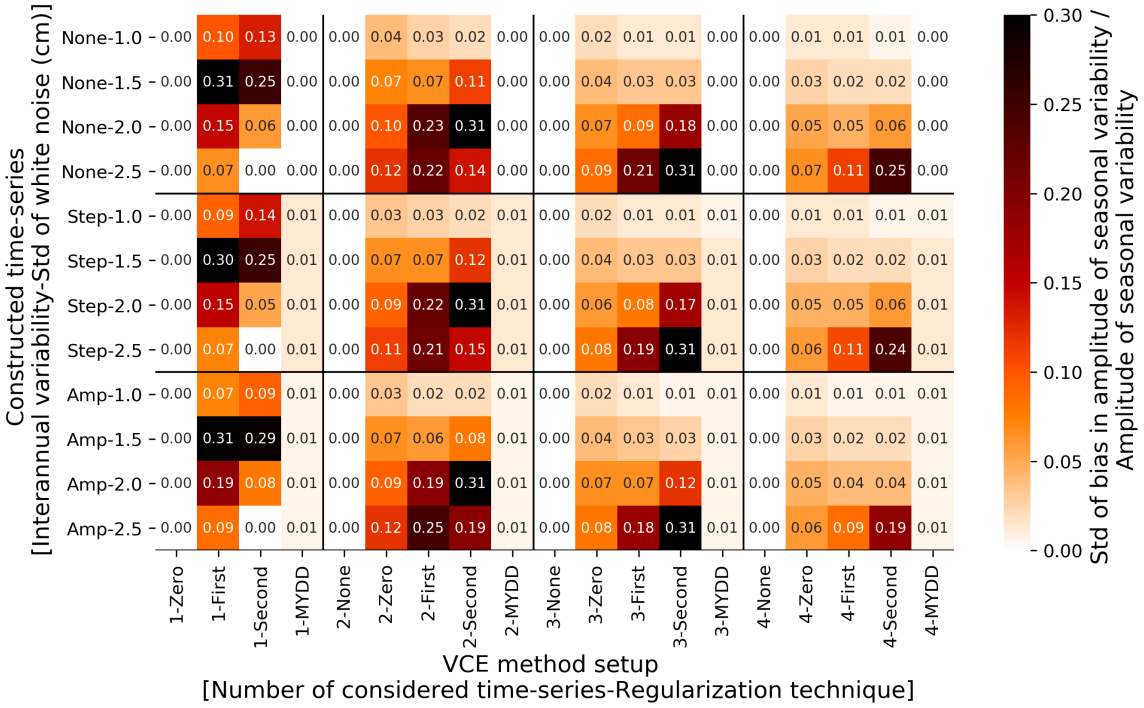

Figure A.8: Standard deviation of the bias in the amplitude of seasonal variability of the combined and/or regularized solution divided by the true amplitude of seasonal variability. Different combinations of signal and noise are shown in the y-direction. Different setups in the VCE method are shown in the x-direction. The signals contain the same linear trend and seasonal variability but differ in interannual variability (none, step function or amplified seasonal variability during half-year).

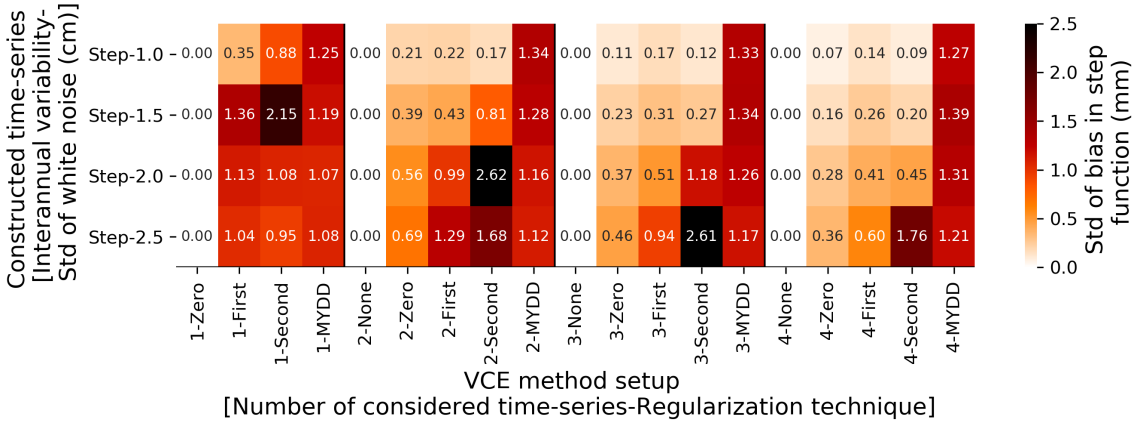

Figure A.9: Standard deviation of the bias in the step-wise increase in mass-anomaly of the combined and/or regularized solution. Different combinations of signal and noise are shown in the y-direction. Different setups in the VCE method are shown in the x-direction.

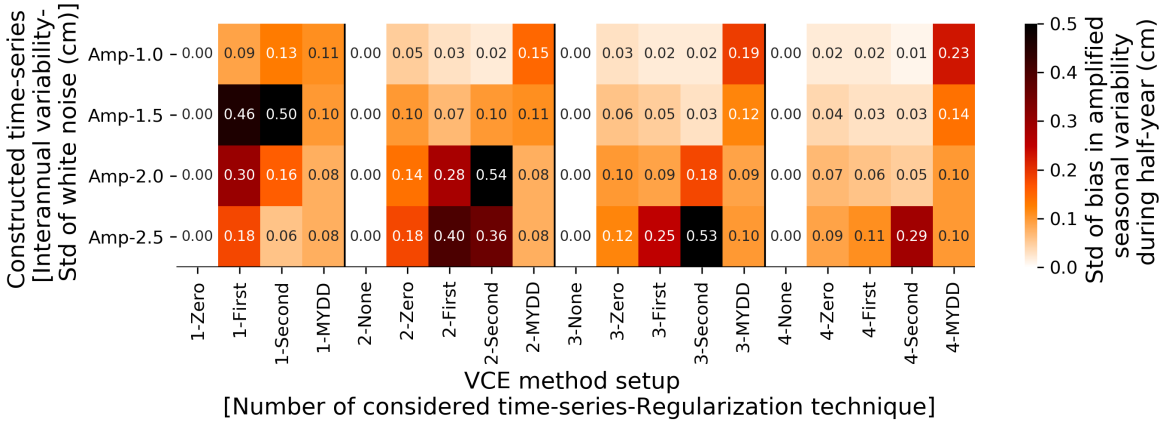

Figure A.10: Standard deviation of the bias in the amplified seasonal variability during half-year of the combined and/or regularized solution. Different combinations of signal and noise are shown in the y-direction. Different setups in the VCE method are shown in the x-direction.

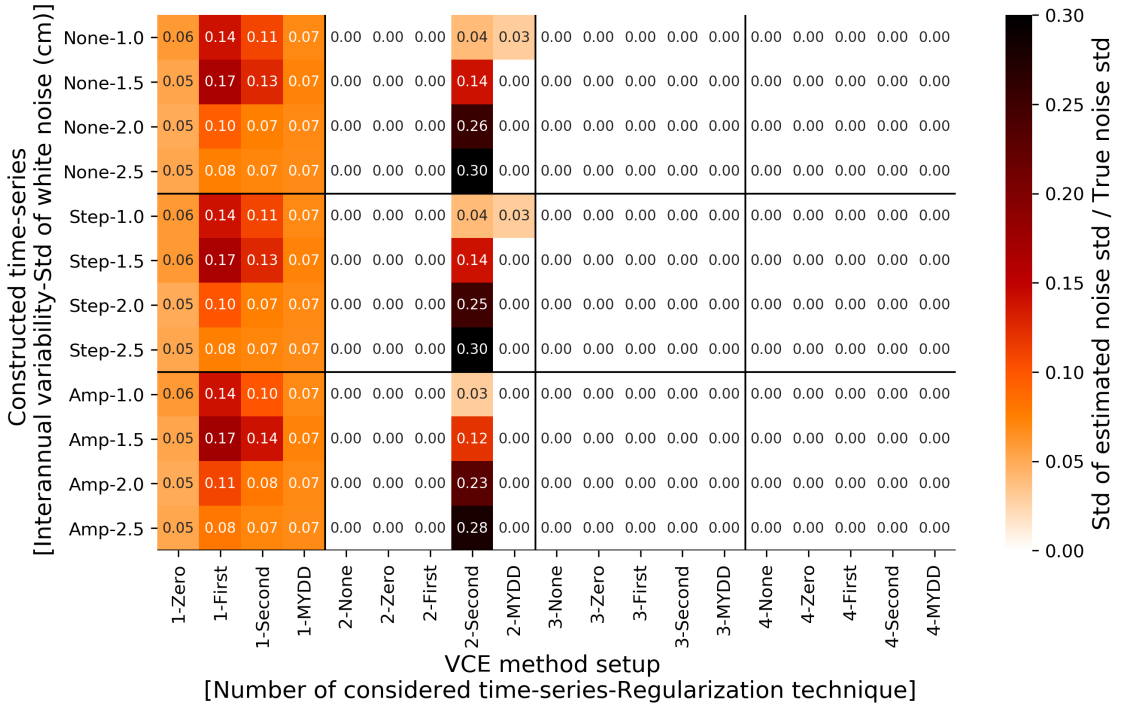

Figure A.11: Standard deviation of estimated noise standard deviation divided by the true noise standard deviation of the time-series. Different combinations of signal and noise are shown in the y-direction. When multiple time-series are considered in the VCE the noise in the time-series is fully cross-correlated. Different setups in the VCE method are shown in the x-direction. The signals contain the same linear trend and seasonal variability but differ in interannual variability (none, step function or amplified seasonal variability during half-year).

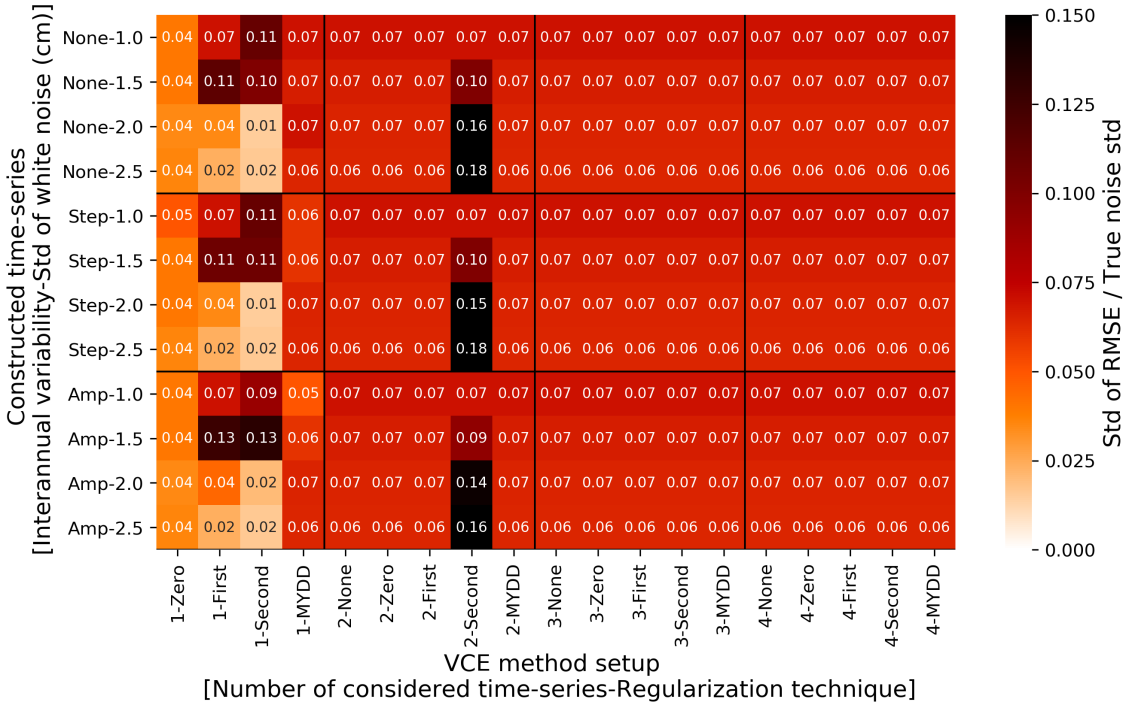

Figure A.12: Standard deviation of RMSE divided by the true noise standard deviation of the time-series. Different combinations of signal and noise are shown in the y-direction. When multiple time-series are considered in the VCE the noise in the time-series is fully cross-correlated. Different setups in the VCE method are shown in the x-direction. The signals contain the same linear trend and seasonal variability but differ in interannual variability (none, step function or amplified seasonal variability during half-year).

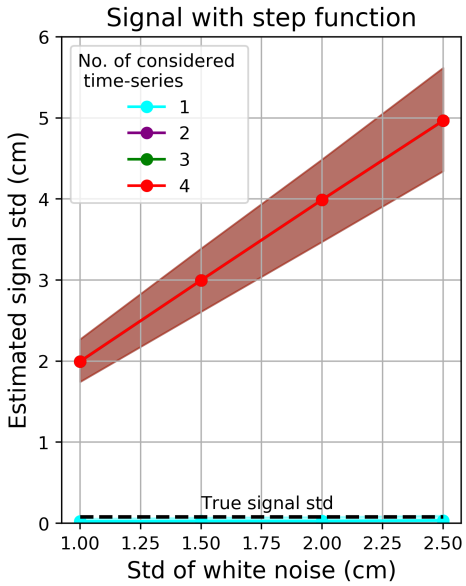

Figure A.13: Estimated signal standard deviation for a signal with interannual variability (in this case a step function) by using MYDD minimization as the regularization technique in the VCE and different numbers of time-series. The true standard deviation of the white noise is shown in the x-direction. The shaded area is the region between the 5 percent and 95 percent quantiles of the estimated signal standard deviation. The noise in the considered time-series is fully cross-correlated.

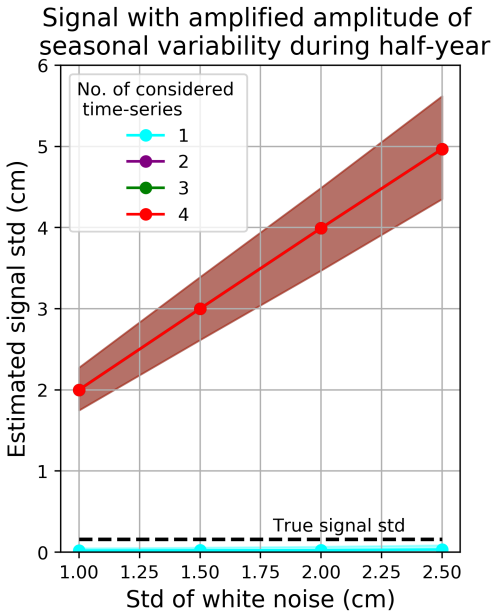

Figure A.14: Estimated signal standard deviation for a signal with interannual variability (in this case an amplified amplitude of seasonal variability during half-year) by using MYDD minimization as the regularization technique in the VCE and different numbers of time-series. The true standard deviation of the white noise is shown in the x-direction. The shaded area is the region between the 5 percent and 95 percent quantiles of the estimated signal standard deviation. The noise in the considered time-series is fully cross-correlated.

B

Complete set of figures of estimated signal and noise in chapter 3

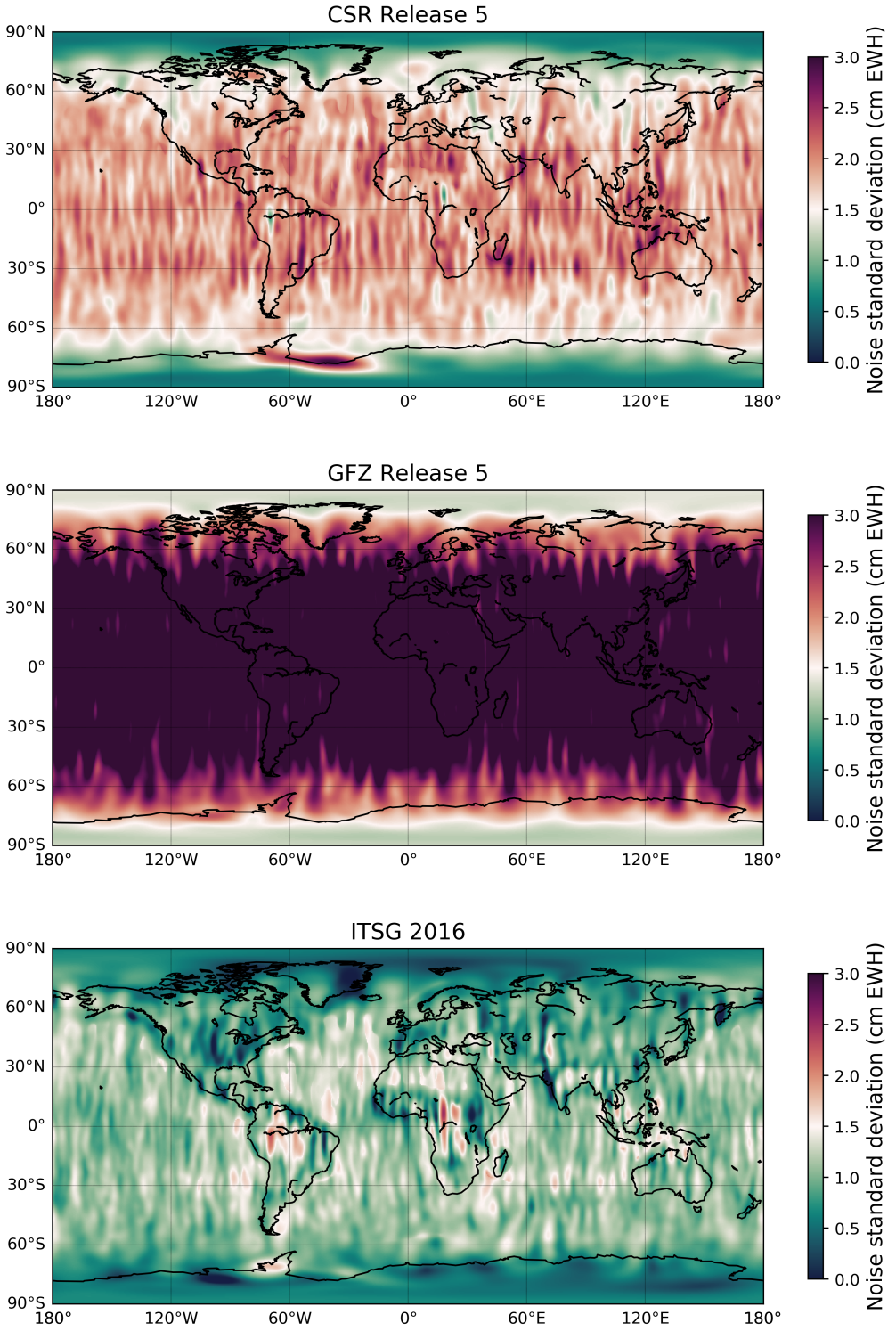

Figure B.1: Estimated noise standard deviation for GRACE Release 5 solutions (CSR Release 5, GFZ Release 5, ITSG 2016) by considering three mass-anomaly time-series in the VCE and Tikhonov first-order as regularization technique.

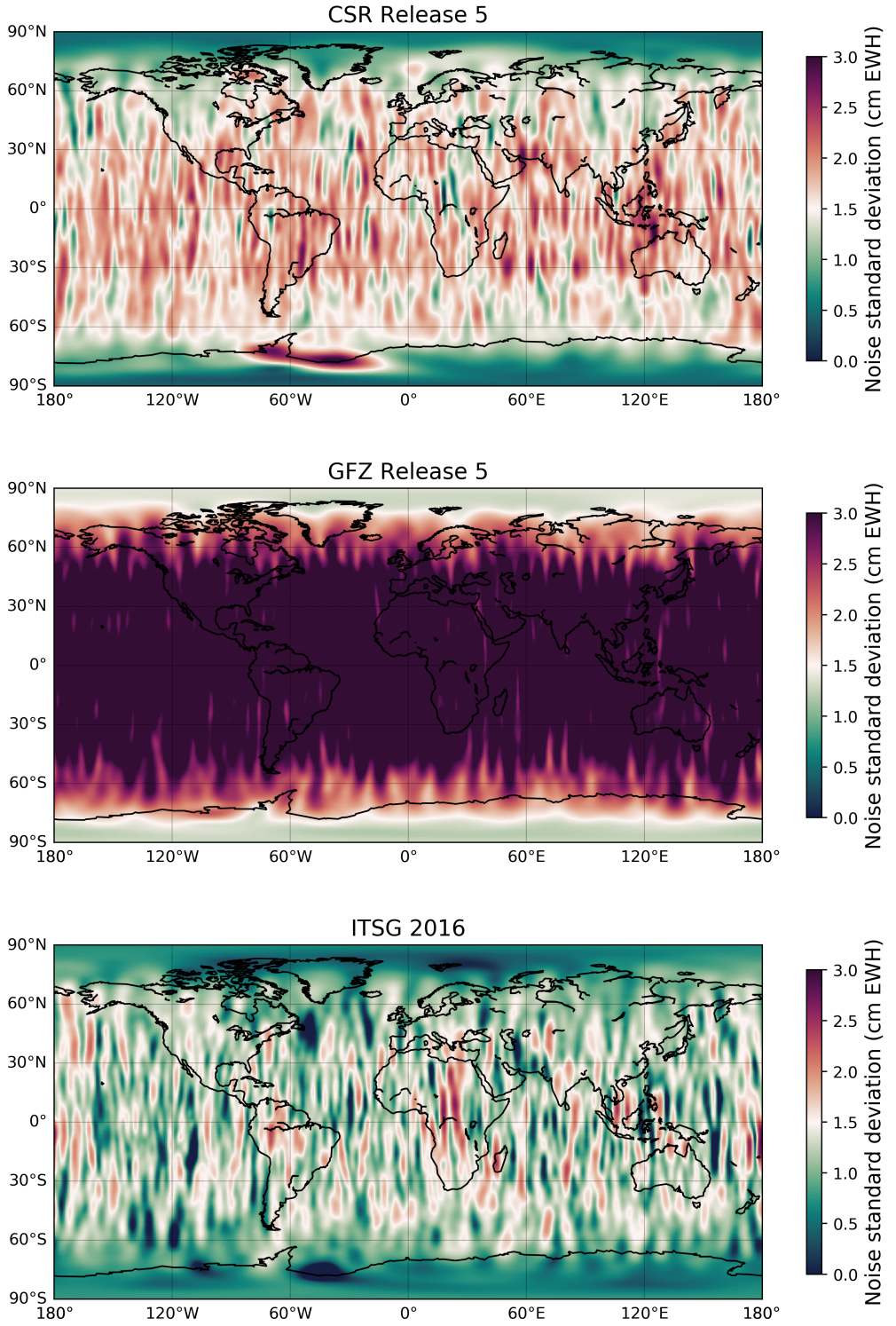

Figure B.2: Estimated noise standard deviation for GRACE Release 5 solutions (CSR Release 5, GFZ Release 5, ITSG 2016) by considering three mass-anomaly time-series in the VCE and applying no regularization.

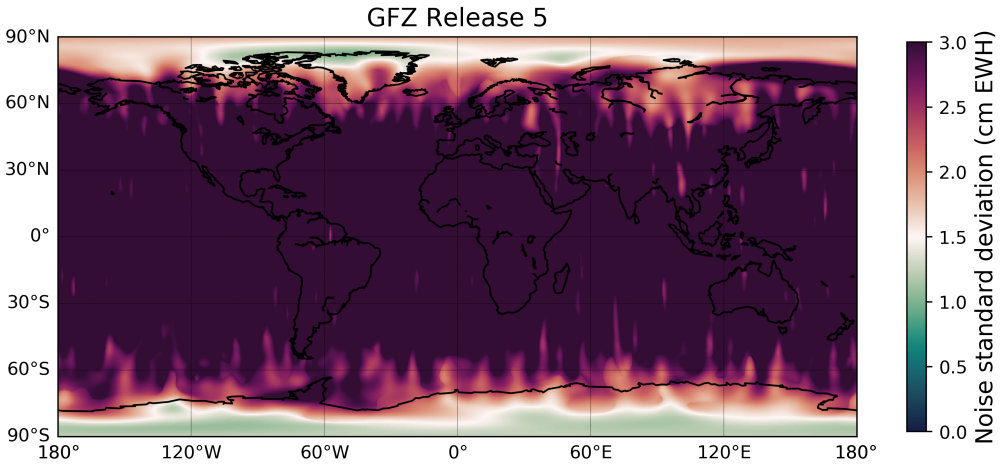

Figure B.3: Estimated noise standard deviation for GRACE solution GFZ Release 5 by considering one mass-anomaly time-series in the VCE and MYDD minimization as regularization technique.

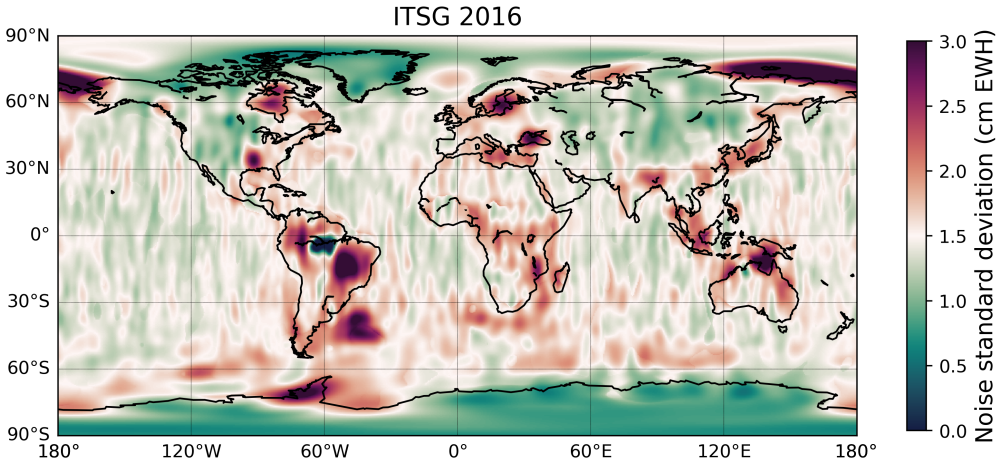

Figure B.4: Estimated noise standard deviation for GRACE solution ITSG 2016 by considering one mass-anomaly time-series in the VCE and MYDD minimization as regularization technique.

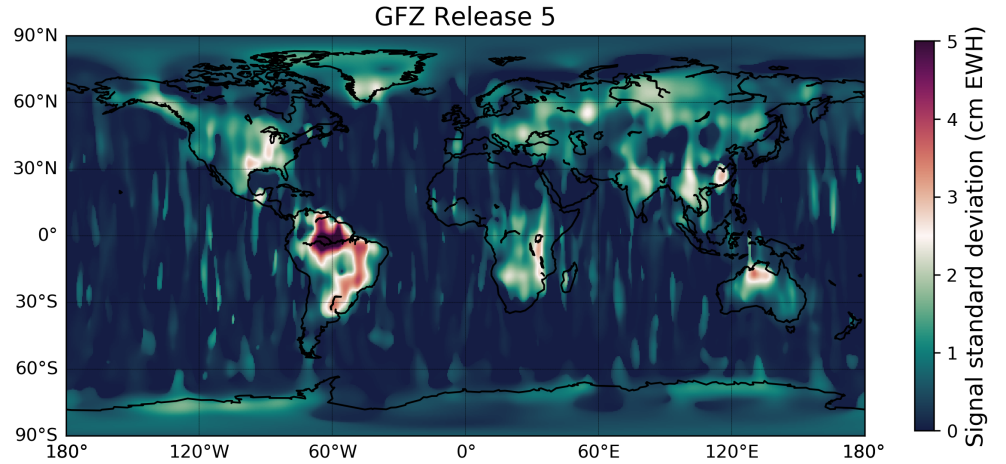

Figure B.5: Estimated signal standard deviation for GRACE solution GFZ Release 5 by considering one mass-anomaly time-series in the VCE and MYDD minimization as regularization technique.

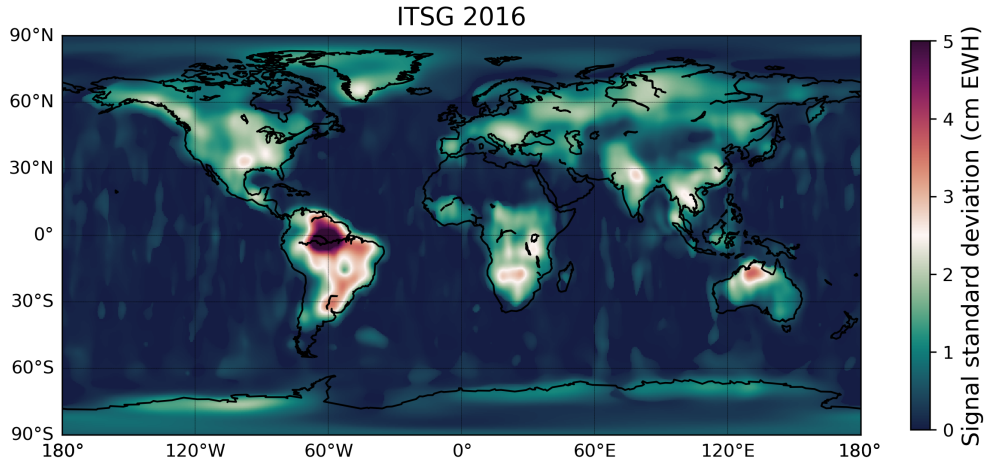

Figure B.6: Estimated signal standard deviation for GRACE solution ITSG 2016 by considering one mass-anomaly time-series in the VCE and MYDD minimization as regularization technique.

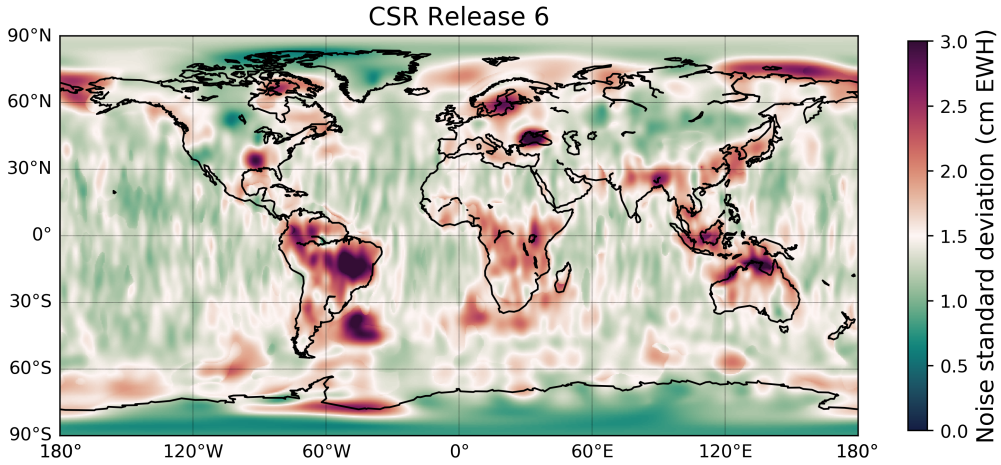

Figure B.7: Estimated noise standard deviation for GRACE solution CSR Release 6 by considering one mass-anomaly time-series in the VCE and MYDD minimization as regularization technique.

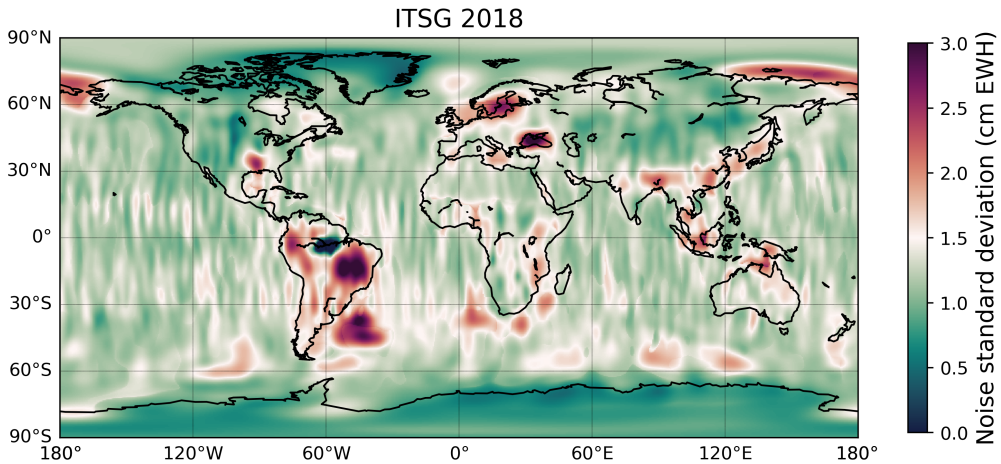

Figure B.8: Estimated noise standard deviation for GRACE solution ITSG 2018 by considering one mass-anomaly time-series in the VCE and MYDD minimization as regularization technique.

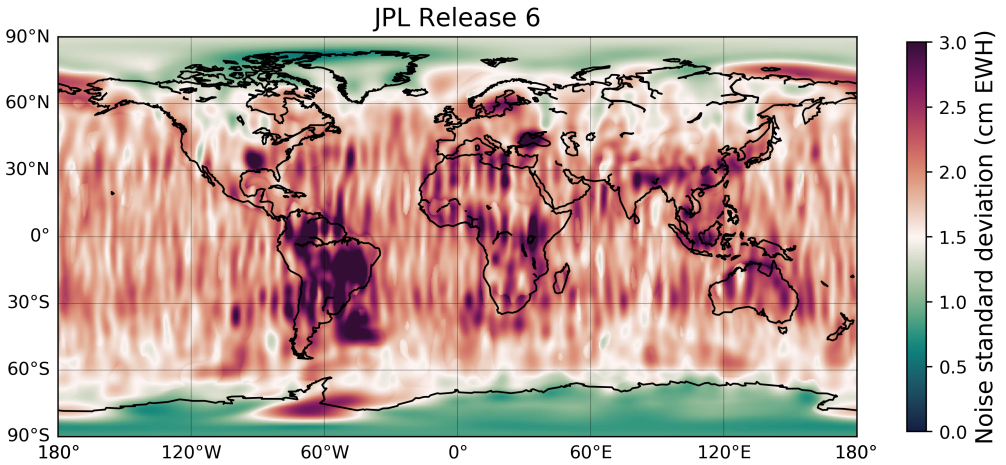

Figure B.9: Estimated noise standard deviation for GRACE solution JPL Release 6 by considering one mass-anomaly time-series in the VCE and MYDD minimization as regularization technique.

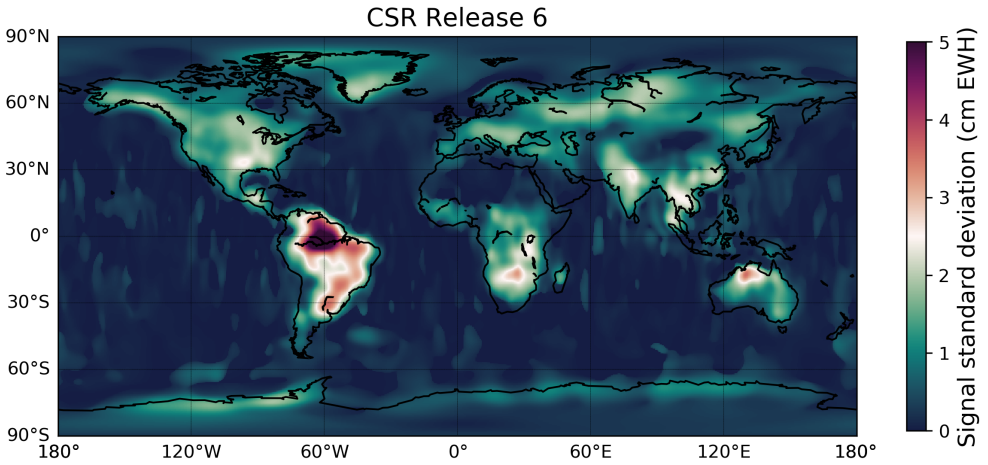

Figure B.10: Estimated signal standard deviation for GRACE solution CSR Release 6 by considering one mass-anomaly time-series in the VCE and MYDD minimization as regularization technique.

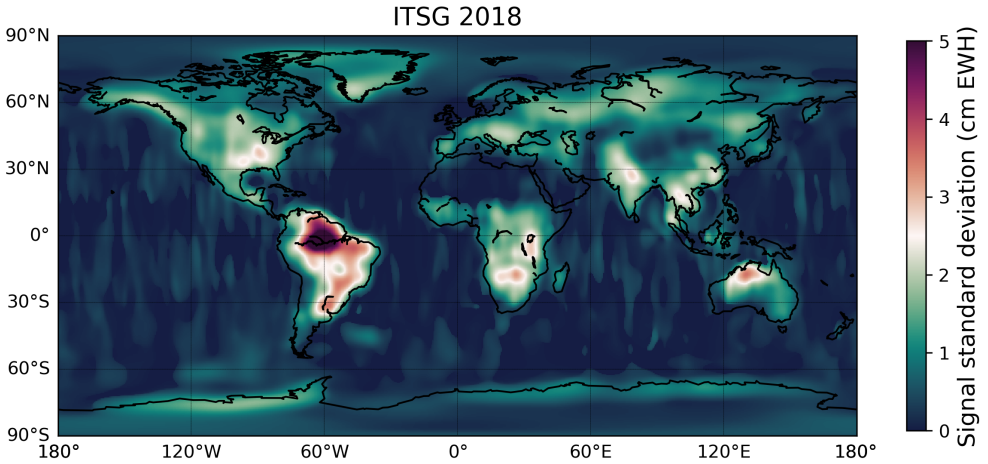

Figure B.11: Estimated signal standard deviation for GRACE solution ITSG 2018 by considering one mass-anomaly time-series in the VCE and MYDD minimization as regularization technique.

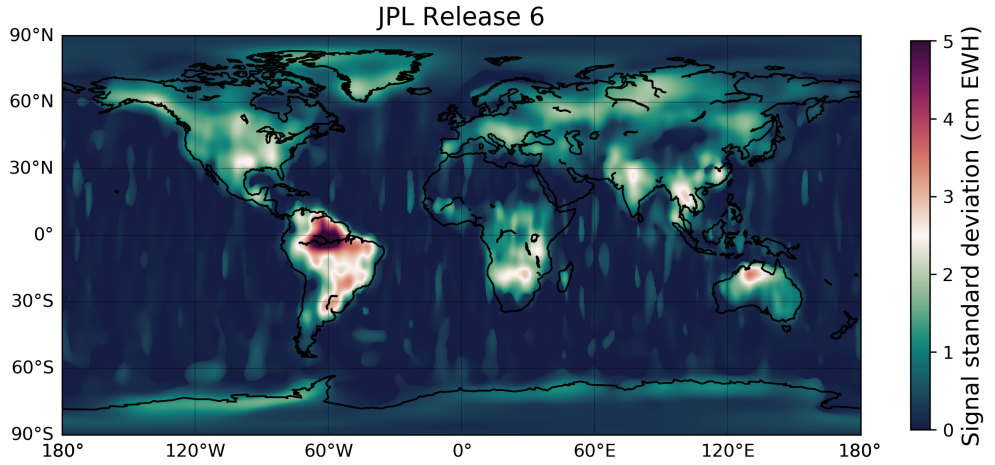

Figure B.12: Estimated signal standard deviation for GRACE solution JPL Release 6 by considering one mass-anomaly time-series in the VCE and MYDD minimization as regularization technique.

C

Supplementing set of figures for section 4.3

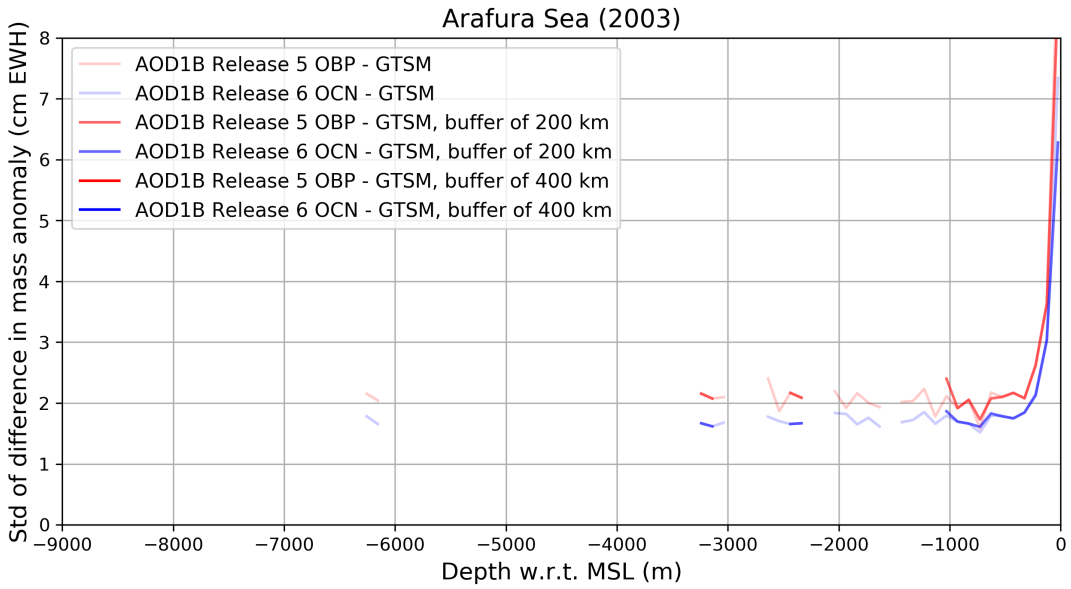

Figure C.1: Standard deviation of the 3/6-hourly difference mass-anomaly time-series (year 2003) versus bathymetry for the Arafura Sea. These difference mass-anomaly time-series are computed by subtracting GTSM from AOD1B OBP Release 5 (red) and subtracting GTSM from AOD1B OCN Release 6 (blue).

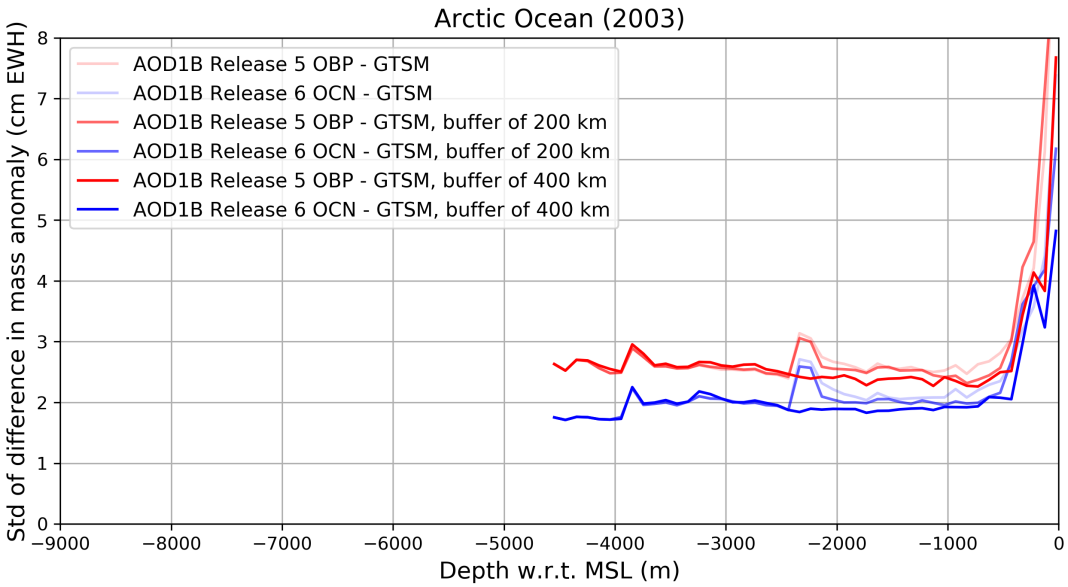

Figure C.2: Standard deviation of the 3/6-hourly difference mass-anomaly time-series (year 2003) versus bathymetry for the Arctic Ocean. These difference mass-anomaly time-series are computed by subtracting GTSM from AOD1B OBP Release 5 (red) and subtracting GTSM from AOD1B OCN Release 6 (blue).

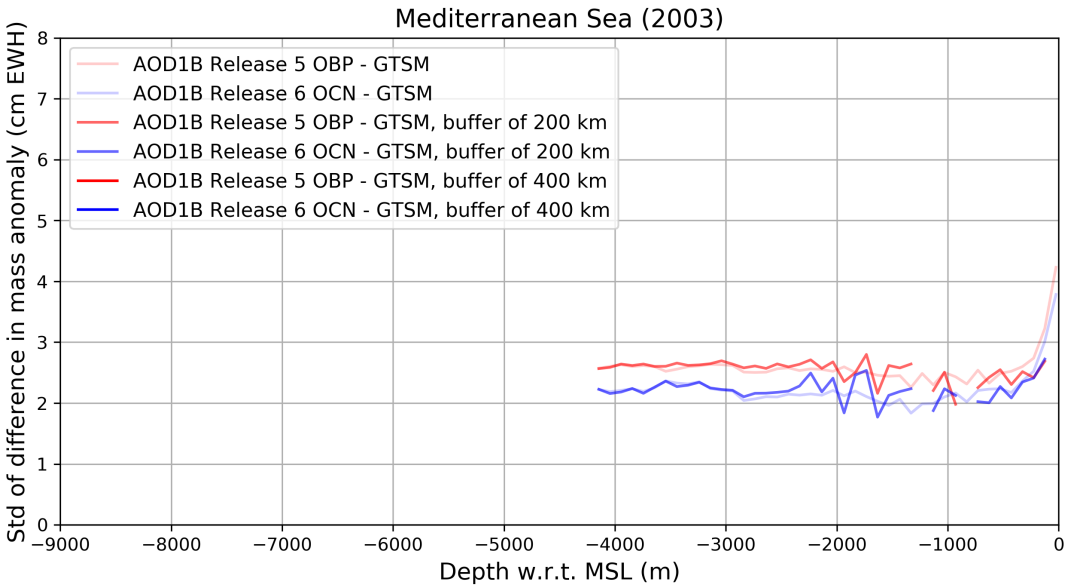

Figure C.3: Standard deviation of the 3/6-hourly difference mass-anomaly time-series (year 2003) versus bathymetry for the Mediterranean Sea. These difference mass-anomaly time-series are computed by subtracting GTSM from AOD1B OBP Release 5 (red) and subtracting GTSM from AOD1B OCN Release 6 (blue).

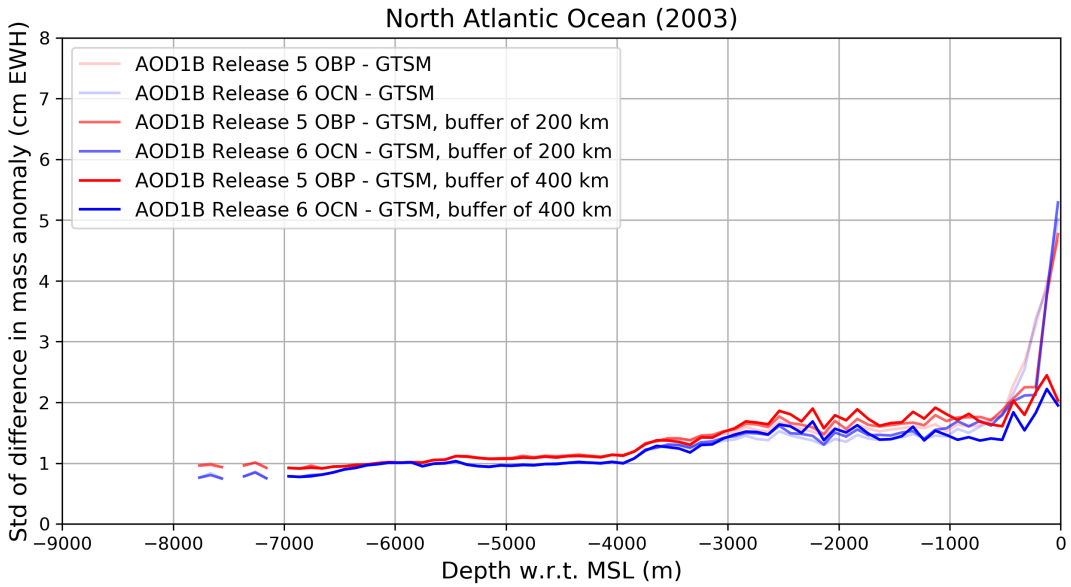

Figure C.4: Standard deviation of the 3/6-hourly difference mass-anomaly time-series (year 2003) versus bathymetry for the North Atlantic Ocean. These difference mass-anomaly time-series are computed by subtracting GTSM from AOD1B OBP Release 5 (red) and subtracting GTSM from AOD1B OCN Release 6 (blue).

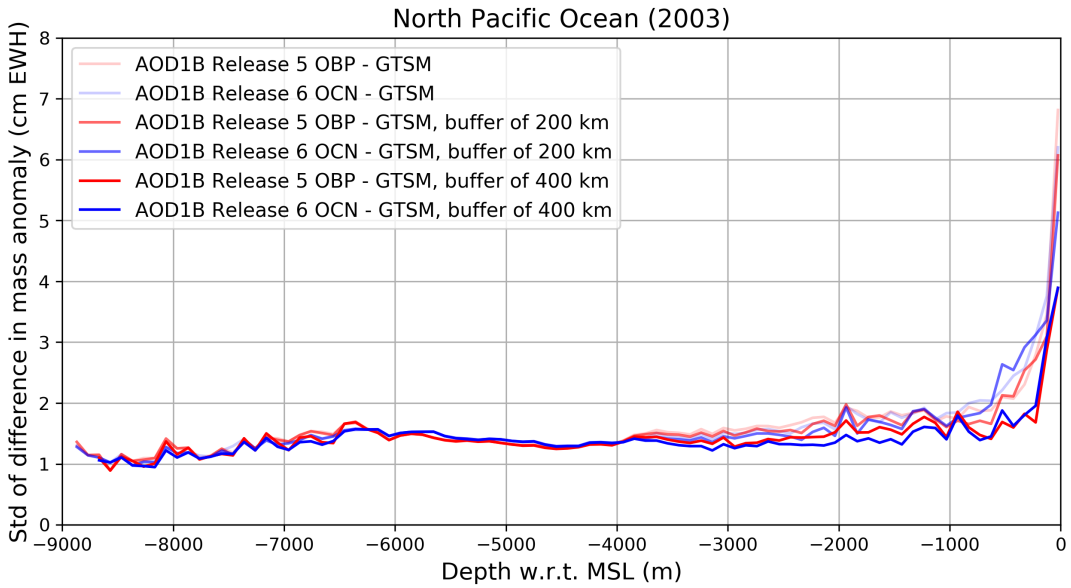

Figure C.5: Standard deviation of the 3/6-hourly difference mass-anomaly time-series (year 2003) versus bathymetry for the North Pacific Ocean. These difference mass-anomaly time-series are computed by subtracting GTSM from AOD1B OBP Release 5 (red) and subtracting GTSM from AOD1B OCN Release 6 (blue).

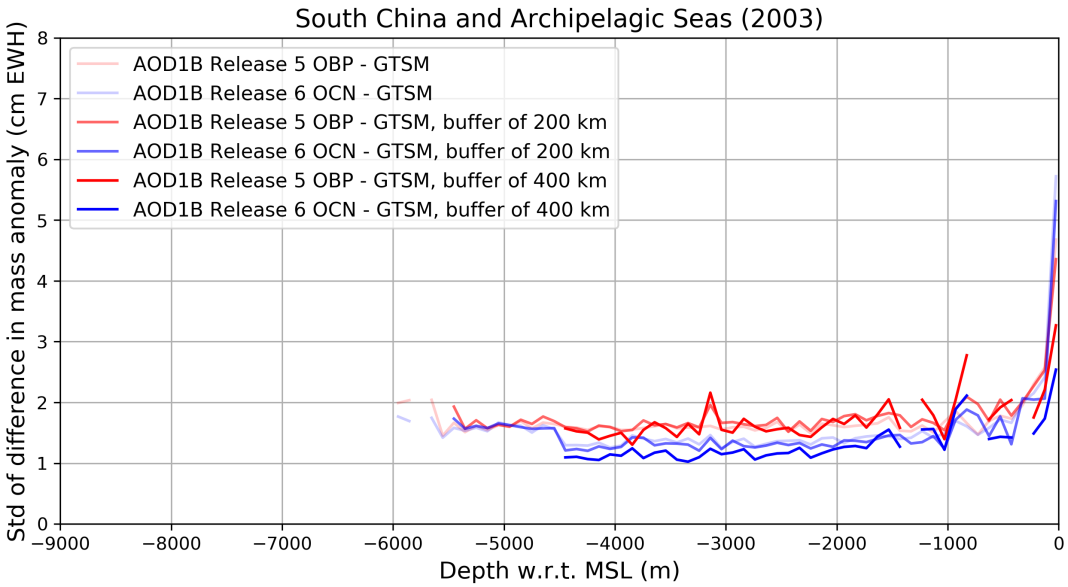

Figure C.6: Standard deviation of the 3/6-hourly difference mass-anomaly time-series (year 2003) versus bathymetry for the South China and Archipelagic Seas. These difference mass-anomaly time-series are computed by subtracting GTSM from AOD1B OBP Release 5 (red) and subtracting GTSM from AOD1B OCN Release 6 (blue).

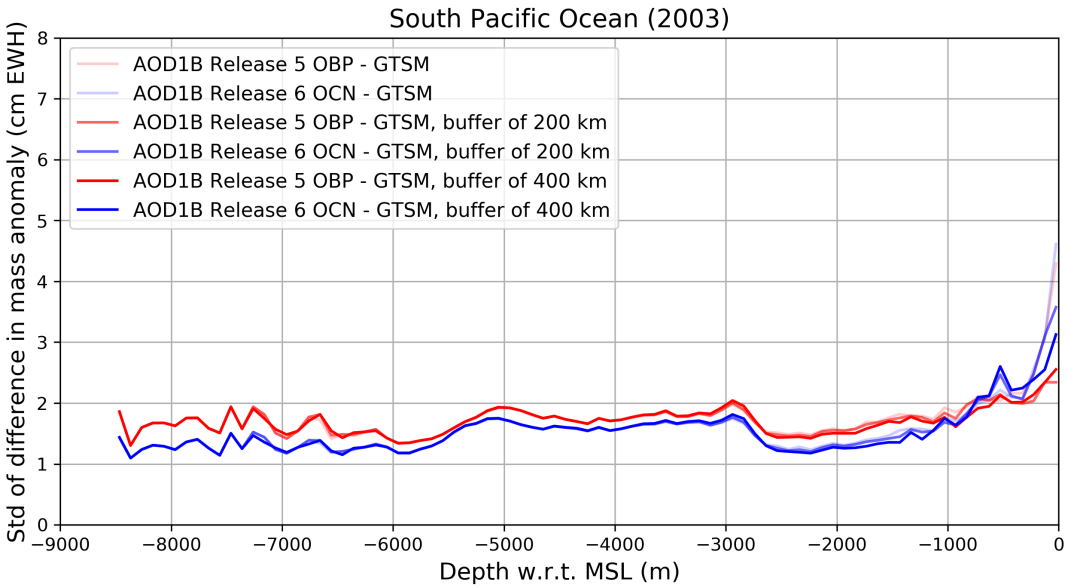

Figure C.7: Standard deviation of the 3/6-hourly difference mass-anomaly time-series (year 2003) versus bathymetry for the South Pacific Ocean. These difference mass-anomaly time-series are computed by subtracting GTSM from AOD1B OBP Release 5 (red) and subtracting GTSM from AOD1B OCN Release 6 (blue).

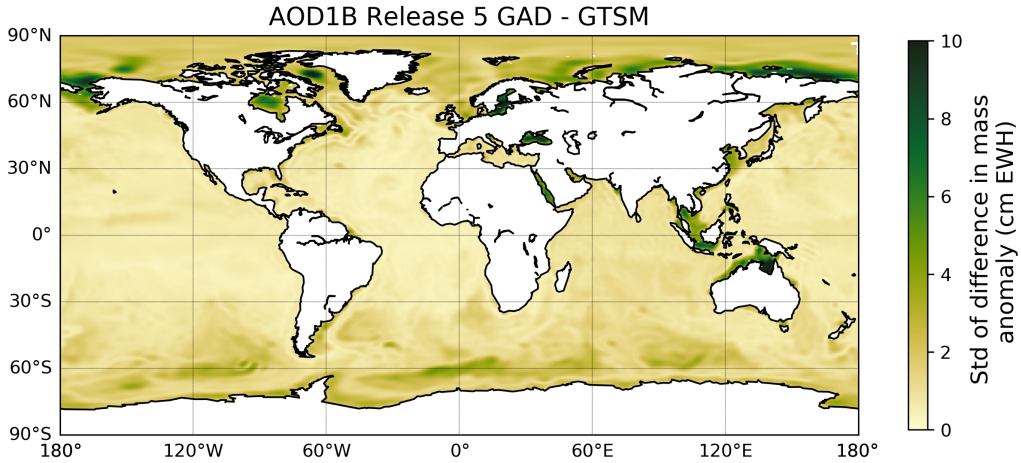

Figure C.8: Standard deviation of the monthly difference mass-anomaly time-series. This difference mass-anomaly time-series is computed by subtracting GTSM (run with only meteorological forcing) from the AOD1B GAD Release 5 product.

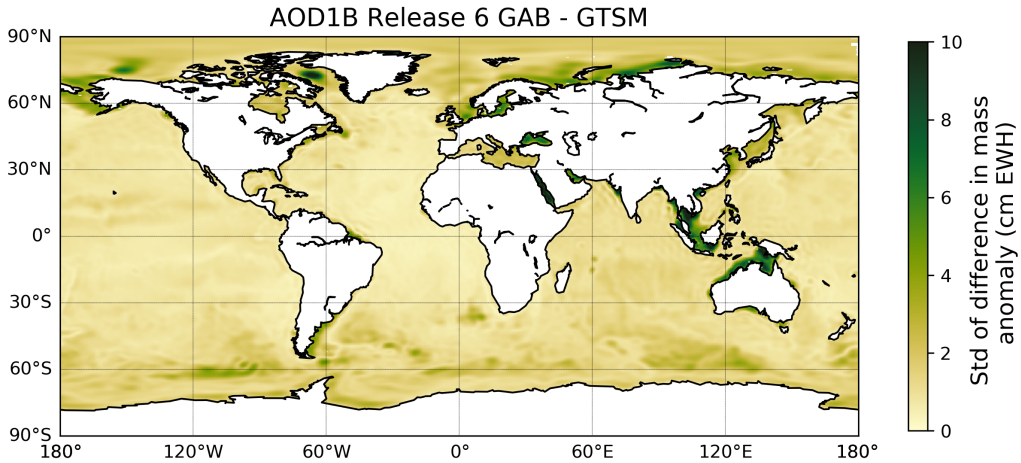

Figure C.9: Standard deviation of the monthly difference mass-anomaly time-series. This difference mass-anomaly time-series is computed by subtracting GTSM (run with only meteorological forcing) from the AOD1B GAB Release 6 product.

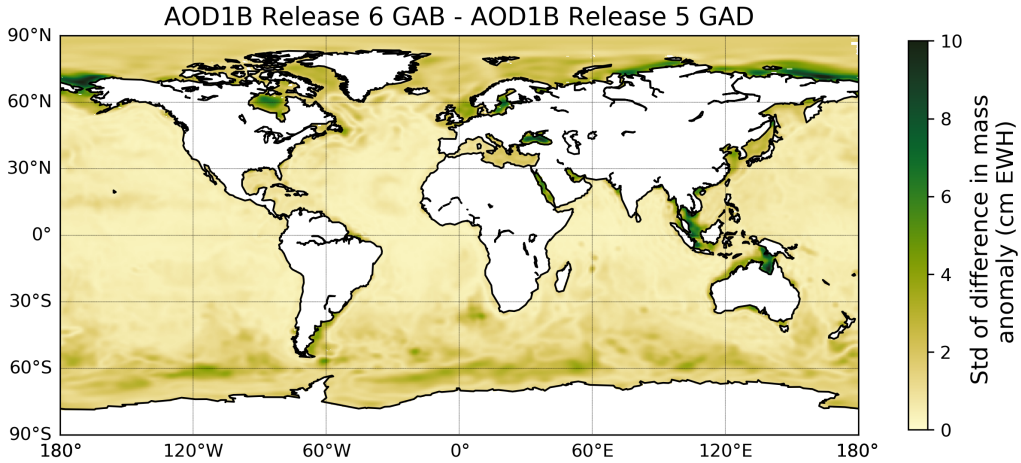

Figure C.10: Standard deviation of the monthly difference mass-anomaly time-series. This difference mass-anomaly time-series is computed by subtracting the AOD1B GAD Release 5 product (after removal of the ocean mean) from the AOD1B GAB Release 6 product.

D

Strange features in GTSM when run with only tidal forcing

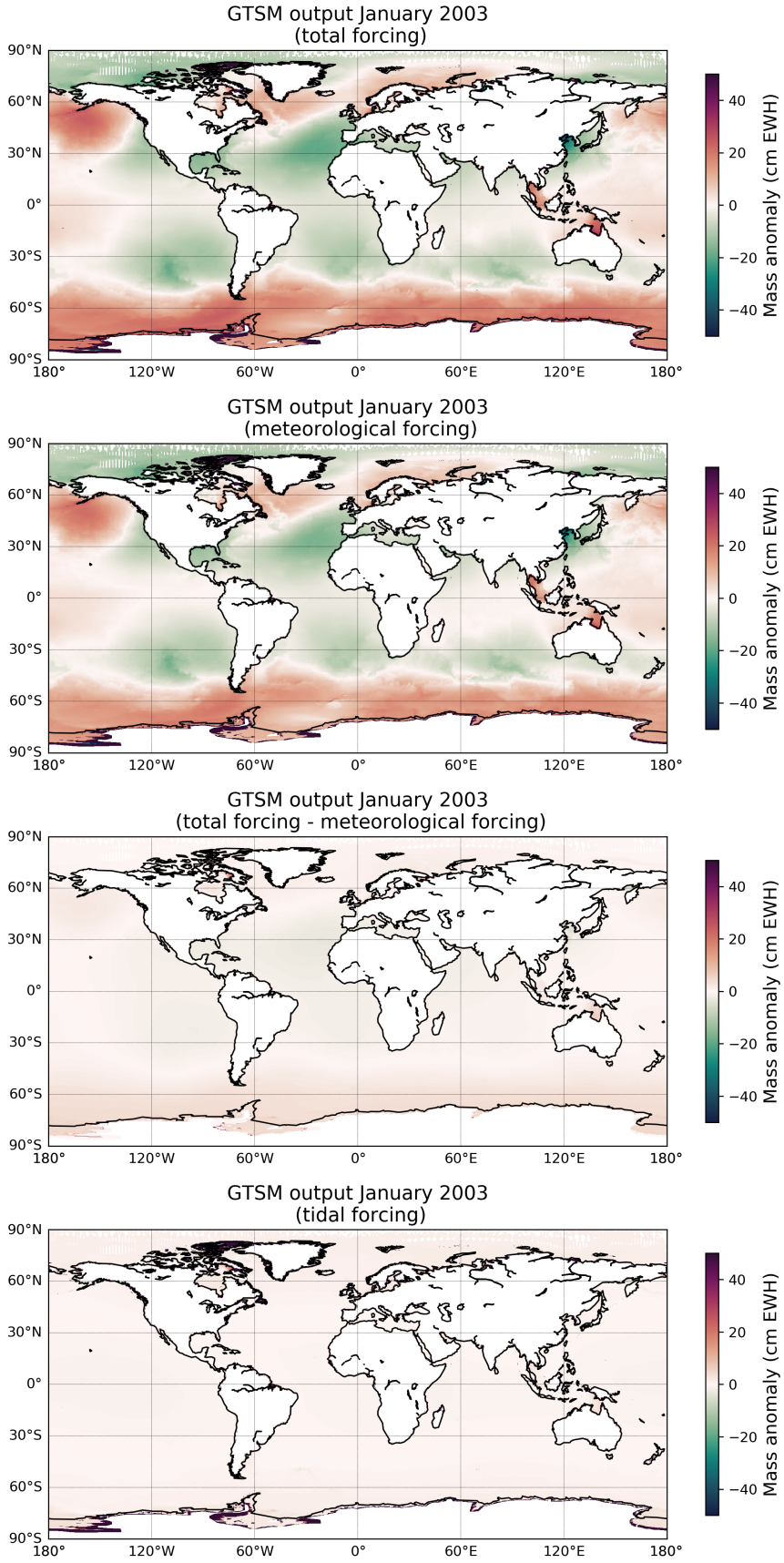

Figure D.1: Monthly mean output at the computational grid for different runs of GTSM for the year 2003. The runs differ in the applied forcing to the model. The third plot is a difference plot of the first and second plot. The monthly mean values for January are shown.

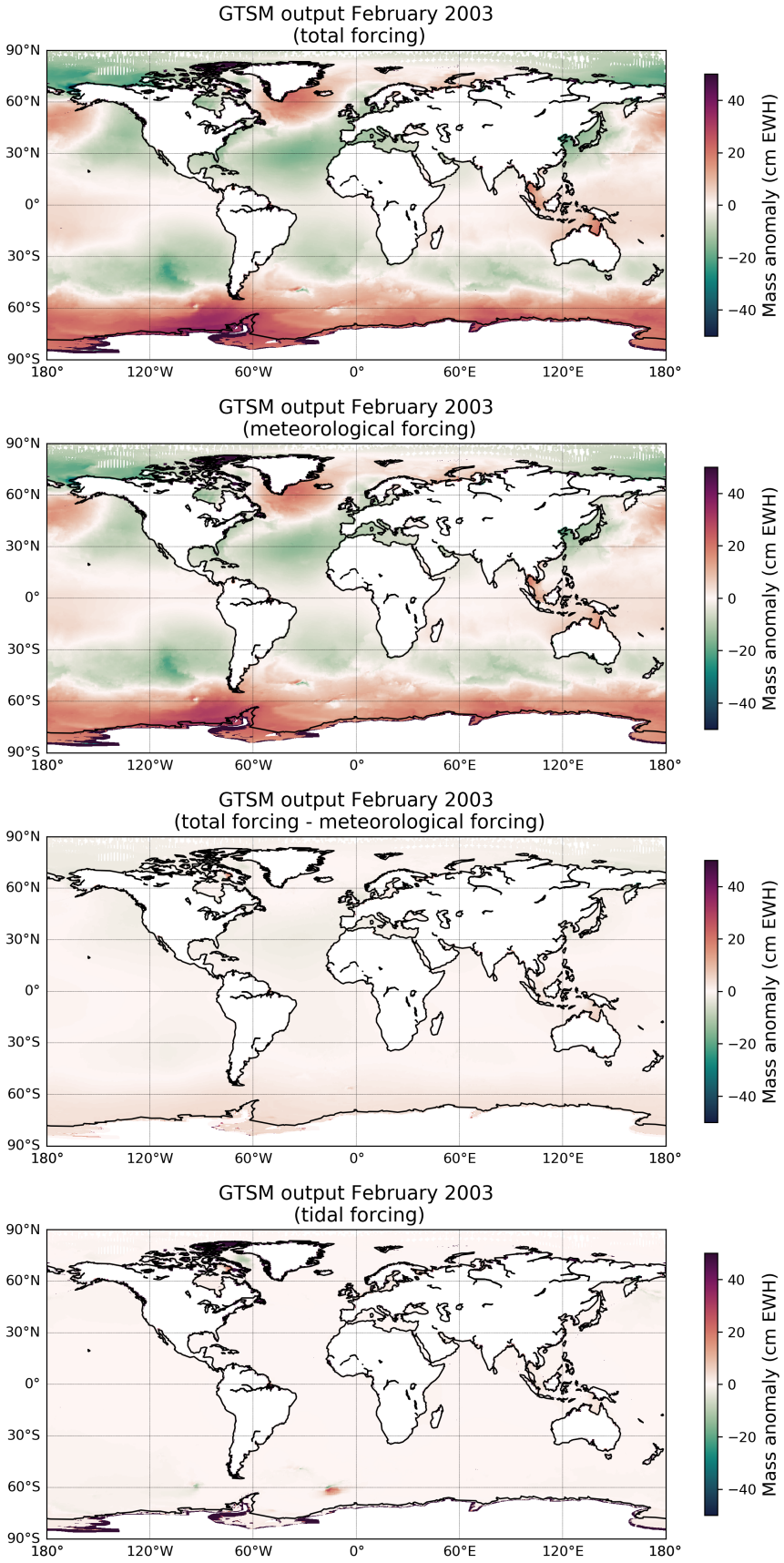

Figure D.2: Monthly mean output at the computational grid for different runs of GTSM for the year 2003. The runs differ in the applied forcing to the model. The third plot is a difference plot of the first and second plot. The monthly mean values for February are shown.

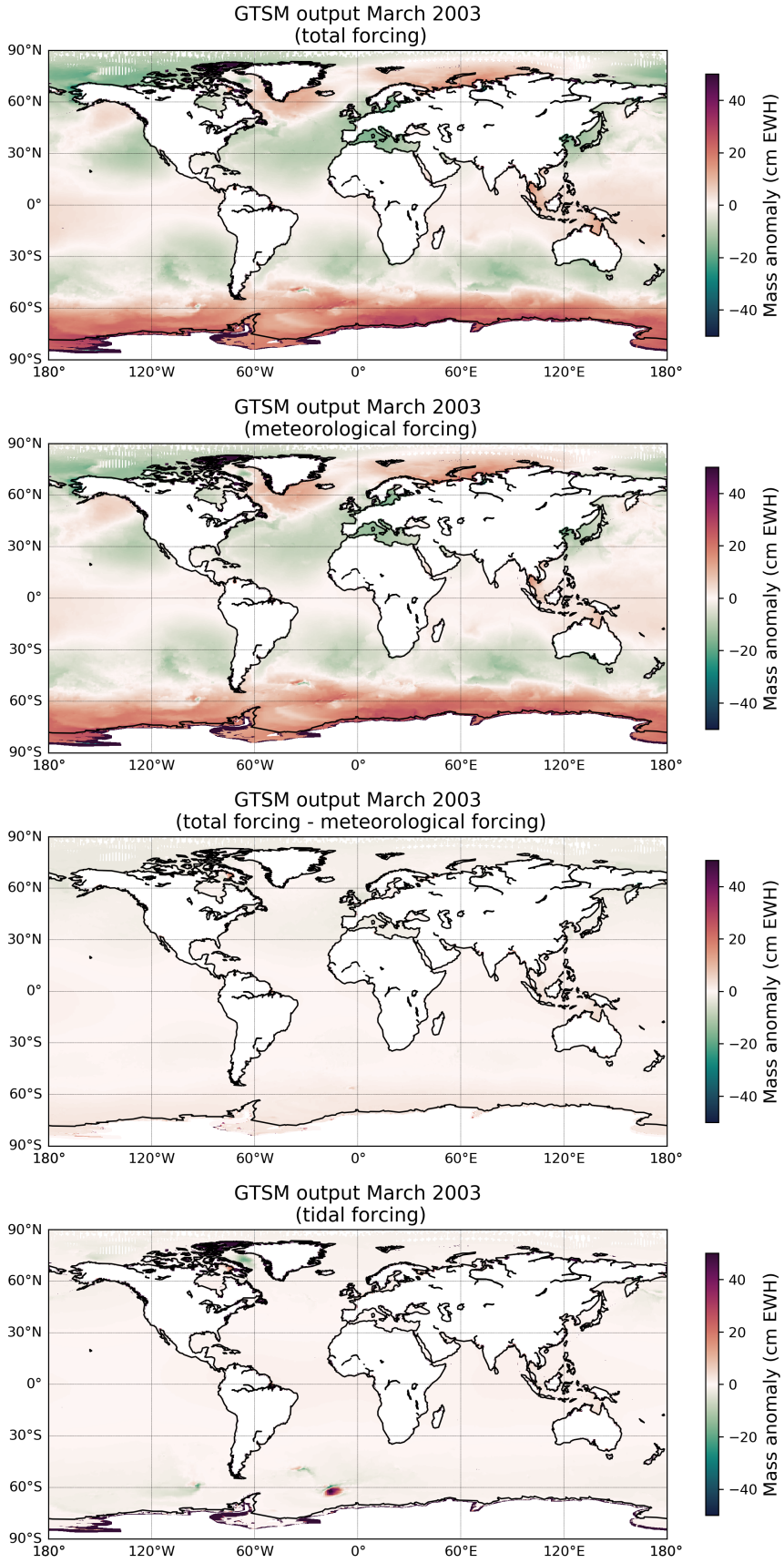

Figure D.3: Monthly mean output at the computational grid for different runs of GTSM for the year 2003. The runs differ in the applied forcing to the model. The third plot is a difference plot of the first and second plot. The monthly mean values for March are shown.

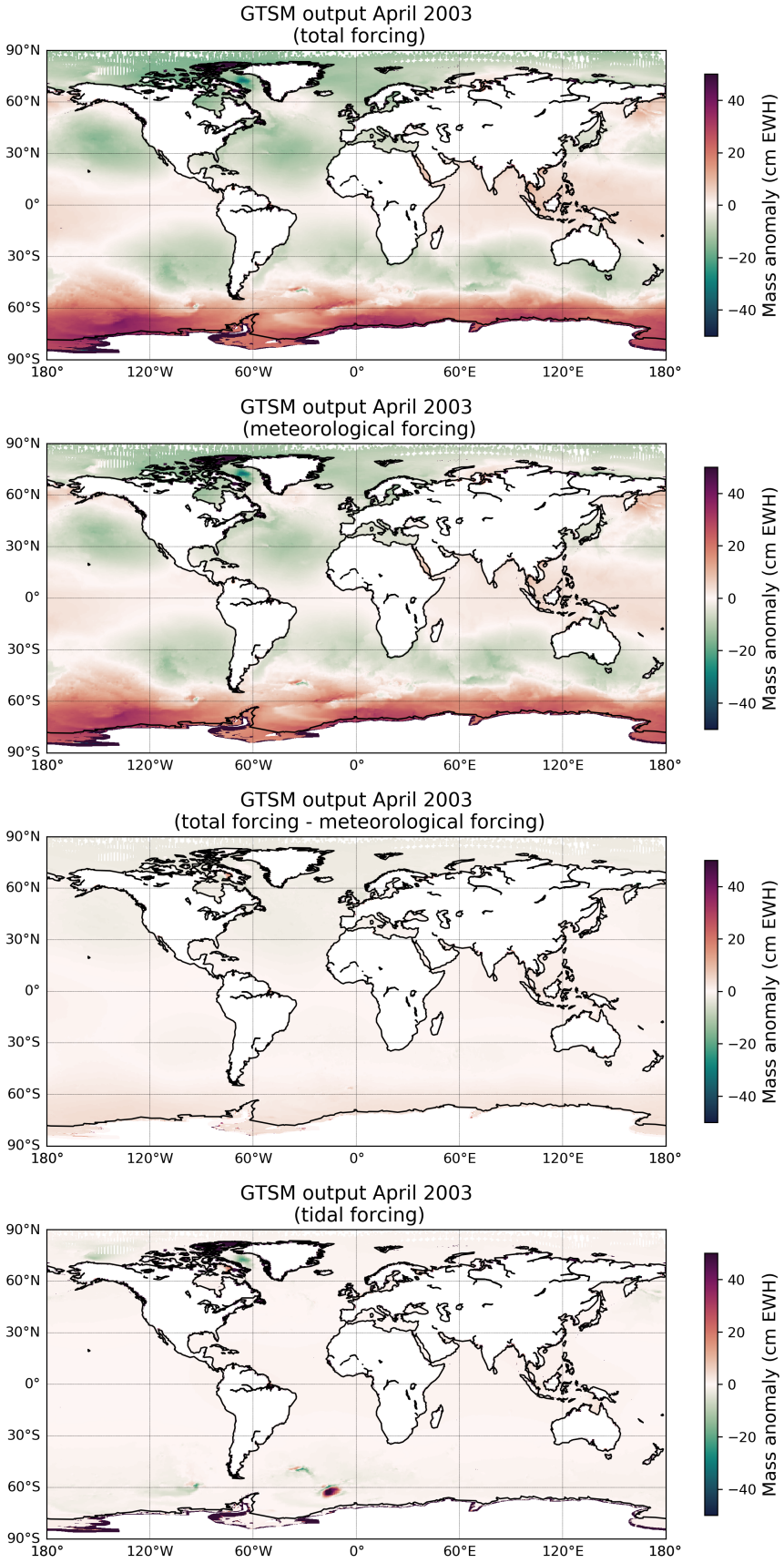

Figure D.4: Monthly mean output at the computational grid for different runs of GTSM for the year 2003. The runs differ in the applied forcing to the model. The third plot is a difference plot of the first and second plot. The monthly mean values for April are shown.

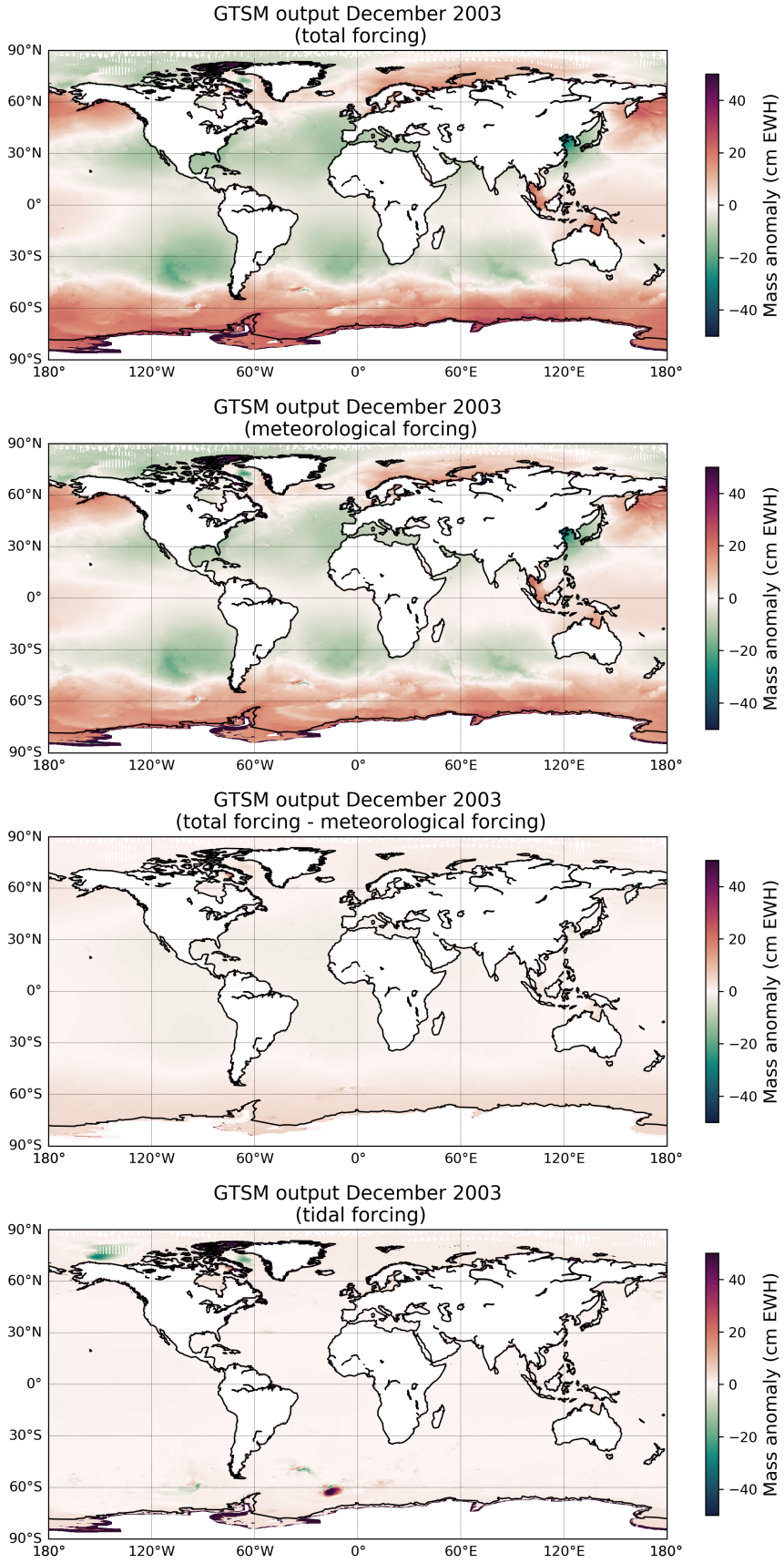

Figure D.5: Monthly mean output at the computational grid for different runs of GTSM for the year 2003. The runs differ in the applied forcing to the model. The third plot is a difference plot of the first and second plot. The monthly mean values for December are shown.

Bibliography

[1] Emodnet bathymetry consortium (2016): Emodnet digital bathymetry (dtm).

[2] March 2003. URL http://www.oc.nps.edu/nom/main.html.

[3] Grace gravity measurement, February 2004. URL http://www2.csr.utexas.edu/grace/science/gravity_measurement.html.

[4] Grace gravity recovery and climate experiment, March 2018. URL http://www2.csr.utexas.edu/grace/.

[5] S. A. Holmes and Will Featherstone. A unified approach to the clenshaw summation and the recursive computation of very high degree and order normalised associated legendre functions. 76:279–299, 05 2002.

[6] M. Apecechea, J. Rego, and M Verlaan. Gtsm setup and validation. Technical report, Deltares, 2017.

[7] Richard C. Aster, Brian Borchers, and Clifford Thurber. *Parameter Estimation and Inverse Problems*. Academic Press, Boston, second edition edition, 2013.

[8] S. Bettadpur. Utcsr level-2 processing standards document for level-2 product release 0005. Technical report, Center for Space Research, The University of Texas at Austin, 2012.

[9] S. Bettadpur. Utcsr level-2 processing standards document for level-2 product release 0006. Technical report, Center for Space Research, The University of Texas at Austin, 2018.

[10] Srinivas Bettadpur. Gravity recovery and climate experiment - level-2 gravity field product user handbook. Technical report, Center of Space Research - The University of Texas at Austin, April 2018.

[11] R. Biancale and A. Bode. Mean annual and seasonal atmospheric tide models based on 3-hourly and 6-hourly ecmwf surface pressure data. Technical report, Deutsches GeoForschungsZentrum GFZ, Potsdam, 2006.

[12] S. Callery, November 2018. URL https://climate.nasa.gov/effects/.

[13] D. P. Chambers, J. Wahr, and R. Steven Nerem. Preliminary observations of global ocean mass variations with grace. *Geophysical Research Letters*, 31(13), 2004.

[14] H. Charnock. Wind-stress on a water surface. *Q. J. Royal Meteorol. Soc.*, pages 638–640, 1955.

[15] Eric Chaumillon, Xavier Bertin, André B. Fortunato, Marco Bajo, Jean-Luc Schneider, Laurent Dezileau, John Patrick Walsh, Agnès Michelot, Etienne Chauveau, Axel Créach, Alain Hénaff, Thierry Sauzeau, Benoit Waeles, Bruno Gervais, Gwenaële Jan, Juliette Baumann, Jean-François Breilh, and Rodrigo Pedreros. Storm-induced marine flooding: Lessons from a multidisciplinary approach. *Earth-Science Reviews*, 165:151 – 184, 2017. ISSN 0012-8252. doi: https://doi.org/10.1016/j.earscirev.2016.12.005. URL http://www.sciencedirect.com/science/article/pii/S0012825216304597.

[16] J. Chen, C. Wilson, and J. Ries. Broad-band assessment of degree-2 gravitational changes from grace and other estimates, 2002–2015. *J. Geophys. Res. Solid Earth*, 2016.

[17] C. Dahle, F. Flechtner, C. Gruber, D. König, R. König, G. Michalak, and K. Neumayer. Gfz grace level-2 processing standards document for level-2 product release 0005. Technical report, GFZ German Research Centre for Geosciences, Potsdam, 2013.

[18] Simone De Kleermaeker, Martin Verlaan, Thomas Mortlock, Joao Lima Rego, Maialen Irazoqui, Kun Yan, and Daniel Twigt. Global-to-local scale storm surge modelling on tropical cyclone affected coasts. In *Coasts & Ports 2017 Conference*, June 2017.

[19] *Delft3D-Flow - Simulation of multi-dimentsional hydrodynamic flows and transport phenomena, including sediments - User Manual*. Deltares, 3.15.20508 edition, January 2012.

[20] *D-Flow Flexible Mesh - User Manual*. Deltares, 1.2.1 edition, July 2018.

[21] S. Desai. Observing the pole tide with satellite altimetry. *Journal of Geophysical Research*, 2002.

[22] S. D. Desai and D.-N. Yuan. Application of the convolution formalism to the ocean tide potential: Results from the gravity recovery and climate experiment (grace). *Journal of Geophysical Research: Oceans*, 2006.

[23] P. Ditmar. Cie4610: Mass transport in the earth system - lecture notes, June 2018.

[24] P. Ditmar. Conversion of time-varying stokes coefficients into mass anomalies at the earth's surface considering the earth's oblateness. *Journal of Geodesy*, February 2018.

[25] P. Ditmar, N. Tangdamrongsub, J. Ran, and R. Klees. Estimation and reduction of random noise in mass anomaly time-series from satellite gravity data by minimization of month-to-month year-to-year double differences. *Journal of Geodynamics*, 119:9–22, March 2018.

[26] H. Dobslaw, I. Bergmann-Wolf, R. Dill, L. Poropat, M. Thomas, C. Dahle, S. Esselborn, R. Konig, and F. Flechtner. A new high-resolution model of non-tidal atmosphere and ocean mass variability for de-aliasing of satellite gravity observations: Aod1b rl06. *Geophysical Journal International*, 2013.

[27] H. Dobslaw, I. Bergmann-Wolf, E. Forootan, C. Dahle, T. Mayer-Gürr, J. Kusche, and F. Flechtner. Modeling of present-day atmosphere and ocean non-tidal de-aliasing errors for future gravity mission simulations. *Journal of Geodesy*, 2016.

[28] F. Flechtner, K.-H. Neumayer, C. Dahle, H. Dobslaw, E. Fagiolini, J.-C. Raimondo, and A. Güntner. What can be expected from the grace-fo laser ranging interferometer for earth science applications? *Surveys in Geophysics*, 37(2):453—470, 2016.

[29] Frank Flechtner, Roland Schmidt, and Ulrich Meyer. *De-aliasing of Short-term Atmospheric and Oceanic Mass Variations for GRACE*, pages 83–97. Springer Berlin Heidelberg, Berlin, Heidelberg, 2006. ISBN 978-3-540-29522-8. doi: 10.1007/3-540-29522-4_7. URL https://doi.org/10.1007/3-540-29522-4_7.

[30] Elisa Fagiolini Frank Flechtner, Henryk Dobslaw. Aod1b product description document for product release 05. Technical report, GFZ German Research Centre for Geosciences, December 2015.

[31] P. Fretwell, H.D. Pritchard, D.G. Vaughan, J.L. Bamber, N.E. Barrand, R. Bell, C. Bianchi, R. G. Bingham, D.D. Blankenship, G. Casassa, G. Catania, D. Callens, H. Conway, A.J. Cook, H.F.J. Corr, D. Damaske, V. Damm, F. Ferraccioli, R. Forsberg, S. Fujita, Y. Gim, P. Gogineni, J.A. Griggs, R.C.A. Hindmarsh, P. Holmlund, J.W. Holt, R.W. Jacobel, A. Jenkins, W. Jokat, T. Jordan, E.C. King, J. Kohler, W. Krabill, M. Riger-Kusk, K.A. Langley, G. Leitchenkov, C. Leuschen, B.P. Luyendyk, K. Matsuoka, J. Mouginot, F.O. Nitsche, Y. Nogi, O.A. Nost, S.V. Popov, E. Rignot, D.M. Rippin, A. Rivera, J. Roberts, N. Ross, M.J. Siegert, A.M. Smith, D. Steinhage, M. Studinger, B. Sun, B.K. Tinto, B.C. Welch, D. Wilson, D.A. Young, C. Xiangbin, and A. Zirizzotti. Bedmap2: improved ice bed, surface and thickness datasets for antarctica. *The Cryosphere*, 7(1):375–393, 2013.

[32] T. Greicius. Grace mission: 15 years of watching water on earth, February 2018. URL https://www.nasa.gov/feature/jpl/grace-mission-15-years-of-watching-water-on-earth.

[33] Tony Greicius. Grace gravity recovery and climate experiment, July 2014. URL https://www.nasa.gov/mission_pages/Grace/.

[34] M. Haasnoot, L. Bouwer, F. Diermanse, J. Kwadijk, A. van der Spek, G. Oude Essink, J. Delsman, O. Weiler, M. Mens, J. ter Maat, Y. Huismans, K. Sloff, and E. Mosselman. Mogelijke gevolgen van versnelde zeespiegelstijging voor het deltaprogramma. een verkenning. Technical report, Deltares, 2018.

[35] Ryan A. Hardy, R. Steven Nerem, and David N. Wiese. The impact of atmospheric modeling errors on grace estimates of mass loss in greenland and antarctica. *Journal of Geophysical Research: Solid Earth*, 122(12):10,440–10,458, 2017. doi: 10.1002/2017JB014556. URL https://agupubs.onlinelibrary.wiley.com/doi/abs/10.1002/2017JB014556.

[36] H. Hersbach and D. Dee. Era5 reanalysis is in production. *ECMWF Newsletter*, 147(7), 2016.

[37] B. Hofmann-Wellenhof and H. Moritz. *Physical geodesy*. SpringerWienNewYork, Wien, Austria, 2005.

[38] National Imagery and Mapping Agency. Department of defense world geodetic system 1984 - its definition and relationships with local geodetic systems. Technical report, 2000.

[39] IPCC. *Climate Change 2013: The Physical Science Basis. Contribution of Working Group I to the Fifth Assessment Report of the Intergovernmental Panel on Climate Change*. Cambridge University Press, 2013. doi: 10.1017/CBO9781107415324.

[40] IPCC. *Climate Change 2014: Impacts, Adaptation, and Vulnerability. Part A: Global and Sectoral Aspects. Contribution of Working Group II to the Fifth Assessment Report of the Intergovernmental Panel on Climate Change*. Cambridge University Press, Campridge, United Kindom and New York, NY, USA, 2014.

[41] Maialen Irazoqui Apecechea, Martin Verlaan, Firmijn Zijl, Camille Le Coz, and Herman Kernkamp. Effects of self-attraction and loading at a regional scale: a test case for the northwest european shelf. *Ocean Dynamics*, 67(6):729–749, Jun 2017. ISSN 1616-7228. doi: 10.1007/s10236-017-1053-4. URL https://doi.org/10.1007/s10236-017-1053-4.

[42] M. J. F. Stive J. Bosboom. *Coastal Dynamics 1 - lecture notes CIE4305*. VSSD, 2012.

[43] G Joodaki. *Earth Mass Change Tracking Using GRACE Satellite Gravity Data*. PhD thesis, Norwegian University of Science and Technology, Trondheim, January 2014.

[44] H. W. J. Kernkamp, A. Van Dam, G. S. Stelling, and E. D. De Goede. Efficient scheme for the shallow water equations on unstructured grids with application to the continental shelf. *Ocean Dynamics*, 61:1175–1188, 2011.

[45] K.-R. Koch and J. Kusche. Regularization of geopotential determination from satellite data by variance components. *Journal of Geodesy*, 76(5):259–268, May 2002. ISSN 1432-1394. doi: 10.1007/s00190-002-0245-x. URL https://doi.org/10.1007/s00190-002-0245-x.

[46] J. Kuhlmann, H. Dobslaw, and M. Thomas. Improved modeling of sea level patterns by incorporating self-attraction and loading. *Journal of Geophysical Research: Oceans*, 116(C11), 2011. doi: 10.1029/2011JC007399. URL https://agupubs.onlinelibrary.wiley.com/doi/abs/10.1029/2011JC007399.

[47] Jet Propulsion Laboratory. Jpl, csr or gfz - which solution should i use?, . URL https://grace.jpl.nasa.gov/data/choosing-a-solution/.

[48] Jet Propulsion Laboratory. Sea level, . URL https://gracefo.jpl.nasa.gov/science/sea-level/.

[49] International Hydrographic Bureau Monaco. Names and limits of oceans and seas. June 2002. URL https://www.iho.int/mtg_docs/com_wg/S-23WG/S-23WG_Misc/Draft_2002/Draft_2002.htm.

[50] H. Moritz. *Advanced Physical Geodesy*. Herbert Wichmann Verlag, Karlsruhe, 1980.

[51] S. Muis, M. Verlaan, H. C. Winsemius, Jeroen C. J. H. Aerts, and P.J. Ward. A global reanalysis of storm surges and extreme sea levels. *Nature Communications*, 7, 2016.

[52] T. Patterson N. V. Kelso. Natural earth downloads, 2018. URL http://www.naturalearthdata.com/downloads/.

[53] Yufeng Nie, Yunzhong Shen, and Qiujie Chen. Combination analysis of future polar-type gravity mission and grace follow-on. *Remote Sensing*, 11, 01 2019. doi: 10.3390/rs11020200.

[54] Graz University of Technology. Itsg-grace2016, . URL https://www.tugraz.at/institute/ifg/downloads/gravity-field-models/itsg-grace2016/.

[55] Graz University of Technology. Itsg-grace2018, . URL https://www.tugraz.at/institute/ifg/downloads/gravity-field-models/itsg-grace2018/.

[56] J. Jungclaus P. Wetzel, H. Haak and E. Maier-Reimer. The max-planck-institute global ocean/sea-ice model mpi-om. Technical report, Max-Planck-Institute for Meteorology, Bundestrasse 53 20146 Hamburg, Germany.

[57] R.D. Ray and R.M. Ponte. Barometric tides from ecmwf operational analyses. *Barometric tides from ECMWF operational analyses*, 2003.

[58] M. Rodell, P.R. Houser, U. Jambor, J. Gottschalck, K. Mitchell, C.-J. Meng, K. Arsenault, B. Cosgrove, J. Radakovich, M. Bosilovich, J.K. Entin, J.P. Walker, D. Lohmann, and D. Toll. The global land data assimilation system. *Bull. Amer. Meteor. Soc.*, 2004.

[59] D. T. Sandwell. Reference earth model - wgs84. University of California San Diego, 2002. URL http://topex.ucsd.edu/geodynamics/14gravity1_2.pdf.

[60] D.C. Slobbe. The earth's gravity field. CIE4606 Lecture slides, 2018.

[61] Y. Sun, R. Riva, and P. Ditmar. Degree-1 and c20 coefficients. URL https://www.tudelft.nl/en/ceg/about-faculty/departments/geoscience-remote-sensing/research/research-themes/gravity/models-data/champgracegoce-gravity-models-data/degree-1-and-c20-coefficients/.

[62] Yu Sun, Riccardo Riva, and Pavel Ditmar. Optimizing estimates of annual variations and trends in geocenter motion and j2 from a combination of grace data and geophysical models. *Journal of Geophysical Research: Solid Earth*, 121(11):8352–8370, 2016.

[63] Yu Sun, Riccardo Riva, Pavel Ditmar, and Roelof Rietbroek. Using grace to explain variations in the earth's oblateness. *Geophysical Research Letters*, 46(1):158–168, 2019.

[64] S. Swenson and J. Wahr. Methods for inferring regional surface-mass anomalies from gravity recovery and climate experiment (grace) measurements of time-variable gravity. *J. Geophys. Res.*, 107, 2002.

[65] Sean Swenson and John Wahr. Estimated effects of the vertical structure of atmospheric mass on the time□variable geoid. *Journal of Geophysical Research: Solid Earth (1978–2012)*, 107 (B9):ETG 4–1–ETG 4–11, 9 2002. ISSN 2156-2202. doi: 10.1029/2000JB000024. URL http:https://doi.org/10.1029/2000JB000024.

[66] M. Thomas and H. Dobslaw. On the impact of baroclinic ocean dynamics on the earth's gravity field. In *Proceedings of Joint CHAMP/GRACE Science Team Meeting 2004*, 2004.

[67] T. van Dam and R. Ray. S1 and s2 atmospheric tide loading effects for geodetic applications, 2010. URL http://geophy.uni.lu/ggfc-atmosphere/tide-loading-calculator.html.

[68] H. van der Marel. *Reference Systems for Surveying and Mapping - Lecture notes CTB3310*. Faculty of Civil Engineering and Geosciences - Delft University of Technology, February 2016.

[69] J. Virtanen, J. Mäkinen, M. Bilker-Koivula, H. Virtanen, M. Nordman, A. Kangas, M. Johansson, C.K. Shum, H. Lee, L. Wang, and M. Thomas. *Gravity, Geoid and Earth Observation*, chapter Baltic Sea Mass Variations from GRACE: Comparison with In Situ and Modelled Sea Level Heights, pages 571–577. Springer-Verlag Berlin Heidelberg, 2010.

[70] John Wahr, Mery Molenaar, and Frank Bryan. Time variability of the earth's gravity field: Hydrological and oceanic effects and their possible detection using grace. 103:30205–30230, 12 1998.

[71] K. F. Wakker. *Fundamentals of Astrodynamics*. Institutional Repository Library Delft University of Technology, Delft, January 2015. ISBN 978-94-6186-419-2.

[72] J. Wassink. Nieuw nederlandje. *Delft Integraal*, December 2018.

[73] P. Weatherall, K. M. Marks, M. Jakobsson, T. Schmitt, S. Tani, J. E. Arndt, M. Rovere, D. Chayes, V. Ferrini, and R. Wigley. A new digital bathymetric model of teh world's oceans. *Earth and Space Science*, 2(8):331–345, 2015.

[74] P. Wessel and W. H. F. Smith. A global self-consistent, hierarchical, high-resolution shoreline database. *J. Geophys. Res.*, pages 8741–8743, 1996.

[75] T. G. Whiteway. Australian bathymetry and topography grid. Technical report, Goescience Australia, 2009.

[76] D. R. Williams. Earth fact sheet, March 2017. URL `https://nssdc.gsfc.nasa.gov/planetary/factsheet/earthfact.html`.

[77] B. Wouters, J. A. Bonin, D. P. Chambers, R. E. Riva, I. Sasgen, and J. Wahr. Grace, time-varying gravity, earth system dynamics and climate change. *Rep Prog Phys*, 77(11), 2014.

[78] D. Yuan. Jpl level-2 processing standards document for level-2 product release 06. Technical report, Jet Propulsion Laboratory, California Institute of Technology, 2018.

[79] Lieselotte Zenner, Elisa Fagiolini, Ilias Daras, Frank Flechtner, Thomas Gruber, Torsten Schmidt, and Gottfried Schwarz. Non-tidal atmospheric and oceanic mass variations and their impact on grace data analysis. *Journal of Geodynamics*, 59-60:9 – 15, 2012. ISSN 0264-3707. doi: https://doi.org/10.1016/j.jog.2012.01.010. URL `http://www.sciencedirect.com/science/article/pii/S0264370712000282`. Mass Transport and Mass Distribution in the System Earth.

[80] Hao Zhou, Zhicai Luo, Yihao Wu, Qiong Li, and Chuang Xu. Impact of geophysical model error for recovering temporal gravity field model. *Journal of Applied Geophysics*, 130:177 – 185, 2016. ISSN 0926-9851. doi: https://doi.org/10.1016/j.jappgeo.2016.04.004. URL `http://www.sciencedirect.com/science/article/pii/S0926985116300982`.